

CARDIFF UNIVERSITY

***In vivo* measurement and
objective classification of
healthy, injured and pathological
shoulder complex function**

by

Lindsay Ann Stroud Larreal

PhD Thesis

Institute of Medical Engineering & Medical Physics
School of Engineering

October 2011

Declaration of Authorship

DECLARATION

This work has not been previously been accepted in substance for any degree and is not concurrently submitted in candidature from any degree.

Signed (candidate) Date

STATEMENT 1

This thesis is being submitted in partial fulfillment of the requirements for the degree of PhD.

Signed (candidate) Date

STATEMENT 2

This thesis is the result of my own independent work/investigation, except where otherwise stated.. Other sources are acknowledged by explicit references.

Signed (candidate) Date

STATEMENT 3

I hereby give consent for my thesis, if accepted, to be available for photocopying and for library loan, and for the title and summary to be made available to outside organisations.

Signed(candidate) Date

Abstract

Valuable insight into healthy and injured or pathological (IoP) shoulder function is gained by analysing the three dimensional (3D) joint kinematics. Motion Analysis (MA) techniques have been previously developed at Cardiff University to assess shoulder function following International Society of Biomechanics (ISB) recommendations. However, errors in the system significantly affect shoulder kinematics measurements.

Image registration techniques (IRT) were developed to accurately measure GH joint kinematics using dynamic single-plane fluoroscopy. 3D computer bone models of the humerus and scapula were generated from magnetic resonance imaging (MRI) scans using Simpleware Software (Simpleware Ltd). Accurate 3D to two dimensional (2D) image registration was performed using JointTrack software (Banks, S.A.). Full kinematics descriptions of the GH joint and of the scapula were obtained. The pattern of rotation agrees with what other researchers have previously measured. Humeral head translation was measured towards the glenoid centre ($3\pm 0.9\text{mm}$ medially, $2.7\pm 0.9\text{mm}$ inferiorly and then superiorly and $6.7\pm 2\text{mm}$ posteriorly) during abduction and ($2.8\pm 0.9\text{mm}$ medially, $3.6\pm 0.9\text{mm}$ superiorly and then inferiorly and $5.3\pm 2.1\text{mm}$ anteriorly) during scaption. The centering of the humeral head is believed to provide joint congruency for optimal shoulder function.

To investigate the errors commonly associated with MA, a comparison between the kinematics outputs from the MA measuring system and IRT was performed. Greater GH joint elevation was recorded with IRT (54.8° and 82.6° for abduction and scaption respectively) compared to MA (51.1° and 75.2° for abduction and scaption respectively). Furthermore, differences between IRT and MA recordings in GH joint plane of elevation (6.7° and 1.9° abduction and scaption respectively) and axial rotation (24.1° and 23.0° abduction and scaption respectively) were measured. Discrepancies in measured rotations between MA and IRT can be attributed to factors related to differences in the analytical approach as well as the errors commonly associated with the techniques.

Additions and improvements to the original Cardiff MA protocol for measuring and analysing shoulder biomechanics were made and healthy and shoulder patient function was subsequently investigated. The glenohumeral (GH) joint centre of rotation (CoR) estimation by means of the instantaneous helical axis (IHA) method was included in the Cardiff model using International Shoulder Group (ISG) routines. With the original protocol, only regression equations (MRE) based on scapula geometry were used to estimate GH joint CoR. Differences between IHA and MRE were investigated by comparing the estimated CoR positions relative to the scapula anatomical coordinate system (ACS). The MRE significantly overestimated the GH joint CoR in the anterior position (by 4 cm) compared to the IHA method and to the work of other research groups. The

MRE also estimated the GH joint CoR laterally to the scapula ACS although imaging studies identified GH joint CoR medially to the scapula ACS.

Trunk contribution to overall arm elevation was assessed between unilateral (UE) and bilateral (BE) arm elevations. BE was found to significantly decrease trunk lateral and axial rotation with respect to UE; however, trunk flexion was significantly greater. This in turn resulted in significantly different scapula rotations between UE and BE with up to 3° difference in scapula retraction during abduction between UE and BE. Consequently in shoulder complex biomechanics studies, particular attention should be made to minimise trunk rotations.

Shoulder function asymmetry was investigated between dominant and non-dominant shoulders. Significantly greater GH elevation and scapula lateral rotation were measured in dominant arms compared to non-dominant arms, with a difference of up to 7.6° and 7.0° respectively between the two arms. Asymmetry between the two shoulders could be attributed to soft tissue imbalance from more frequent use of the dominant shoulder compared to the non-dominant.

Physiological range of motion (during static and dynamic trials) and 15 activities of daily living (ADLs) were recorded with skin markers attached to bony landmarks as well as with the AMC (and the SL for physiological ROMs). Static and dynamic trials measured differences in thorax and scapula rotations which may have arisen from muscle stabilisation. Acromioclavicular (AC) and scapula lateral rotations were underestimated (by up to 8° and 20° respectively) using the skin fixed markers. Joint and segment rotations are comparable to published studies that follow ISB recommendations

The kinematics of patients with four different shoulder conditions (clavicle fracture, multidirectional instability, irreparable rotator cuff tear and GH dislocation) was measured. The effect and the extent of the IoP was investigated during physiological ROMs elevation and ADLs recordings by comparing their function to healthy and contralateral shoulders. The results from this study were used to develop a novel application for the Cardiff Dempster Shafer (DS) objective classifier. The classification tool was used to characterise shoulder complex function of 40 participants. Non injured or pathological (NloP) and IoP shoulder function was characterised with 72.5% accuracy. Eight patients were misclassified as having NloP shoulder function while two healthy participants were misclassified as having IoP function. A weak correlation between scoring questionnaires with the NloP and IoP classification indices was found (-0.16298 and 0.180187 respectively). This might be explained by the subjective nature of the scores.

The studies described in this thesis contributed towards advancements in shoulder complex kinematics studies at Cardiff University as well as with the international shoulder researcher's community. An appreciation was gained of the challenges faced when using MA and IRT to measure shoulder motion as well as a better understanding of joint function in healthy and IoP shoulders.

Acknowledgements

I would like to express my gratitude to the people that helped make my PhD an enriching and invaluable experience.

I am heartily thankful to my supervisor, Dr. Cathy Holt, whose encouragement, guidance and support from the initial to the final level enabled me to develop an enthusiasm for the subject. I am also thankful to my second supervisor, Dr. Sam Evans for his technical support and advice.

My appreciation goes to Mr. Richard Evans as well as his registrars and medical students. Their determination to continually improve the care of their patients is exceptional.

I would also like to sincerely thank Dr. Scott Banks and Shang Mu for their software, training and for making me feel so welcome during my time at the University of Florida.

I am very grateful to Dr. John Evans at CUBRIC for his support in the acquisition of the MRI scans. Thanks also to Rebecca Vaughan-Roberts at the University Hospital of Wales for the acquisition of the fluoroscopy images. And to Dr. Arnold Rust from the Radiation Protraction Service, for calculating a safe radiation dose.

A very special thanks goes out to Barry, Dan and Gemma. Without your continual help and support I would not have been able to complete this thesis. It was a pleasure working with you.

I am lucky to be surrounded by a supportive network of friends since being far away from home is not always easy. To my friends and colleagues in Cardiff, you became part of my family here. Thank you all for the good times we spent together, I hope we can share many more.

A mi Mama, Papa y Hermana, apesar de la distancia que nos separa, siempre hay un lugar que se llama hogar y esta donde quiera que se encuentren ustedes. Muchisimas gracias por el apoyo incondicional y por siempre exijirme a dar lo mejor de mi. Mis logros son gracias a ustedes.

Contents

Declaration of Authorship	i
Abstract	ii
Acknowledgements	iv
List of Figures	x
List of Tables	xiv
Abbreviations	xvi
Symbols	xviii
1 Introduction and literature review	1
1.1 Introduction	1
1.2 Literature Review	2
1.2.1 Anatomy of the shoulder complex	3
1.2.1.1 The sternoclavicular and acromioclavicular joints	3
1.2.1.2 The glenohumeral joint	4
1.2.1.3 The scapulothoracic articulation	5
1.2.1.4 Other shoulder complex relationships	6
1.2.1.5 Shoulder muscle activity and function	7
1.2.2 Measurement tools used to record shoulder motion	9
1.2.3 Measuring shoulder complex function	11
1.2.3.1 Challenges of measuring accurate shoulder kinematics	13
1.2.4 The Dempster-Shafer objective function classifier	19
1.3 Aim and objectives of the study	20
1.4 Hypothesis	21
1.5 Thesis summary	21
2 Measuring glenohumeral joint kinematics using model-based image registration techniques	23

2.1	Background	24
2.2	Development of image registration studies at Cardiff	28
2.3	Data collection protocol	29
2.3.1	Participants recruitment	29
2.3.2	Measuring systems	30
2.3.2.1	X-ray department at the University Hospital of Wales	30
2.3.2.2	Cardiff University Brain Repair Imaging Centre	34
2.4	Data handling protocol	35
2.4.1	Magnetic resonance imaging protocol	36
2.4.1.1	3D bone models generated from MRI scans	36
2.4.1.2	Humerus head sphere fitting	36
2.4.1.3	Changing the embedded axes systems on the 3D models	37
2.4.2	Fluoroscopy images handling protocol	39
2.4.2.1	Geometry correction	39
2.4.2.2	Geometry calibration	40
2.4.3	JointTack 3D to 2D image registration	41
2.5	Data analysis protocol	42
2.5.1	Glenohumeral joint kinematics	43
2.5.2	Scapula kinematics relative to JointTrack GCS	46
2.6	Methods	48
2.6.1	Measuring GH and scapula kinematics using image reg- istration	48
2.6.2	Comparison of image registration and motion analysis mea- surements	49
2.6.3	Repeatability	49
2.7	Results	50
2.7.1	Measuring GH and scapula kinematics using image reg- istration	50
2.7.2	Comparison of image registration and motion analysis mea- surements	56
2.7.3	Repeatability	58
2.8	Discussion and Conclusions	58
2.8.1	Measuring GH and scapula kinematics using image reg- istration techniques	59
2.8.2	Comparison of image registration and motion analysis mea- surements	60
2.8.3	Repeatability	64
2.9	Study limitations and recommendations for future work	65
3	The Cardiff protocol for measuring and calculating shoulder com- plex function	67
3.1	Healthy volunteers and patients recruitment	69
3.2	Measurement system	69

3.3	Data collection	71
3.3.1	System calibration	71
3.3.2	Informed consent	73
3.3.3	Shoulder outcome questionnaires	74
3.3.4	Anthropometric measurements	74
3.3.5	Marker placement	74
3.3.6	Neutral position measurement	77
3.3.7	Circumduction recording	77
3.3.8	Physiological range of motion	78
3.3.9	Activities of daily living	80
3.4	Data handling and analysis	82
3.4.1	Computing shoulder complex kinematics	82
3.4.2	The Global Coordinate System	86
3.4.3	Establishing anatomical coordinate systems on shoulder complex segments	86
3.4.3.1	Thorax anatomical coordinate system	87
3.4.3.2	Clavicle anatomical coordinate system	89
3.4.3.3	Scapula anatomical coordinate system	90
3.4.3.4	Humerus anatomical coordinate system	94
3.4.4	Shoulder complex rotations calculations	97
3.4.4.1	Thorax relative to GCS	97
3.4.4.2	The sternoclavicular joint	100
3.4.4.3	The acromioclavicular joint	101
3.4.4.4	The glenohumeral joint	103
3.4.4.5	The scapulothoracic articulation	106
3.4.4.6	Rotations of the humerus relative to the thorax .	108
3.4.5	Outputs	111
4	Measuring shoulder complex kinematics in healthy volunteers	112
4.1	Glenohumeral joint centre estimation using regression equations and a functional method	113
4.1.1	Method	115
4.1.2	Results	116
4.1.3	Discussion and Conclusions	116
4.2	Comparison between two different acromium marker clusters used to record scapula motion	119
4.2.1	Methods	120
4.2.2	Results	122
4.2.3	Discussion and Conclusions	123
4.3	The effect of unilateral and bilateral arm elevation on thorax and scapulothoracic articulation kinematics	125
4.3.1	Methods	126
4.3.2	Results	126
4.3.3	Discussion and Conclusions	127

4.3.3.1	Trunk rotations during arm elevation	128
4.3.3.2	Scapula rotations during arm elevation	129
4.4	Investigating shoulder function asymmetry in dominant and non-dominant arms	130
4.4.1	Methods	131
4.4.2	Results	131
4.4.3	Discussion and Conclusions	133
4.5	Shoulder complex kinematics during physiological ranges of motion and activities of daily living	134
4.5.1	Methods	134
4.5.2	Results	135
4.5.3	Discussion and Conclusions	141
4.5.3.1	Physiological ROM	141
4.5.3.2	Activities of Daily Living	143
4.6	Repeatability of bony landmark identification and scapula locator placement	144
4.6.1	Methods	145
4.6.2	Results	146
4.6.3	Discussion and Conclusions	148
4.7	Overall conclusions	149
5	Assessing shoulder complex kinematics in injured or pathological patients	151
5.1	Background	152
5.2	Analysis of shoulder patients' kinematics using motion capture techniques	153
5.2.1	Clavicle fracture patients	154
5.2.1.1	Methods	155
5.2.1.2	Results	156
5.2.1.3	Discussion and Conclusions	156
5.2.2	Glenohumeral joint instability patients	160
5.2.2.1	Multidirectional instability patients	161
5.2.2.2	Irreparable Rotator Cuff tear patients	166
5.2.2.3	GH joint dislocation patients	172
5.2.3	Activities of Daily Living	176
5.2.3.1	Methods	177
5.2.3.2	Results	177
5.2.3.3	Discussion and conclusions	180
5.3	Functional classification of shoulder complex data	182
5.3.1	The Dempster-Shafer classification method	183
5.3.1.1	Conversion of input variables into confidence factors	184
5.3.1.2	Conversion of confidence factors to BOE	185
5.3.1.3	Combination of individual BOE	185
5.3.1.4	Visualisation of BOE using simplex plots	186

5.3.1.5	Classification based on BOE_C	186
5.3.1.6	Classification accuracy and ranking of input variables	187
5.3.2	Novel application for the Cardiff DS classifier	187
5.3.2.1	Selecting input variables	188
5.3.2.2	Shoulder function classification	191
5.3.2.3	Comparing objective classification with subjective score measures	195
5.3.2.4	Discussion and Conclusions	196
5.4	Limitations	199
6	Conclusions and Further Work	201
6.1	Conclusions	201
6.2	Further work	210
A	Image registration information sheet and consent form	213
B	Image registration protocol	221
C	Motion analysis information pack and consent form	243
D	Complete healthy and patient shoulder complex kinematics description during physiological ROM	259
D.1	Clavicle fracture patients	260
D.2	Multiple directional instability patients	264
D.3	Irreparable rotator cuff tear patients	268
D.4	GH dislocation patients	272
E	Functional classification using different input variables	276
	References	279

List of Figures

1.1	The shoulder complex	3
1.2	Frontal section of the glenohumeral joint	4
1.3	The scapulothoracic articulation	6
1.4	Shoulder girdle muscles	8
2.1	Session at the X-ray department to estimate the study radiation dose	29
2.2	Qualisys camera layout for simultaneous fluoroscopic and Motion Analysis recordings	31
2.3	Calibration of the Portable Qualisys camera system in the fluoroscopy screening room	32
2.4	Calibration frame used to undistort fluoroscopy images	33
2.5	Simultaneous fluoroscopy and motion analysis recordings	33
2.6	Shoulder MRI data collection in CUBRIC	34
2.7	MRI scans of the shoulder	35
2.8	Flow diagram of the data handling protocol to perform 3D to 2D image registration	35
2.9	Segmenting the humerus and scapula to create 3D bone models	36
2.10	3D fine model of the scapula (a) prior to applying a smoothing filter and (b) after smoothing filter	37
2.11	Fitting a sphere on the humerus head. The position of the sphere centroid is known.	37
2.12	Scapula anatomical coordinate system for IRT	38
2.13	Humerus anatomical coordinate system for IRT	39
2.14	Schematic representation of (a) the magnification distortion and (b) correction of fluoroscopic images	39
2.15	Fluoroscopic image of control points in the calibration frame	40
2.16	Calibration grid of control points	40
2.17	Star shaped distribution of control points	41
2.18	JointTrack registration	42
2.19	Canny edge detection	42
2.20	Registered models onto fluoroscopic images using JointTrack	43
2.21	Two dimensional illustration of glenohumeral elevation	44
2.22	Two dimensional illustration of glenohumeral plane of elevation	45
2.23	Two dimensional illustration of glenohumeral axial rotation	45
2.24	Two dimensional illustration of scapula retraction	46

2.25	Two dimensional illustration of scapula lateral rotation	47
2.26	Two dimensional illustration of scapula anterior tilt	48
2.27	Average GH joint kinematics during abduction calculated using IRT	51
2.28	Average GH joint kinematics during scaption calculated using IRT	52
2.29	Average GH joint kinematics axial rotation calculated using IRT .	53
2.30	Average scapula kinematics during abduction calculated using IRT	54
2.31	Average scapula kinematics during scaption calculated using IRT	54
2.32	Average scapula kinematics during axial rotation calculated using IRT	55
2.33	Assessing MRI model registration repeatability	58
3.1	Camera layout for shoulder complex studies	70
3.2	Summary of the motion analysis data collection protocol	72
3.3	Qualisys calibration kit	72
3.4	Laboratory set up for wand calibration	73
3.5	Marker placement according to ISB recommendations	75
3.6	A schematic of the scapula locator	76
3.7	A schematic of the acromium marker cluster	76
3.8	Neutral position measurement	77
3.9	Circumduction recording	78
3.10	Illustration of arm elevation in abduction, scaption and flexion . .	79
3.11	Posterior view of participant's positioning and measurement frame for static trials.	79
3.12	Activities of daily living	81
3.13	Defining a segment's position (a) location and (b) orientation . .	83
3.14	Summary of motion analysis data handling and analysis protocol	85
3.15	Thorax anatomical coordinate system	87
3.16	Pointer local coordinate system	88
3.17	Thorax technical coordinate system for PX landmark calibration .	89
3.18	Clavicle anatomical coordinate system	90
3.19	Scapula recording methods	91
3.20	Scapula anatomical coordinate system	91
3.21	Scapula locator local coordinate system	92
3.22	Acromium marker cluster local coordinate system	93
3.23	Humerus marker cluster local coordinate system	94
3.24	3D transformation matrix	95
3.25	Humerus anatomical coordinate system	96
3.26	Two dimensional illustration of thorax flexion	98
3.27	Two dimensional illustration of thorax right lateral rotation	99
3.28	Two dimensional illustration of thorax right axial rotation	99
3.29	Two dimensional illustration of sternoclavicular protraction	100
3.30	Two dimensional illustration of sternoclavicular elevation	101
3.31	Two dimensional illustration of acromioclavicular protraction . . .	102
3.32	Two dimensional illustration of acromioclavicular lateral rotation .	103

3.33	Two dimensional illustration of acromioclavicular anterior tilt	104
3.34	Two dimensional illustration of glenohumeral plane of elevation	104
3.35	Two dimensional illustration of glenohumeral depression	105
3.36	Two dimensional illustration of glenohumeral axial rotation	106
3.37	Two dimensional illustration of scapulothoracic protraction	107
3.38	Two dimensional illustration of scapulothoracic lateral rotation	107
3.39	Two dimensional illustration of scapulothoracic anterior tilt	108
3.40	Two dimensional illustration of humerothoracic plane of elevation	109
3.41	Two dimensional illustration of humerothoracic depression	110
3.42	Two dimensional illustration of humerothoracic axial rotation	110
4.1	Measurements recorded for GH estimation	115
4.2	Scapula ACS position and orientation	116
4.3	Average GH joint position in Scapula ACS axes	117
4.4	Two different AMCs	120
4.5	Average ST articulation kinematics measured with AMC1 and AMC2 as well as with the SL	122
4.6	Complete shoulder complex kinematics during abduction	136
4.7	Complete shoulder complex kinematics during scaption	137
4.8	Complete shoulder complex kinematics during flexion	138
5.1	Average healthy participants and clavicle fracture patients' injured and contralateral (a) sternoclavicular and (b) acromioclavicular kinematics during abduction	157
5.2	Average healthy participants and clavicle fracture patients' injured and contralateral (a) sternoclavicular and (b) acromioclavicular kinematics during scaption	157
5.3	Average healthy participants and clavicle fracture patients' injured and contralateral (a) sternoclavicular and (b) acromioclavicular kinematics during flexion	158
5.4	Average healthy and MDI patients' injured and contralateral (a) glenohumeral and (b) scapulothoracic kinematics during abduction	163
5.5	Average healthy and MDI patients injured and contralateral (a) glenohumeral and (b) scapulothoracic kinematics during scaption	164
5.6	Average healthy and MDI patients' injured and contralateral (a) glenohumeral and (b) scapulothoracic kinematics during flexion	164
5.7	Average healthy and IRCT patients' injured and contralateral (a) glenohumeral and (b) scapulothoracic kinematics during abduction	168
5.8	Average healthy and IRCT patients' injured and contralateral (a) glenohumeral and (b) scapulothoracic kinematics during scaption	169
5.9	Average healthy and IRCT patients' injured and contralateral (a) glenohumeral and (b) scapulothoracic kinematics during flexion	169
5.10	Average healthy and GH dislocation patients' injured and contralateral (a) glenohumeral and (b) scapulothoracic kinematics during abduction	173

5.11 Average healthy and GH dislocation patients' injured and contralateral (a) glenohumeral and (b) scapulothoracic kinematics during scaption	174
5.12 Average healthy and GH dislocation patients' injured and contralateral (a) glenohumeral and (b) scapulothoracic kinematics during flexion	175
5.13 DS classification stages	184
5.14 Visualising DS objective classification using simplex plots	186
5.15 Simplex plot participants' shoulder classification using 21 input variables	190
5.16 Simplex plot participants' shoulder classification using 10 input variables	191
5.17 Simplex plot showing the simplex coordinate representation of the BOE_C for all study participants	194
6.1 AnyBody upper limb musculoskeletal model	212
D.1 Complete healthy and clavicle fracture patient shoulder complex kinematics during abduction	260
D.2 Complete healthy and clavicle fracture patient shoulder complex kinematics during scaption	261
D.3 Complete healthy and clavicle fracture patient shoulder complex kinematics during flexion	262
D.4 Complete healthy and MDI patient shoulder complex kinematics during abduction	264
D.5 Complete healthy and MDI patient shoulder complex kinematics during scaption	265
D.6 Complete healthy and MDI patient shoulder complex kinematics during flexion	266
D.7 Complete healthy and IRCT patient shoulder complex kinematics during abduction	268
D.8 Complete healthy and IRCT patient shoulder complex kinematics during scaption	269
D.9 Complete healthy and IRCT patient shoulder complex kinematics during flexion	270
D.10 Complete healthy and GH dislocation patient shoulder complex kinematics during abduction	272
D.11 Complete healthy and GH dislocation patient shoulder complex kinematics during scaption	273
D.12 Complete healthy and GH dislocation patient shoulder complex kinematics during flexion	274
E.1 Simplex plot showing the simplex coordinate representation of the BOE_C for all study participants using different input variables	278

List of Tables

1.1	Shoulder girdle muscles and individual functions	8
2.1	Recent studies that employ model based 3D to 2D IRT to measure shoulder function	27
2.2	QTM workspace configuration for MA recordings fluoroscopy screening room.	30
2.3	Fluoroscope settings for glenohumeral joint screening	32
2.4	MRI settings for shoulder scans	35
2.5	Shoulder kinematics measured with the MA system and with IRT during abduction	56
2.6	Shoulder kinematics measured with the MA system and with IRT during scaption	56
2.7	Shoulder kinematics measured with the MA system and with IRT during axial rotation	57
3.1	Workspace configuration	71
3.2	Marker placement according to ISB recommendations	75
3.3	Activities of daily living	80
3.4	Euler and Cardan angle sequence of rotations	97
4.1	Arm elevation angle for which significant differences between AMC and SL recordings were first measured	123
4.2	Unilateral and bilateral arm elevation kinematics during abduction	127
4.3	Unilateral and bilateral arm elevation kinematics during flexion .	127
4.4	Joint and segment rotations ROM and SD for dominant and non-dominant shoulders during abduction, scaption and flexion	132
4.5	Investigating significant differences between recording protocols	139
4.6	Average shoulder complex ROM and SD during ADL	140
4.7	Intra-class and inter-class variation of shoulder complex kinematics	147
5.1	ANOVA <i>p</i> values associated with SC and AC joint kinematics of healthy and clavicle fracture patients' injured and CL shoulders during physiological ROM	158
5.2	ANOVA <i>p</i> values associated with GH joint and ST articulation kinematics of healthy and MDI patients' injured and contralateral shoulders during physiological ROM	165

5.3	ANOVA p values associated with GH joint and ST articulation kinematics of healthy and IRCT patients' injured and contralateral shoulders during physiological ROM	170
5.4	ANOVA p values associated with GH joint and ST articulation kinematics of healthy and GH dislocation patients' injured and contralateral shoulders during physiological ROM	175
5.5	Average patients' injured or pathological shoulder complex ROM and SD during ADLs	178
5.6	Average patients' contralateral shoulder complex ROM and SD during ADLs	179
5.7	Summary of the input variables used to explore for classification	189
5.8	Ranking of input variables used in the classification	190
5.9	BOE _C values for the study participants	192
5.10	Ranking of input variables used in the classification	195
5.11	Correlation between objective classification and subjective score measures	196
D.1	Differences between healthy and clavicle fracture patient shoulder complex kinematics during physiological ROM	263
D.2	Differences between healthy and MDI patient shoulder complex kinematics during physiological ROM	267
D.3	Differences between healthy and IRCT patient shoulder complex kinematics during physiological ROM	271
D.4	Differences between healthy and GH dislocation patient shoulder complex kinematics during physiological ROM	275
E.1	Classification trials	277

Abbreviations

2D/3D	2 dimensional / 3 dimensional
AC	Acromioclavicular
ACS	Anatomical coordinate system
ADL	Activity of daily living
AMC	Acromium marker cluster
ANOVA	Analysis of Variance
BE	Bilateral elevation
BMI	Body mass index
BOE	Body of evidence
BOE _C	Combined body of evidence
CAD	Computer-aided design
CoR	Centre of rotation
CT	Computed Tomography
CUBRIC	Cardiff University Brain Research Imaging Centre
DOF	Degrees of freedom
DS	Dempster-Shafer
DST	Dempster-Shafer theory
FHA	Finite helical axis
GCS	Global coordinate system
GH	Glenohumeral
HMC	Humerus marker cluster
HT	Humerothoracic
ICC	Intraclass correlation coefficient
IHA	Instantaneous helical axis

IoP	Injured or pathological
IRCT	Irreparable rotator cuff tear
IRT	Image Registration technique
ISB	International Society of Biomechanics
ISG	International Shoulder Group
LCS	Local coordinate system
LOO	Leave-one-out
MA	Motion Analysis
MDI	Multidirectional instability
MRE	Meskers' regression equations
MRI	Magnetic resonance imaging
NIoP	Non injured or pathological
NP	Neutral Position
OA	Osteoarthritic
OB	Objective function
OSIS	Oxford Shoulder Instability Score
OSS	Oxford Shoulder Score
PLCS	Pointer local coordinate system
QTM	Qualisys Track Manager
RC	Rotator cuff
RCT	Rotator cuff tear
ROM	Range of motion
SC	Sternoclavicular
SCoRE	Symmetrical Centre of Rotation Estimation
SD	Standard deviation
SHR	Scapulohumeral rhythm
SL	Scapula locator
ST	Scapulothoracic
TCS	Technical coordinate system
TKR	Total knee replacement
UE	Unilateral elevation

Symbols

P_p	The PLCS coordinates of the pointer's point
T_{pg}	Transformation matrix relating orientation of the PLCS in the GCS
T_{ag}	Transformation matrix relating orientation of the ACS in the GCS
T_{ma}	Transformation matrix relating the orientation of the MCLCS in the ACS
T_{gm}	Transformation matrix relating orientation of the GCS in the thorax TCS
T_{ma}	Transformation matrix relating the orientation of the MCLCS in the ACS
T_{am}	Inverse of the matrix T_{ma}
L	Position vector
R	Rotation matrix
α_{TG}	Thorax flexion-extension angle
β_{TG}	Thorax lateral rotation angle
γ_{TG}	Thorax axial rotation angle
α_{SC}	SC protraction-retraction angle
β_{SC}	SC elevation-depression angle
α_{AC}	AC protraction-retraction angle
β_{AC}	AC medial-lateral rotation
γ_{AC}	AC anterior-posterior tilt
α_{GH}	GH plane of elevation
β_{GH}	GH elevation
γ_{GH}	GH axial rotation
α_{ST}	ST retraction-protraction angle
β_{ST}	ST medial-lateral angle
γ_{ST}	ST anterior-posterior tilt

α_{HT}	Humerothoracic plane of elevation
β_{HT}	Humerothoracic elevation
γ_{HT}	Humerothoracic axial rotation
ω	Angular velocity
v	Input variable
$cf(v)$	Confidence factor
$m_c(\{IoP\})$	Belief in the subject's joint function being IoP
$m_c(\{NIoP\})$	Belief in the subject's joint function being NIoP
$m_c(\Theta)$	Belief in either the subject's joint function being IoP or NIoP

Chapter 1

Introduction and literature review

1.1 Introduction

The shoulder is highly susceptible to musculoskeletal injury and pathology due to the lack of inherent stability provided by the articulating segments and its wide range of motion (ROM). It is likely that the reader has a family member, friend or colleague that has suffered from a dislocation or has disability and pain in the shoulder. As a result, there has been an increase in interest to better understand joint injury and disease to help prevent them as well as to improve treatment, evaluate surgical outcome and enhance rehabilitation regimes .

Accurate descriptions of the motions occurring at each joint of the shoulder complex are necessary to assess shoulder function. Valuable insight into healthy and injured or pathological (IoP) shoulder musculoskeletal function is gained by analysing three dimensional (3D) joint complex kinematics. These biomechanical measurements are essential for the understanding and evaluation of the joint complex. They provide knowledge of how the bony structures interact to maintain stability within the joint; of the mechanisms which lead to IoP as well as give an indication of the extent of the condition.

Shoulder complex function is commonly investigated using Motion Analysis (MA) systems. MA is a highly sensitive, non-invasive and objective technique in which motion can be assessed. Measuring shoulder function is challenging and its complexity becomes apparent as soon as one considers the following: firstly, shoulder motion is the result of the intricate interaction of four segments; this results in the greatest ROM as compared to any other joint complex in the human body. Secondly, movement is not cyclic and is much more unpredictable as compared, for example, to the lower limbs; furthermore, there is no one single way of performing a motor task. Finally, soft tissue surrounding the joint complex complicates the reliability of the measurements.

This thesis is devoted to increasing the understanding of shoulder complex kinematics, contributing to improving MA measuring techniques employed at Cardiff University and hence to a better understanding of the shoulder complex function.

1.2 Literature Review

The motion at the shoulder joint is a result of the independent yet simultaneous contributions of the four articulations that make up the shoulder complex. Similar to lower limb gait analysis, shoulder function analysis is performed to aid in the treatment of individual patients, to monitor the results of medical treatment, and to improve the understanding of the elaborate motions of the joint complex by analysing the separate components needed to achieve any one position.

A basic anatomy description of the joints that make up the shoulder complex, as well as the muscles that contribute to shoulder movement and stability is given below.

1.2.1 Anatomy of the shoulder complex

The shoulder complex is the upper limb's first mechanical chain which connects the arm to the trunk. Four bony structures make up the shoulder kinematic chain: the sternum, the clavicle, the scapula and the proximal end of the humerus. The relations between the bone segments form four articulations: the sternoclavicular (SC) joint, the acromioclavicular (AC) joint, the glenohumeral (GH) joint and the scapulothoracic (ST) articulation, shown in Figure 1.1. The shoulder functions together with the elbow and the wrist for the positioning of the hand in space. Its complex construction provides “a unique mobility that surpasses the mobility of any other joint in the body” [1].

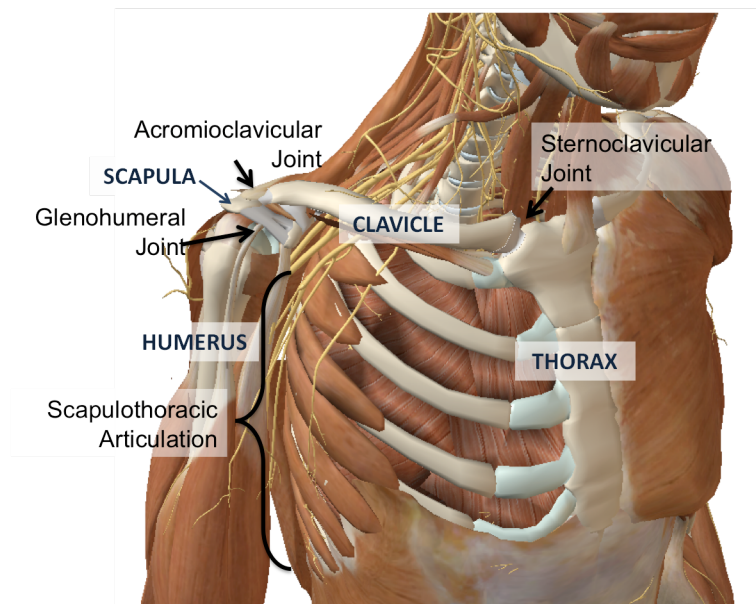


FIGURE 1.1: The shoulder complex, comprising of the sternoclavicular joint, the acromioclavicular joint, the glenohumeral joint and the scapulothoracic articulation. Adapted from [2]

1.2.1.1 The sternoclavicular and acromioclavicular joints

The SC joint is a small synovial articulation between the medial end of the clavicle and the manubrium of the sternum. It is the only bony connection between the upper extremity and the trunk. A meniscus lies between the two bony

surfaces, dividing the joint into two functional units for gliding, where anteroposterior gliding takes place between the sternum and the meniscus, and superior inferior gliding takes place between the clavicle and the meniscus [3].

The AC joint is a small synovial joint between the medial surface of the acromion and lateral end of the clavicle. A dense fibrous capsule surrounds the joint, which includes the superior and inferior acromioclavicular ligaments [4]. The anatomical joint stability is provided by the two components of the coracoclavicular ligament, the conoid and the trapezoid.

1.2.1.2 The glenohumeral joint

The GH joint is a synovial ball and socket articulation between the humerus head and the glenoid fossa of the scapula (Figure 1.2). The humerus head has the shape of half a sphere and it projects medially and slightly superiorly to articulate with the much smaller glenoid cavity [3]. The surfaces are quite congruent, with a radii within a 3mm difference [1]. Both surfaces are covered with hyaline cartilage and the glenoid is deepened and expanded peripherally by the glenoid labrum [3].

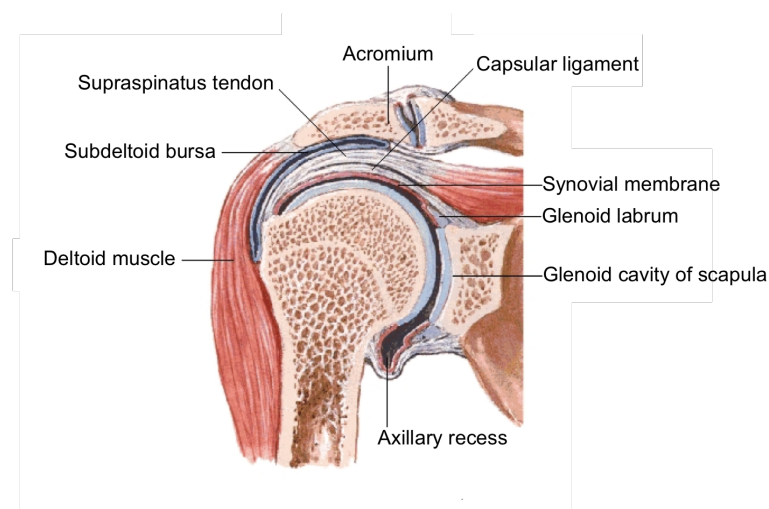


FIGURE 1.2: Frontal section of the glenohumeral joint. Adapted from [5]

The GH joint is commonly described as a “beach ball balancing on seal’s nose” [6] or a “golf ball on a tee” [7] referring to the lack of inherent stability provided by

the bony structures. Its anatomical joint configuration yields significant freedom of movement of the humerus head: the glenoid has a radius of curvature less than half that of the humeral head, and covers only about 25 to 33% of the humeral head [7].

Minimal coupled translation does accompany all GH joint rotation, even in normal or healthy shoulders [8]. This wide range of motion exposes the joint to skeletal instability, with recurrent subluxation and dislocation commonly observed.

Stability in the GH joint

Stability of the GH joint is dependent on both static and dynamic stabilisers. Static stability is achieved by the integrated function of:

- The bony architecture
- The labrum
- The joint capsule
- The GH ligaments
- Internal negative pressure gradient

On the other hand, the rotator cuff tendon provides dynamic stability. The rotator cuff muscles are the supraspinatus, infraspinatus, teres minor and subscapularis muscles. Their function is summarised in Subsection 1.2.1.5.

1.2.1.3 The scapulothoracic articulation

The ST articulation is a bone-muscle-bone articulation that is not synovial. The two bone segments (the scapula and the thorax) are separated by the subscapularis and serratus muscles (Figure 1.3), which glide over each other during motion. Since the scapula has no bony or ligamentous connection to the

thorax apart from its attachment through the AC joint, a wide range of scapular motion is possible [4].

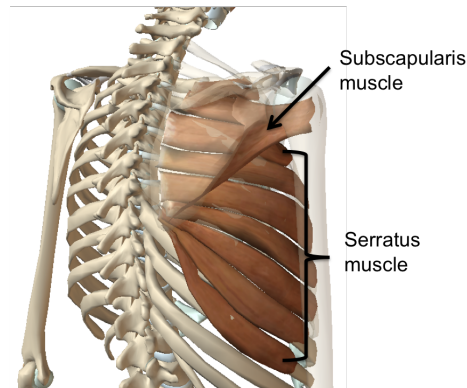


FIGURE 1.3: The scapulothoracic articulation. Adapted from [2]

ST motion is essential for normal shoulder complex function. Its motion specifically influences GH joint stability as well as the size of the subacromial space [9]. Altered ST kinematics are referred to as scapular dyskinesis; with altered muscle activation or coordination the most commonly proposed causes [9].

1.2.1.4 Other shoulder complex relationships

A further two relationships between segments of the shoulder complex are commonly identified: humerothoracic (HT) motion and the scapulohumeral rhythm (SHR).

Humerothoracic motion

HT motion is the movement of the humerus relative to the thorax. Motion is generally described as abduction-adduction, flexion-extension and axial rotation. Elevation of the arm is considered the movement of the arm away from the thorax in any plane; where flexion is elevation in the sagittal plane, scaption is elevation in the scapula plane and abduction is elevation in the frontal plane. Scaption is considered the most clinically meaningful out of the three elevation planes, since elevation in the scapula plane “does not deform the inferior GH

joint capsule and the deltoid and supraspinatus muscles are optimally aligned for elevation of the arm” [10].

Scapulohumeral rhythm

The coordinated humerus and scapula motions is termed the SHR and their kinematic relationship has been researched extensively [11–17]. Arm elevation at the GH joint is accompanied by ST movement, an arrangement that according to Inman et al “enhances the power of the attendant muscles” [11]. Inman et al first described the SHR as the relationship between GH elevation and ST lateral rotation. They measured a 2:1 GH joint to ST articulation movement ratio during arm abduction [11]. Many researchers have since expanded Inman’s original description to also include scapula protraction-retraction and anterior-posterior tilt [17–19].

1.2.1.5 Shoulder muscle activity and function

The coordinated activation of the muscles of the shoulder have an essential role in ensuring the simultaneous mobility whilst maintaining stability at the joint complex. Their contribution is essential due to a lack of bony stability provided by the shallow glenoid cavity. The muscles involved in shoulder movement and stability are illustrated in Figure 1.4 and their individual contributions are summarised in Table 1.1.

A comprehensive review of the literature was performed. It is not surprising that there is no single method of analysis and numerous methodologies using various techniques have been developed. The next section of this Chapter provides an overview of methodologies and studies that have assessed shoulder complex function. A mathematical tool developed for the functional classification of joint function based on MA data is also described.

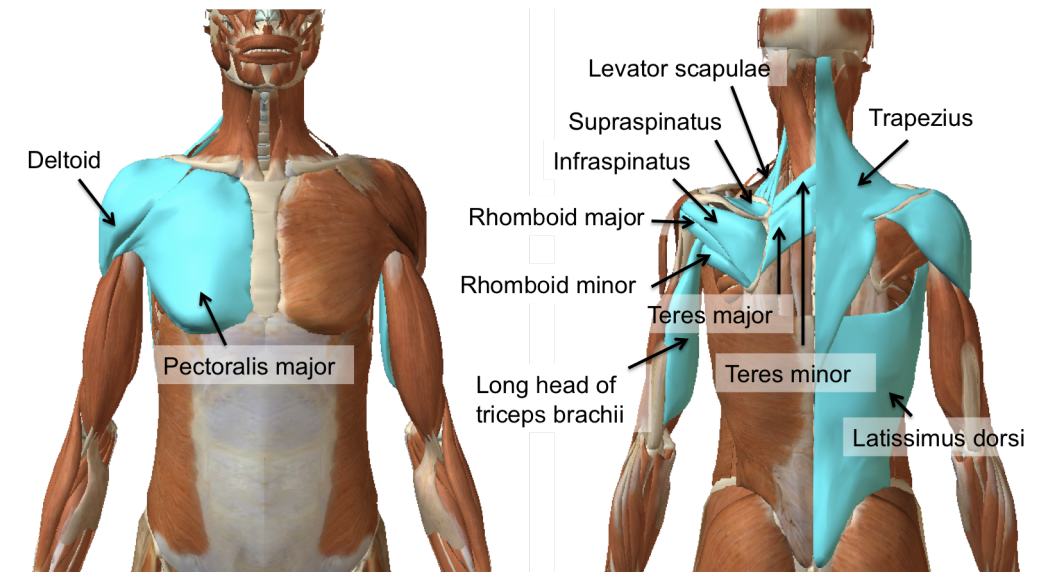


FIGURE 1.4: Shoulder girdle muscles (a) anterior view and (b) posterior view. Adapted from [2]

TABLE 1.1: Shoulder girdle muscles and functions. Reproduced from [3]

Muscle	Function
Trapezius	Powerful elevator of the scapula; rotates the scapula during abduction of humerus above horizontal; middle fibres retract the scapula; lower fibres depress scapula
Deltoid	Major abductor of arm (abducts arm beyond initial 15° done by supraspinatus); clavicular fibres assist in flexing the arm; posterior fibres assist in extending the arm
Levator scapulae	Elevates the scapula
Rhomboid minor and major	Elevates and retracts the scapula
Supraspinatus	Rotator cuff muscle (GH stabiliser); initiation of abduction of arm to 15° at GH joint
Infraspinatus and teres minor	Rotator cuff muscles (GH stabilisers); lateral rotation of arm at GH joint
Subscapularis	Rotator cuff muscle (GH stabilisers); internally rotates the humerus
Teres major	Internal rotation and extension of the arm at the GH joint
Long head of triceps brachii	Extension of the forearm at the elbow joint; accessory adductor and extensor of the arm at the GH joint

The review is intentionally brief as each subsequent Chapter contains an associated theoretical background with appropriate references to the relevant literature.

1.2.2 Measurement tools used to record shoulder motion

Questionnaires are commonly used to assess treatment outcome [20]. A score is assigned to an individual based upon patient perceptions of pain, function and overall satisfaction [21, 22]. The assessment is highly subjective, resulting in an often incomplete evaluation of a patient's progress [23]. Consequently, objective assessment methods have been developed over the decades to obtain complete information of a patient's condition as well as to better understand the contribution of the individual segments to overall arm positioning.

Two dimensional (2D) roentgenogram and radiograph systems have been used to analyse shoulder complex kinematics [11, 24]. Although highly reproducible kinematics have been measured with such systems [8], planar motion cannot fully address the complex 3D motions of the shoulder. Furthermore, measurements can only be taken statically whereas shoulder complex movements are, in their majority, dynamic.

Electromagnetic systems have been extensively used to measure *in vivo*, non-invasive shoulder complex kinematics [13, 25–28] in a relatively fast and easy manner with little restriction to motion. An electromagnetic field is set up around a source. The segments' 3D positions and orientations are recorded by firmly attaching sensors on meaningful locations on the body. Subsequently, bony landmarks are identified and related to the sensors for the kinematics analysis. Metal interference (from for example structural metal in the laboratory) reduces the accuracy and increases the variability of data collected with the electromagnetic devices [29] since it distorts the electromagnetic field.

Optoelectronic measuring systems are also used to collect *in vivo*, non-invasive 3D kinematics data [30–36]. Three or more retro-reflective markers are attached to the skin surface on meaningful locations on the body segments of interest. As the subject performs a motor task, the marker trajectories are recorded using infrared light emitting cameras. The position and orientation

of the segments can be obtained from the marker recordings using vector analysis. However, when a marker becomes occluded in the field of view of the cameras, for example as a result of body interposition, the kinematics data for the period where the markers is missing cannot be computed.

Electromagnetic and optoelectronic systems are subject to common measurement errors. Perhaps the biggest source of error is due to skin movement artefact [37]. The electromagnetic sensors and the retro-reflective markers attempt to measure the kinematics of the bones of the human body; however, they are fixed onto the skin. Relative movement between the skin and the underlying bone significantly affects the accuracy of the measurements. Furthermore, miss identification of the bony landmarks required to perform the kinematics analysis introduces additional errors to the measurements. Despite the challenges, high levels of agreement between electromagnetic and optoelectronic systems have been reached (mean difference between both systems did not exceed 2°), suggesting measurements obtained from either system are clinically comparable [38].

Magnetic resonance imaging (MRI) and computer tomography (CT) can be used to collect shoulder kinematics data [39–42]. Bone segments are reconstructed in 3D and their position and orientation relative to other segments can be calculated at different arm elevations. GH joint translations have been recorded using these 3D techniques [40]. However, due to the nature of the measuring systems, only static positions can be recorded.

3D to 2D image registration techniques (IRT) were originally developed to measure natural knee and total knee replacement kinematics [43–47]. More recently, the technique has been used to measure shoulder complex kinematics [15, 48–52]. 3D bone models, created from MRI or CT scans, are registered onto fluoroscopic images taken during dynamic arm movements. The silhouette of the bone models is manually adjusted to match its silhouette in the fluoroscopy images to obtain a kinematics description of the GH joint. Researchers have reported an accuracy in recordings of approximately 1° for rotations and

within 0.5mm sagittal plane translations [15, 50]. Although accurate measurements are recorded, the IRT requires participant exposure to ionising radiation; limiting measurement times.

Some measurement techniques are more appropriate than others, with all of them having merits and disadvantages. Therefore, the technique employed to record and measure shoulder complex kinematics is dependent on the variable being investigated.

1.2.3 Measuring shoulder complex function

Arm elevation is the movement of the arm away from the thorax, with elevation in the plane of the scapula (referred to as scaption) considered as the most efficient type of elevation [53]. The deltoid and rotator cuff (RC) muscles are optimally aligned on this plane and the inferior joint capsule has an untwisted configuration [10, 54]. However, shoulder kinematics during abduction and flexion are also commonly investigated and reported.

The interaction of the segments that make up the shoulder result in the largest ROM achieved by any joint complex in the human body. GH joint and ST articulation motions account for the majority of shoulder ROM while the SC and AC joint rotations aid in the positioning and motion of the ST articulation.

Few studies have investigated the coupled rotations of the scapula and clavicle dynamically since it is difficult to track clavicle axial rotation *in vivo* without the use of non-invasive techniques [55]. Optimisation algorithms provide a method to estimate clavicle axial rotation [56, 57]. Motion of the shoulder is represented in a closed loop mechanism in which the motion at the SC and AC joints are coupled [57] with the costoclavicular and the coracoclavicular ligaments limiting the SC and AC motions respectively. Pronk et al [58] found that, by optimising clavicle axial rotation, AC rotations were reduced from over 40° lateral rotation and posterior tilting, to less than 10°.

The GH joint is mainly responsible for the first 40 to 50° of arm elevation, during which the scapula is a supportive base [19, 27]. Beyond this initial stage, the movement of the arm is mainly due to GH and ST elevations. During arm elevation, the humerus moves around a mobile scapula. If the shoulder girdle were to remain fixed, the humerus would not be elevated more than 120° [1]. If scapula movement and position is altered, this normal pattern of integrated movement is expected to be affected [59].

The GH joint has six degrees of freedom (DOF), namely three rotations and three translations. In the healthy population, translations are usually neglected due to their small magnitude (in the order of 1–2mm [40, 60]). However, unstable shoulders may demonstrate a dysfunction of the GH translation behaviour [61], with up to 16mm anterior translations in GH joint instability patients [62]. Excessive superior humeral translation has also been reported in patients with rotator cuff tears (RCT) [8, 63]. GH joint translations may lead to dislocations and subluxations that in turn may result in the onset of osteoarthritis (OA) of the joint due to cartilage degeneration [64].

Several studies have investigated (atypical) scapula kinematics and its relationship with shoulder dysfunction since abnormal scapula kinematics is commonly measured in patients with disability. Compensatory ST strategies for GH weakness or motion loss have been observed in patients with frozen shoulder [25, 65] while patients with OA in the GH joint or frozen shoulder present an increased scapula lateral rotation [66, 67]. Scapula winging is a common shoulder disorder and may be indicative of neuromuscular, musculoskeletal and/or structural damage [68, 69].

Alterations in GH joint or scapula kinematics affects the SHR. Altered SHR may be indicative of impingement syndrome, GH instability, frozen shoulder, OA, amongst others [25, 67, 70, 71]; with the degree of abnormality correlated with the severity of shoulder ROM restriction [67].

Quantifying upper extremity movements during activities of daily living (ADL) is challenging because of the high DOF, coordinated movement from multiple

joints and between trial and between individual variability in the execution of the task [72], with Klopkar et al measuring 5° and 20° variability respectively in healthy participants [33]. Furthermore, there are no standardised activities described for the upper extremity. Over 20 ADLs have been recorded by various shoulder complex researchers. It would be difficult to measure only a small number of ADLs on all patient groups since pathology and injury may affect different joints. Standardising activities, even though highly desirable for ease in data collection and analysis, would seem to be highly unlikely. However, a standardised set of activities could be proposed for each shoulder condition.

The variety of different data collection and analysis protocols between different research groups makes comparison of results difficult. As a result, the International Society of Biomechanics (ISB) suggested recommendations when analysing the motion of the upper limb [73]. The aim was to encourage communication between researchers by providing guidelines as to how to best measure shoulder function, so that measurements taken by different research groups could be comparable.

1.2.3.1 Challenges of measuring accurate shoulder kinematics

Due to the shoulder's complicated anatomy and large ROM, measuring dynamic, *in vivo* shoulder joint kinematics is challenging [74]. The main challenges faced by researchers will now be discussed.

Glenohumeral joint rotation estimation

For the kinematics analysis of human motion using vector analysis, three non-collinear landmarks must be identified on each segment to create an anatomical coordinate system (ACS). Only two landmarks can be identified on the humerus by means of palpation, the medial and lateral epicondyles. The third landmark, the GH joint centre of rotation (CoR), must be estimated. This virtual landmark

can be estimated through a number of different techniques. They include regression equations based on the participant's anatomy and functional methods [75–77] which estimate the CoR from the relative motion of the humerus and scapula.

Regression equations were first developed by Meskers et al to establish a relationship between scapula geometry and the position of the GH joint CoR (in a cadaveric study) [78]. The predictive method requires the identification of five scapula landmarks used in three regression equations. To develop the equations, they constructed spheres to fit the glenoid and humeral head by using around 40 data points on the surface of the glenoid and humeral head. The centre of the sphere sitting on the glenoid was considered the CoR. Recently, Campbell et al developed and validated a new regression model for GH joint CoR estimation [79, 80] using six distances between different anatomical landmarks as well as the subject's height and weight. However, the GH joint CoR estimation by means of regression equations is affected by errors from landmark calibration and the regression uncertainty [75].

Sphere fitting has also been used to estimate the GH joint CoR [60, 74, 77]. The technique consists in fitting a sphere on 3D models of the humerus head reconstructed from either MRI or CT scans. The centre of the sphere is taken as the GH joint CoR. Stockdijk et al reported high reliability using the current method [77]. However, they found the method too time consuming to be practical for large patient cohorts.

Functional methods for estimating subject specific joint CoR have increased in popularity in clinical and research laboratories [75, 77, 81, 82]. Amongst the functional methods, the instantaneous helical axes (IHA) method, based on the work by Woltring et al [83–85], is used and recommended by the ISB [73]. The method is based on Chasles' theorem, which proposes that any general motion can be represented as “the sum of translations along and rotations around the helical axis in any sequence”. Position vectors of the IHA are determined through a motion pattern. The GH joint CoR is calculated as the optimum pivot

point of all position vectors [76, 77]. Functional methods are considered more accurate than landmark-based methods [77, 86]. Nevertheless, the IHA method is very sensitive to low angular velocities [75, 77, 83].

Recently, Monnet et al validated the use of the Symmetrical Centre of Rotation Estimation (SCoRE) method to estimate the GH joint rotation centre *in vivo* [75]. As well as being a more precise method for estimating GH than IHA, SCoRE was also able to locate GH even at slow velocities, contrary to the IHA.

For normal GH joint kinematics, the previously discussed methods could be used to estimate the GH CoR since the joint acts as a ball-and-socket joint with a fixed rotation centre [63]. However, abnormal kinematics due to instability caused by structural damage, alter joint behaviour, and translations in the joint are observed [49, 87–89]. When this is the case, the methods outlined above should not be used since they introduce errors to the calculations. Instead, the finite helical axes method (FHA) should be adopted [76]; where helical axes are estimated from single finite displacements [83].

Skin movement artefact and scapula kinematics measurements

Two assumptions are employed during human MA: firstly, there is no relative movement between the skin and the underlying bone segment to which the retro-reflective markers are attached; and secondly, the body is treated as a rigid body [1].

As highlighted previously, a major concern associated with skin fixed marker based MA is the error introduced due to skin movement artefacts [37, 90–92]. This error is the result of the movement between the marker, attached to the skin, and the underlying bone. It is mostly associated with “the interposition of both passive and active soft tissues” [92]. Significantly overestimated or underestimated joint angles and translations are recorded when these errors affect the measurements. The extent of skin artefact errors is magnified in upper limb kinematics studies due to the wide ROM of the upper arm [37, 93].

A typical example of erroneous measurements as a result of skin movement artefact is that of the scapula. Its motion presents a significant challenge to quantifying the biomechanical function of the shoulder complex *in vivo* as a large amount of bony movement occurs under the skin [17, 18, 94], with Meskers et al estimating errors in lateral rotation measurements with skin fixed methods by up to 7° during flexion and 13° during abduction [94].

Accurate scapula function has been reported from cadaveric studies [95]. However, doubt exists as to the validity of these results since it is difficult to reproduce *in vivo* loading conditions; i.e. the complex muscle contractions as well as soft tissue constraints necessary to maintain joint stability [96].

Pronk [58] used a single point locator attached to a 3D spatial linkage instrument to measure the spatial position of the three bony landmarks used to create the scapula ACS. Although accurate, this method was found to be too time consuming for clinical practice.

Johnson et al [18] developed a technique using an electromagnetic sensor on top of a three pointed palpator applied over the scapula bony landmarks, referred to as the scapula locator (SL). The SL facilitates the identification of the scapula bony landmarks at any arm elevation. Since the scapula is regarded as a rigid body, the relationship between its bony landmarks remains fixed. For every new arm position, the SL is readjusted on to the bony landmarks. Numerous researchers have used the SL to record scapula movement [27, 30, 97, 98] since it is considered the “gold” standard for scapula function measurements. However, the measurement technique is constrained to static recordings.

Percutaneous pins attached directly onto the bone provide accurate scapula measurements [99, 100] during functional dynamic tasks. However, the technique is invasive, therefore it has limited uses due to ethical implications. Moreover, it is unclear how much the pins restrict soft tissue motion and hence affect segment movement.

Van Andel et al developed an acromium marker cluster (AMC) to perform dynamic scapula tracking [30]. The AMC consists of a cluster of 3 retro-reflective markers which are attached on top of the acromium of the scapula. Through an initial anatomical calibration, the scapula bony landmarks are related to a technical coordinate system fixed to the AMC so that dynamic tracking is possible. Scapula function has been reported accurately with the AMC up until 100° of arm elevation [30]. At higher elevations, soft tissue bulging, mainly the deltoid muscle, introduces significant measurement errors. Brochard et al suggested a double calibration of the AMC [101], where a combination of the resting calibration of the scapula and a high angle calibration (which serves to correct for artefacts caused by bulging tissue above 90°) is performed. The accuracy of 3D scapular motion recordings using the double calibration is improved; however, the inter-trial and inter-session reliability was not as good as when only a single calibration is performed [101].

Leardini et al proposed that soft tissue artefacts are reproducible within subjects but not between subjects [102] thus suggesting subject-specific skin correction

factors could be developed to correct for scapula skin artefact errors [103]. As a result, Bourne et al performed multiple digitalisations of scapula landmarks at static positions through the ROM coupled with percutaneous pins drilled into the lateral scapula spine to accurately measure its movement [103]. The data was then used to correct dynamic kinematic data obtained from skin markers. They found that the correction factor significantly improves the accuracy of the skin marker measurements. However, the method is considered complex and too time consuming for daily clinical analysis [101].

Model-based 3D to 2D image registration techniques have been used to measure accurate dynamic scapula function. 3D models of the scapula and humerus are obtained by segmenting bone from other soft tissue on MRI or CT scans. The segment's position and orientation are tracked by determining the pose of their silhouette in the low dose X-rays, therefore the technique is not susceptible to skin artefact errors. However the technique requires the patient to be exposed to ionising radiation from the fluoroscopy recordings (and to further radiation when the 3D bone models are reconstructed from CT scans). Furthermore, errors due to segmentation and manual matching of the 3D models to the fluoroscopy images can reduce measurement accuracy.

Bony landmark identification by means of palpation

The markers on bony landmarks are used to create orthogonal coordinate systems on each segment and to track their movement. They are usually identified by means of external palpation. Misplacement of the retro-reflective markers on the bony landmarks results in erroneous definitions of the anatomical embedded reference frames [37] which affect the joint kinematics measurements. De Groot investigated the precision of shoulder anatomical landmark palpation and measured 8.8° inter-trial variability in shoulder complex kinematics due to errors in landmark identification [104].

Della Croce et al identified three specific factors that affect digitising the landmarks: landmarks are surfaces, not points; there is inter-subject variation in soft

tissue thickness and composition; and there is a dependence in the specific palpation technique used [105].

Rotation sequences and the “gimbal lock” effect

The movement of shoulder complex segments is expressed by three Cardan angles for each bone. The sequence of rotation around these angles is non-commutative [1]; in other words, they must be performed in a specific order. A disadvantage of using Cardan angles is the decreasing measurement accuracy at positions near the singular position [104]. At this joint angular position, the Cardan angles cannot be precisely defined since the axes of the two adjacent segments are collinear [1]. This occurrence is referred to as “gimbal lock”.

“Gimbal lock” particularly affects GH and HT measurements when using the ISB recommendations to record and analyse motion [19, 27]. At positions where the arm is hanging by the side of the body and at extremes of arm elevation, the first and third rotations cannot be calculated, and consequently unrealistic rotations are computed. However, singularity can be minimised by an appropriate choice of coordinate systems and rotation order [104].

1.2.4 The Dempster-Shafer objective function classifier

Detailed and objective quantitative analysis can be performed using MA since the individual contribution of the joints towards overall arm positioning or elevation is measured. However, a wealth of biomechanical data is collected which can be extremely difficult to analyse. To interpret the MA data, researchers sometimes focus on a single variable; however, no individual variable is capable of providing a complete description of a subject’s motion [106].

Jones et al developed an automated tool capable of objectively assessing OA knee function and quantify functional recovery following total knee replacement (TKR) from MA data [107]. The classifier is based around the Dempster-Shafer

(DS) theory of evidence. It enables decision making in “the presence of uncertain, inadequate, and conflicting evidence” [107]; a common problem in the MA laboratory.

The tool addresses common challenges in MA data such as the “difficulty in comprehending large amounts of both corroborating and conflicting information; the subjectivity of data interpretation; the need for visualisation; and the quantitative comparison of temporal waveform data” [108]. A subject’s classification, as well as the contribution of each input variable towards classification, is visualised in simplex plots [107, 109]. Different regions in the simplex triangle support the classification of the subject as pathological or healthy depending on the joint characteristics.

To the authors’ knowledge, no such tools have been developed or employed to aid in the assessment of shoulder kinematics data. Simple clinical interpretation of the results from the quantitative analysis would be most advantageous since surgeons still rely on visual assessment, imaging examination and subjective questionnaires.

1.3 Aim and objectives of the study

The aim of this thesis was to contribute towards the development and improvement of shoulder complex kinematics research by introducing novel approaches to measure motions more accurately as well as aid in the interpretation of motion analysis data.

To achieve the aim of the study, a set of objectives were established:

1. Develop and collect data with an image based method to accurately measure glenohumeral joint function.
2. Develop and use a data collection and analysis method to assess shoulder complex function on healthy volunteers using motion analysis techniques.

3. Investigate skin artefact and marker placement errors in motion analysis measurements by comparing simultaneous image registration and motion analysis recordings.
4. Investigate differences between patients' injured or pathological shoulder function with that of the contralateral shoulder as well as healthy shoulder function using motion analysis techniques.
5. Investigate the suitability of using functional variables obtained in the motion analysis Laboratory to objectively characterise healthy and pathological or injured shoulder function applying the Cardiff DS objective classifier method.

1.4 Hypothesis

Considering both the advantages and limitations of motion analysis techniques, this study raises the question; can motion analysis be used to objectively quantify healthy, injured and pathological shoulder complex function? It was hypothesised that this should be possible and that biomechanical differences between the study's patient cohorts and healthy subjects can be measured using such techniques. However, errors in the motion analysis system due to marker placement and skin movement artefact would need to be investigated first by comparing the measurements taken simultaneously with the motion analysis and image registration systems.

1.5 Thesis summary

The aim and objectives of the thesis were addressed in the following chapters:

Chapter 2 presents a novel study at Cardiff University using model based 2D to 3D image registration to accurately measure glenohumeral joint kinematics. Errors in the motion capture system were investigated by comparing synchronous measurements taken with the motion analysis system and with image registration technique. Work stemming from this Chapter was presented at the British Elbow & Shoulder Society Meeting, 2011 [110].

Chapter 3 provides a detailed description of the motion analysis methods of data collection and analysis currently employed at Cardiff University for shoulder complex biomechanics studies.

Chapter 4 presents healthy participants' kinematics data collected in the motion analysis Laboratory. Different studies were carried out for the better understanding of shoulder complex kinematics as well as subsequent improvement of the data collection and analysis methods. Work stemming from this chapter was presented in 8th and 9th International Symposia on Computer Methods in Biomechanics and Biomedical Engineering [97, 111], XXII and XXIII Congresses of the International Society of Biomechanics [112, 113], 17th Conference of the European Society of Biomechanics [114], 10th International Symposium 3D analysis of human movement [115], and at UK Shoulder Group Meetings (years 2008, 2009 and 2010).

Chapter 5 presents kinematics data of patients with different conditions in their shoulder due to trauma or pathology (clavicle fracture, multidirectional instability, irreparable rotator cuff tear and glenohumeral joint dislocation), as well as measurements from their contralateral shoulder. The DS classification method was explored and used to characterise patient and healthy shoulder function.

Chapter 6 Draws conclusions from the research carried out for the fulfilment of the thesis as well as proposes direction for future shoulder research at Cardiff University.

Chapter 2

Measuring glenohumeral joint kinematics using model-based image registration techniques

Measurement of glenohumeral (GH) joint motion is essential for the understanding and evaluation of shoulder complex function. Measuring accurate GH joint kinematics during dynamic activities is challenging using conventional techniques due to the wide ranging, complex joint motions and relative movement between the skin and the underlying bone, called skin movement artifact.

Model-based image registration techniques (IRT) are used to accurately measure joint kinematics by matching three-dimensional (3D) computer models of orthopaedic implants or bones to a sequence of two-dimensional (2D) fluoroscopic images. The technique has been used extensively to measure knee joint kinematics; with reported accuracy of approximately 1° for rotations and within 0.5mm sagittal plane translations [43].

Within Cardiff University, Dr. Whatling successfully applied IRT to measure knee joint kinematics on healthy volunteers and total knee replacement (TKR) patients [47] using the protocol established by Banks and Hodge [44]. Her goal was to assess errors in the motion capture system by comparing the kinematics

waveforms derived from the IRT to passive motion capture in a simple step-up and down task. Critical analysis of the study is focused on the fact that the measurements were taken non-simultaneously, and thus it does not represent a true comparison between the two systems.

The aim of this study was to develop an effective method to register 3D bone models to a sequence of 2D fluoroscopic images in order to identify errors associated with motion analysis (MA) using skin fixed markers. To achieve this, a suitable, practical and repeatable protocol applied to the shoulder was developed to measure accurate GH joint kinematics.

To achieve the aim of the study, a set of objectives was established:

- Describe GH joint kinematics (rotations and translations) during physiological arm elevations using single-plane fluoroscopy.
- Compare kinematics waveforms of GH joint motion measured using IRT and motion capture on two healthy volunteers and determine whether systematic differences in the kinematics were present.
- Investigate use of magnetic resonance imaging (MRI) scans to create accurate 3D bone models of the humerus and scapula to match to the 2D fluoroscopic images by performing a registration repeatability trial.

This study forms part of a 5 year clinical investigation of which the initial exploration is attributed to this thesis.

2.1 Background

Shoulder kinematics studies consist of tracking the 3D rigid body motions of the segments that make up the shoulder complex. Accurately measuring shoulder kinematics is challenging due to the complex nature of shoulder motions and the errors associated with conventional measurement techniques.

Standard 2D X-rays [63, 116–118], and fluoroscopy [71, 89, 119, 120] measurements are not sufficient to describe the complex six degrees of freedom (DOF) motions of the GH joint. Skin markers attached to bony landmarks are widely used to measure shoulder function [97, 121]. An anatomical coordinate system (ACS) is fixed on to a segment using skin markers to describe its changing position with respect to a global coordinate system (GCS) or to another segment's ACS. Accuracy is compromised due to the undesired relative movement of the skin and the underlying bone. This error is commonly known as skin movement artifact [122, 123]. Electromagnetic tracking devices use an electromagnetic field with sensors attached to segments to determine their position and orientation [13, 27]. Manual point digitalisation of anatomical landmarks is performed to fix an ACS onto the body. These devices are subject to skin artifact errors since the sensors are attached to the skin. Another source of error for both skin markers attached to bony landmarks as well as the electromagnetic tracking systems is related to the accuracy and repeatability of manual digitalisation of the bony landmarks [124]. Percutaneous pins inserted in the skin, and directly attached to the bones, are an accurate method for measuring scapular kinematics during dynamic activities [99, 100]. However, a high risk of infection associated with the percutaneous pins limits its use. Cadaveric investigations [95, 125, 126] provide accurate measurement of the motion, although doubt exists as to whether the results bear a true resemblance to in vivo kinematics given the limited degree to which the muscle action can be replicated. Recently, researchers have investigated shoulder motions using 3D imaging with magnetic resonance imaging (MRI) scans [39, 40] although they are currently constrained to static measurements only.

The majority of the reported techniques are unable to either precisely measure shoulder motion during dynamic activities, or the method used is not suitable. IRT were originally developed around 20 years ago to assess total knee replacement (TKR) kinematics [43–46] during dynamic activities. The technique involves projecting the 3D computer-aided design (CAD) models (from the manufacturer) of the implants' metallic components onto single-plane fluoroscopic

images. The object's pose is manually adjusted to match its silhouette with the silhouette of the fluoroscopic image, thereby recreating the position and orientation of the TKR components [44, 45, 127]. When the poses are determined for a sequence of fluoroscopic images, the kinematics of the knee replacement joint can be calculated during dynamic activities. Challenges associated with IRT are that objects in the fluoroscopic images with similar appearance to the implant component can clutter the image. Furthermore, overlap of the other leg or another implant causes occlusion and low object-to-background contrast may lead to inaccuracies in the measurements [127]. Despite the challenges, knee rotations have been measured accurately to approximately 1° and sagittal plane translations within approximately 0.5mm [43].

Natural knee kinematics have also been measured using IRT. Three-dimensional bone models of the tibia and femur can be created from either computerised tomography (CT) scans [128–130] or MRI scans [47, 131, 132] for the 2D matching. CT generated models are generally more accurate than MRI generated models since CT provides higher bone contrast than MRI and does not suffer from spatial distortions compared to MRI [129, 133, 134]. The downside of CT is that the study volunteer is exposed to further ionising radiation, which leads to a higher risk to the study participants. Independently of the imaging modality used to create the 3D bone models, registration is more difficult since human bones are of weaker contrast compared to the metallic components of implants [123].

Single-plane fluoroscopic techniques are subject to measurement uncertainties in translations perpendicular to the image plane [132]. To overcome this, bi-plane fluoroscopic image sequences were developed to measure accurate joint motion [135, 136]. The fluoroscope consists of two X-ray sources and image intensifiers configured in such a way that allow recordings of the joint from two different views (usually anterior-posterior and oblique). The 3D models are thus registered to two fluoroscopic images obtained simultaneously, minimising in-plane translation errors. However, ionising radiation is greater compared to single-plane fluoroscopy.

Despite the success of measuring TKR and natural knee kinematics using IRT, limited studies have applied the technique to measure shoulder function (see Table 2.1).

TABLE 2.1: Recent studies that employ model based 3D to 2D IRT to measure shoulder function

Paper	Aim	Imaging modality	Fluoroscopy
Bey et al. 2006 [48]	Validate a model-based tracking technique to measure in vivo, 3D GH joint kinematics	CT scans	Bi-plane radiographs
Kon et al. 2008 [15]	Determine influence of a handheld weight on the scapulohumeral rhythm in healthy participants	CT scans	Single-plane fluoroscopy
Bey et al. 2008 [49]	Measure GH joint translations in patients with a repaired rotator cuff shoulders and their contralateral shoulder	CT scans	Bi-plane X-ray
Nishinaka et al. 2008 [50]	Measure in-vivo GH translation in healthy shoulders	CT scans	Single-plane fluoroscopy
Bishop et al. 2009 [51]	Assess the relationship between GH inclination and superior translation in shoulder patients	CT scans	Bi-plane fluoroscopy
Matsuki et al. 2010 [52]	Compare scapular kinematics between dominant and non-dominant shoulders in healthy participants	CT scans	Single-plane fluoroscopy

Even though the GH joint is treated as a perfect ball and socket joint, humerus translations relative to the scapula have been measured in both healthy and injured or pathological shoulders using several different techniques. However, a greater appreciation of GH joint translations has been gained through these studies [49–51], since researchers have measured GH joint translations accurately to 0.5mm.

Furthermore, accurate scapula function is measured during dynamic activities using IRT [15, 52]. The scapula moves significantly under the skin during arm elevation. However, its position and orientation is tracked by determining the pose of its silhouette in the low dose X-rays, therefore the technique is not susceptible to skin artifact errors.

CT scans have been the imaging modality for the creation of the 3D natural shoulder bone models for the aforementioned research groups, with no other group investigating IRT with MRI scans generated bone models despite studies

suggesting bone models generated from MRI scans are appropriate for image registration [47, 132].

2.2 Development of image registration studies at Cardiff

It was considered appropriate to explore the feasibility and set-up of the technique at Cardiff to measure GH function following the methodology established by Banks and Hodge [44]. A protocol was developed where both data collection methods were used simultaneously to allow a direct comparison between IRT and MA. This way, the errors that are commonly associated with MA could be assessed.

Ethical approval was necessary from the NHS Research and Development Department, the Local Research Ethics Committee and from the School of Engineering within Cardiff University. The Integrated Research Application was used to complete the forms for ethical approval, which involved several meetings with different NHS personnel to develop the testing protocol.

The Radiation Protection Adviser and MPE (diagnostic radiology) from Vellindre Hospital, Arnold Rust, estimated the radiation dose associated with the study. Monte-Carlo based radiation dose calculations software was used to produce a dose estimate based on exposure factors provided for a typical clinical examination. The effect of the presence of a shoulder prosthesis on fluoroscopic exposure factors was estimated using a pail of water and a typical prosthesis. Exposure factors were noted under automatic brightness control using a range of X-ray beam pulse rates both with and without the prosthesis present (Figure 2.1).

The radiation effective dose in microSieverts (μSv) were estimated to be 4.5 and 4.1 with and without the prostheses respectively. The risk presented by these



FIGURE 2.1: Session at the X-ray department to estimate the study radiation dose

exposures can be regarded to be trivially low, with the level of risk from one exposure approximately equivalent to one day of exposure to natural background radiation.

2.3 Data collection protocol

The South East Wales Research Ethics Committee and the NHS R&D Department granted ethical approval for the recruitment of healthy participants and patients presenting shoulder pathology or instability to measure their GH joint function using shape matching techniques (Study details: Assessment of shoulder function using imaging techniques. REC number: 06/WSE03/57).

2.3.1 Participants recruitment

Initially two healthy participants were recruited for the study: one healthy female volunteer (44 year old, weight 68 Kg) and one healthy male volunteer (22 year old, weight: 78Kg). An information pack was given to the participants and written informed consent was obtained (Refer to Appendix A for information sheets and consent forms).

2.3.2 Measuring systems

Participants were asked to attend a session at the X-ray Department, University Hospital, Heath Park, Cardiff (lasting approximately 1 hour) to record GH joint motion using dynamic fluoroscopy, as well as two sessions at the Cardiff University Brain Research Imaging Centre, CUBRIC, (lasting approximately 3 hours between the two sessions) to obtain MRI scans of their tested shoulder.

2.3.2.1 X-ray department at the University Hospital of Wales

A screening room at the University Hospital of Wales X-ray department was booked through Miss Rebecca Vaughan-Roberts, a study collaborator. The room is equipped with a Philips Eleva dynamic fluoroscope (Philips).

During this session, simultaneous dynamic single-plane fluoroscopic recording and motion capture measurements were taken. A Qualysis ProReflex MCU portable five camera motion capture system was set-up as shown in Figure 2.2. The Qualysis Track Manager (QTM) Workspace Options and calibration procedure are summarised in Table 2.2.

TABLE 2.2: QTM workspace configuration for MA recordings fluoroscopy screening room.

Capture rate	60 Hz
Capture period	20 s
Maximum number of markers	100
Calibration settings	Wand calibration Wand kit 110 mm Exact wand length 110.9 mm
Tracking settings	Bounding box X \pm 1000 mm Y \pm 1000 mm Z \pm 1000 mm

The Qualysis system L-shaped calibration frame was placed on a stool in front of the fluoroscope image intensifier so that all five cameras had the frame within their field of view (see Figure 2.3). The calibration frame X axis was pointing

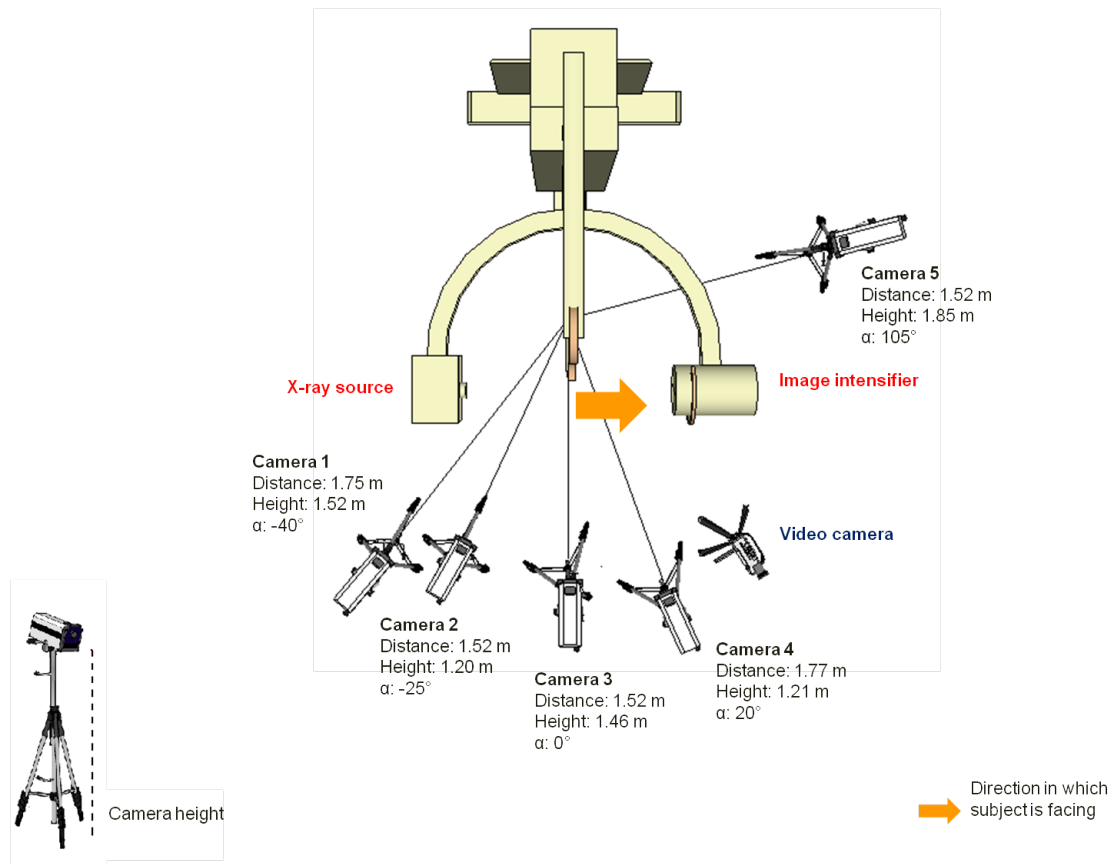


FIGURE 2.2: Qualisys camera layout for simultaneous fluoroscopic and Motion Analysis recordings

horizontally to the right and the Y axis was pointing horizontally towards the image intensifier. The calibration procedure described in Chapter 3 was followed.

International Society of Biomechanics (ISB) recommended bony landmarks (Table 3.2 in Chapter 3) were identified with retro-reflective markers. The markers were first coated with Zinc paint and then with the necessary retro-reflective material. The markers would then be radio-opaque and thus would be visible in the fluoroscopy recordings as well as in QTM camera system. The GH joint centre of rotation (CoR) was estimated through Mesker's regression equations (MRE) [78].

The fluoroscope settings were set as shown in Table 2.3

Prior to recording shoulder movement, a fluoroscope calibration frame consisting of two Plexiglas sheets with lead markers was placed precisely 2cm in front

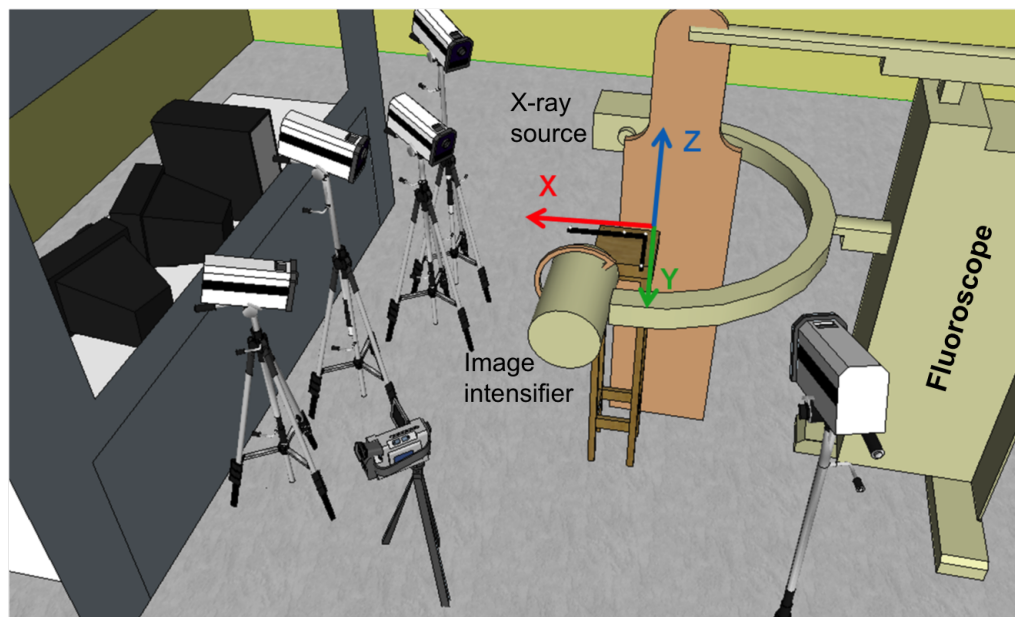


FIGURE 2.3: Calibration of the Portable Qualisys camera system in the fluoroscopy screening room

TABLE 2.3: Philips dynamic fluoroscope settings for glenohumeral joint screening

Source to image intensifier distance	105 cm
Image intensifier image size	25 cm
Added X-ray beam filtration	0.1mm Cu 1 mm Al
Pulse rate	"half"
Exposure duration	60 seconds
Screening direction	Anterior-Posterior

of the image intensifier (Figure 2.4a). The central markers on both grids were aligned with the centre of the image intensifier, marked by a stainless steel ball bearing fixed to the intensifier (Figure 2.4b). The acquired calibration frame image was used in the post processing analysis to remove geometric distortions in the fluoroscopic images. Details on how the calibration frame was constructed can be found in [47].

The participants' right shoulder was centred within the image intensifier. Dynamic arm elevation and lowering in abduction and scaption were recorded

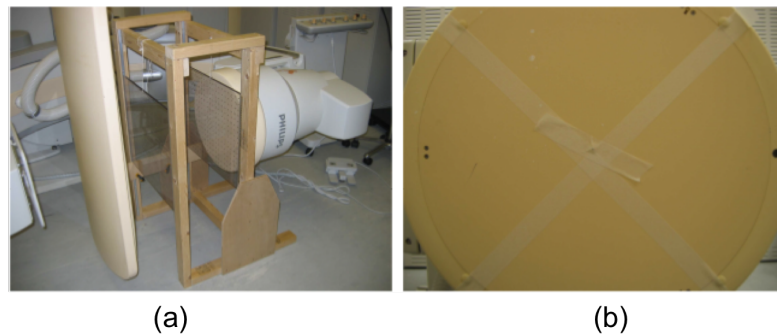


FIGURE 2.4: (a) Calibration frame used to undistort fluoroscopy images and (b) determining the origin of the image intensifier (from [47]).

from the arm hanging by the side of the body to full physiological elevation (Figure 2.5a,b). Physiological internal and external rotation was measured from the arm hanging by the side of the body with the elbow flexed to 90° to full external rotation (Figure 2.5c). A 2lb handheld weight was used during all recording trials.



FIGURE 2.5: Simultaneous fluoroscopy and motion analysis recordings (a) frontal plane elevation, (b) scapular elevation and (c) external rotation

Subjects were allowed to practise the movements prior to recording. Elevation trials lasted approximately 4s each.

2.3.2.2 Cardiff University Brain Repair Imaging Centre

MRI was the preferred imaging modality for the construction of the 3D bone models. Scan data of the study participants was obtained at CUBRIC at Cardiff University with a 3T GE scanner (General Electric Company), as shown in Figure 2.6.



FIGURE 2.6: Shoulder MRI data collection in CUBRIC

The participants were asked to complete the CUBRIC standard questionnaire to make sure they were suitable candidates for MRI scanning. Subjects were asked to remove all metal objects from themselves prior to entering the scanner. A blanket and ear plugs were provided for comfort.

In the absence of a dedicated shoulder coil, a flexible head coil and a thorax coil were used around the segments to collect the MRI data. A range of scanner settings were explored in an attempt to obtain the best possible quality images. The optimum images were obtained when the scanner settings for data acquisition were as shown in Table 2.4.

Sets of 1mm slice thickness scans were obtained (Figure 2.7) for the creation of high resolution models of the superior humerus and the entire scapula necessary for accurate image registration.

TABLE 2.4: MRI settings for shoulder scans

Sequence	SPGR3D
Slice thickness	1x1x1
Field of view	25.6mm
Coil	GP Flex

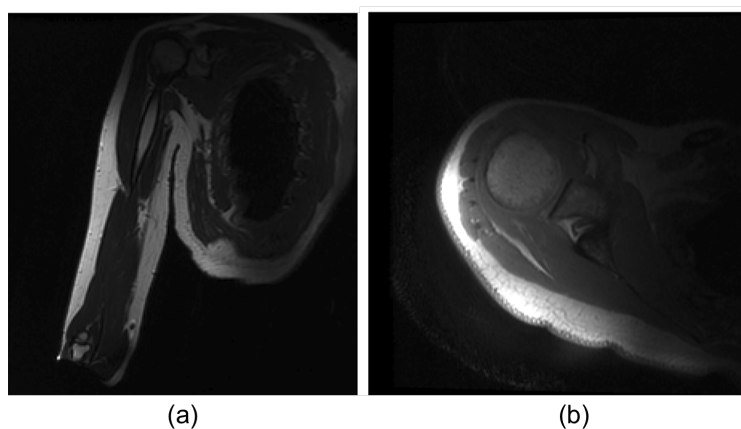


FIGURE 2.7: MRI scans of the shoulder (a) in the frontal plane and (b) in the transverse plane

2.4 Data handling protocol

Extensive image data processing is required to perform accurate image registration. A flow diagram of the data handling protocol is shown in Figure 2.8. For detailed instructions on how to perform 3D to 2D image registration using the Cardiff protocol, refer to the Image Registration Manual in Appendix B.

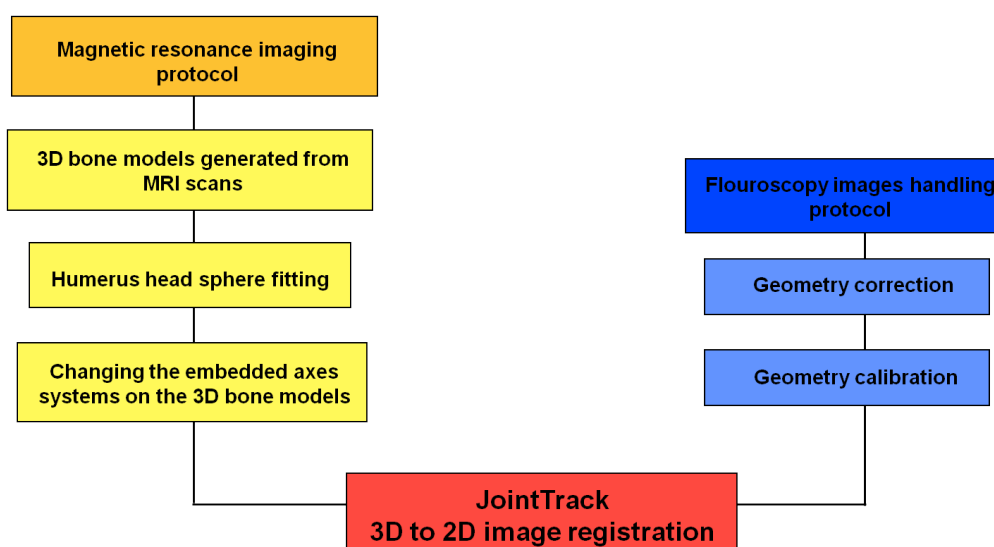


FIGURE 2.8: Flow diagram of the data handling protocol to perform 3D to 2D image registration

2.4.1 Magnetic resonance imaging protocol

2.4.1.1 3D bone models generated from MRI scans

Commercial software (Simpleware, Ltd) was used for the construction of the 3D models from MRI data. The scans were segmented in ScanIP (Simpleware, Ltd.). Cortical bone gives a dark, low intensity signal on MRI scans, thus appearing as a black area. The humerus and scapula were segmented (Figure 2.9 using various automated tools that are available in ScanIP. These included manipulating the threshold value of the grey value of the pixels as well as floodfill, a tool which facilitates the filling of the bone. When convenient, a manual paint tool was also used to segment scans.

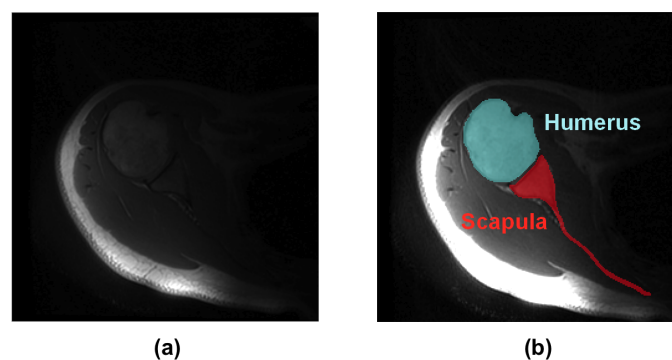


FIGURE 2.9: Segmenting the humerus and scapula to create 3D bone models

A smoothing algorithm was applied to the 3D models in order to remove inconsistencies from the manual segmentation. A basic gaussian-recursion filter was applied to smooth the models (Figure 2.10), thus improving the quality of the mask. The filter X, Y and Z Gaussian sigma values were set to the spacing of the data, which in this case was 1mm x 1mm x 1mm.

2.4.1.2 Humerus head sphere fitting

To identify the GH joint CoR, a sphere is fitted on to the humerus head. The smoothed humerus model as well as a sphere of unit diameter were imported into ScanCAD (Simpleware, Ltd.). The sphere was then manually fitted to the

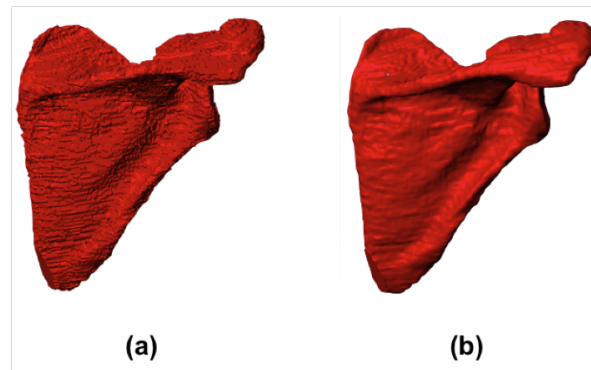


FIGURE 2.10: 3D fine model of the scapula (a) prior to applying a smoothing filter and (b) after smoothing filter

humeral head using the *translation* tool found in ScanCAD (Figure 2.11). The position of its centroid was defined as the GH joint CoR.



FIGURE 2.11: Fitting a sphere on the humerus head. The position of the sphere centroid is known.

2.4.1.3 Changing the embedded axes systems on the 3D models

An ACS was embedded on the high resolution models for the kinematics analysis using JointTrack image registration software. The orientation of the new ACSs was estimated from the coordinate data of bony landmarks in an excel sheet using vector multiplication, according to the convention followed at the University of Florida.

The scapula origin was defined as the centre of the line connecting the most superior and inferior bony edges of the glenoid surface. From Figure 2.12a, a vector S_1 is defined from the most inferior glenoid bony edge to the most superior glenoid bony edge. Vector S_1 divided by its length gives unit vector s_1 . A vector S_2 is defined from the most posterior glenoid bony edge to the most anterior glenoid bony edge. The cross product of s_1 and S_2 gives vector S_3 .

Vector S_3 divided by its length gives unit vector s_3 . The cross product of s_3 and s_1 gives unit vector s_4 . The unit vectors s_3 , s_1 and s_4 produce the x_S , y_S , z_S axes respectively, attached to the origin, as shown in Figure 2.12b.

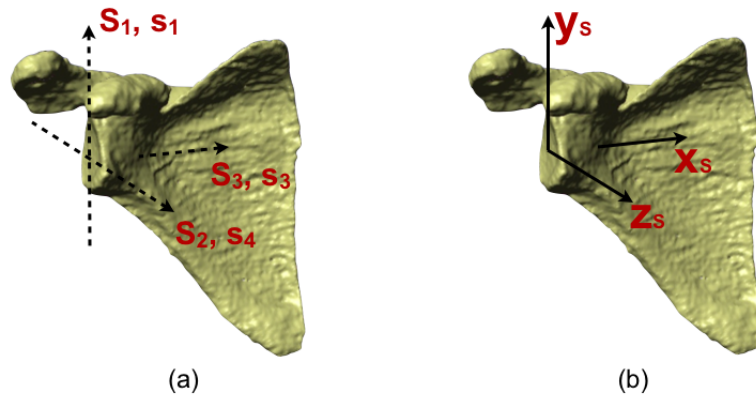


FIGURE 2.12: Scapula anatomical coordinate system
(a) construction and (b) position and orientation

The humerus origin was defined as the centre of the sphere fitted on the humerus head. From Figure 2.13a, a vector H_1 is defined from an inferior position along the humerus shaft to a superior position along the shaft. Vector H_1 divided by its length gives unit vector h_1 . A vector H_2 is defined from the GH joint CoR to the intertubercular groove. The cross product of vectors h_1 and H_2 gives the vector H_3 . Vector H_3 divided by its length gives unit vector h_3 . The cross product of vectors h_3 and h_1 gives the unit vector h_4 . The unit vectors h_3 , h_1 and h_4 produce the x_H , y_H , z_H axes respectively, attached to the origin at GH joint CoR as shown in Figure 2.13b.

Once the models were rotated in ScanIP, the position of the glenoid centre and GH joint CoR landmarks were recorded in the new ACS in order to translate the origin position. The translation of the ACSs origins was performed using Rhinoceros 4.0 software. The models were imported into the software and the origin was moved from 0,0,0 position to where the new origin coordinates were recorded in ScanIP.

Once this was completed, the 3D models were ready to be registered to the fluoroscopic images.

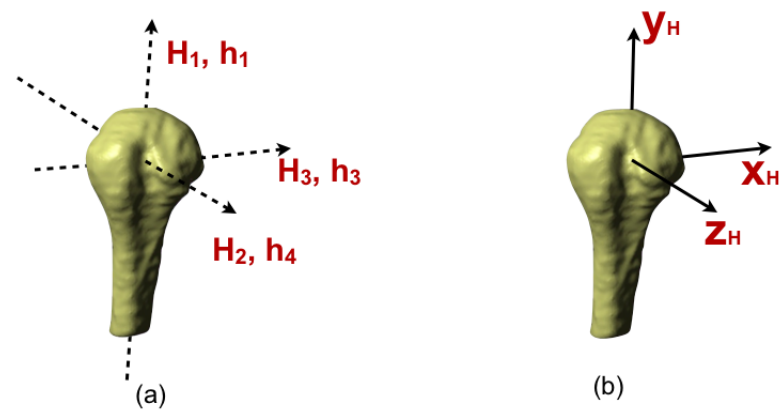


FIGURE 2.13: Humerus anatomical coordinate system
(a) construction and (b) position and orientation

2.4.2 Fluoroscopy images handling protocol

Fluoroscopy images present significant geometric distortion [43, 137] mainly due to the curved shape of the image intensifier screen. This results in a magnification of the image towards the periphery of the screen (Figure 2.14a). All images were corrected for distortion (Figure 2.14b) through the calibration procedure described below.

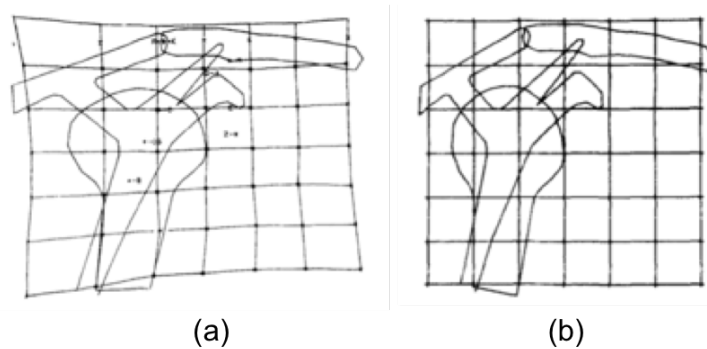


FIGURE 2.14: Schematic representation of (a) the magnification distortion and (b) correction of fluoroscopic images. Adapted from [137]

2.4.2.1 Geometry correction

Geometric distortion was corrected by determining and applying the transformation between known control points on the calibration frame (shown in Figure 2.15) and measured coordinates of the same points to the entire region

bounded by control points [43].

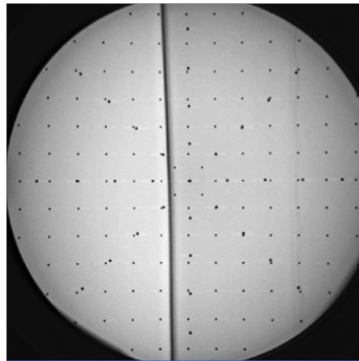


FIGURE 2.15: Fluoroscopic image of control points in the calibration frame

A rectangular grid of precisely placed markers (lead shot) was imaged (Figure 2.16) in a calibration program written in Matlab at the University of Florida. Corrections to the resulting image were applied so that the markers returned to their known positions using bilinear interpolation. The distortions only needed to be measured once during each session and the same correction could then be applied to all images.

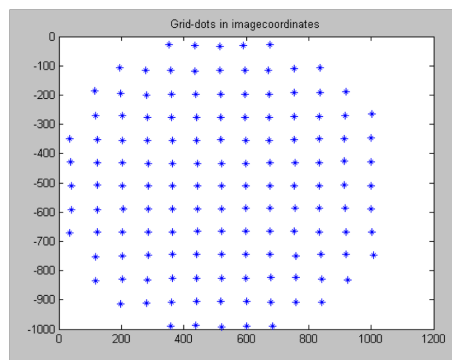


FIGURE 2.16: Calibration grid of control points

2.4.2.2 Geometry calibration

The internal orientation parameters (principal distance and principal point) were determined by imaging a star shaped distribution of the control points (Figure 2.17) on a Plexiglas plate.

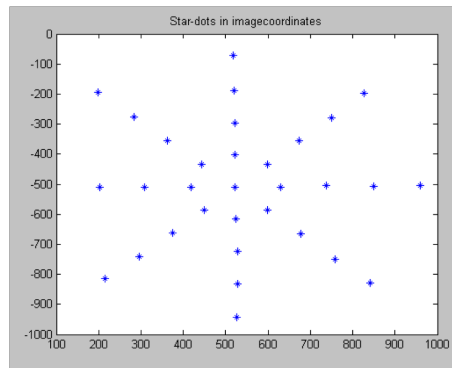


FIGURE 2.17: Star shaped distribution of control points

Once the images were corrected for distortion and the internal orientation parameters were calculated, 3D to 2D image registration was performed.

2.4.3 JointTack 3D to 2D image registration

The 3D models of the humerus and scapula were registered to a sequence of fluoroscopic images using model-based 3D to 2D image registration software called JointTrack. The software was developed in the University of Florida based on a software known as KneeTrack by Banks and Hodge [44].

The internal calibration parameters were used to establish the local coordinate system (LCS) within JointTrack. The system is orientated so that:

- The origin is placed at the X-ray source point
- The X axis corresponds to the horizontal axis of the image, positive to the right.
- The Y axis corresponds to the vertical axis of the image, positive upwards.
- The Z axis pointing from the image intensifier to the X-ray source

The silhouette of the 3D models was manually adjusted to fit the silhouette of the bones on the distortion corrected fluoroscopic images (Figure 2.18a). The models were rotated around and about all three planes for the registration. The

3D poses were iteratively adjusted to match their silhouette with the silhouette of the fluoroscopic image. JointTrack uses a “copy previous” tool to copy the models’ poses from the previous registered image on to the subsequent image therefore only minor adjustments are necessary (Figure 2.18b). A canny edge detection tool was used to highlight the bone edges in the fluoroscopic images to aid with registration (Figure 2.19).

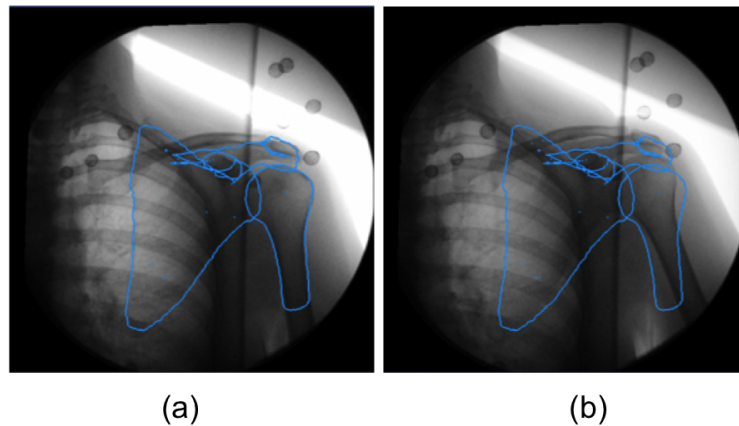


FIGURE 2.18: JointTrack registration: (a) Models silhouette matching fluoroscopic images and (b) “copy preview” tool

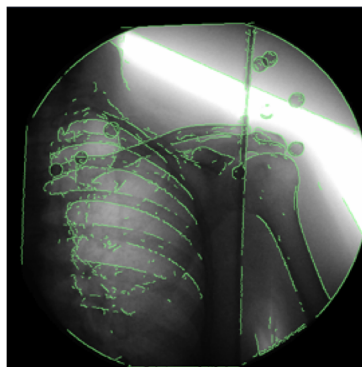


FIGURE 2.19: Canny edge detection

2.5 Data analysis protocol

A customised Matlab program, written by PhD student Shang Mu at University of Florida, was used to compute GH joint and scapula kinematics measured

with IRT (Figure 2.20) from the transformation matrix T (Equation (2.1)) which relates the two segments.

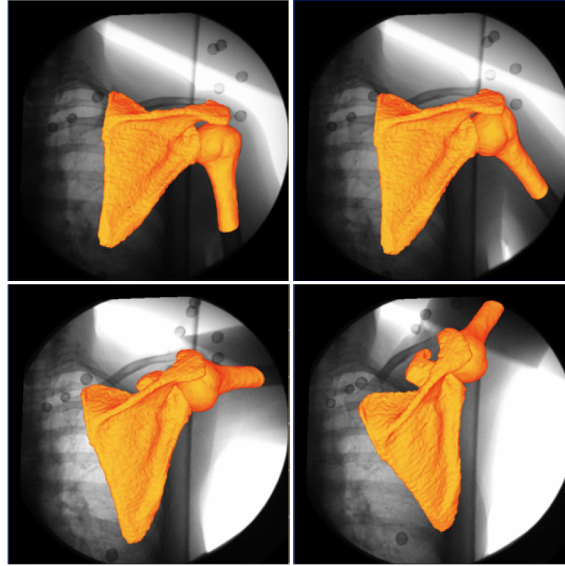


FIGURE 2.20: Registered models onto fluoroscopic images using JointTrack 3D to 2D image registration software

$$[T] = \begin{bmatrix} \cos X_x & \cos X_y & \cos X_z & L_X \\ \cos Y_x & \cos Y_y & \cos Y_z & L_Y \\ \cos Z_x & \cos Z_y & \cos Z_z & L_Z \\ 0 & 0 & 0 & 1 \end{bmatrix} = \begin{bmatrix} T_{11} & T_{12} & T_{13} & T_{14} \\ T_{21} & T_{22} & T_{23} & T_{24} \\ T_{31} & T_{32} & T_{33} & T_{34} \\ 0 & 0 & 0 & 1 \end{bmatrix} \quad (2.1)$$

2.5.1 Glenohumeral joint kinematics

The program calculates the transformation matrix relating the humerus ACS to the scapula ACS (T_{gh}) from their absolute poses using Equation (2.2).

$$T_{gh} = [T_{ga,S}][T_{ag,H}] \quad (2.2)$$

Where $T_{ga,S}$ is the transformation matrix relating JointTrack GCS to the Scapula ACS and $T_{ag,H}$ is the transformation matrix relating the humerus ACS to JointTrack GCS

GH joint rotations are resolved according to the Euler sequence of rotation ZXY.

GH elevation α_{GH}

GH joint elevation is the humerus rotation around the coincident z_S and z_H axes, as shown in Figure 2.21a. It is defined as the angle between x_S and y_H in the frontal plane using Equation (2.3). GH joint elevation is defined as a positive angle.

$$\alpha_{GH} = \tan^{-1} \left(\frac{T_{12}}{T_{22}} \right) \quad (2.3)$$

Where T refers to the transformation matrix T_{gh} , T_{12} is the projection of y_H onto x_S , indicated by Xy in Figure 2.21b and T_{22} is the projection of y_H in y_S , represented by Yy in Figure 2.21b.

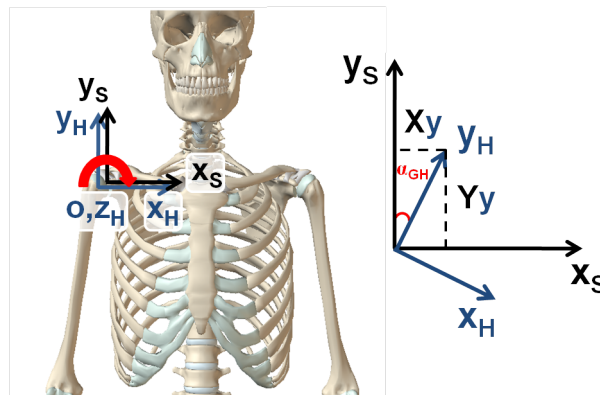


FIGURE 2.21: Two dimensional illustration of glenohumeral elevation, where x_S, y_S, z_S denotes the axes of the scapula ACS while x_H, y_H, z_H denotes the axes of the humerus ACS (a) elevation defined as rotation around z_H and (b) elevation angle

GH plane of elevation β_{GH}

GH joint plane of elevation is the humerus rotation around x_S , as shown in Figure 2.22a. It is defined as the angle between y_S and y_H in the sagittal plane using Equation (2.4).

$$\beta_{GH} = -\sin^{-1}(T_{32}) \quad (2.4)$$

Where T refers to the transformation matrix T_{gh} and T_{32} is the projection of y_H onto z_S , indicated by Zy in Figure 2.22b.

GH axial rotation γ_{GH}

GH axial rotation is the humerus rotation around y_S , as shown in Figure 2.23a. It is defined as the angle between x_S and x_H in the transverse plane using

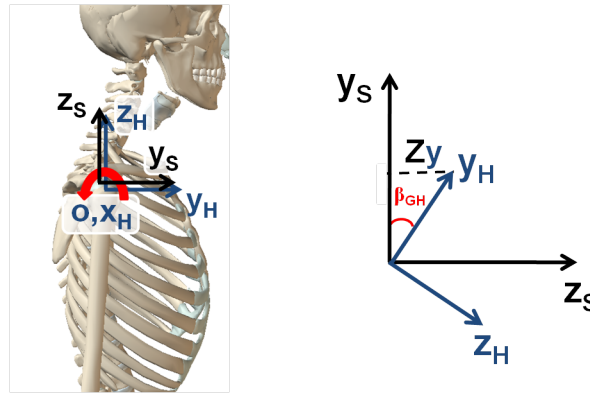


FIGURE 2.22: Two dimensional illustration of glenohumeral plane of elevation in the sagittal plane, where x_S, y_S, z_S denotes the axes of the scapula ACS while x_H, y_H, z_H denotes the axes of the humerus ACS (a) plane of elevation defined as rotation around x_S and (b) plane of elevation angle

Equation (2.5). Internal rotation is defined as a positive angle while external rotation is defined as a negative angle.

$$\gamma_{GH} = \tan^{-1} \left(\frac{-T_{31}}{T_{33}} \right) \quad (2.5)$$

Where T refers to the transformation matrix T_{gh} , T_{31} is the projection of x_H onto Z_S , indicated by Zx in Figure 2.23b and T_{33} is the projection of z_H in z_S , represented by Zz in Figure 2.23b.

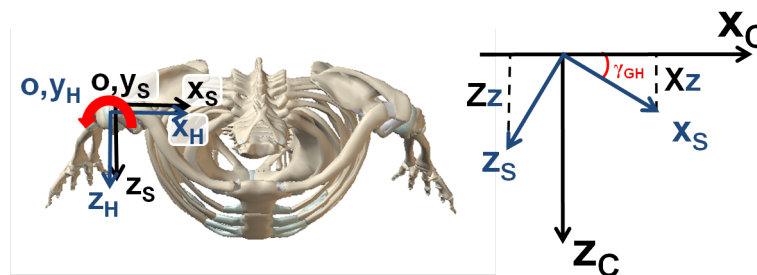


FIGURE 2.23: Two dimensional illustration of glenohumeral axial rotation in the transverse plane, where x_S, y_S, z_S denotes the axes of the scapula ACS while x_H, y_H, z_H denotes the axes of the humerus ACS (a) axial rotation defined as rotation around y_S and (b) external rotation angle

2.5.2 Scapula kinematics relative to JointTrack GCS

The program calculates the transformation matrix relating the scapula ACS to JointTrack GCS (T_s) from its absolute poses. Scapula rotations are resolved according to the Euler sequence of rotation Y-Z-X.

Retraction - protraction α_S

Retraction and protraction are scapula rotations around the coincident Y and y_S axes, as shown in Figure 2.24a. It is defined as the angle between x_S and X in the transverse plane using Equation (2.6). Protraction is defined as a positive angle while retraction is defined as a negative angle.

$$\alpha_{GH} = \tan^{-1} \left(\frac{-T_{31}}{T_{11}} \right) \quad (2.6)$$

Where T refers to the transformation matrix T_s , T_{31} is the projection of x_S onto Z, indicated by Zx in Figure 2.24b and T_{11} is the projection of x_S in X, represented by Xx in Figure 3.34b.

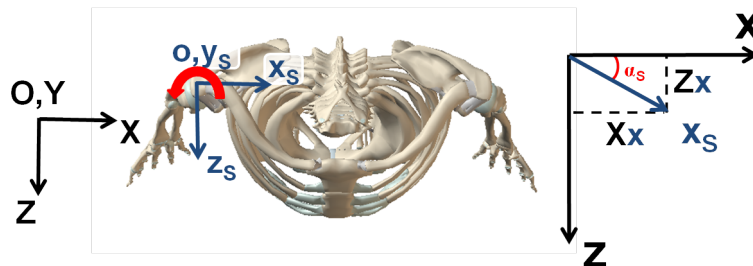


FIGURE 2.24: Two dimensional illustration of scapula retraction in the transverse plane, where x_S, y_S, z_S denotes the axes of the scapula ACS while X, Y, Z denotes the axes of JointTrack GCS (a) retraction - protraction is defined as rotation around z_S and (b) retraction angle

Medial - Lateral rotation β_S

Medial and lateral rotation is the scapula rotation around Z, as shown in Figure 2.25a. It is defined as the angle between x_S and X in the frontal plane using Equation (2.7).

$$\beta_{GH} = -\sin^{-1}(T_{21}) \quad (2.7)$$

Where T refers to the transformation matrix T_s and T_{21} is the projection of x_s onto Y , indicated by Yx in Figure 2.25b.

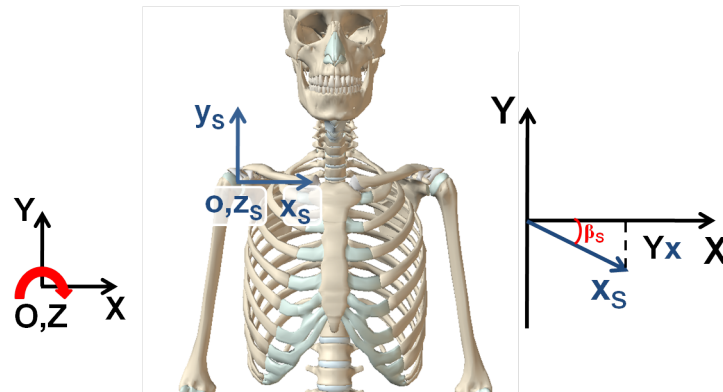


FIGURE 2.25: Two dimensional illustration of scapula lateral rotation in the frontal plane, where x_s, y_s, z_s denotes the axes of the scapula ACS while X, Y, Z denotes the axes of JointTrack GCS (a) plane of elevation defined as rotation around x_s and (b) lateral rotation angle

Anterior - posterior tilt γ_s

Anterior and posterior tilt is the scapula rotation around X , as shown in Figure 2.26a. It is defined as the angle between z_s and Z in the sagittal plane using Equation (2.8). Anterior rotation is defined as a positive angle while posterior rotation is defined as a negative angle.

$$\gamma_{GH} = \tan^{-1} \left(\frac{-T_{23}}{T_{22}} \right) \quad (2.8)$$

Where T refers to the transformation matrix T_s , T_{23} is the projection of z_s onto Y , indicated by Yz in Figure 2.26b and T_{22} is the projection of y_s in Y , represented by Yy in Figure 3.36b.

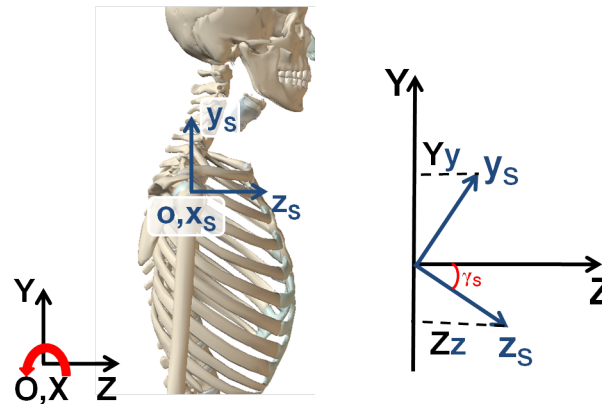


FIGURE 2.26: Two dimensional illustration of scapula anterior tilt in the sagittal plane, where x_s , y_s , z_s denotes the axes of the scapula ACS while X , Y , Z denotes the axes of JointTrack GCS (a) axial rotation defined as rotation around y_s and (b) posterior tilt angle

2.6 Methods

2.6.1 Measuring GH and scapula kinematics using image registration

Each model was registered three times for each elevation trial. GH joint rotations and translations were calculated for the complete arm movement trials. The three rotations defined the GH elevation, GH plane of elevation and axial rotation. GH joint translations represented the change of humerus ACS position in the scapula ACS. Translation along x_s was defined as medial-lateral, translation along y_s was defined as superior-inferior, and translation along and along the z_s was defined as anterior-posterior. The measured 3D kinematics of the humerus was analysed to determine humerus elevation relative to JointTrack GCS.

The average of the kinematics from the three-times-registered models and standard deviation (SD) were computed.

2.6.2 Comparison of image registration and motion analysis measurements

The motion capture data was analysed using the ISB convention described in Chapter 3. The IRT measurements were registered three times

The kinematics data from both the MA and the IRT was resampled over 100 points. When MA markers became occluded at high arm elevations, the image registration angles were discarded for the same resampled data to the MA to allow comparison of the results measured with both systems.

The convention used in JointTrack calculations defines elevation as a positive angle whereas ISB convention defines elevation as a negative angle. For consistency, the negative sign for the elevation angles computed using MA were modified to positive so that the sign convention was in agreement with that of JointTrack.

Whenever singularity occurred in the plane of elevation and axial joint rotations, the section of the waveform that presented it was discarded. This is because the steep slopes of the waveform do not represent true rotations for they reflect “gimbal lock” effects.

From each elevation trial, the peak and minimum joint angles as well as the ROM was recorded.

2.6.3 Repeatability

The repeatability of matching 3D models (created from MRI images) to distortion corrected fluoroscopic images was investigated. A single observer matched in three separate occasions the 3D models to a sequence of 2D images during scapion. The Kruskal-Wallis (non-parametric) test (SPSS 16.0) was used to detect significant differences between the registered poses from the three trials for both humerus and scapula Z translations relative to JointTrack coordinate

system. One way Analysis of Variance, ANOVA, (SPSS 16.0) was used to detect significant differences ($p < 0.05$) between the registered poses from the three trials for all other translations and rotations relative to JointTrack GCS.

2.7 Results

2.7.1 Measuring GH and scapula kinematics using image registration

GH joint kinematics during arm elevation and lowering in the frontal and scapular planes as well as axial rotation were calculated using IRT for the healthy female volunteer. Average humerus translations and rotations \pm SD relative to the scapula are plotted in Figure 2.27 to Figure 2.29 during abduction, scaption and axial rotation respectively.

Absolute scapula function was investigated during the elevation trials around JointTrack's X, Y and Z axes (Figure 2.30 to Figure 2.32 for abduction, scaption and axial rotation respectively). Error bars represent the SD.

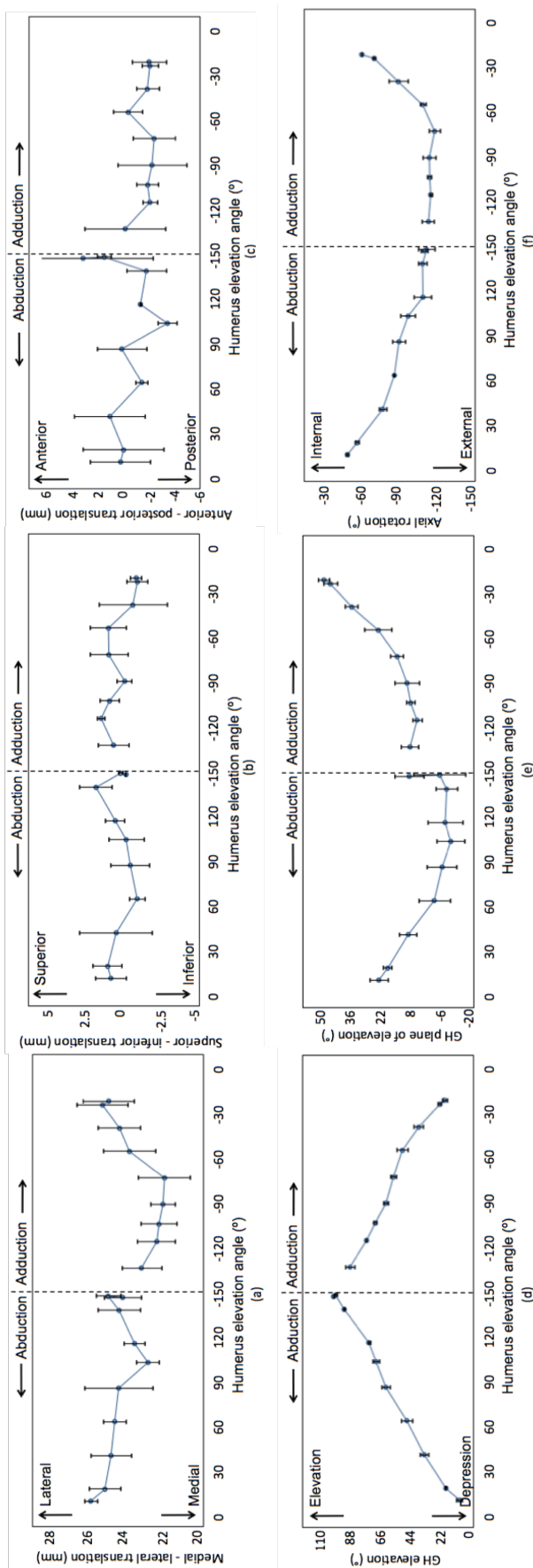


FIGURE 2.27: Average GH joint kinematics \pm SD during **abduction** calculated using IRT. (a) Medial (-) and lateral (+) translation, (b) superior (+) and inferior (-) translation, (c) Anterior (+) and posterior (-) translation, (d) Elevation (e) Plane of elevation and (f) internal (+) and external (-) rotation

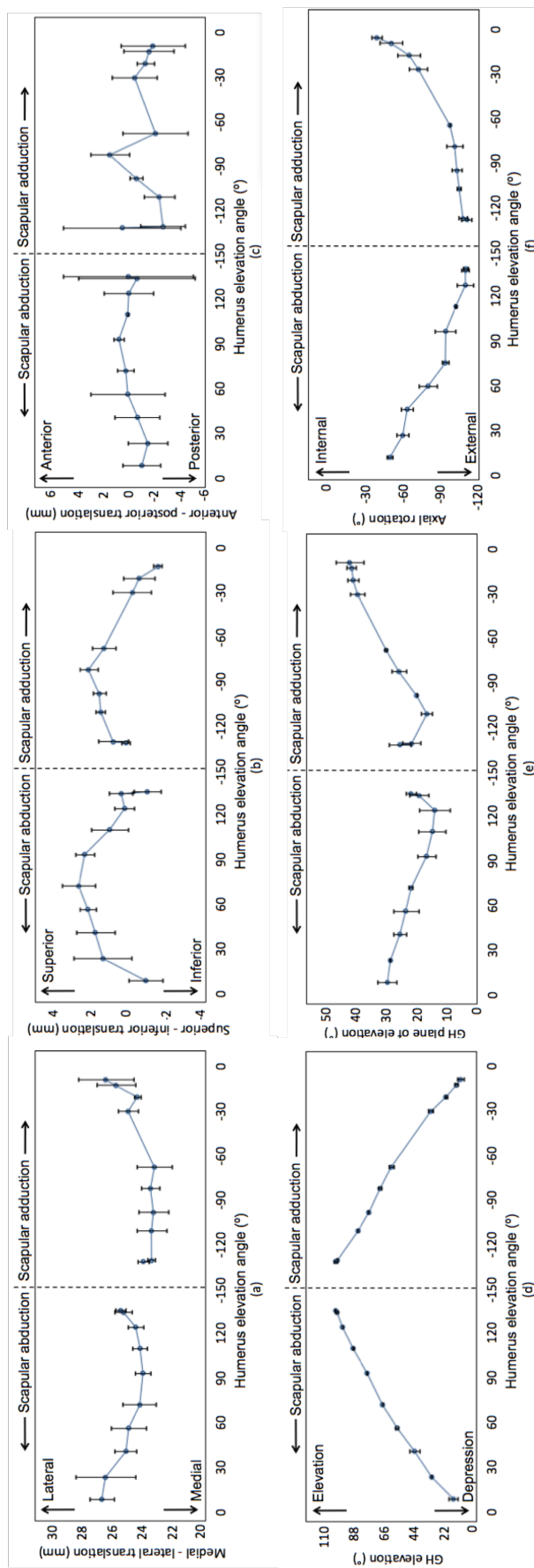


FIGURE 2.28: Average GH joint kinematics \pm SD during **scapion** calculated using IRT. (a) Medial (-) and lateral (+) translation, (b) superior (+) and inferior (-) translation, (c) Anterior (+) and posterior (-) translation, (d) Elevation (e) Plane of elevation and (f) internal (+) and external (-) rotation

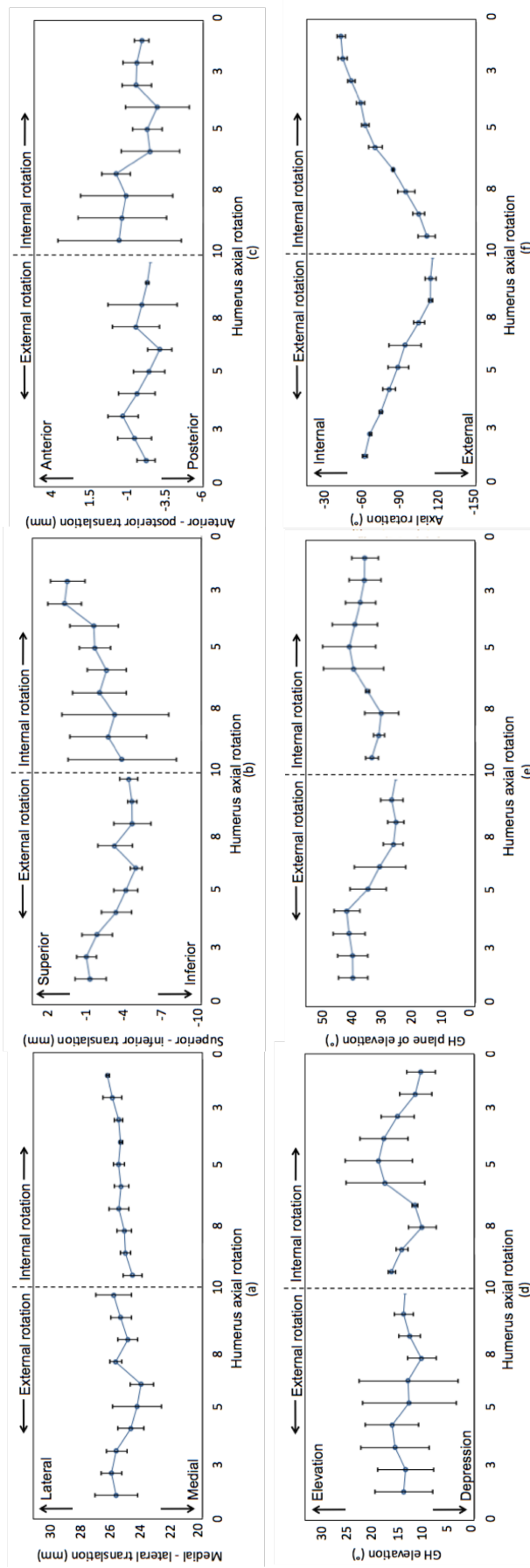


FIGURE 2.29: Average GH joint kinematics \pm SD during **axial rotation** calculated using IRT. (a) Medial (-) and lateral (+) translation, (b) superior (+) and inferior (-) translation, (c) Anterior (+) and posterior (-) translation, (d) Elevation (+) and depression (-) rotation, (e) internal (+) and external (-) rotation, (f) internal (+) and external (-) rotation

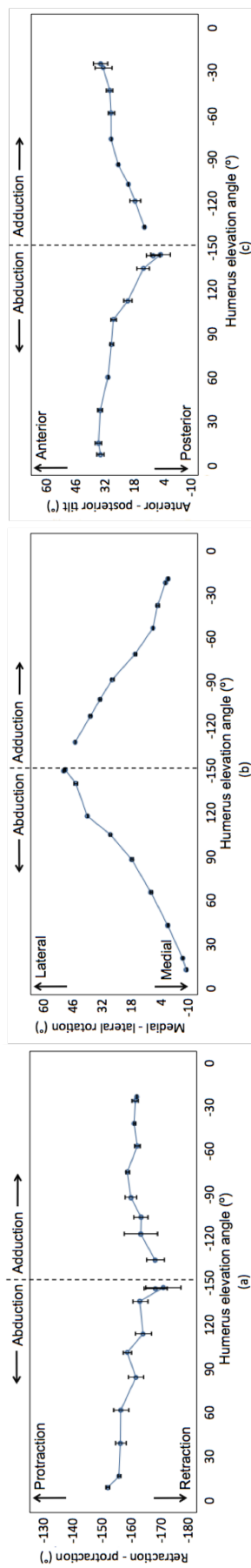


FIGURE 2.30: Average scapula kinematics \pm SD during **abduction** calculated using IRT. (a) Retraction (-) and protraction (+) rotation, (b) lateral (+) and medial (-) rotation, and (c) Anterior (+) and posterior (-) tilt

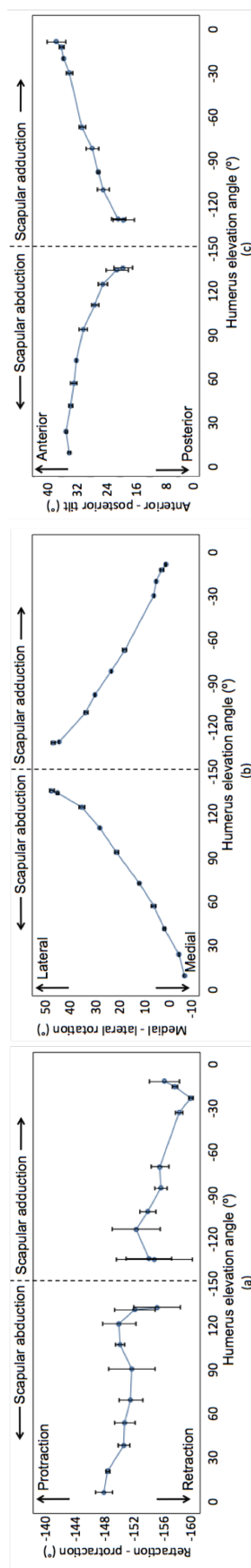


FIGURE 2.31: Average scapula kinematics \pm SD during **scaption** calculated using IRT. (a) Retraction (-) and protraction (+) rotation, (b) lateral (+) and medial (-) rotation, and (c) Anterior (+) and posterior (-) tilt

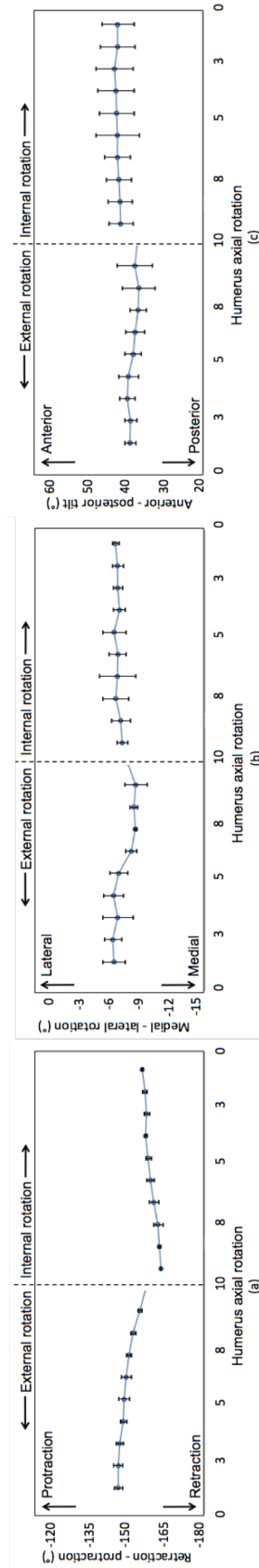


FIGURE 2.32: Average scapula kinematics \pm SD during **axial rotation** calculated using IRT. (a) Retraction (-) and protraction (+) rotation, (b) lateral (+) and medial (-) rotation, and (c) Anterior (+) and posterior (-) tilt

2.7.2 Comparison of image registration and motion analysis measurements

Differences between MA and IRT are compared in Table 2.5 through to Table 2.7 for the three arm elevation and lowering trials for the healthy female volunteer.

TABLE 2.5: Shoulder kinematics measured with the MA system and with IRT for a healthy participant during **abduction**. The greatest ROMs are highlighted

Elevation trial	Variable	X	MA&skin	IRT
Abduction	Plane of elevation	MAX	5.47	24.72
		MIN	-19.98	-6.96
		ROM	25.45	31.68
	Elevation	MAX	66.81	63.10
		MIN	15.75	8.31
		ROM	51.06	54.79
	Axial rotation	MAX	-5.00	-50.13
		MIN	-31.89	-91.13
		ROM	26.89	41.00
Adduction	Plane of elevation	MAX	8.97	53.49
		MIN	-14.90	19.71
		ROM	23.88	33.78
	Elevation	MAX	53.66	67.971
		MIN	10.91	21.88
		ROM	42.75	46.09
	Axial rotation	MAX	-31.26	-69.91
		MIN	-52.62	-111
		ROM	21.36	41.09

TABLE 2.6: Shoulder kinematics measured with the MA system and with IRT for a healthy participant during **scaption**. The greatest ROMs are highlighted

Elevation trial	Variable	X	MA&skin	IR
Scap. Abduction	Plane of elevation	MAX	28.13	26.68
		MIN	13.27	13.74
		ROM	14.86	12.94
	Elevation	MAX	94.29	98.40
		MIN	19.07	15.76
		ROM	75.21	82.64
	Axial rotation	MAX	-19.85	-58.01
		MIN	-51.79	-112.96
		ROM	31.94	54.95
Scap. Adduction	Plane of elevation	MAX	35.83	47.66
		MIN	12.36	18.58
		ROM	23.47	29.09
	Elevation	MAX	80.99	78.7
		MIN	20.82	11.68
		ROM	60.18	67.02
	Axial rotation	MAX	-26.38	-45.97
		MIN	-49.69	-104.99
		ROM	23.29	59.02

TABLE 2.7: Shoulder kinematics measured with the MA system and with IRT for a healthy participant during **axial rotation**.
The greatest ROMs are highlighted

Elevation trial	Variable	X	MA&skin	IR
External rotation	Plane of elevation	MAX	–	45.10
		MIN	–	24.26
		ROM	–	20.84
	Elevation	MAX	6.65	16.96
		MIN	3.25	9.84
		ROM	3.41	7.12
	Axial rotation	MAX	–	–63.21
		MIN	–	–133.08
		ROM	–	69.87
Internal rotation	Plane of elevation	MAX	–	41.33
		MIN	–	27.09
		ROM	–	14.24
	Elevation	MAX	14.07	18.93
		MIN	6.35	9.79
		ROM	7.72	9.14
	Axial rotation	MAX	–	–45.37
		MIN	–	–127.47
		ROM	–	82.10

2.7.3 Repeatability

Absolute humerus and scapula poses relative to JointTrack GCS (rotations and translations) were computed during scaption. The average poses were plotted in Figure 2.33. Error bars represent the SD of three model matching trials.

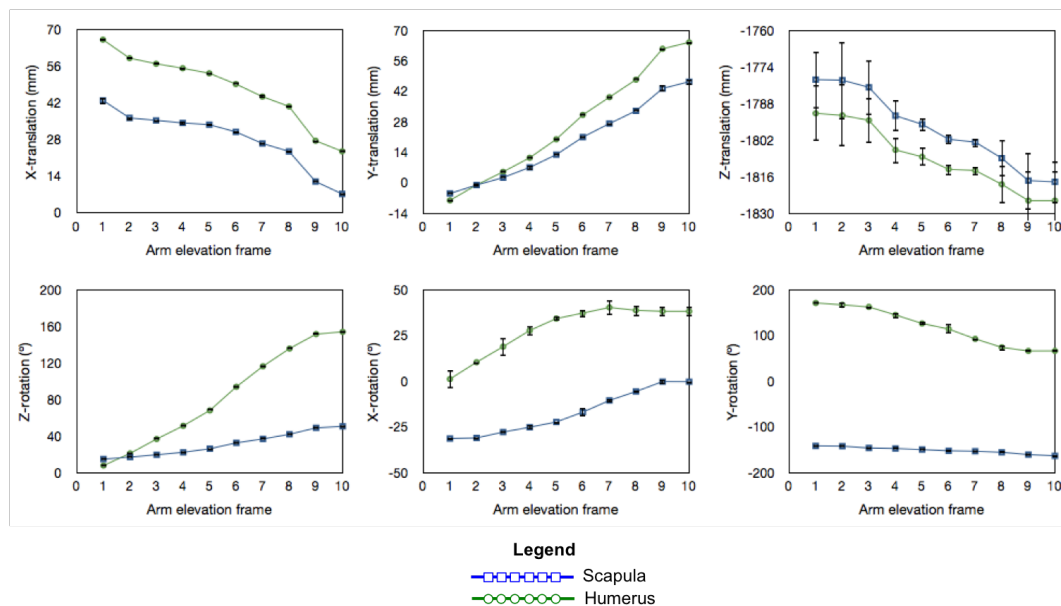


FIGURE 2.33: Assessing MRI model registration repeatability from JointTrack absolute poses during scaption. Translations along JointTrack's (a) X, (b) Y and (c) Z axes and rotations around JointTrack's (d) X, (e) Y, and (f) Z axes

2.8 Discussion and Conclusions

IRT were developed in the current study to measure GH joint kinematics using dynamic single-plane fluoroscopy. The technique used was based on the original protocol developed by Banks and Hodge [44] at the University of Florida to measure knee joint kinematics. Simultaneous motion capture measurements following ISB recommendations [73] were performed to investigate the errors associated with the Cardiff measurement protocol.

Accurate registration of the 3D bone models to the fluoroscopic images was only possible with the female volunteer's data. The male volunteer's model could not

be matched to the fluoroscopic images. It is believed that the models were not accurate enough for registration, mainly due to the MRI image quality used to segment the models and different fluoroscope settings used.

2.8.1 Measuring GH and scapula kinematics using image registration techniques

Full kinematic description of the GH joint was obtained for the movement trials using IRT. From Figure 2.27 and Figure 2.28, the GH joint was recorded elevating $92.1 \pm 2.3^\circ$ and $85.7 \pm 1.6^\circ$ during abduction and scaption respectively. GH elevation was responsible for the first 40° of arm elevation, with small scapula lateral rotation angles recorded during this phase of motion (under 9° for both abduction (Figure 2.30b) and scaption (Figure 2.31b) elevations). Beyond 40° , arm elevation appears to be a combined movement of GH elevation and scapula lateral rotation.

The choice for describing scapula rotations with respect to JointTrack's GCS means that an absolute orientation of the segment was obtained. During arm elevation, the scapula retracted ($18.8 \pm 2.8^\circ$ and $7.5 \pm 1.8^\circ$ during abduction and scaption respectively), tilted posteriorly ($29.4 \pm 2.4^\circ$ and $15.8 \pm 1.3^\circ$ during abduction and scaption respectively) and rotated laterally ($58 \pm 1^\circ$ and $54 \pm 2^\circ$ during abduction and scaption respectively). The pattern of elevation agrees with what other researchers have previously measured [19, 27].

During axial rotation measurements, the volunteers were asked to maintain their arm by the side of the body. The GH externally rotated $54.4 \pm 5.1^\circ$ (Figure 2.29) and maintained the plane of elevation at $16.5 \pm 5.1^\circ$ and elevation $5.8 \pm 5.2^\circ$. Small scapula rotations were recorded (Figure 2.32), in the order of $2.3 \pm 0.9^\circ$ lateral rotation and $3.0 \pm 3.1^\circ$ posterior tilt. $11.1 \pm 1.9^\circ$ scapula retraction was also measured.

The position of the humerus ACS was evaluated along the three scapula ACS axes. Humeral head translation was measured towards the glenoid centre

(3 ± 0.9 mm medially, 2.7 ± 0.9 mm inferiorly and then superiorly and 6.7 ± 2 mm posteriorly) during abduction (Figure 2.27) and (2.8 ± 0.9 mm medially, 3.6 ± 0.9 mm superiorly and then inferiorly and 5.3 ± 2.1 mm anteriorly) during scaption (Figure 2.28). The centering of the humeral head is believed to provide “maximum joint congruency for optimal shoulder function and longevity” [50].

Other studies have also measured GH joint translations on healthy volunteers using imaging techniques [40, 50]. Graichen et al measured 1.2mm inferior GH translation and 1.62mm posterior translation during abduction [40] while Nishinaka et al measured 1.7mm superior translation during abduction [50]. Discrepancies between the image registration results and kinematics outputs obtained by other research groups may be explained by the different measurement devices used to collect the shoulder data as well as differences in the analysis of the data. These differences ranged from the anatomical landmarks used to create the segments' ACSs as well as the location of the origin.

Translations along the z-axis (anterior-posterior) in the current study are greater than expected and there does not seem to be a clear pattern of motion. This could be a result of errors in the registration process which are expected from single-plane fluoroscopy.

2.8.2 Comparison of image registration and motion analysis measurements

To investigate the errors commonly associated with MA, a comparison between the kinematics outputs from the MA measuring system and IRT was performed. However, GH joint kinematics could not be measured with MA at arm elevations ranging beyond 70° to 90° since the retro-reflective markers became occluded with the fluoroscope examination table during arm elevations. Therefore, comparisons between the two methods during abduction (Table 2.5) and scaption (Table 2.6) were performed up to the last point where MA was recorded and.

GH motion during humerus axial rotation was recorded with both methods for the entire movement trial (Table 2.7).

Greater GH joint elevation was recorded with IRT (54.8° and 82.6° for abduction and scaption respectively) compared to MA (51.1° and 75.2° for abduction and scaption respectively). Discrepancies between the two measurement systems appears larger for the scaption recordings. This is because greater humerothoracic angles could be measured since the markers became occluded beyond 90° of arm elevation compared to 70° during abduction. Skin artifact errors would thus affect the scaption measurements more than the abduction measurements since greater arm elevations were achieved during scaption. Furthermore, differences between IRT and MA recordings in GH joint plane of elevation (6.7° and 1.9° abduction and scaption respectively) and axial rotation (24.1° and 23.0° abduction and scaption respectively) were measured.

During axial rotation measurements, similar GH joint elevation angles were measured with the two measurement systems (Table 2.7), with maximum difference of 3.7° measured during external rotation. The GH joint plane of elevation and axial rotations measured with the MA system is subject to “gimbal lock” errors and so are not reported.

Discrepancies in measured rotations between MA and IRT can be attributed to factors related to differences in the analytical approach as well as the errors associated with the techniques:

The choice of anatomical landmarks used to create the embedded scapula and humerus ACSs affects the results. All of the identified landmarks used to create the ACSs were different for the two methods. According to Zatsiorsky, results using different axes systems may differ substantially because the reference frames are slightly rotated and translated relative to each other [1].

The GH joint CoR was estimated through MRE for the MA measurements and by fitting a sphere in the humerus' head for the IRT measurements. The centre

of the sphere was considered the CoR. Differences in the estimated GH joint positions have been previously recorded by up to 2cm [77]; with the sphere fitting method considered more accurate in estimating GH position than regression equations [77, 80].

Different rotation sequences used to analyse the kinematics data may also be responsible for discrepancies between MA and image registration measurements. MA uses the ISB recommended YXY Euler angle sequence of rotation while IRT uses the ZXY Cardan angle convention. Phadke et al [138] observed a 24° difference between YXY and XZY sequences when analysis GH rotations.

Plane of elevation and axial rotation rotations are susceptible to singularity near 0 and 180° of arm elevation using the YXY sequence of rotation. Recent MA studies recommend the use of the ZXY sequence of rotation to measure GH function [138–140] during humerus elevation in abduction and scaption. As a result, GH first and third rotations of humerus axial rotation measured with MA techniques could not be measured since the arm was hanging by the side of the body; and the technique cannot accurately measure axial rotation and plane of elevation at this arm elevation [138].

The radio-opaque markers created with the Zinc coat allowed for the visual qualitative assessment of marker placement for MA measurements. It was thus possible to observe that the AI scapula marker was not accurately placed on the bony landmark, but instead was placed inferiorly. Bony landmark identification errors lead to inaccuracies in the MA measurements with de Groot measuring 3° variance during a inter-individual palpation study on the shoulder complex [104].

MA measurements are also sensitive to skin movement artefact. The scapula moves significantly under the skin [18, 94, 104, 121] therefore skin markers are not fully representative of scapula movement. Scapula movement under the skin was observed with the radio-opaque markers, therefore skin artifact errors are to be expected in the MA results. Furthermore, the humerus marker cluster used in MA measurements also appears to introduce errors due to skin

artefacts. The markers are fixed to muscle insertions and the belly of the biceps, which lead to the underestimation of GH axis rotation.

The IRT is also subject to measurement and computational errors. The 3D models were created from MRI scans. Discrepancies between the original bone and the one created from MRI scans is considered as noise. Small motions of participants during scanning can degrade boundary resolution and spatial integrity of the resulting models. This is of particular concern when sequences requiring long scan times are used, when the anatomy of interest is affected by normal breathing movements, and when immobilisation of the area is not easily accomplished.

MRI model-based shape matching provides kinematic measurements with sufficient certainty to assess normal GH function. MoroOka compared bone models produced from CT and MRI data and found that in some areas, the surfaces differed by several millimetres. Therefore, different shape matching performances between the two models are expected. Shape registration based motion measurement requires sub-millimetre model accuracy for many clinically relevant measurement scenarios [132].

Furthermore, human bones are difficult to identify in fluoroscopic images since they are weaker contrast, resulting in reduced accuracy [123]. A canny edge detection was used to aid in identifying the silhouette of the bone on the fluoroscopic images. However, the tool was not suitable for the scapula silhouette since there was a low object to background contrast as well as clutter and occlusion [127] caused by the ribs and clavicle.

Single-plane fluoroscopy is sensitive to translations perpendicular to the image plane. Biplane would give more accurate results. However, in addition to a greater radiation dose associated with the measurement system, it also constrains the movements further.

2.8.3 Repeatability

Both the scapula and humerus segments presented similar patterns of translation along JointTrack's X, Y and Z axes. The translations correspond to not only to translations of the segments due to the natural movement, but also due to the volunteer experiencing a certain amount of swaying or moving during arm elevation. During the trial, the volunteer moved towards the left (Figure 2.33a), superiorly (Figure 2.33b) and closer to the image intensifier (Figure 2.33c).

The starting position of the translation along the three axes is indicative of the centering of the participant's shoulder in the image intensifier. Therefore, the large Z translation shown in Figure 2.33c can be explained by the distance between the tested shoulder and the image intensifier.

Small scapula rotations were measured in the first half of the registered frames, whereas humerus rotations were measured from the beginning of motion (Figure 2.33 d, e and f). This can be explained by the fact that GH motion (humerus relative to the scapula) is responsible for the first 50° of humerus elevation relative to the thorax. Beyond that, humerus elevation is a result of the combined movement of the GH joint and the scapulothoracic articulation.

One way ANOVA was used to investigate significant differences between the registration poses for all rotation and translations values except for Z-axis translations. For these translations, the Kruskal-Wallis non-parametric test was used since the data violated the equal variance assumption. No significant differences in the registration trial was detected between the three-times-registered poses. Therefore, 3D bone models of the scapula and humerus rendered from MRI scans may be of sufficient accuracy to perform image registration. The position variability of registering the models in the Z axis could then be attributed to the single-plane fluoroscopic images.

This study is laying the grounds for enabling comparison of image registration methods and motion capture systems to evaluate the errors associated with motion capture when measuring GH joint kinematics. Marker occlusion needs

to be addressed in order to obtain an appreciation of the errors for the entire movement trials.

2.9 Study limitations and recommendations for future work

The two measurement techniques used different axis systems and different decomposition formats. To perform a direct comparison between the two systems, it would be necessary to embed ACS calculated from the same anatomical landmarks as well as to use the same decomposition format to obtain the kinematics outputs.

The retro-reflective markers were occluded by the table attached to the fluoroscope. It would be highly desirable to take the table off the fluoroscope prior to recording GH motion. If it is not possible, perhaps using a different fluoroscope would be necessary if simultaneous motion capture and image registration recordings are desirable.

A circumduction movement recorded with motion capture data would allow the estimation of the GH joint CoR using the instantaneous helical axis (IHA) method. This is desirable since the GH joint positions estimated with the IHA and with a sphere fitted on the humerus head are not statistically different [81].

A shoulder coil was not used to obtain the MRI images of the humerus and scapula. This may have resulted in reduced accuracy of the 3D models. An especially dedicated shoulder coil should be used to obtain the MRI data in order to obtain better quality images for segmentation.

Variations in the contrast of fluoroscopic images was an important issue that should be addressed. The image contrast at high elevations made registration difficult since anatomical details of the bones were not easily distinguishable. It would thus be desirable to take an image of the static shoulder prior to recording

arm elevation movements and fix the fluoroscopy so that the contrasts maintains constant throughout the movement trials.

This work represents the initial stages of developing an accurate protocol for measuring dynamic GH motion during physiological movements. A controlled validation study should be carried out to assess the system's accuracy. This could be performed in a cadaveric study or using animal bones. A jig would need to be constructed in order to perform controlled GH joint movements.

Finally, the comparison of the two systems was only made when recording arm movement for one healthy volunteer. Therefore, meaningful statistical analysis to characterise the discrepancies between skin fixed markers using a motion capture technique and IRT is limited. The sample size of healthy participants measured with the developed IRT needs to be increased. It would also be beneficial to include shoulder replacement patients since the implant matching to the fluoroscopic image should be easier than with natural bones. Furthermore, the arm elevation trials could be constrained to 2s only so that 3 elevation trials per movement can be recorded.

Chapter 3

The Cardiff protocol for measuring and calculating shoulder complex function

The previous Chapter described an accurate image registration study which made it possible to investigate errors in the motion analysis system. It is necessary to understand how these errors affect the kinematics measurements of the shoulder complex, more specifically of the glenohumeral joint, and to attempt to reduce the errors. This Chapter details the data collection and analysis protocols developed and used at Cardiff University to measure healthy and patient shoulder complex kinematics.

Initial work on the shoulder complex within the University was undertaken following a suggestion by a collaborating surgeon from a study on the classification of pathology of subjects with osteoarthritic (OA) knee function [141]. The surgeon indicated that the method would be beneficial when applied to the shoulder since there is a lot more *grey areas* and an objective classification would aid surgeons in treatment and management of injuries or pathologies. Thus Jones et al [142] developed a measurement protocol to study movement of the

shoulder complex through a motion analysis (MA) based technique following International Society of Biomechanics (ISB) recommendations [73]. Healthy volunteers were recorded during dynamic physiological ranges of motion (ROM). Three 3rd year undergraduate students adopted shoulder projects for their final year dissertations. Amy Bowles (year 2005 to 2006) helped develop the original measurement protocol used in [142] to measure dynamic movements using skin markers attached to bony landmarks. Lindsay Stroud (year 2006 to 2007) introduced the Newcastle Scapula Locator [18], to measure scapula function more accurately, to the measurement protocol. Todd Burrows (year 2007 to 2008) investigated the use of a Polhemus electromagnetic system to measure shoulder function. Dr. Barry Lovern's PhD (2006 to 2010) expanded the study to include shoulder patients diagnosed with either shoulder injury or pathology as well as developing the use of an acromium marker cluster to measure dynamic scapula movements. Finally, Nicholas Ferran's Orthopaedic Engineering MSc dissertation (2008-2009) aimed to measure glenohumeral (GH) joint translations on healthy volunteers and multidirectional instability patients.

Cardiff University School of Engineering has a state of the art Qualisys Motion Capture system (Qualisys, Sweden). The South East Wales Research Ethics Committee and the NHS R&D Department granted ethical approval for the recruitment of healthy participants and patients presenting shoulder pathology or instability to the MA Laboratory to measure their shoulder function (Study details: Assessment of shoulder function in healthy and pathological subjects using three dimensional motion analysis techniques. REC number: 08/WSE02/37). ISB recommendations for the upper extremity [73] were adopted for this study. Their aim is to encourage communication between research groups. Bony landmark identification, segments' coordinate systems and Euler and Cardan angles sequence of rotations are followed according to the proposed ISB standards.

3.1 Healthy volunteers and patients recruitment

Healthy volunteers with no previously identified shoulder injuries, disability or pain are chosen as part of the standard recruitment procedure for this study. They are approached within the University and invited to take part in the shoulder MA trial. An Information Sheet with details of the study is provided to the volunteers prior to the Laboratory session.

Suitable patients for the trial are selected and approached by Mr. Richard Evans (an Orthopaedic Consultant from University Hospital of Wales) or a member of his team during follow-up clinics. Once the patient has given verbal consent to be contacted by researchers at Cardiff University School of Engineering, a phone call is made to provide them with further information about the trial. An information pack, consisting of an Information Sheet with details of the study and an explanation of the trial in the MA Laboratory, the Shoulder Oxford Questionnaire, and a map of how to get to the Engineering Department are sent to the patient's home address. The patients are given a week to read the information pack and make a decision as to whether they would like to participate in the study or not. They are contacted once more to arrange a date for testing. The patient information pack and consent form can be found in Appendix C.

3.2 Measurement system

The MA Laboratory at Cardiff University consists of an eight camera Qualisys ProReflex MCU array (Qualisys, Sweden). The cameras emit pulses of infrared light at 120Hz which are reflected back into the camera lenses from retro-reflective markers attached to bony landmarks or marker clusters attached to segments.

Three-dimensional (3D) marker positions are obtained from the triangulation of the two-dimensional (2D) marker positions recorded by each camera. Two

or more cameras must record a marker in a calibrated camera layout for the Qualysis software to perform the triangulation. A map of the camera layout for shoulder complex measurements is shown in Figure 3.1. The cameras are firmly mounted on tripods to achieve the desired height positions. Synchronised QTM and video recordings are taken for visual feedback and qualitative analysis.

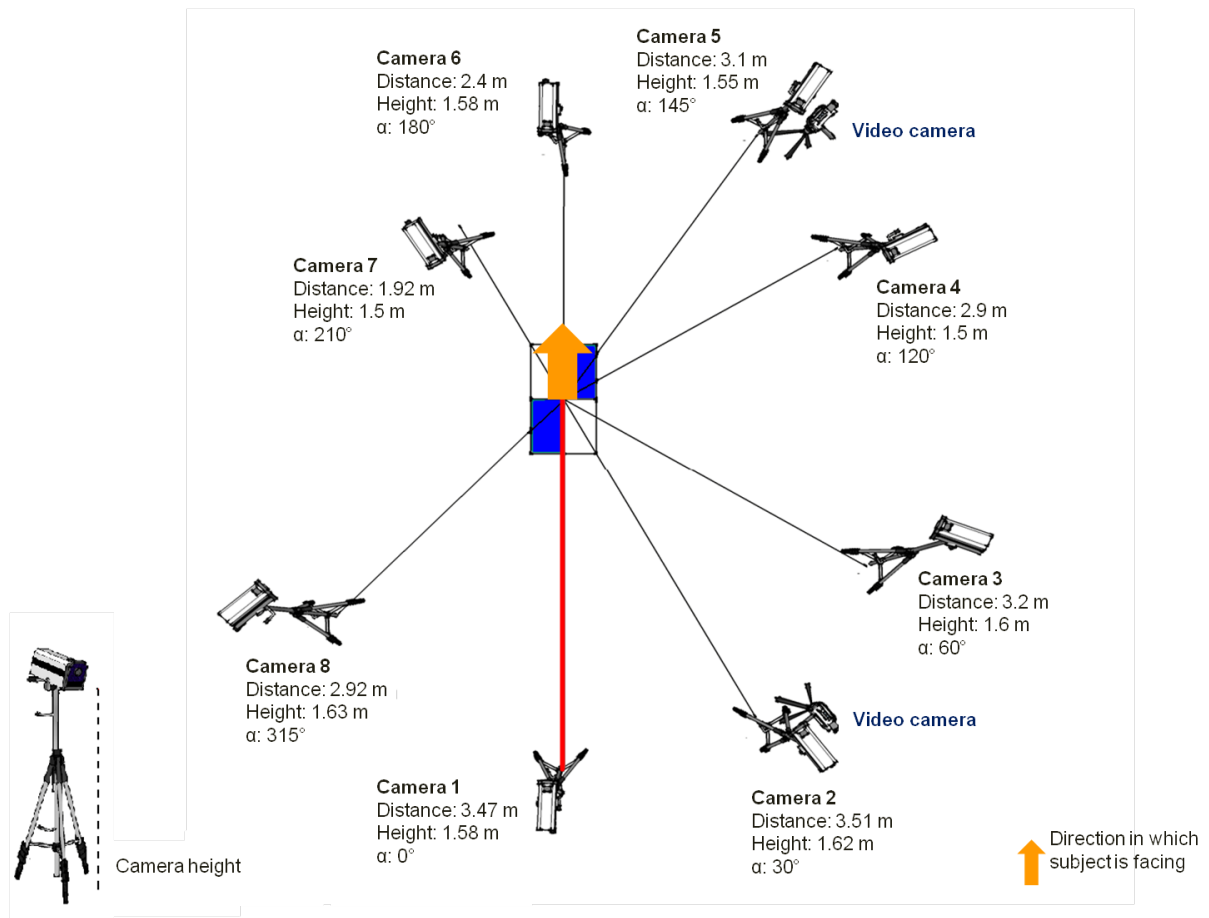


FIGURE 3.1: Camera layout for shoulder complex studies

Qualisys' proprietary tracking software, Qualisys Track Manager (QTM), is used to record and identify marker trajectory data.

The QTM software configuration and settings are changed in the Workspace Options. A summary of the settings used in the study is shown in Table 3.1.

TABLE 3.1: Workspace configuration

Capture rate	60 Hz
Maximum number of markers	100
Calibration settings	Wand calibration Wand kit 750 mm Exact wand length 750.9 mm Coordinate system
Tracking settings	Bounding box X ± 1500 mm Y ± 1500 mm Z ± 1500 mm

3.3 Data collection

Participants are asked to attend a session at the Cardiff University School of Engineering MA Laboratory. The healthy volunteer's dominant arm is tested. For patients, their injured or pathological shoulder is tested first to ensure that complete measurements for the shoulder are recorded should the patient decide to withdraw from the trial. The contralateral shoulder is then tested.

Sessions take on average three hours. Regular rests and beverages are provided.

The data collection protocol is summarised in Figure 3.2. A more detailed description of the method follows the diagram.

3.3.1 System calibration

A system calibration is necessary to establish the global coordinate system (GCS) within the Laboratory. A wand calibration with a 30s capture period and 100Hz capture frequency is performed prior to the participant's arrival to the Laboratory. This calibration method uses a two part kit: an L-shaped reference structure and a calibration wand, both shown in Figure 3.3.

The 'L' shaped reference structure is placed on a 1m high stool where the subject to be measured would be positioned (Figure 3.4) so that all of its markers

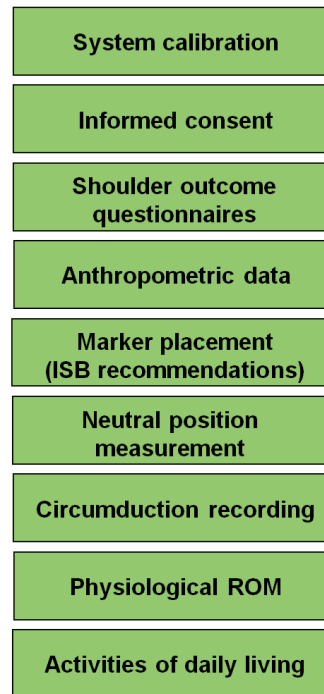


FIGURE 3.2: Summary of the motion analysis data collection protocol

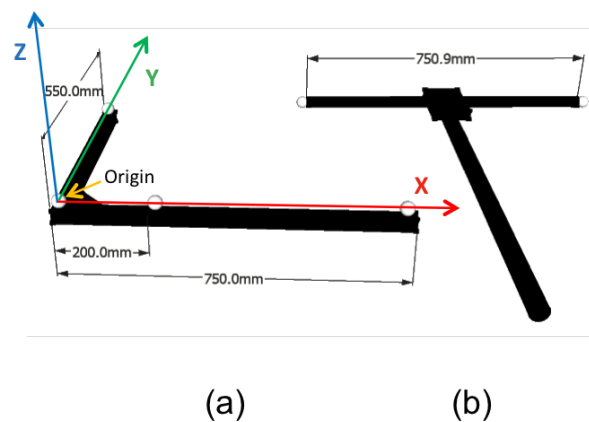


FIGURE 3.3: Qualisys 750mm calibration kit:
(a) 'L' shaped frame and (b) calibration wand

are seen in the 2D view of every camera. The structure has four reflective markers with known and fixed positions. The calibration frame defines the GCS as follows:

- The origin is defined by the marker at the corner of the 'L' shaped frame.
- The X axis is on the long axis of the frame, pointing to the right.
- The Y axis is the short axis on the frame, pointing forwards.

- The Z axis is established from the cross-product of the other two axes, pointing upwards.



FIGURE 3.4: Laboratory set up for wand calibration

The calibration wand is moved inside the measurement volume in all three directions to ensure that all axes are properly scaled. The movement of the wand is performed in a smooth and consistent motion while the cameras record the movement of the two markers on the wand that are 750mm apart. The cameras' position and orientation is obtained by evaluating the cameras' view of the wand during the calibration.

3.3.2 Informed consent

An informal interview is conducted at the start of the laboratory session. During the interview, the participant's date of birth, age and arm dominance are documented in the protocol sheet. When testing patients, details of the pathology or the mechanism of the sustained injury as well as the treatment received are also recorded.

Participants are given the opportunity to ask questions and written informed consent is obtained.

3.3.3 Shoulder outcome questionnaires

The shoulder outcome questionnaires are sent out to the patients only. The questionnaires rely on the patient's subjective assessment of pain and activities of daily living impairment over the previous 4 weeks. Patients with shoulder pathology or injury, excluding GH joint dislocation, are sent the *Shoulder Oxford Score* while GH joint instability patients are sent the *Oxford Shoulder Instability Score*. Patients rate the extent to which their injury or pathology has affected their daily living over 12 questions, each scored between 0 and 4. The questionnaires accumulate to a total score with a maximum value of 48.

3.3.4 Anthropometric measurements

Once the participants have signed the consent form, their anthropometric data is collected. The subject's height (m) is measured with a Seca Ltd. wall mounted measuring tape. Weighing scales are used to measure the participant's weight (kg). Trunk circumference and upper arm circumference, both when the arm is flexed and when it is extended, are measured with measuring tape (cm) to provide an indication of muscle mass.

3.3.5 Marker placement

During the landmark identification process, subjects are asked to adopt the neutral position (NP), that is standing up straight, elbows flexed at 90°, hands pronated. The bony landmarks are identified by means of palpation. A retro-reflective marker is attached onto the landmark using double-sided tape.

The identified bony landmarks and their anatomical description are summarised in Table 3.2 and represented graphically in Figure 3.5. Additionally, a humerus marker cluster (HMC) is attached to the upper arm with individual markers on

the deltoid insertion (DI), the belly of the brachius (BB) and the brachius insertion (BI).

TABLE 3.2: Marker placement according to ISB recommendations

Segment	Landmark	Description of location
Thorax	C7	Spinous process of the 7 th cervical vertebra
	T8	Spinous process of the 8 th thoracic vertebra
	IJ	Deepest point of Incisura Jugularis
	PX	Processus Xiphoideus, most caudal point on the sternum
Clavicle	SC	Most ventral point on the sternoclavicular joint
	AC	Most dorsal point on the acromioclavicular joint
Scapula	TS	Trigonium Spinae, the midpoint of the triangular surface on the medial border of the scapula in line with the scapular spine
	AI	Aungulus Inferior, most caudal point of the scapula
	AA	Angulus Acromialis, most laterodorsal point of the scapula
	PC	Most ventral point of processus coracoideus
Humerus	GH	Glenohumeral joint rotation centre, estimated using the helical axis method
	EL	Most caudal point on lateral epicondyle
	EM	Most caudal point on medial epicondyle

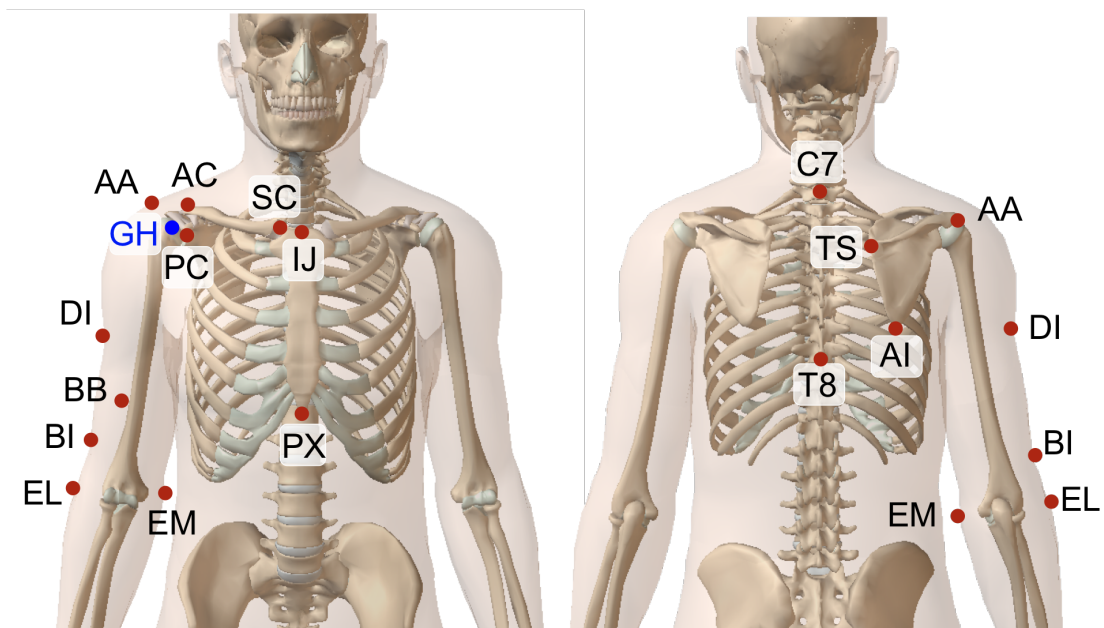


FIGURE 3.5: Marker placement according to ISB recommendations (adapted from [2])

A scapula locator (SL), developed at Newcastle University, is used in the measurement protocol to accurately track scapula movement during static arm elevations. The SL consists of a Perspex (Perspex, Ltd.) device with three palpating legs (Figure 3.6). The legs are adjusted along slots on the base plate to

match and have the best contact with the individual's scapula bony landmarks [18]. The legs are fixed in place by tightening the screws on them to keep a fix relationship between the landmarks. A retro-reflective marker is attached on top of each peg to record the SL's position. The SL is held in place by the observer during each static measurement.

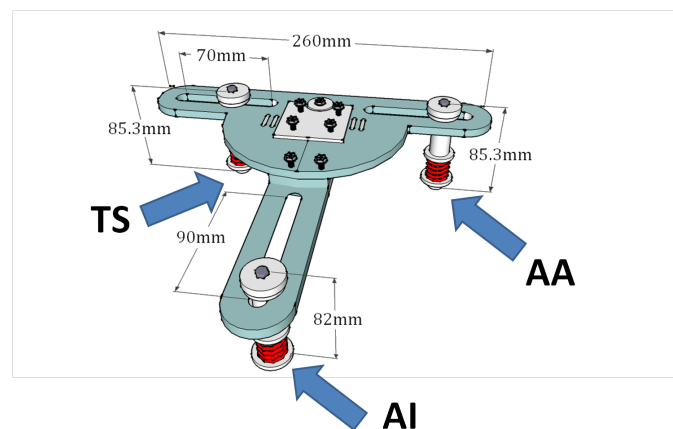


FIGURE 3.6: A schematic of the scapula locator

An acromium marker cluster (AMC), shown in Figure 3.7, was built in the Mechanical Workshop at the School of Engineering. The AMC enables unconstrained 3D measurements of scapula kinematics during dynamic arm movements. It consists of a 10mm diameter plastic base and three carbon fibre rods with retro-reflective markers attached onto them. The AMC can be accurately placed in the flat part of the acromium using Velcro. Its accuracy has been reported up to 90° of arm elevation using optoelectronic systems [30] and up to 120° of arm elevation using an electromagnetic tracking device [94, 100].

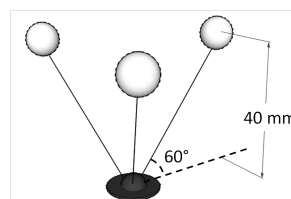


FIGURE 3.7: A schematic of the acromium marker cluster

3.3.6 Neutral position measurement

During the one second NP measurement, subjects maintain both arms by the side of the body with the elbows flexed to 90°, hands pronated (Figure 3.8). During the recording, the system measures the positions of the HMC, the AMC and the individual markers attached to bony landmarks in the GCS.

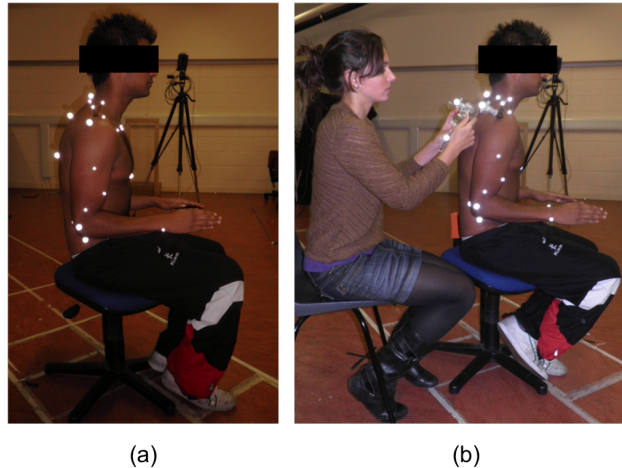


FIGURE 3.8: Neutral position measurement (a) with skin fixed markers on scapula landmarks and (b) with the scapula locator

The NP measurement is repeated when any marker falls off and has to be repositioned for fear that the marker changes position.

3.3.7 Circumduction recording

A 10s recording of the subject performing passive circumduction is made. The observer moves the participant's humerus in small circular movements while applying pressure on the scapula to minimise its movement, as shown in Figure 3.9. During the measurement, the system records the movement of the scapula tracking markers as well as the movement of the HMC.



FIGURE 3.9: Circumduction recording

3.3.8 Physiological range of motion

The physiological ROM is evaluated during static and dynamic trials starting with the arm hanging by the side of the body up to 180° and 120° of arm elevation for healthy participants and shoulder patients respectively:

- During the static trials, a one second recording is taken with the observer holding the SL over the scapula bony landmarks. The AMC is also used to record scapula kinematics. A frame is used to standardise static positions at 20° intervals.
- During the dynamic trials, scapula kinematics is recorded with skin markers attached to bony landmarks as well as with the AMC.

Participants are instructed to perform bilateral physiological arm elevation in abduction, scaption and flexion (Figure 3.10) in a seated, upright position (their backs unsupported) with elbows fully extended. Throughout arm abduction and scaption, subjects maintain a supinated arm (the palm of the hands is facing forwards as the arm is being elevated). During flexion elevation measurements, subjects perform the movements with the forearm pronated (palm of hands facing backwards, downwards and forwards as the arm is being elevated).

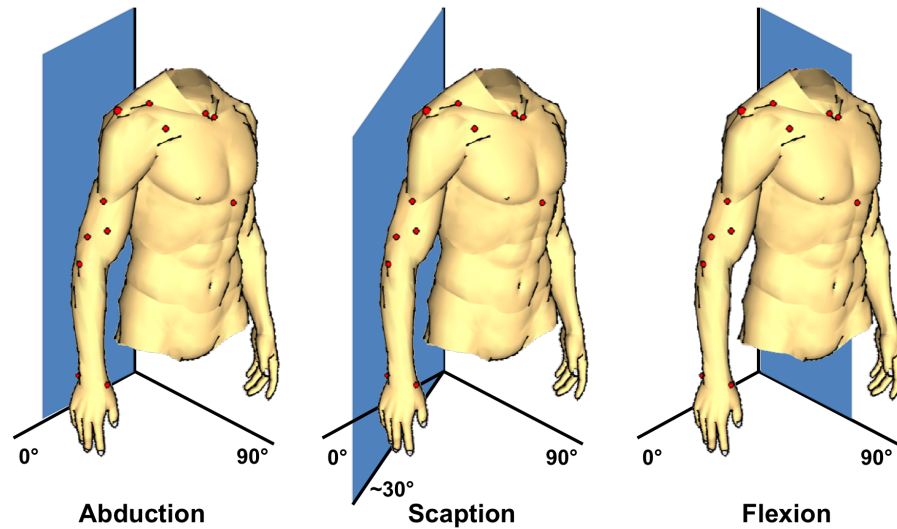


FIGURE 3.10: Illustration of arm elevation in abduction, scaption and flexion

A mirror is placed in front of subjects to aid in identification of the required angle on the frame during static recordings and also to maintain their posture throughout each measurement (Figure 3.11).

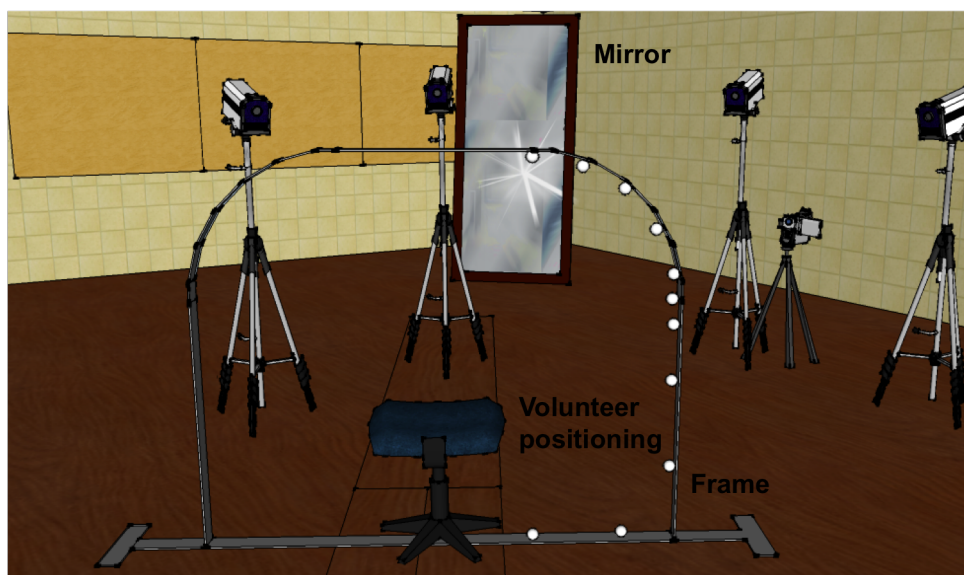


FIGURE 3.11: Posterior view of participant's positioning and measurement frame for static trials.

3.3.9 Activities of daily living

Participants are recorded while they complete a series of tasks that are typical of everyday life, based on the measurement protocol developed in Newcastle University. The tasks aim to measure shoulder movement during hygiene, feeding and reaching activities [143, 144]. Five measurements were added to the protocol. During the activities of daily living (ADLs), scapula function is measured with skin fixed markers and the AMC. The list of ADLs is summarised in Table 3.3 and represented graphically in Figure 3.12.

TABLE 3.3: Activities of daily living

Section	Activity
Hygiene	Reach to opposite axilla Reach opposite side of neck Reach side and back of head Brush opposite side of head Clean upper back Clean lower back
Feeding	Eat with hand to mouth Drink from mug
Reaching	Answer phone Reach as far forward as possible [§] Lift block to shoulder height (20N) [†] Lift block to head height (20N) [†] Cross body abduction [§] Internal rotation [§] External rotation [§] 90° abduction, external rotation [§]

[§]New ADL

[†]Patients were given the choice of a 10N load if they were not comfortable lifting 20N

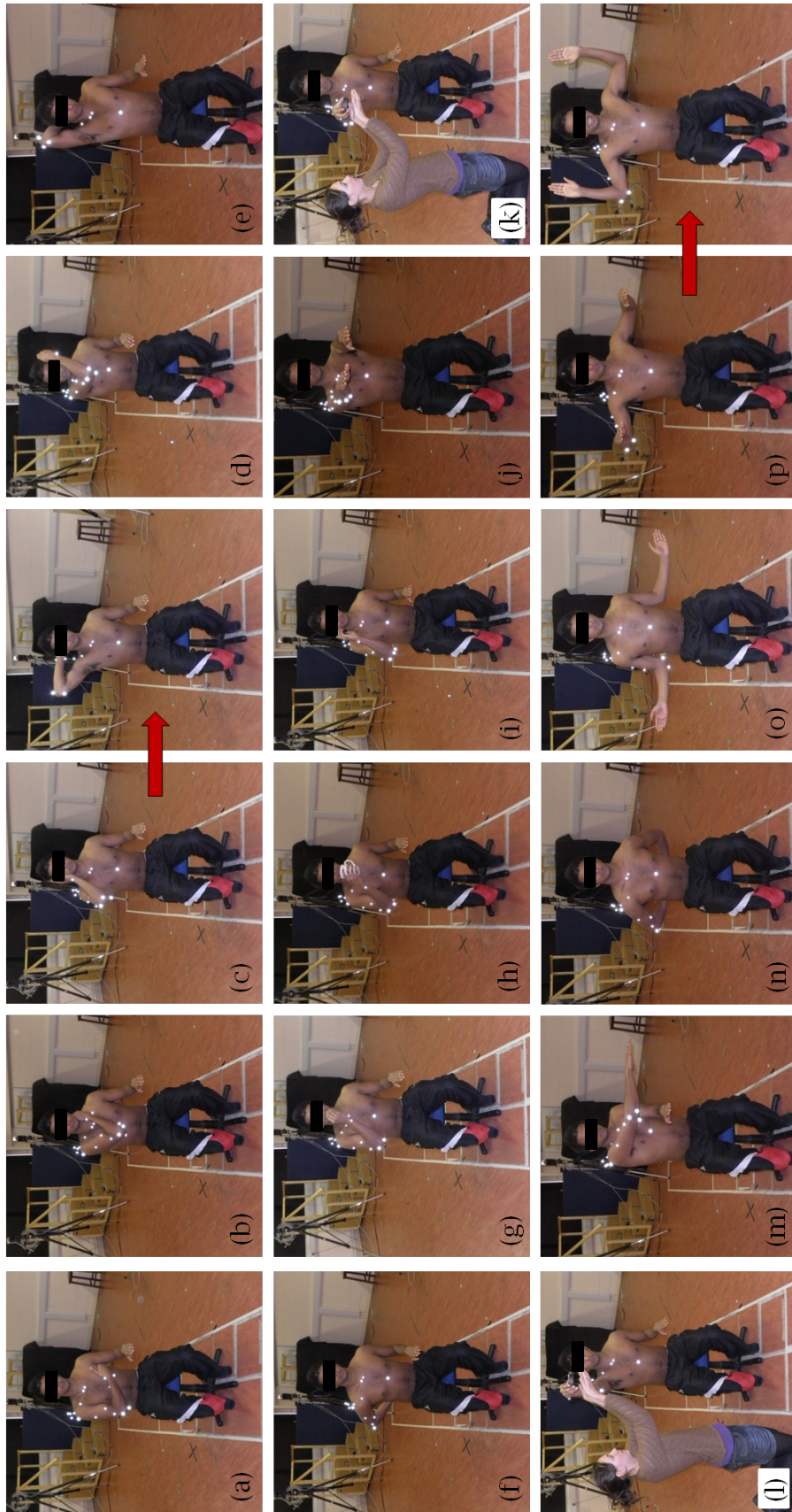


FIGURE 3.12: Activities of daily living: (a) Reach opposite axilla, (b) Reach opposite side of neck, (c) Reach opposite side of head, (d) Brush opposite side of head, (e) Clean upper back, (f) Clean lower back, (g) Eat with hand to mouth, (h) Drink from mug, (i) Answer phone, (j) Reach as far forward as possible, (k) Lift block to shoulder height, (l) Lift block to head height, (m) Cross body abduction, (n) Internal Rotation, (o) External rotation, (p) 90° abduction, external rotation

Participants are asked to begin and end each ADL in the NP. The researcher demonstrates all of the movements and the participants are encouraged to practise them before the measurements are taken. Verbal feedback is provided whenever it is necessary.

3.4 Data handling and analysis

A one second recording produces 60 frames of data that contain the 3D positions of all the retro-reflective markers. The raw data from the retro-reflective markers is tracked in QTM (Qualisys, Sweden). The data tracking process consists in assigning each marker its name for the duration of the movement. An automatic identification of markers (AIM) model is created for each participant and applied to the captured measurements.

Whenever any marker goes missing for 10 frames or less (due to body interposition obscuring markers), QTM gives the user the option to *gap fill* the missing marker. *Frame splitting* is necessary whenever a marker interchanges positions with another marker or changes to a noticeably wrong position. If a marker is missing from one of the measurements, the marker is exported as having position (0,0,0).

3.4.1 Computing shoulder complex kinematics

The 3D positions of the markers attached to bony landmarks is given relative to the GCS origin. The tracked data is exported in tab separated variable (.tsv) format to be analysed using in-house Matlab software (The Mathworks, Inc.).

An anatomical coordinate system (ACS) is constructed and fixed onto each of the shoulder complex segments. To create an orthogonal coordinate system,

three non-collinear landmarks within the segment must be identified. Two vectors created with the landmarks define a plane and the cross products of these vectors are used to define the reference frame.

The position of the segments' ACSs must be computed in order to analyse their movement. It is defined by the location (Figure 3.13a) and orientation (Figure 3.13b) of its fixed coordinate system in space using the Cartesian reference system.

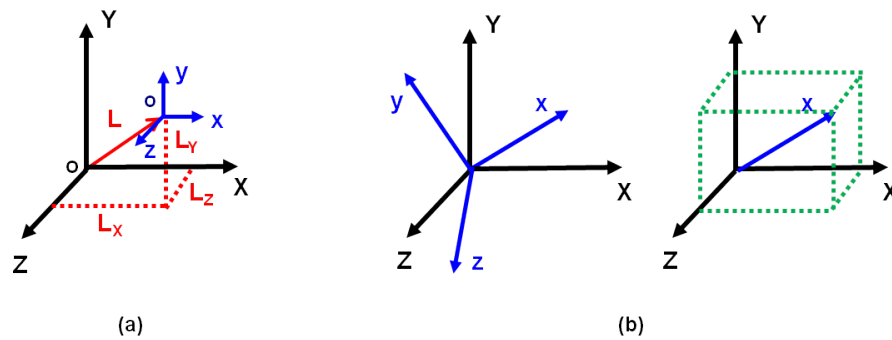


FIGURE 3.13: Defining a segment's position (a) location and (b) orientation. O, X, Y and Z defines the origin and axes of the GCS and o, x, y and z defines the origin and axes of a LCS.

The 3×1 position vector L (shown in Figure 3.13a) defines the location of the origin of a moving system relative to a fixed system using Equation (3.1).

$$[L] = \begin{bmatrix} L_X \\ L_Y \\ L_Z \end{bmatrix} \quad (3.1)$$

The 3×3 rotation matrix R defines the orientation of the system (shown in Figure 3.13b). The matrix is constructed with the cosine of the angles described by the component of each of the axes of a moving system (x, y, z) on the axes of a fixed system (X, Y, Z) using Equation (3.2).

$$[R] = \begin{bmatrix} \cos_{Xx} & \cos_{Xy} & \cos_{Xz} \\ \cos_{Yx} & \cos_{Yy} & \cos_{Yz} \\ \cos_{Zx} & \cos_{Zy} & \cos_{Zz} \end{bmatrix} \quad (3.2)$$

A transformation matrix T is a 4×4 homogeneous matrix where both translation and rotation of a moving reference system are expressed relative to a fixed reference system in one common mathematical operation. It is constructed using Equation (3.3).

$$[T] = \begin{bmatrix} \cos_{Xx} & \cos_{Xy} & \cos_{Xz} & L_X \\ \cos_{Yx} & \cos_{Yy} & \cos_{Yz} & L_Y \\ \cos_{Zx} & \cos_{Zy} & \cos_{Zz} & L_Z \\ 0 & 0 & 0 & 1 \end{bmatrix} = \begin{bmatrix} T_{11} & T_{12} & T_{13} & T_{14} \\ T_{21} & T_{22} & T_{23} & T_{24} \\ T_{31} & T_{32} & T_{33} & T_{34} \\ 0 & 0 & 0 & 1 \end{bmatrix} \quad (3.3)$$

The in house Matlab program (The Mathworks, Inc.) uses the Soderkvist and Wedin method [145] to calculate the transformation matrices that relate the shoulder complex segments together. The joint rotations are then calculated using matrix decomposition.

A flow diagram summarising the methods used to calculate shoulder complex function is shown in Figure 3.14. A more detailed description of the methods follows from the diagram.

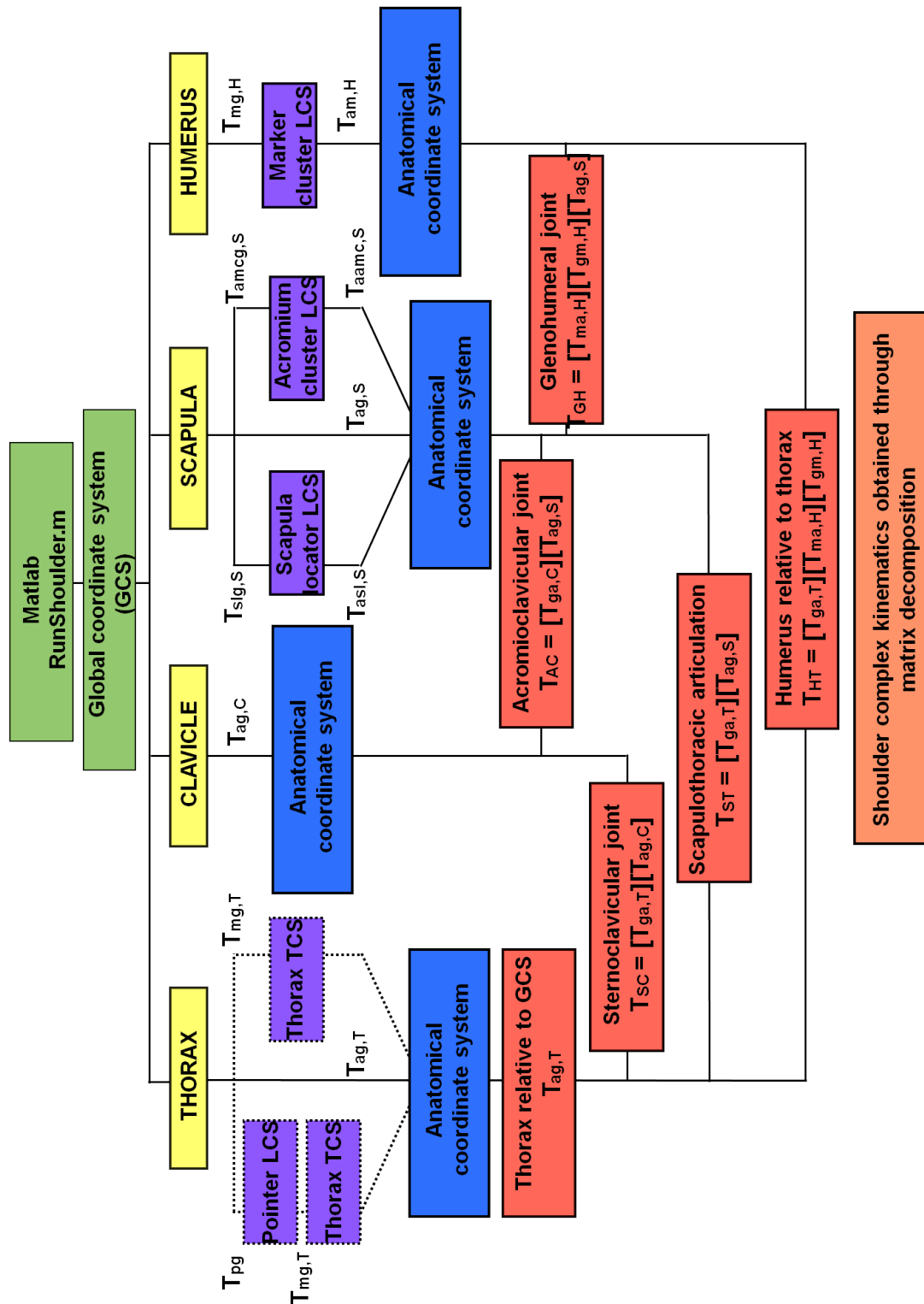


FIGURE 3.14: Summary of motion analysis data handling and analysis protocol

3.4.2 The Global Coordinate System

The GCS is rotated so that its orientation conforms to ISB standards. The rotation (R_{GCS}) is performed using Equation (3.4).

$$[R_{GCS}] = \begin{bmatrix} 0 & 1 & 0 \\ 0 & 0 & 1 \\ 1 & 0 & 0 \end{bmatrix} \quad (3.4)$$

The new GCS is orientated so that:

- The X axis points horizontally forwards
- The Y axis points vertically upwards
- The Z axis points horizontally outwards.

3.4.3 Establishing anatomical coordinate systems on shoulder complex segments

For the purposes of MA, the human body may be viewed as a system of rigid links connected by joints. Although the human body is not in fact rigid, it is a simplifying yet necessary assumption that must be made in order to make the investigation of human motion possible. An ACS is attached to a rigid body if three or more non-collinear markers are identified on the body.

ISB recommendations for the upper extremity were adopted in the current study [73]. Their convention will now be described for right shoulders. Whenever left shoulders are measured, the raw position data with respect to the sagittal plane is mirrored so that the convention for the right shoulder applies.

3.4.3.1 Thorax anatomical coordinate system

The thorax ACS is established from the GCS coordinates of markers C7, T8, IJ and PX. From Figure 3.15a, the origin of the thorax ACS is located in the centre of marker IJ. A vector T_1 is defined from the midpoint between PX and T8 to the midpoint between IJ and C7. Vector T_1 divided by its length gives the unit vector t_1 . A vector T_2 is defined from T8 to PX. The cross product of T_2 and t_1 gives the vector T_3 . Vector T_3 divided by its length gives the unit vector t_3 . The cross product of t_1 and t_3 gives the unit vector t_4 . The unit vectors t_4 , t_1 and t_3 produce the x_T, y_T, z_T axes respectively, attached to the origin as shown in Figure 3.15b.

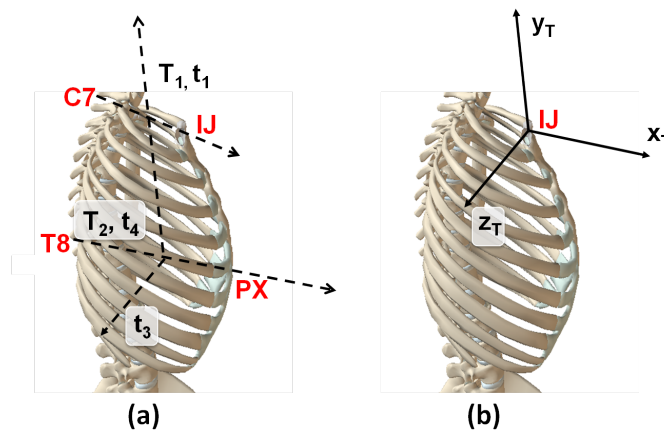


FIGURE 3.15: Thorax anatomical coordinate system
(a) construction and (b) position and orientation

The transformation matrix $T_{ag,T}$ is then computed to relate the position and orientation of the thorax ACS to the GCS.

When testing female participants, PX landmark is sometimes difficult to identify with a marker since it may become occluded with the participant's breasts. In this instance, an anatomical calibration with a pointer is necessary. The anatomical calibration consists on identifying the bony landmark with the pointer and relating its position to a technical device on the thorax.

The GCS coordinates of three of the markers on the pointer are recorded to establish a pointer local coordinate system (PLCS). From Figure 3.16a, the origin of the PLCS is located in marker P2. A vector U_1 is defined from P2 to P1. Vector U_1 divided by its own length gives the unit vector u_1 . A vector U_2 is defined from P3 to P2. The cross product of u_1 and U_2 gives vector U_3 . Vector U_3 divided by its length gives unit vector u_3 . The cross product of u_3 and u_1 gives the unit vector u_4 . The unit vectors u_1, u_4 and u_3 produce the x_P, y_P, z_P axes respectively, attached to the origin as shown in Figure 3.16b.

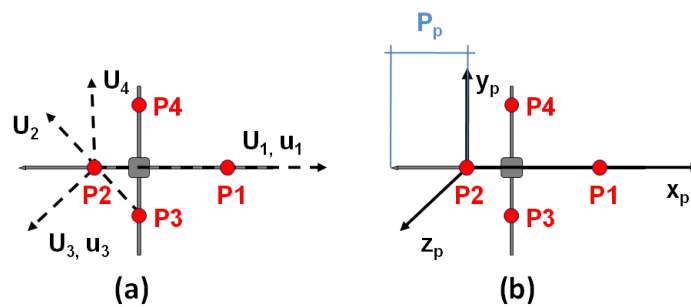


FIGURE 3.16: Pointer local coordinate system

The transformation matrix (T_{pg}) relating the position and orientation of the PLCS relative to the GCS is then computed.

A technical coordinate system (TCS) on the thorax is established from the thorax anatomical landmarks C7, T8 and IJ. From Figure 3.17a, the origin of the TCS is located in marker IJ. A vector V_1 is defined from C7 to IJ. Vector V_1 divided by its length gives unit vector v_1 . A vector V_2 is defined from T8 to IJ. The cross product of v_1 and V_2 gives vector V_3 . Vector V_3 divided by its length gives unit vector v_3 . The cross product of v_3 and v_1 gives the unit vector v_4 . The unit vectors v_1, v_4 and v_3 produce the x_{Tt}, y_{Tt}, z_{Tt} axes respectively, attached to the origin as shown in Figure 3.17b.

The transformation matrix (T_{mg}) relating the position and orientation of the thorax TCS relative to the GCS is computed. The position of PX in the thorax TCS is fixed using Equation (3.5).

$$px = [T_{gm}][T_{pg}][P_p] \quad (3.5)$$

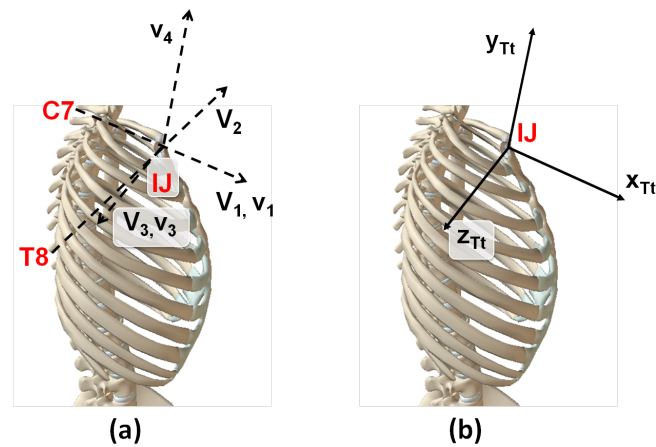


FIGURE 3.17: Thorax technical coordinate system for PX landmark calibration
(a) construction and (b) position and orientation

Where T_{gm} is the inverse of T_{mg} and P_p are the PLCS coordinates of the pointer's point (shown in Figure 3.16)

The thorax ACS can then be created as described above.

During certain measurements, in particular when recording the ADLs, markers on the thorax may become occluded due to the nature of the movement. Without all four markers, the thorax ACS cannot be calculated therefore a new function was written to 'fill in' any one of the four markers that may be occluded. The function file checks for missing data points and fills in the dropouts if only one thorax marker is missing. In this case, the other three markers on the thorax are used to correct the problem. A fixed relationship is established using the NP recording between the missing marker and a technical coordinate system established by the other three markers.

3.4.3.2 Clavicle anatomical coordinate system

It is only possible to palpate two clavicle bony landmarks, therefore the thorax's y-axis is used to construct the clavicle's ACS. From Figure 3.18a, the origin of the clavicle ACS is coincident with SC. A unit vector t_1 is defined as described for the y_T thorax ACS. A vector C_1 is defined from SC to AC. Vector C_1 divided by its length gives unit vector c_1 . The cross product of t_1 and c_1 gives unit vector

c_2 . The cross product of c_1 and c_2 gives unit vector c_3 . The unit vectors c_2 , c_3 and c_1 produce the x_C , y_C , z_C axes respectively, attached to the origin as shown in Figure 3.18b.

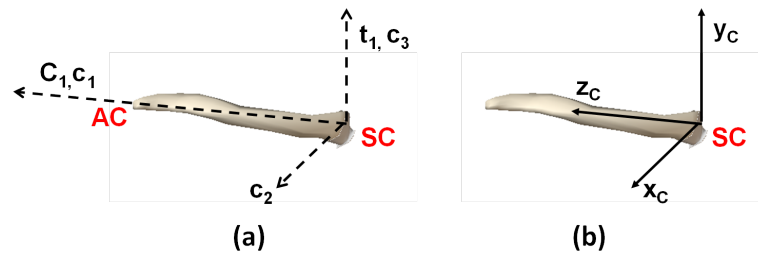


FIGURE 3.18: Clavicle anatomical coordinate system
(a) construction and (b) position and orientation

The transformation matrix $T_{ag,C}$ is then computed to relate the orientation of the clavicle ACS in the GCS.

A limitation of not being able to construct the clavicle ACS without the thorax ACS is that clavicle axial rotation cannot be measured using this protocol.

3.4.3.3 Scapula anatomical coordinate system

Three methods are used to record scapula movement. These are skin markers on bony landmarks, the SL with markers attached to the pegs that identify the bony landmarks and the AMC (shown in Figure 3.19). Some methods are more suitable than others for the measurement required although the SL is considered the most accurate of all three.

- **Skin fixed markers**

The scapula ACS is constructed from the GCS coordinates of markers TS, AI and AA. From Figure 3.20a, the origin of the coordinate system is located in marker AA. A vector S_1 is defined from TS to AA. Vector S_1 divided by its length gives unit vector s_1 . A vector S_2 is defined from AI to AA. The cross product of S_2 and s_1 gives vector S_3 . Vector S_3 divided

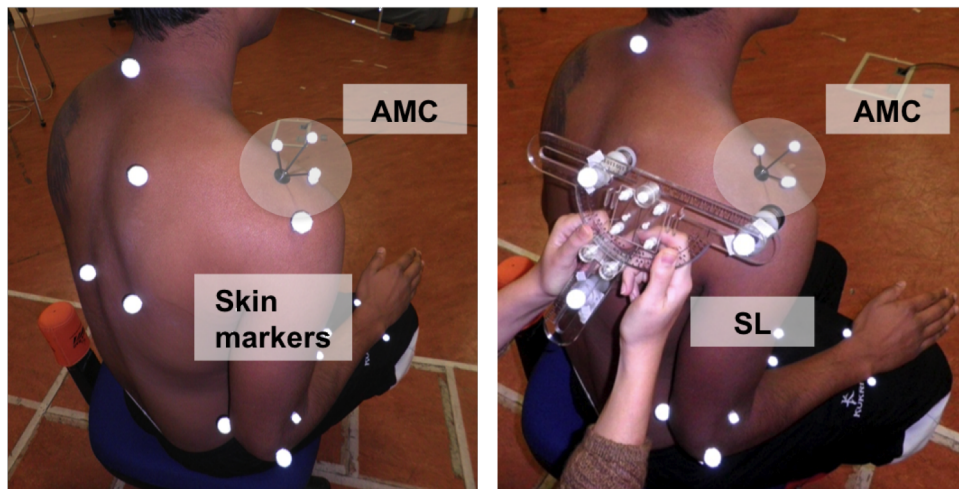


FIGURE 3.19: Scapula recording methods: skin fixed markers attached to bony landmarks, the scapula locator and the acromium marker cluster

by its length gives unit vector s_3 . The cross product of s_1 and s_3 gives unit vector s_4 . The unit vectors s_3 , s_4 and s_1 produce the x_S , y_S , z_S axes respectively, attached to the origin at as shown in Figure 3.20b.

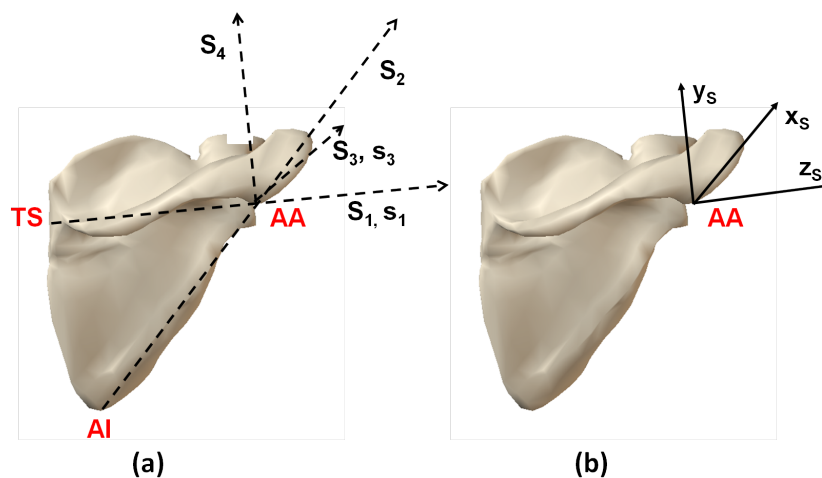


FIGURE 3.20: Scapula anatomical coordinate system (a) construction and (b) position and orientation

The transformation matrix $T_{ag,S}$ is computed to relate the orientation of the scapula ACS in the GCS.

- **Scapula locator (SL)**

A LCS on the SL (SLLCS) is constructed with a similar orientation as described when using skin markers. From Figure 3.21a, the origin of the coordinate system is located in marker SLAA. A vector SL_1 is defined

from SLTS to SLAA. Vector SL_1 divided by its length gives unit vector sl_1 . A vector SL_2 is defined from SLAI to SLAA. The cross product of SL_2 and sl_1 gives a vector SL_3 . Vector SL_3 is divided by its length to give unit vector sl_3 . The cross product of sl_1 and sl_3 gives a unit vector sl_4 . The unit vectors sl_3 , sl_4 and sl_1 produce the x_{SL}, y_{SL}, z_{SL} axes respectively, attached to the origin as shown in Figure 3.21b.

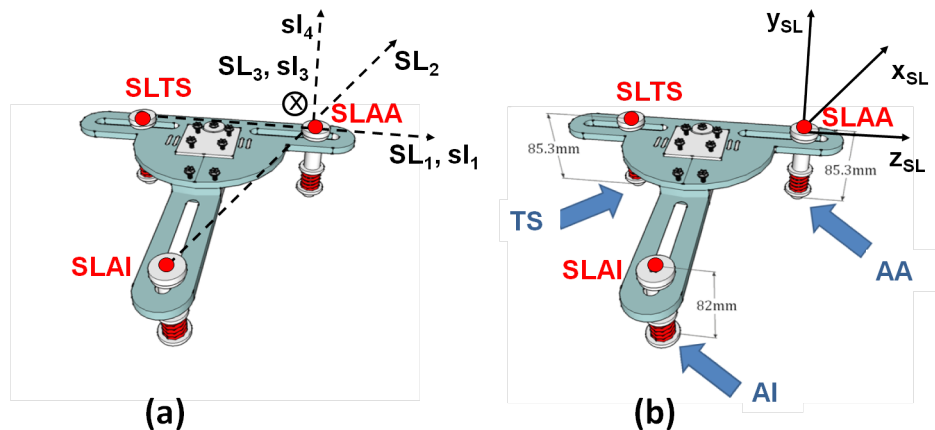


FIGURE 3.21: Scapula locator local coordinate system
(a) construction and (b) orientation

The position of each of the anatomical landmarks is given by the SLLCS on the peg identifying the landmark (SLAA, SLTS and SLAI for AA, TS and AI respectively) and the offset produced by the length of the identifying peg on the x_{SL} axis. Figure 3.21b shows the method of identification of marker AA. The origin of the SLLCS is located on SLAA for this anatomical calibration. TS and AI are similarly computed but with the position of the SLLCS origin on SLTS and SLAI markers respectively and the offset given by the peg identifying the bony landmark.

Once the position of the three anatomical landmarks is calculated, the scapula ACS is constructed as described when using skin markers.

- **Acromium marker cluster (AMC)**

A LCS is established on the AMC (AMCLCS) as shown in Figure 3.22a. The origin of the AMCLCS is located in marker AMCmed. A vector M_1

is defined from AMCmed to AMClat. Vector M_1 is divided by its length to give unit vector m_1 . A vector M_2 is defined from AMCmed to AMCant. The cross product of vectors m_1 and M_2 gives vector M_3 . Vector M_3 divided by its length gives the unit vector m_3 . The cross product of m_3 and m_1 gives unit vector m_4 . The unit vectors m_4 , m_3 and m_1 produce the x_{AMC} , y_{AMC} , z_{AMC} axes respectively, attached to the origin as shown in Figure 3.22b.

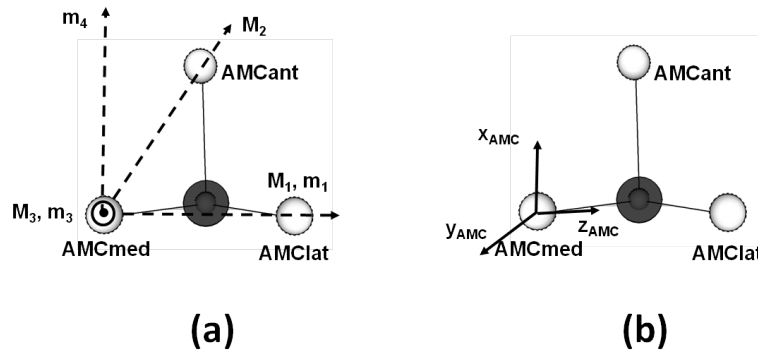


FIGURE 3.22: Acromium marker cluster local coordinate system
(a) construction and (b) position and orientation

The transformation matrix T_{acg} is then computed to relate the orientation of the AMCLCS in the GCS.

The scapula bony landmarks are identified with skin markers. The scapula ACS, constructed as described for skin markers, is related to the AMCLCS through the transformation matrix T_{aac} .

The transformation matrix $T_{ga,S}$ is computed to relate the orientation of the GCS in the scapula ACS using Equation (3.6).

$$T_{ga,S} = [T_{aca}][T_{gac}] \quad (3.6)$$

Where T_{aca} and T_{gac} are the inverse of T_{aac} and T_{acg} respectively.

3.4.3.4 Humerus anatomical coordinate system

The GH joint centre of rotation (CoR) is the third landmark required to construct the humerus ACS. The GH joint CoR lies within the humeral head, and as such it cannot be identified by means of palpation but instead must be estimated. Its position is then fixed relative to the HMC attached to the upper arm.

A LCS is fixed to the HMC (HMCLCS) from the position data of BI, BB and DI in the GCS. From Figure 3.23a, the origin is located in marker BI. A vector P_1 is defined from BI to DI. Vector P_1 divided by its length gives unit vector p_1 . A vector P_2 is defined from BI to BB. The cross product of P_2 and p_1 gives vector P_3 . Vector P_3 divided by its length gives unit vector p_3 . The cross product of p_1 and p_3 gives the unit vector p_4 . The unit vectors p_4 , p_1 and p_3 produce the x_{HMC} , y_{HMC} , z_{HMC} axes respectively, attached to the origin as shown in Figure 3.23b.

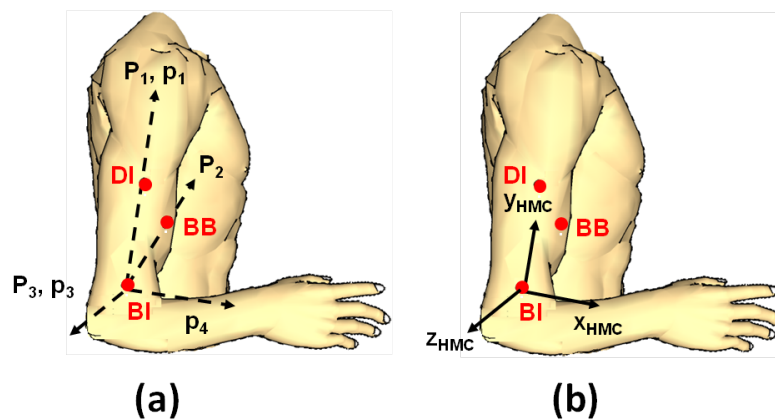


FIGURE 3.23: Humerus marker cluster local coordinate system
(a) construction and (b) position and orientation

The transformation matrix $T_{mg,H}$ relating the position and orientation of the HMCLCS relative to the GCS is computed.

The instantaneous helical axis (IHA) method is used to determine the GH joint CoR. The transformation matrix T_{hs} , which relates the HMCLCS to the Scapula ACS, is calculated using Equation (3.7) for the circumduction movement.

$$T_{hs} = [T_{ga,S}][T_{mg,H}] \quad (3.7)$$

Matrix T_{hs} is stacked to create a 3D transformation matrix as shown in Figure 3.24.

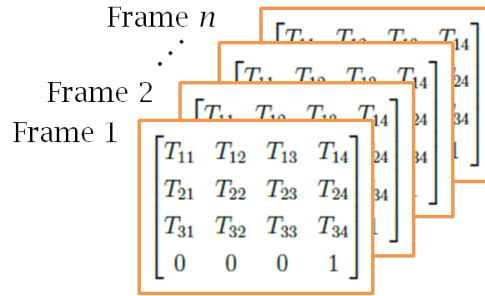


FIGURE 3.24: 3D transformation matrix

The IHA direction vector (\vec{n}), the projection of a point on the IHA (\vec{s}) and the translation velocity along the IHA (v) for T_{hs} are calculated using functions obtained from the International Shoulder Group (ISG) website using Equation (3.8), Equation (3.9) and Equation (3.10) respectively.

$$\vec{n} = \frac{\vec{\omega}}{\omega} \quad (3.8)$$

Where $\vec{\omega}$ is the instantaneous rotation velocity vector of amplitude ω

$$\vec{s}(t) = \vec{p}(t) + \vec{\omega}(t) \times \frac{\dot{\vec{p}}(t)}{\omega^2(t)} \quad (3.9)$$

Where \vec{p} is the position of a point P on the helical axis and $\dot{\vec{p}}$ is its velocity.

$$v = \dot{\vec{p}}' \times n \quad (3.10)$$

These parameters are subsequently used in a second ISG function to calculate the optimum pivot point of all position vectors of the IHA [76, 77]. The pivot point is considered the GH joint CoR, calculated at a fixed position to the scapula ACS.

The position of the humerus landmarks are expressed in the HMCLCS and the humerus ACS is constructed as shown in Figure 3.25a. The origin is located

in the GH joint CoR. A vector H_1 is defined from the midpoint of EL and EM (defined midELEM) to GH. Vector H_1 divided by its length gives unit vector h_1 . A vector H_2 is defined from EM to EL. The cross product of vectors h_1 and H_2 gives the vector H_3 . Vector H_3 divided by its length gives unit vector h_3 . The cross product of vectors h_3 and h_1 gives the unit vector h_4 . The unit vectors h_3 , h_1 and h_4 produce the x_H , y_H , z_H axes respectively, attached to the origin as shown in Figure 3.25b.

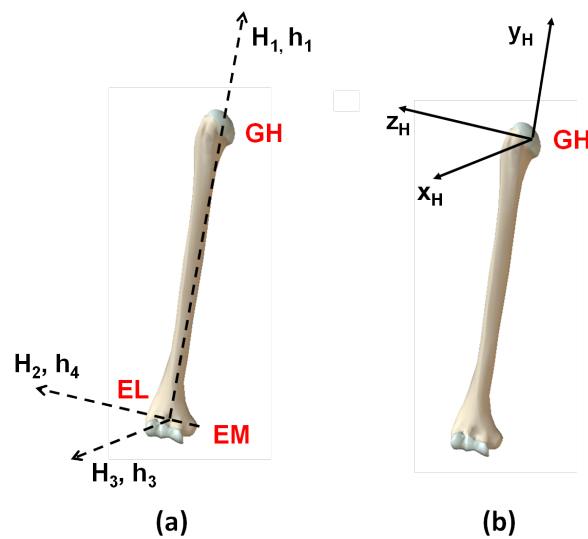


FIGURE 3.25: Humerus anatomical coordinate system
(a) construction and (b) position and orientation

The transformation matrix $T_{am,H}$ relating the humerus ACS relative to the HM-CLCS is computed.

The transformation matrix $T_{ga,H}$ relating the GCS to the humerus ACS is computed using Equation (3.11).

$$T_{ga,H} = [T_{ma,H}][T_{gm,H}] \quad (3.11)$$

Where $T_{ma,H}$ and $T_{gm,H}$ are the inverse of $T_{am,H}$ and $T_{mg,H}$ respectively.

3.4.4 Shoulder complex rotations calculations

The fixed body axes established during the anatomical calibration are similarly computed during the movement trials to track the position and pose of the four segments relative to the GCS.

A transformation matrix, relating the different anatomical systems, is constructed for every frame of data. Joint rotations are described as the movement of the distal segment relative to the proximal segment using either Euler or Cardan angles. The first rotation is around one of the common axes, and the second and third rotations are expressed around the rotated axes of the moving coordinate system.

Shoulder complex kinematics is calculated through matrix decomposition following the sequence of rotation summarised in Table 3.4. The method uses elements from the joint transformation matrices to provide a geometric description of joint and segment rotations.

TABLE 3.4: Euler and Cardan angle sequence of rotations

Joint rotation	Euler sequence
Thorax relative to GCS	Z-X-Y
Sternoclavicular joint	Y-X-Z
Acromioclavicular joint	Y-X-Z
Glenohumeral joint	Y-X-Y
Scapulothoracic articulation	Y-X-Z
Humerus relative to thorax	Y-X-Y

The equations that describe the joint rotations and their interpretation are explained below.

3.4.4.1 Thorax relative to GCS

The transformation matrix $T_{ag,T}$ contains the kinematics information of the thorax in the GCS. Thorax rotations are resolved according to the Cardan sequence of rotation Z-X-Y to describe the segment's rotation.

Flexion - extension angle α_{TG}

Flexion and extension are the rotations of the thorax around the coincident GCS Z axis and z_T , as shown in Figure 3.26a. They are determined as the angle formed by y_T and the GCS Y axis in the sagittal plane, according to Equation (3.12). Extension is defined as a positive angle while flexion is defined as a negative angle.

$$\alpha_{TG} = -\tan^{-1} \left(\frac{T_{12}}{T_{22}} \right) \quad (3.12)$$

Where T refers to the transformation matrix $T_{ag,T}$, T_{12} is the projection of y_T onto the GCS X axis, indicated by Xy in Figure 3.26b and T_{22} is the projection of y_T onto the GCS Y axis, represented as Yy in Figure 3.26b.

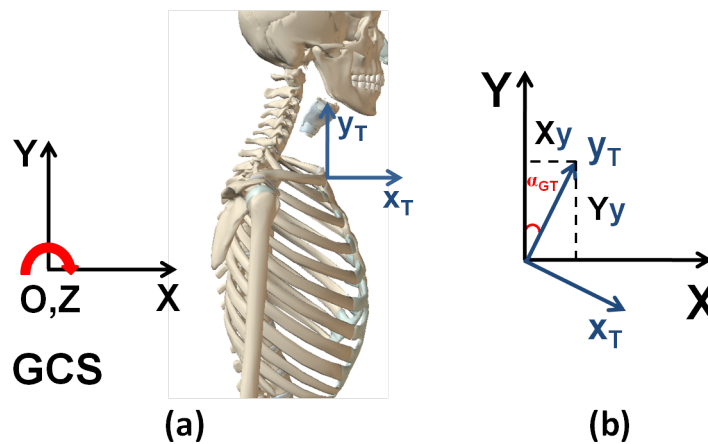


FIGURE 3.26: Sagittal plane illustration of thorax (a) flexion and extension rotations (b) flexion angle. X, Y, Z denotes the axes of the GCS while x_T , y_T , z_T denotes the axes of the thorax ACS

Lateral rotation angle β_{TG}

Lateral rotation is the rotation of the thorax around x_T , as shown in Figure 3.27a. It is defined as the angle between the CGS Y axis and y_T in the frontal plane using Equation (3.13). Right lateral rotation is defined as a positive angle while left lateral rotation is defined as a negative angle.

$$\beta_{TG} = \sin^{-1}(T_{32}) \quad (3.13)$$

Where T refers to the transformation matrix $T_{ag,T}$, and T_{32} is the projection of y_T onto the GCS Z axis, indicated by Zy in Figure 3.27b.

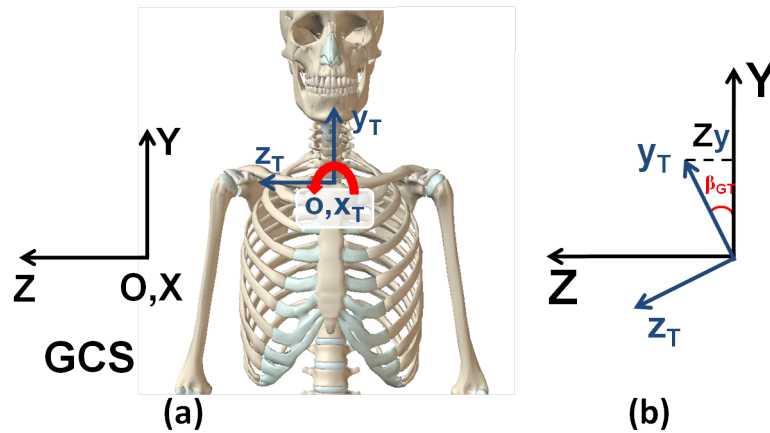


FIGURE 3.27: Frontal plane illustration of thorax (a) lateral rotation and (b) right lateral rotation angle. X, Y, Z denotes the axes of the GCS while x_T , y_T , z_T denotes the axes of the thorax ACS

Axial rotation angle γ_{TG}

Axial rotation is the thorax rotation around y_T , as shown in Figure 3.28a. It is determined as the angle between the GCS X axis and the x_T in the transverse plane using Equation (3.14). Left axial rotation is defined as positive while right lateral rotation is defined as negative.

$$\gamma_{TG} = -\tan^{-1} \left(\frac{T_{31}}{T_{33}} \right) \tag{3.14}$$

Where T refers to transformation matrix $T_{ag,T}$, T_{31} is the projection of x_T onto the GCS Z axis, indicated by Zx in Figure 3.28b and T_{33} is the projection of z_T in the GCS Z axis, represented by Zz in Figure 3.28b.

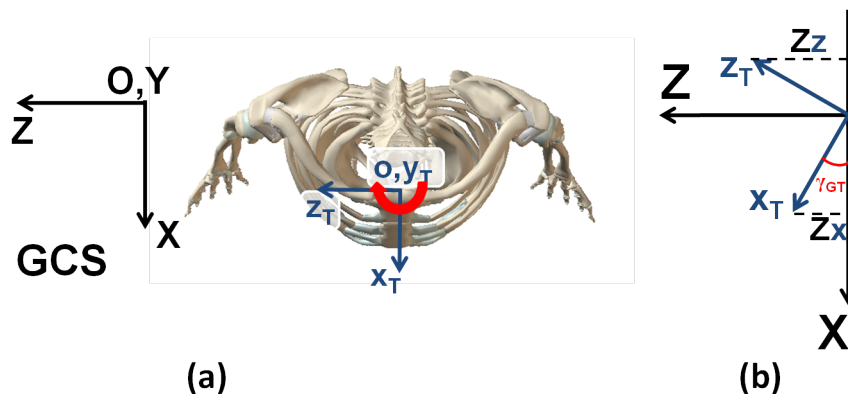


FIGURE 3.28: Transverse plane illustration of thorax (a) axial rotation and (b) right axial rotation. X, Y, Z denotes the axes of the GCS while x_T , y_T , z_T denotes the axes of the thorax ACS

3.4.4.2 The sternoclavicular joint

The transformation matrix T_{sc} relating the position and pose of the clavicle ACS relative to the thorax ACS is calculated using Equation (3.15).

$$T_{sc} = [T_{ga,T}][T_{ag,C}] \quad (3.15)$$

The sternoclavicular (SC) rotations are resolved according to the Cardan sequence of rotation Y-X-Z.

Protraction-retraction angle α_{SC}

Protraction and retraction are the clavicle rotations around the coincident y_T and y_C axes, as shown in Figure 3.29a. They are defined as the angle between z_C and z_T in the transverse plane using Equation (3.13). Protraction is determined as a positive angle while retraction is defined as a negative angle.

$$\alpha_{SC} = \tan^{-1} \left(\frac{T_{13}}{T_{33}} \right) \quad (3.16)$$

Where T refers to the transformation matrix T_{sc} , T_{13} is the projection of z_C onto x_T , indicated by Xz in Figure 3.29b and T_{33} is the projection of z_C in z_T , represented by Zz in Figure 3.29b.

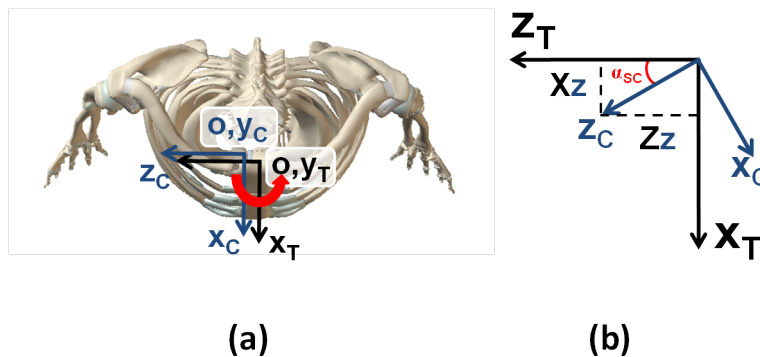


FIGURE 3.29: Transverse plane illustration of sternoclavicular (a) protraction and retraction and (b) protraction angle. x_T , y_T , z_T denotes the axes of the thorax ACS while x_C , y_C , z_C denotes the axes of the clavicle ACS

Elevation-depression angle β_{SC}

Elevation and depression are the clavicle rotations around x_C , as shown in Figure 3.30a. They are defined as the angle between z_C and z_T in the frontal plane using Equation (3.13). Depression is defined as a positive angle while elevation is defined as a negative angle.

$$\beta_{SC} = -\sin^{-1}(T_{23}) \quad (3.17)$$

Where T refers to the transformation matrix T_{sc} and T_{23} is the projection of z_C onto y_T , indicated by Yz in Figure 3.30b.

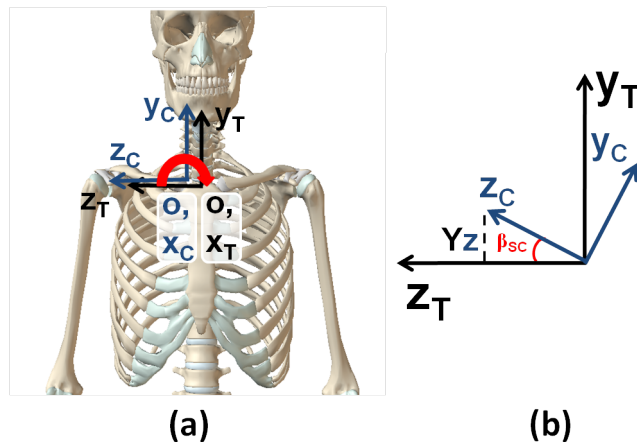


FIGURE 3.30: Frontal plane illustration of sternoclavicular (a) elevation and depression and (b) depression angle. x_T, y_T, z_T denotes the axes of the thorax ACS while x_C, y_C, z_C denotes the axes of the clavicle ACS

3.4.4.3 The acromioclavicular joint

The transformation matrix T_{ac} relating the position and pose of the scapula ACS relative to the clavicle ACS is calculated using Equation (3.18).

$$T_{ac} = [T_{ga,C}][T_{ag,S}] \quad (3.18)$$

Acromioclavicular (AC) joint rotations are resolved according to the Cardan sequence of rotation Y-X-Z.

Protraction-retraction angle α_{AC}

Protraction and retraction are the scapula rotations around the coincident y_S and y_C axes, as shown in Figure 3.31a. They are defined as the angle between z_S and z_C in the transverse plane using Equation (3.13). Protraction is defined as a positive angle while retraction is defined as a negative angle.

$$\alpha_{AC} = \tan^{-1} \left(\frac{T_{13}}{T_{33}} \right) \quad (3.19)$$

Where T refers to the transformation matrix T_{ac} , T_{13} is the projection of z_S onto x_C , indicated by Xz in Figure 3.31b and T_{33} is the projection of z_S in z_C , represented by Zz in Figure 3.31b.

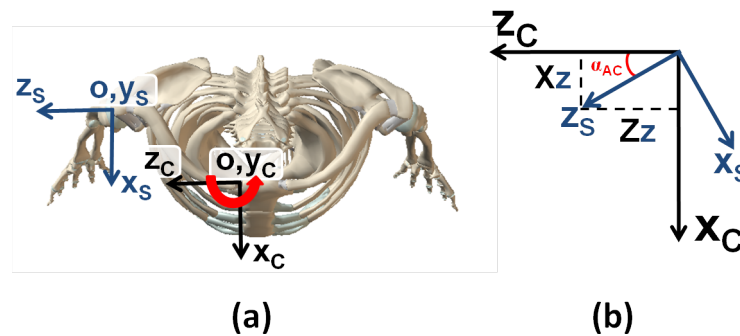


FIGURE 3.31: Transverse plane illustration of acromioclavicular (a) protraction and retraction and (b) protraction angle. x_C, y_C, z_C denotes the axes of the clavicle ACS and x_S, y_S, z_S denotes the axes of the scapula ACS

Medial-lateral rotation β_{AC}

Medial and lateral rotations are defined as the scapula rotations around x_S , as shown in Figure 3.32a. They are defined as the angle between z_S and z_C in the frontal plane using Equation (3.20). Medial rotation is defined as a positive angle while lateral rotation is defined as a negative angle.

$$\beta_{AC} = -\sin^{-1}(T_{23}) \quad (3.20)$$

Where T refers to the transformation matrix T_{ac} and T_{23} is the projection of z_S onto y_C , indicated by Yz in Figure 3.32b.

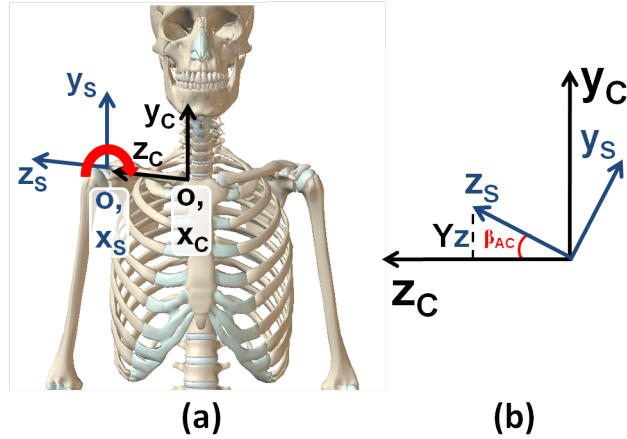


FIGURE 3.32: Frontal plane illustration of acromioclavicular (a) medial and lateral rotation and (b) lateral rotation angle. x_C, y_C, z_C denotes the axes of the clavicle ACS while x_S, y_S, z_S denotes the axes of the scapula ACS

Anterior-posterior tilt γ_{AC}

Anterior and posterior tilt are the scapula rotations around z_S , as shown in Figure 3.33a. They are defined as the angle between x_S and x_C in the sagittal plane using Equation (3.21). Posterior tilt is defined as a positive angle while anterior tilt is defined as a negative angle.

$$\gamma_{AC} = \tan^{-1} \left(\frac{T_{21}}{T_{22}} \right) \quad (3.21)$$

Where T refers to the transformation matrix T_{ac} , T_{21} is the projection of x_S onto y_C , indicated by Yx in Figure 3.33b and T_{22} is the projection of y_S in y_C , represented by Yy in Figure 3.33b.

3.4.4.4 The glenohumeral joint

The transformation matrix T_{gh} relating the position and pose of the humerus ACS relative to the scapula ACS is calculated using Equation (3.22).

$$T_{gh} = [T_{ga,S}][T_{ag,H}] \quad (3.22)$$

Glenohumeral (GH) joint rotations are resolved according to the Euler sequence of rotation Y-X-Y.

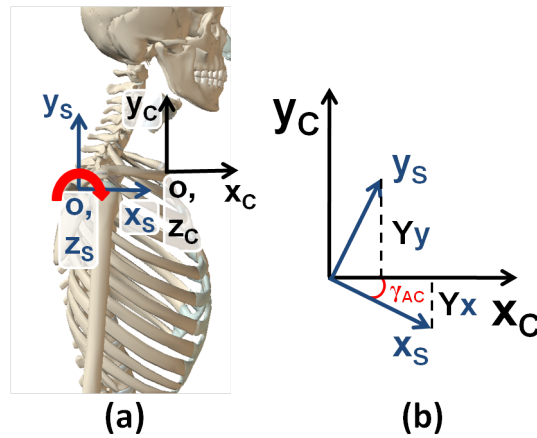


FIGURE 3.33: Sagittal plane illustration of acromioclavicular (a) anterior and posterior tilt and (b) anterior tilt angle. x_C, y_C, z_C denotes the axes of the clavicle ACS while x_S, y_S, z_S denotes the axes of the scapula ACS

GH plane of elevation α_{GH}

GH elevation is the humerus rotation around the coincident y_S and y_H axes, as shown in Figure 3.34a. It is defined as the angle between x_S and x_H using Equation (3.23). Plane of elevation is defined as a negative angle.

$$\alpha_{GH} = \tan^{-1} \left(\frac{T_{12}}{T_{32}} \right) \tag{3.23}$$

Where T refers to the transformation matrix T_{gh} , T_{12} is the projection of y_H onto x_S , indicated by Xy in Figure 3.34b and T_{32} is the projection of y_H in z_S , represented by Zy in Figure 3.34b.

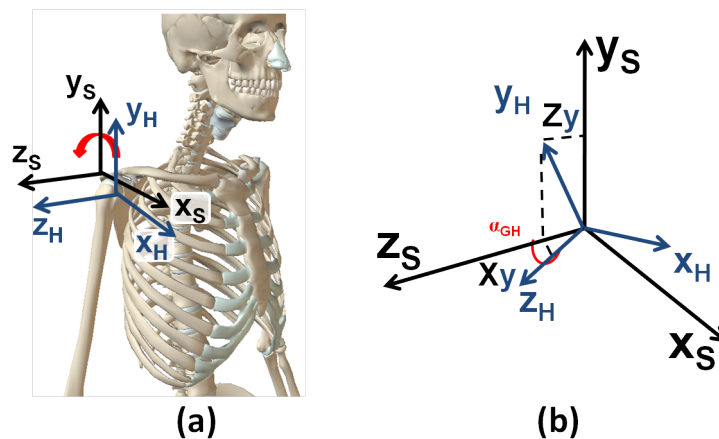


FIGURE 3.34: Two dimensional illustration of glenohumeral (a) plane of elevation and (b) plane of elevation angle. x_S, y_S, z_S denotes the axes of the scapula ACS while x_H, y_H, z_H denotes the axes of the humerus ACS

GH elevation β_{GH}

GH elevation is the humerus rotation around x_H , as shown in Figure 3.35a. It is defined as the angle between y_S and y_H in the frontal plane using Equation (3.24). GH elevation is defined as a negative angle.

$$\beta_{GH} = -\cos^{-1}(T_{22}) \quad (3.24)$$

Where T refers to the transformation matrix T_{gh} and T_{22} is the projection of y_H onto y_S , indicated by Yy in Figure 3.35b.

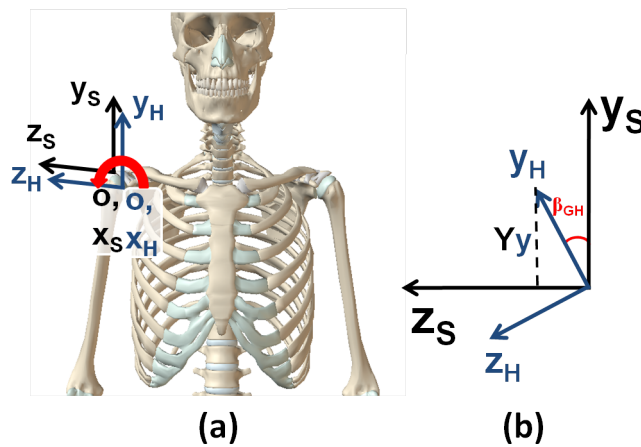


FIGURE 3.35: Frontal plane illustration of glenohumeral (a) elevation and depression and (b) depression angle. x_S, y_S, z_S denotes the axes of the scapula ACS while x_H, y_H, z_H denotes the axes of the humerus ACS

GH axial rotation γ_{GH}

GH axial rotation is the humerus rotation around y_H , as shown in Figure 3.36a. It is defined as the angle between z_S and z_H using Equation (3.25). Internal rotation is defined as a positive angle while external rotation is defined as a negative angle.

$$\gamma_{GH} = \tan^{-1} \left(\frac{-T_{21}}{T_{23}} \right) \quad (3.25)$$

Where T refers to the transformation matrix T_{gh} , T_{21} is the projection of x_H onto y_S , indicated by Yx in Figure 3.36b and T_{23} is the projection of z_H in y_S , represented by Yz in Figure 3.36b.

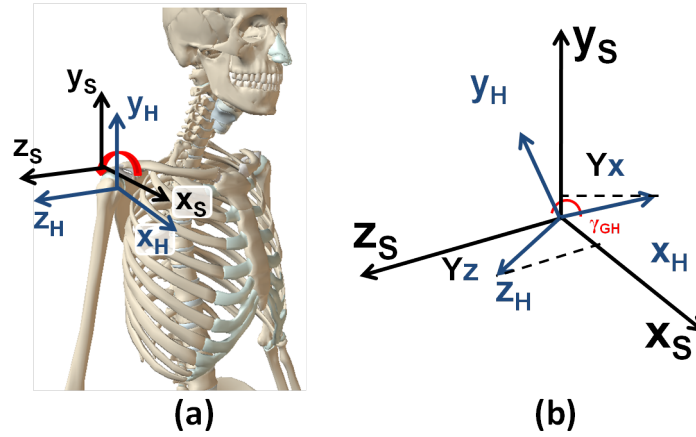


FIGURE 3.36: Two dimensional illustration of glenohumeral (a) axial rotation and (b) internal rotation angle. x_S, y_S, z_S denotes the axes of the scapula ACS while x_H, y_H, z_H denotes the axes of the humerus ACS

3.4.4.5 The scapulothoracic articulation

The transformation matrix T_{st} relating the position and pose of the scapula ACS relative to the thorax ACS is calculated using Equation (3.26).

$$T_{st} = [T_{ga,S}][T_{ag,T}] \quad (3.26)$$

Scapulothoracic (ST) joint rotations are resolved according to the Cardan sequence of rotation Y-X-Z.

Protraction - retraction angle α_{ST}

Protraction and retraction are the scapula rotations around the coincident x_S and x_T axes, as shown in Figure 3.37a. They are defined as the angle between z_S and z_T in the transverse plane using Equation (3.27). Protraction is defined as a positive angle while retraction is defined as a negative angle.

$$\alpha_{ST} = \tan^{-1} \left(\frac{T_{13}}{T_{33}} \right) \quad (3.27)$$

Where T refers to the transformation matrix T_{st} , T_{13} is the projection of z_S onto x_T , indicated by Xz in Figure 3.37b and T_{33} is the projection of z_S in z_T , represented by Zz in Figure 3.37b.

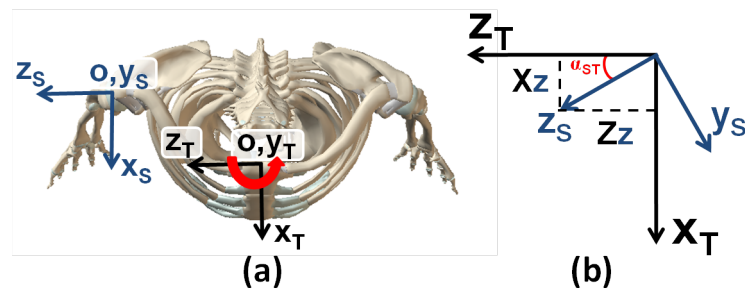


FIGURE 3.37: Transverse plane illustration of scapulothoracic (a) protraction and retraction and (b) protraction angle. x_T, y_T, z_T denotes the axes of the thorax ACS while x_S, y_S, z_S denotes the axes of the scapula ACS

Medial - lateral rotation β_{ST}

Medial and lateral scapula rotation are defined as the scapula rotations around x_S , as shown in Figure 3.38a. They are defined as the angle between z_S and z_T in the frontal plane using Equation (3.28). Medial rotation is defined as a positive angle while lateral rotation is defined as a negative angle.

$$\beta_{ST} = -\sin^{-1}(T_{23}) \quad (3.28)$$

Where T refers to the transformation matrix T_{st} and T_{23} is the projection of z_S onto y_T , indicated by Yz in Figure 3.38b.

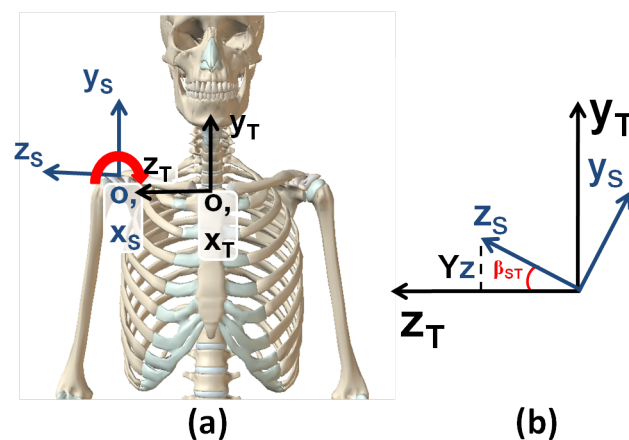


FIGURE 3.38: Frontal plane illustration of scapulothoracic (a) medial and lateral rotation and (b) lateral rotation angle. x_T, y_T, z_T denotes the axes of the thorax ACS while x_S, y_S, z_S denotes the axes of the scapula ACS

Anterior tilt - posterior tilt γ_{ST}

Anterior and posterior tilt are the scapula rotations around z_S , as shown in Figure 3.39a. They are defined as the angle between x_S and x_T in the sagittal plane using Equation (3.29). Posterior tilt is defined as a positive angle while anterior tilt is defined as a negative angle.

$$\gamma_{ST} = \tan^{-1} \left(\frac{T_{21}}{T_{22}} \right) \quad (3.29)$$

Where T refers to the transformation matrix T_{st} , T_{21} is the projection of x_S onto y_T , indicated by Yx in Figure 3.39b and T_{22} is the projection of y_S in y_T , represented by Yy in Figure 3.39b.

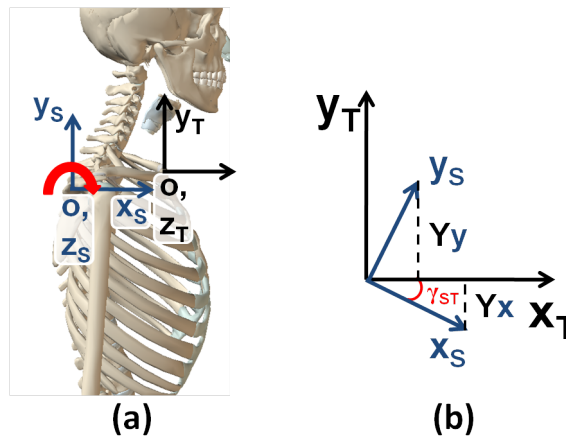


FIGURE 3.39: Sagittal plane illustration of scapulothoracic (a) anterior and posterior tilt and (b) anterior tilt angle. x_T, y_T, z_T denotes the axes of the thorax ACS while x_S, y_S, z_S denotes the axes of the scapula ACS

3.4.4.6 Rotations of the humerus relative to the thorax

The transformation matrix T_{ht} relating the position and pose of the humerus ACS relative to the thorax ACS is calculated using Equation (3.30).

$$T_{ht} = [T_{ga,H}][T_{ag,T}] \quad (3.30)$$

Humerothoracic (HT) rotations are resolved according to the Euler sequence of rotation Y-X-Y.

Plane of elevation α_{HT}

The Plane of elevation is the humerus rotation around the coincident y_H and y_T axes, as shown in Figure 3.40a. It is defined as the angle between x_H and x_T using Equation (3.31).

$$\alpha_{HT} = \tan^{-1} \left(\frac{T_{12}}{T_{32}} \right) \quad (3.31)$$

Where T refers to the transformation matrix T_{ht} , T_{12} is the projection of y_H onto x_T , indicated by Xy in Figure 3.40b and T_{32} is the projection of y_H in z_T , represented by Zy in Figure 3.40b.

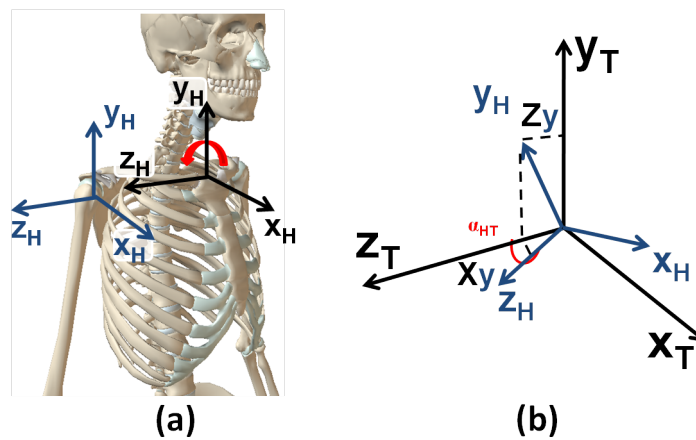


FIGURE 3.40: Two dimensional illustration of humerothoracic (a) plane of elevation and (b) plane of elevation angle. x_T, y_T, z_T denotes the axes of the thorax ACS while x_H, y_H, z_H denotes the axes of the humerus ACS

Elevation β_{HT}

Elevation is the humerus rotation around x_H , as shown in Figure 3.41a. It is defined as the angle between y_H and y_T in the sagittal plane using Equation (3.32). Humerus elevation is defined as a negative angle.

$$\beta_{HT} = -\cos^{-1}(T_{22}) \quad (3.32)$$

Where T refers to the transformation matrix T_{ht} and T_{22} is the projection of y_H onto y_T , indicated by Yy in Figure 3.41b.

Axial rotation: Internal - external rotation γ_{HT}

Axial rotation is the humerus rotation around y_H , as shown in Figure 3.42a. It is

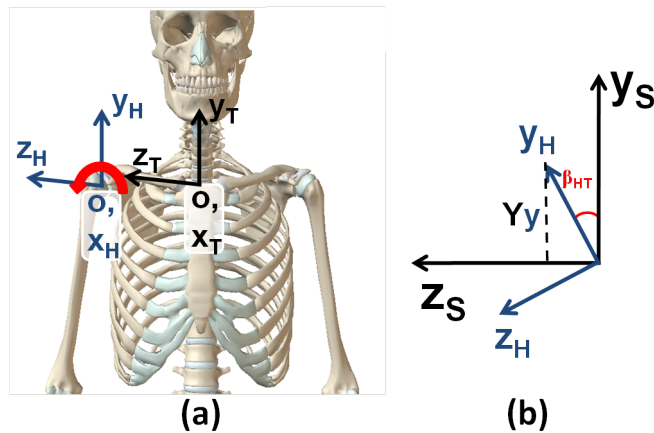


FIGURE 3.41: Frontal plane illustration of humerothoracic (a) elevation and depression and (b) depression angle. x_T, y_T, z_T denotes the axes of the thorax ACS while x_H, y_H, z_H denotes the axes of the humerus ACS

defined as the angle between z_H and z_T using Equation (3.33). Internal rotation is defined as a positive angle while external rotation is defined as a negative angle.

$$\gamma_{HT} = \tan^{-1} \left(\frac{-T_{21}}{T_{23}} \right) \quad (3.33)$$

Where T refers to the transformation matrix T_{ht} , T_{21} is the projection of x_H onto y_T , indicated by Yx in Figure 3.42b and T_{23} is the projection of z_H in y_T , represented by Yz in Figure 3.42b.

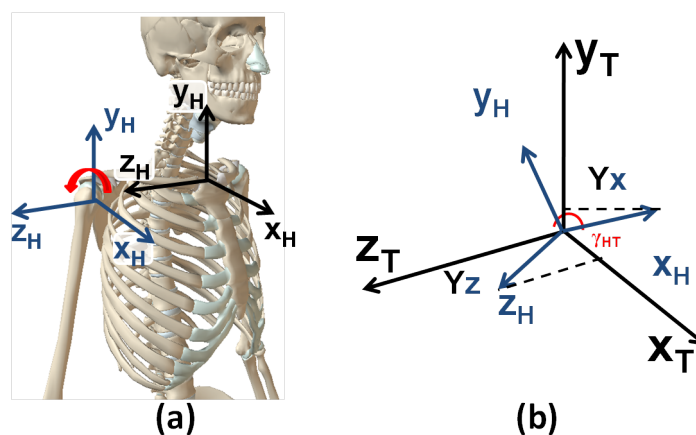


FIGURE 3.42: Two dimensional illustration of humerothoracic (a) axial rotation and (b) internal rotation angle. x_T, y_T, z_T denotes the axes of the thorax ACS while x_H, y_H, z_H denotes the axes of the humerus ACS

3.4.5 Outputs

The kinematics outputs are saved in Excel files. Each column represents a joint or segment rotation in the same order as how is described above. The rows represent the frames. The outputs are subsequently input into a different Excel file with a saved template for further manipulation. The ROM for each rotation is calculated and the rotations are plotted against humerus elevation relative to the thorax.

Chapter 4

Measuring shoulder complex kinematics in healthy volunteers

Biomechanical measurements of healthy shoulder function are essential for the understanding and evaluation of the joint complex. These measurements provide knowledge about how the bony structures interact to maintain stability within the joint. They also provide a reference against which patient shoulder kinematics can be compared for quantitative analysis of the effect of pathology or injury to the joint complex.

This Chapter is directed at further developing and improving the initial Cardiff protocol developed by Jones et al [141] as well as its application to quantify shoulder kinematics on healthy subjects and patients with a compromised shoulder due to trauma or pathology. The author explored, and attempted to replicate, different data collection procedures available from the literature. As knowledge and expertise was gained, improvements to the data collection and analysis procedure were made.

The author conducted several studies for the better understanding, and consequent improvements, in the data collection and analysis protocols developed at Cardiff. All subjects gave written informed consent prior to testing. International

Society of Biomechanics (ISB) recommendations on marker placement and the reporting of motion were followed [73]. The studies presented are as follows:

1. Glenohumeral joint centre estimation using regression equations and a functional method
2. Comparison between two different acromium marker clusters used to record scapula motion
3. The effect of unilateral and bilateral arm elevation in thorax and scapula kinematics
4. Investigating shoulder function asymmetry in dominant and non-dominant arms
5. Shoulder complex kinematics during physiological ranges of motion and activities of daily living
6. Repeatability of bony landmark identification and scapula locator placement

A brief background and summary of the motion analysis (MA) protocol and instructions to the participants is given at the start of each study. For detailed explanation of data collection and analysis, please refer to Chapter 3.

4.1 Glenohumeral joint centre estimation using regression equations and functional method

For the kinematics analysis of human motion, three non-collinear landmarks must be identified to create an anatomical coordinate system (ACS) on a segment. Only two landmarks can be identified on the humerus by means of palpation (the medial and lateral epicondyles). The third landmark, the glenohumeral (GH) joint centre of rotation (CoR), must be estimated. This virtual landmark

can be estimated through a number of different techniques, including regression equations based on the scapula geometry [78, 79] and functional methods [75–77] which estimate the CoR from the relative motion of the humerus and scapula.

Meskers et al developed regression equations (MRE) to estimate the GH position relative to the scapula ACS [78] in a cadaveric study. The predictive method requires the identification of 5 scapula bony landmarks used in three regression equations. The equations were based on the assumption that the position of the geometric CoR can be specified as the centre of a sphere fitted through the glenoid surface [81]. However, the estimation of the GH joint CoR by means of MRE is affected by errors from landmark calibration and the regression uncertainty [75].

Functional methods for estimating subject specific joint CoR have increased in popularity in different clinical and research laboratories [75, 77, 81, 82] since they can be more accurate than landmark-based methods [86]. Amongst the functional methods, the instantaneous helical axis (IHA) is used and recommended by the ISB [73]. The method is based on Chasles' theorem, which proposes that any general motion can be represented as "the sum of translations along and rotations around the helical axis in any sequence". The GH joint CoR is calculated as the optimum pivot point of all position vectors of the instantaneous helical axes [76, 77].

The original Cardiff protocol could only estimate the GH joint CoR through MRE. It was desirable to modify the custom developed Matlab program to allow for the estimation of GH joint CoR through the IHA method. The author incorporated two analyses programs found in the International Shoulder Group (ISG) website [146] to estimate the optimum pivot point into the in house Cardiff analysis program.

The aim of this study was to evaluate the position of the GH joint CoR when estimated using the IHA method, and compare its position to when calculated using MRE.

4.1.1 Method

Twenty three healthy participants (8♀, 15♂, age 23.7 ± 2.2 years, height 1.73 ± 0.09 m, weight 69.9 ± 14.6 Kg, and BMI 22.9 ± 2.8 Kg/m²) were included in the study. Retro-reflective markers were attached to bony landmarks according to ISB recommendations. Two measurements on their right shoulder were recorded to estimate the GH joint CoR using both techniques:

- A one second recording of the subject in an upright neutral position, NP, (i.e. sitting down, elbow flexed at 90°, hand pronated), Figure 4.1a, was used to estimate GH joint CoR using MRE.
- A 10s recording of the subject performing small passive circumduction movements was recorded to estimate the GH joint CoR using the IHA method. Participants maintained their elbow flexed to 90° whilst the observer moved their arm (Figure 4.1b). They were instructed neither to move their arm themselves nor to oppose the movement that was performed by the observer. The observer also applied pressure on the top of the scapula whilst rotating the volunteer's upper arm to minimise scapula rotation during the measurement.

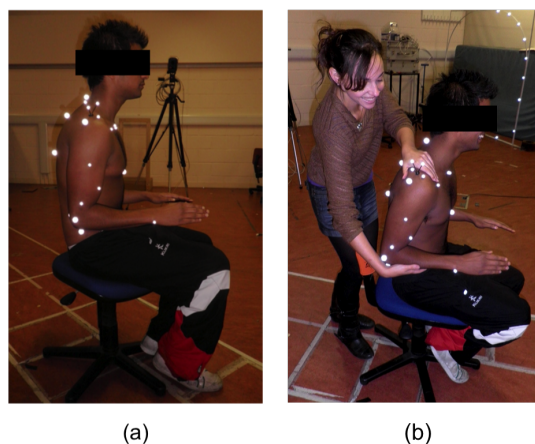


FIGURE 4.1: Measurements recorded for GH estimation through (a) regression equations and (b) instantaneous helical axis method

The positions of the GH joint CoR were computed relative to the Scapula ACS axes with the origin established on the Acromium Angle (AA), as shown in Figure 4.2.

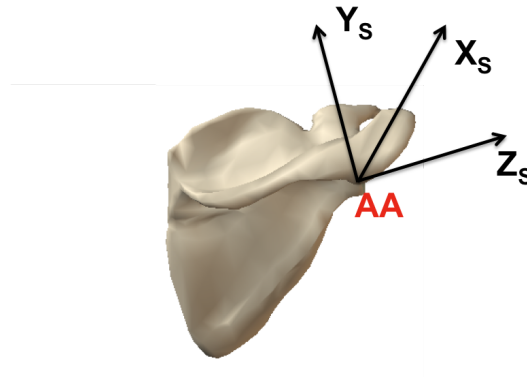


FIGURE 4.2: Scapula X_s , Y_s , and Z_s ACS axes orientation and origin on AA landmark. Adapted from [2]

Significant differences between the two GH estimation methods were explored using a paired sample t-test ($p < 0.05$) in IBM Statistics SPSS 19.

4.1.2 Results

The average location coordinates of the GH joint CoR in the scapula ACS (X_s , Y_s , and Z_s axes) are shown in Figure 4.3. Error bars represent the standard deviation (SD). Significant differences between the GH positions are denoted with *.

4.1.3 Discussion and Conclusions

The ability to accurately determine the GH joint CoR can lead to improved kinematics measurements of the shoulder complex. This virtual landmark is essential for the definition of the embedded humerus ACS, and errors in its identification may significantly alter the derived humerus kinematics [80, 147].

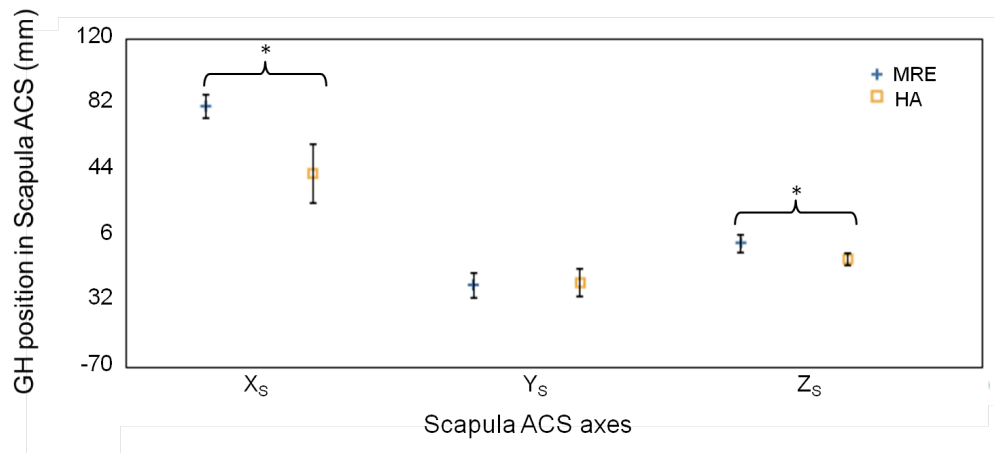


FIGURE 4.3: Average GH joint position in Scapula ACS axes. Error bars represent SD. Significant differences are denoted with *

When GH joint CoR was estimated using MRE, the average location was calculated at $(8.1 \pm 0.7, -2.2 \pm 0.8, 0.3 \pm 0.5)$ cm to the scapula ACS. In a similar study, Stokdijk et al [77] measured GH joint CoR at $(4.85, -2.52, 0.88)$ cm from the scapula ACS (their results were transformed into the ISB recommended coordinate system to facilitate data comparison). Discrepancies in the current study's GH joint CoR position with that of Stokdijk's are likely due to scapula bony landmark identification differences, since MRE are highly susceptible to these errors [75]. Muscle mass surrounding the shoulder joint as well as morphological differences between participants can difficult bony landmark identification. As a result, Stokdijk et al reported low reliability of GH joint CoR estimation using MRE [77].

When the GH joint CoR was estimated using the IHA method, its average location relative to the scapula ACS was calculated at $(4.2 \pm 1.8, -2.1 \pm 0.9, -0.7 \pm 0.4)$ cm. Other researchers have also investigated the estimation of the GH joint CoR, both *in vivo* and in cadaveric studies, using the IHA method. Stokdijks et al [77] estimated GH joint CoR *in vivo* at $(4.48 \pm 0.71, -3.82 \pm 0.83, -0.98 \pm 0.54)$ cm to the scapula ACS while Monnet estimated it at $(3.15 \pm 1.18, -1.45 \pm 0.62, -0.32 \pm 1.24)$ cm [75]. In a cadaveric study, Veeger et al [76] calculated GH joint CoR at $(4.32, -3.29, -0.73)$ cm from the scapula ACS. All sets of results were transformed into ISB recommended ACS to facilitate data comparisons.

Discrepancies between the results can be attributed to errors in landmark identification as well as to the different complexity movement patterns recorded to estimate the landmark [75]). In the current study, the GH joint CoR was estimated from a circumduction movement with the arm hanging by the side of the body while in the previous studies, movement patterns including flexion-extension, abduction-adduction and circumduction were used to estimate the landmark.

Through imaging studies, Inman identified the GH joint CoR anteriorly (positive X_S), inferiorly (negative Y_S) and medially (negative Z_S) to the scapula ACS [11]. The IHA method estimated the landmark at a similar position as Inman; however, MRE significantly overestimated the position along X_S as well as placed the GH joint CoR laterally instead of medially to the scapula ACS.

Both the IHA method and MRE assume that there is a single joint centre. While this assumption is reasonable when measuring healthy volunteers, it is not considered applicable when measuring patients with shoulder instability since translations at the joint may occur [87, 88]. For such patients, the finite helical axis (FHA) would be the preferred method to estimate GH joint CoR [76]. The FHA describes discrete relative motion of a body by a finite rotation around and a finite translation along a fixed axis.

Recently, the Symmetrical Centre of Rotation Estimation (SCoRE) method was validated for GH centre estimation *in vivo* [75]. As well as being a more precise method for estimating GH joint CoR than IHA, SCoRE was also able to locate GH even at slow velocities, contrary to IHA [85]. For this reason, frames with angular velocity (ω) of less than 10 percent maximum ω were removed in the current study in the IHA measurements.

A different approach to estimating GH joint CoR by anatomical landmark regression was incorporated into the Cardiff testing protocol. Following this study, all data collected at Cardiff is now analysed using the IHA method to estimate the GH joint CoR since it locates the GH joint CoR at a more anatomically meaningful position compared to MRE. Other, more complex, movement patterns could

be used to collect the data since published studies have demonstrated improved GH estimation with them [75, 77].

4.2 Comparison between two different acromium marker clusters used to record scapula motion

Skin fixed marker based MA is a technique commonly used to measure the kinematics of the shoulder complex [30–34, 148]. The main concern associated with this technique is the error introduced due to skin movement artefacts [37, 90, 91]. A typical example is that of the scapula, where motion presents a significant challenge to quantifying the biomechanical function of the shoulder complex *in vivo* as a large amount of bony movement occurs under the skin [17, 18, 94]. As a result, Johnson et al [18] developed a three pointed palpator (referred to as the scapula locator, SL) that facilitates the identification of the scapula bony landmarks at any arm elevation, thus providing a more accurate measurement tool. However, it is only possible to measure static positions of the scapula using the SL. Thus, van Andel et al [30], developed an acromium marker cluster (AMC) to perform dynamic scapula tracking. The AMC consists of a cluster of 3 retro-reflective markers that are attached on top of the acromium of the scapula. Through an initial anatomical calibration, the scapula bony landmarks are related to a technical coordinate system fixed to the AMC so that dynamic tracking is possible. Scapula function has been reported accurately with the AMC up until 100° of arm elevation [30].

In his PhD studies, Dr Lovern designed and developed an AMC (referred to as AMC1) to measure scapula function with the Cardiff protocol [149], shown in Figure 4.4a. However, during testing of participants, the design of the AMC appeared not to be optimum for the following reasons:

- Due to the AMC's height and weight, the cluster tipped downwards and was unstable, often pulling on the skin to which it was attached.
- The AMC frequently interfered with the SL at elevations higher than 80° marked on the reference frame.

As a result, the author designed and developed a different, more compact and lighter AMC (referred to as AMC2) for recording scapula movement (shown in Figure 4.4b). The aim of this study was to quantify differences in scapula kinematics measured with the two AMCs. It was hypothesized that scapula function would be tracked more accurately with AMC2 compared to AMC1. The recordings were also performed with the SL in order to make a direct comparison between SL and AMC recordings, with the SL considered the more accurate method of the two for recording scapula function.

4.2.1 Methods

An AMC and a SL were simultaneously used to track scapula function during static physiological arm elevation trials in abduction, scaption and flexion. Twelve subjects (3♀, 9♂, mean age 23.3 ± 2.1 years, height 1.77 ± 0.09 m, weight 74.5 ± 17.1 Kg, and BMI 23.4 ± 3.5 Kg/m²) were tested with AMC1, shown in Figure 4.4a and 11 different subjects (5♀, 6♂, mean age 24.1 ± 2.3 years, height 1.68 ± 0.08 m, weight 63.9 ± 9.0 Kg and BMI 22.4 ± 1.6 Kg/m²) were tested with AMC2, shown in Figure 4.4b.

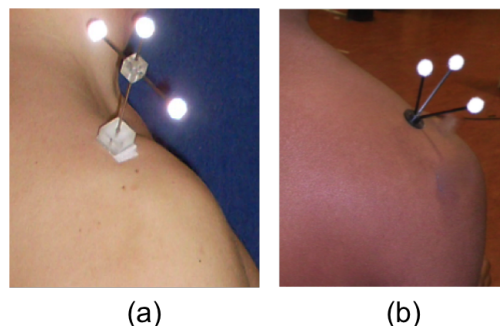


FIGURE 4.4: (a) AMC1 and (b) AMC2

The SL was repositioned on the scapula for each arm elevation position to account for its movement relative to the overlying skin. For AMC1 recordings, the SL recordings are referred to as SL1 and similarly SL2 for AMC2 trials. A frame was used to standardise arm elevations at 20° intervals starting with the arm beside the body up to 180° of arm elevation. The humerus CoR was estimated with the IHA method.

Validity of scapula orientations obtained with the AMCs was investigated against those measured with the SL by a repeated measurement One-Way Analysis of Variance (ANOVA) ($p < 0.05$) in IBM Statistics SPSS 19 for each elevation angle marked on the reference frame.

To assess the variability of the AMCs, repeatability trials were performed using each AMC.

- The right shoulder kinematics of a right handed, healthy male participant (age 26 years, weight 70 kg, height 161.5 cm and a BMI of 21.1 Kg/m²) was recorded using AMC1. The reliability was assessed over two visits to the MA Laboratory by three observers. During each visit, the observers performed three trials where the AMC was repositioned at the beginning of each trial and bilateral scaption from the arm hanging by the side of the body to 120° at 30° intervals was recorded.
- The right shoulder kinematics of a right handed, healthy female participant (age 23.3, height 1.77 m, weight 74.5 Kg, and BMI 23.4 Kg/m²) was tested over two sessions in the MA Laboratory by a single observer using AMC2. In each session, the AMC was repositioned and scapula kinematics was measured five times with the AMC and the SL simultaneously starting from the arm hanging by the side of the body up to 120° marked on the frame in 20° interval during scaption. The AMC was repositioned at the beginning of each elevation trial.

The intraclass correlation coefficient (ICC) was calculated in SPSS ($p < 0.05$) to investigate measured scapula kinematics repeatability recorded with both AMCs.

4.2.2 Results

Average scapulothoracic (ST) articulation kinematics measured with AMC1 and AMC2 as well as with the SL are plotted against arm elevation relative to the thorax in Figure 4.5 for the three elevation trials.

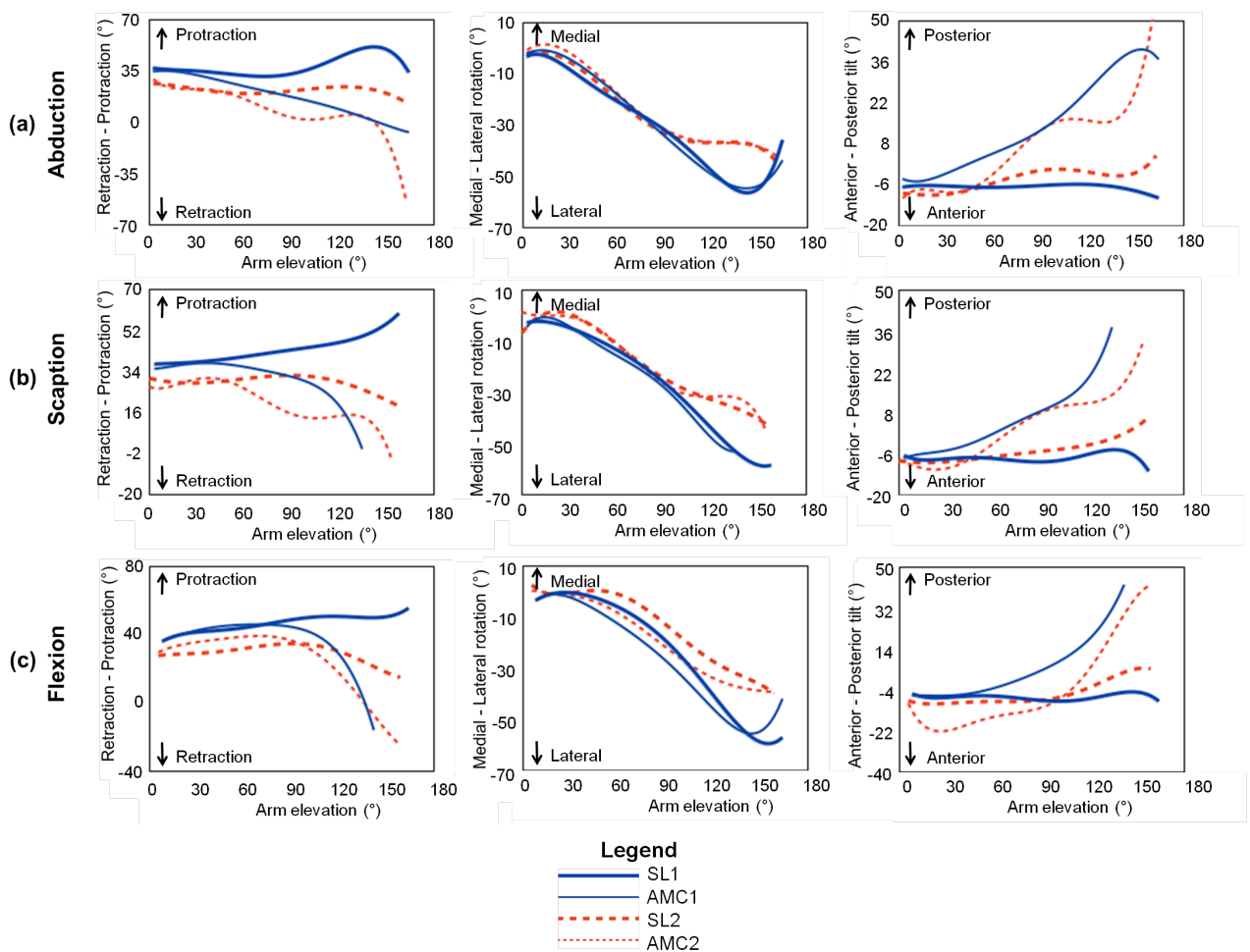


FIGURE 4.5: Average ST articulation kinematics measured with AMC1 and AMC2 as well as with the SL during (a) abduction, (b) scaption and (c) flexion

Results from the One-Way ANOVA were used to determine the arm elevation angle relative to the thorax where significant differences between AMC recordings and SL were first measured. Results are summarised in Table 4.1.

TABLE 4.1: Arm elevation angle (\pm SD) for which significant differences between AMC and SL recordings were first measured

Movement	Retraction ($^{\circ}$)		Lateral rotation ($^{\circ}$)		Posterior tilt ($^{\circ}$)	
	AMC1	AMC2	AMC1	AMC2	AMC1	AMC2
Abduction	44 \pm 8	65 \pm 8	135 \pm 7	140 \pm 13	25 \pm 7	65 \pm 8
Scaption	53 \pm 14	75 \pm 7	131 \pm 13	137 \pm 14	34 \pm 14	75 \pm 7
Flexion	44 \pm 9	82 \pm 6	137 \pm 13	140 \pm 11	64 \pm 10	82 \pm 6

The ICC for AMC1 and AMC2 were measured as 0.975 and 0.925 respectively.

4.2.3 Discussion and Conclusions

Skin markers attached to bony landmarks significantly underestimate scapula motion due to skin artefacts [18, 30, 94, 100]. To account for scapula movement under the skin, Johnson et al developed the SL although it is constrained to static measurements [18]; however, dynamic, unconstrained measurements of shoulder function are possible with the use of the AMC [30].

During the entire elevation trials in all three planes of elevation, both AMCs consistently measured greater scapula retraction (e.g. 9 $^{\circ}$ AMC1 and 21 $^{\circ}$ AMC2 during scaption) and posterior tilting (e.g. 26 $^{\circ}$ AMC1 and 32 $^{\circ}$ AMC2 during scaption) compared with the SL measurements (shown in Figure 4.5). On the other hand, similar lateral rotations were measured with the AMCs compared to the SL (e.g. 2 $^{\circ}$ AMC1 and 3 $^{\circ}$ AMC2 during scaption). Errors in the measurements recorded with both AMCs are likely to have been introduced due to changes in the shape of the soft tissue surrounding the acromium due to deltoid contraction. Furthermore, the AMC mass may result in inertial translations and rotations of the cluster [94]. Skin manipulation around the AMC attachment

may have introduced further errors since it was required to palpate close to the acromium in order to place the SL.

Significant differences between AMC1 and SL1 were first recorded in scapula posterior tilt at $25\pm 7^\circ$ of arm elevation during abduction and at $44\pm 9^\circ$ arm elevation for scapula retraction during flexion. On the other hand, AMC2 recorded scapula retraction and posterior tilt similarly to SL2 up to $65\pm 8^\circ$ of arm elevation during abduction (Table 4.1).

AMC2 consistently measured scapula lateral rotation more accurately than AMC1 when compared to differences between the two AMCs relative to the SL measurements. Lateral rotation was recorded accurately up to $131\pm 13^\circ$ of arm elevation in scaption with AMC1 and to $137\pm 14^\circ$ of arm elevation for AMC2 (Table 4.1). Similar findings have been reported by Meskers et al [94] and Karduna et al [100] who both tracked scapula lateral rotation accurately using a sensor mounted on the acromium up to 120° of arm elevation with an electromagnetic system.

The accuracy and reproducibility of the AMC measurements is heavily dependent on AMC placement [30, 94, 150]. AMC1 showed marginally better reproducibility of the measured kinematics (ICC 0.975) compared to AMC2 (0.925) in the intra-observer reliability trial.

It would be desirable to establish regression equations that compensate or calibrate the errors in the AMC recordings from the known SL rotations. However, Meskers et al found that it was practically impossible to develop such equations [94] since the inter-individual and inter-measure determinants are too unpredictable.

AMC2 measured rotations accurately at higher elevations compared to AMC1. In general, the results of this study support previous research suggesting that AMC is reliable for measuring scapula function although caution should be taken at high arm elevations.

4.3 The Effect of Unilateral and Bilateral arm elevation on thorax and scapulothoracic articulation kinematics

Positioning the arm during certain tasks, particularly at high elevations, may involve a combination of the synchronized shoulder complex movement and trunk rotations [16, 151]. Consequently in shoulder complex biomechanics studies, particular attention is made to minimise trunk rotations. In some instances, participants have been constrained physically [19, 152] from moving their trunk to isolate the movement of the arm. Simultaneous arm elevations have also been performed to reduce trunk rotations [33] as opposed to unilateral arm elevations [30, 153] as, according to Crosbie et al [16], significantly different ranges of thoracic motions are achieved when volunteers perform unilateral and bilateral arm elevations. It is necessary to understand how these rotations affect shoulder kinematics. The effect of thoracic posture on scapular kinematics has been documented in several studies [152, 154]. The studies conclude that thoracic spine position significantly affects shoulder complex kinematics by decreasing scapular ROM.

During clinical assessment of a patient's injury or the outcome of surgery, orthopaedic surgeons commonly use a range of shoulder scoring systems. The scoring systems contain subjective assessment of pain and limitations to the activities of daily living (ADLs) as well as measurements of the active physiological range of motion (ROM) [21, 22] carried out during arm elevation. It is thus important, when performing clinical assessments, to consider the effect of compensatory mechanisms, where trunk rotations could play a significant role in the subjective assessment.

The aim of this study was to quantify the differences in scapula and trunk rotations when subjects perform unilateral elevation (UE) and bilateral elevation (BE) of the arm during physiological ROM.

4.3.1 Methods

Eleven subjects were included in the study (4♀, 7♂, age 23.6 ± 2.1 years, height 1.72 ± 0.1 m, weight 67 ± 13.2 Kg, and BMI 22.4 ± 2.2 Kg/m²). Participants were instructed to perform full physiological arm elevation in the frontal (abduction) and sagittal (flexion) planes in a seated, upright position (their back was unsupported) with the elbow fully extended. Static measurements were taken using the SL which was repositioned on the scapula for each arm elevation position to account for its movement relative to the overlying skin for both UE and BE. A frame was used to standardise arm elevations at 20° intervals starting with the arm beside the body up to 180° of arm elevation. It also assisted the volunteers to maintain the correct plane of elevation. A mirror was placed in front of the subject to aid in identification of the required angle on the frame and to assist in maintaining posture throughout each measurement.

Throughout arm abduction elevation, subjects maintained a supinated arm (palm of hands facing forwards as the arm was elevated). During flexion elevation measurements, subjects performed the movements with the forearm pronated (palm of hands facing backwards, downwards and forwards as the arm was elevated). Measurements were taken with the subjects performing UE of the right arm. They were given no instruction as to left arm posture during these measurements. Following UE, the subjects performed BE for which only the right arm was assessed.

Significant differences between the two measuring protocols were calculated using paired sample t-test ($p < 0.05$) in IBM Statistics SPSS 19 software.

4.3.2 Results

Each participant's ROM for trunk rotations and scapula rotations were calculated. The average ROMs and SD are summarised in Table 4.2 for abduction and Table 4.3 for flexion.

TABLE 4.2: Unilateral and bilateral arm elevation kinematics during **abduction**. Significant differences are denoted with *

Joint Kinematics		Unilateral		Bilateral		P value
		ROM (°)	SD (°)	ROM (°)	SD (°)	
Thorax	Flexion-Extension	12.9	2.5	16.3	4.0	*.000
	Lateral rotation	7.9	2.8	4.5	1.8	*.000
	Axial rotation	5.6	2.3	3.6	1.8	.360
ST artic.	Retraction-Protraction	15.1	7.0	19.6	9.3	*.008
	Medial-Lateral rotation	45.8	8.1	48.8	7.1	*.000
	Anterior-Posterior tilt	12.1	7.7	13.1	6.4	.051

TABLE 4.3: Unilateral and bilateral arm elevation kinematics during **flexion**. Significant differences are denoted with *

Joint Kinematics		Unilateral		Bilateral		P value
		ROM (°)	SD (°)	ROM (°)	SD (°)	
Thorax	Flexion-Extension	11.8	3.6	15.9	3.5	*.000
	Lateral rotation	6.9	3.4	3.3	1.6	*.000
	Axial rotation	6.3	3.1	3.9	2.4	*.000
ST artic.	Retraction-Protraction	16.0	4.6	16.4	5.3	.225
	Medial-Lateral rotation	45.9	9.7	46.8	5.3	.074
	Anterior-Posterior tilt	11.6	5.9	13.0	8.2	.056

4.3.3 Discussion and Conclusions

A full 3D kinematics description of the trunk and scapula was obtained (Table 4.2 for abduction and Table 4.3 for flexion) for healthy participants using marker based MA techniques and the ISB recommendations for the upper limb. Although previous studies have quantified trunk rotations or scapula rotations [16, 151, 155, 156] minimal attention has been given to quantifying the combined movement of both trunk and scapula during arm elevation.

4.3.3.1 Trunk rotations during arm elevation

The thorax provides a stable postural basis of arm movement. Even though participants were asked to maintain their trunks as straight as possible, rotations along all three axes were recorded during UE and BE.

Significantly larger trunk extension was recorded with the subjects performing BE compared to UE during both abduction and flexion. Gatchev and Dimitrova [155] found an increase in electromyographic recordings of erector spinae muscle activity during right arm elevation. This observation might explain the greater trunk extension during BE (where both the right and left erector spinae would be active). The pattern of observed trunk extension was consistent with other studies [156, 157] suggesting it is necessary for full shoulder ROM.

During UE, lateral rotation of the trunk was contralateral to the arm being elevated. Small trunk rotations were recorded below 80° of arm elevation and rapidly increased beyond 80° with up to 14° of left lateral trunk rotation recorded for one of the volunteers during abduction. Although Theodoridis and Ruston found ipsilateral trunk rotation in a study of 25 healthy female participants [151], Stewart et al found that lateral rotation could be either ipsilateral or contralateral during UE [158]. On the other hand, BE resulted in significantly smaller lateral rotation during both abduction and flexion although no clear pattern (contralateral or ipsilateral) was observed amongst the study cohort. Lateral rotations of the trunk during UE in the current study were found to be twice as large compared to those found by Theodoridis and Ruston. Differences in ROM may be attributed to the recording protocols where Theodoridis and Ruston assessed the movement dynamically and, in the current study, movement was assessed statically. Another possible reason for the discrepancies may be explained by variations in the age group (Theodoridis and Ruston measured women aged between 45 and 64 years) and recording protocols (the thorax in the present study was modelled as a rigid body identified by bony landmarks whereas Theodoridis and Ruston fixed an electromagnetic source over the T2 spinous process).

Trunk axial rotation remained constant and close to that recorded for the trunk's starting position during BE for both abduction and flexion. However, trunk axial rotations were significantly different between BE and UE. It is suggested that, during BE, the trunk segment is stabilized by muscular forces to produce an equilibrium; which also reduces axial trunk rotation.

4.3.3.2 Scapula rotations during arm elevation

Scapula motion aids in arm position by maintaining a better congruence between the humerus and the glenoid of the scapula, thus reducing the risk of GH dislocation. The present study showed that retraction, lateral rotation and posterior tilting of the scapula occur during arm elevation. Similar observations have been made in previous studies [19, 27, 97, 154].

The patterns and ROM of scapula retraction during arm elevations are comparable to those recorded by Fayad et al [26]. Significant differences were measured for scapula retraction during abduction between BE ($19.6 \pm 9.3^\circ$) and UE ($15.1 \pm 7.0^\circ$).

The average scapula lateral rotation ROM was significantly different between the two measurement protocols. Greater lateral rotation was measured during abduction for BE ($48.8 \pm 7.1^\circ$) compared to UE ($45.8 \pm 8.1^\circ$). Thoracic posture is thought to influence scapula lateral rotation, with underestimation by as much as 4° during different sitting postures [154].

Posterior scapula tilting was similar between BE ($13.1 \pm 6.4^\circ$ during abduction and $13.0 \pm 8.2^\circ$ during flexion) and UE ($12.1 \pm 7.7^\circ$ during abduction and $11.6 \pm 5.9^\circ$ during flexion). However, the present study measured a smaller magnitude of posterior tilting during arm elevations when compared to the study of Finley et al [154]. Differences may be attributed to variations in the subjects cohort and differences in computing scapula motions (where the axes of the technical coordinate systems fixed by the electromagnetic sensors to describe the segments' motions since the ACSs were unknown).

It is possible that recording the data trials statically, and with a SL, might influence participants' normal trunk and shoulder motion. Therefore dynamic trials might show different movement patterns or ROM although the accuracy of the scapula recordings would be compromised due to skin artefacts.

Trunk and scapula motions were significantly different when participants elevate one or both arms, similar to those found by Klopkar et al [33]. Therefore it is suggested that, to measure shoulder function more precisely, the contribution of the thorax rotations should be minimised through BE.

4.4 Investigating shoulder function asymmetry in dominant and non-dominant arms

Conflicting evidence exists concerning the differences in shoulder ROM and function in dominant and non-dominant arms. Some authors have found similar ROM between the two shoulders [159], whilst others have measured significant differences [160–162] and others have measured varied results depending on the motion being tested [163]. At present, the literature is contradictory and confusing and no clear pattern is available. Study characteristics, such as population size and composition, the design of the protocol and the measuring techniques used, probably all contribute to the inconsistencies in the results.

The importance of determining whether significant differences exist between dominant and non-dominant shoulders is related to the general assumption that a patient's un-injured shoulder is a measure of how the affected shoulder moved prior to injury or pathology [164]. Some authors believe that there are natural differences between sides due to joint usage [160, 163], therefore using the contralateral shoulder as an estimate of pre-injury would not be appropriate [164].

The aim of this study was to compare shoulder complex kinematics in healthy volunteers' dominant and non-dominant arms to determine whether similar or significantly different patterns and ROM are measured.

4.4.1 Methods

Five healthy participants (4♀, 1♂, mean age 23.6 ± 2.2 years, height 1.73 ± 0.1 m, weight 68.9 ± 23.8 Kg, and BMI 22.5 ± 4.9 Kg/m²) were included in the study. ISB recommendations for marker placement and the reporting of motion were followed. Dominant arm shoulder function was measured from the arm starting beside the body to 120° of arm elevation in abduction, scaption and flexion in 20° intervals during bilateral arm elevation. Scapula kinematics was recorded with the SL. Following this, the non-dominant shoulder was similarly tested.

Differences between GH joint, ST articulation and humerothoracic (HT) motion were investigated using a paired sample t-test ($p < 0.05$) in IBM Statistics SPSS 19.

4.4.2 Results

The average dominant and non-dominant shoulder ROM and SD are shown in Table 4.4 for abduction, scaption and flexion. Significant differences in the measured ROM between the two arms are denoted with *.

TABLE 4.4: Joint and segment rotations ROM and SD for dominant and non-dominant shoulders during abduction, scaption and flexion. Significant differences obtained with a paired t-test are denoted with *

Joint Kinematics	Abduction					Scaption					Flexion					
	Dominant		Non Dominant		P value	Dominant		Non Dominant		P value	Dominant		Non Dominant		P value	
	ROM (°)	SD (°)	ROM (°)	SD (°)		ROM (°)	SD (°)	ROM (°)	SD (°)		ROM (°)	SD (°)	ROM (°)	SD (°)		
GH joint	Plane of Elevation	16.0	5.4	21.7	7.3	*.000	12.0	2.7	12.0	3.9	*.000	17.5	6.5	22.4	6.6	*.002
	Elevation	63.7	5.1	63.3	5.0	.735	72.7	6.0	65.1	5.1	*.001	76.9	7.5	74.3	17.5	*.008
	Axial rotation	16.0	6.3	13.2	6.5	.152	11.8	5.2	14.4	7.3	*.000	7.8	3.1	13.8	2.3	*.000
ST artic.	Retraction-Protraction	9.0	4.9	9.2	3.8	*.001	8.1	2.1	10.7	7.7	*.001	12.4	4.4	13.7	6.5	*.000
	Medial-Lateral rotation	30.6	4.5	28.6	4.0	*.001	23.4	5.6	25.9	2.5	*.000	20.6	4.9	13.7	5.0	*.005
	Anterior-Posterior tilt	6.6	3.2	5.2	2.7	*.000	4.3	1.4	6.5	2.3	*.000	7.0	1.5	6.7	3.1	*.000
HF	Plane of elevation	16.8	5.8	13.2	7.7	.058	7.4	3.2	7.6	3.1	*.006	10.5	6.2	12.6	4.0	.377
	Elevation	92.6	4.0	87.8	8.5	.152	91.6	6.3	92.1	7.8	.686	86.5	6.8	89.3	12.0	.704
	Axial rotation	17.7	8.2	26.1	13.4	.301	13.9	1.5	14.0	5.1	.520	19.2	5.2	20.2	11.5	*.000

4.4.3 Discussion and Conclusions

There are few studies comparing shoulder function and motion between dominant and non-dominant arms, and the feeling in general is that it is still unclear as to whether clinically relevant differences indeed exist.

Significantly greater GH joint elevation was measured with the dominant shoulders compared to the non-dominant shoulders during scaption (difference of 7.6°) and flexion (difference of 2.6°). Differences were also recorded in the GH plane of elevation and axial rotation, with the non-dominant shoulders generally showing greater plane of elevation angles and larger external rotations during arm elevations (Table 4.4). However, these rotations may be subject to “gimbal lock” errors and so caution should be taken when interpreting these measurements.

Significant differences were measured for all ST articulation rotations in the current study (Table 4.4), contrary to previous studies [14, 161, 165, 166] which mostly found significant differences in scapula lateral rotation only. Larger scapula lateral rotations were measured in dominant shoulders, with a maximum difference of 7° between both shoulders during flexion.

Similar humerothoracic elevation angles were achieved with the dominant and non-dominant arms (Table 4.4). Humerus axial rotation showed SD of up to 13° which could be explained by the variation of measured angles due to presence of “gimbal lock” at the beginning and final stages of motion.

Macedo et al found significant differences between the two shoulders of healthy participants in 34 out of 60 measured motions [164]. Despite the differences, they support the practise of the contralateral shoulder as a measure of pre-injury since differences ranged between 0.3° to 7.5° .

Asymmetry between the two shoulders could be attributed to soft tissue imbalance from more frequent use of the dominant shoulder compared to the non-dominant [161]. Large variations in joint movement based on factors such as

age, sex, posture and ligament laxity [163, 167] can also influence shoulder motion.

4.5 Shoulder complex kinematics during physiological ranges of motion and activities of daily living

The motion at the shoulder joint is a result of the independent yet simultaneous contributions of the four articulations that make up the shoulder complex [11]. It is through the understanding of the interactions between the joints that better suited rehabilitation and treatment options could become available for shoulder patients.

The techniques available at Cardiff University allow for the kinematic analysis of all joints in the shoulder complex (the sternoclavicular joint, SC; the acromioclavicular joint, AC; the glenohumeral joint, GH; and the scapulothoracic articulation ST). The aim of this study was to develop a database with healthy shoulder complex function for physiological arm elevations and ADLs measurements. Different techniques were used to collect shoulder kinematics data: skin markers attached to bony landmarks (during both static and dynamic measurements), the SL to record scapula kinematics, as well as the AMC for dynamic measurements, with the objective of making a comparison of the different measurement techniques.

4.5.1 Methods

Dominant shoulder complex function was measured in 23 healthy volunteers (8♀, 15♂, age 23.7 ± 2.2 years, height 1.73 ± 0.09 m, weight 69.5 ± 14.6 Kg, and BMI 22.9 ± 2.8 Kg/m²) in the MA Laboratory following ISB recommendations for marker placement and the reporting of motion. The physiological ROM of the shoulder complex was assessed during bilateral full arm elevation in abduction,

scaption and flexion at 20° intervals from the arm hanging by the side of the body to 180° of elevation marked on a reference frame.

Three recording methods were implemented:

1. Dynamic measurements with markers fixed to the skin as well as AMC to measure scapula function.
2. Static measurements with markers fixed to the skin.
3. Static measurements using the SL, adjusted on the scapula for each arm elevation to account for its movement relative to the overlying skin.

Differences between the scapula recording methods were investigated using One-Way ANOVA ($p < 0.05$) in IBM Statistics SPSS 19.

Fifteen ADLs were recorded for the same arm using an AMC to measure scapula motion. The list of activities can be found in Chapter 3, Table 3.3. All subjects began and ended the measurements in the NP (arm hanging by the side of the body, elbow flexed to 90°, hand pronated). Participants were instructed to perform the activities at their own speed.

Sessions took on average 3 hours.

4.5.2 Results

Complete kinematics descriptions of the right arm shoulder complex were obtained for the 23 volunteers. The mean values of the ROM are shown in Figure 4.6 through to Figure 4.8 for abduction, scaption and flexion respectively. Joint and segment rotations are plotted against humerus elevation relative to the thorax for the given plane of elevation. The results from the ANOVA test to investigate significant differences between the recording approaches are summarised in Table 4.5. The average joint rotations ROM \pm SD during the ADLs are summarised in Table 4.6.

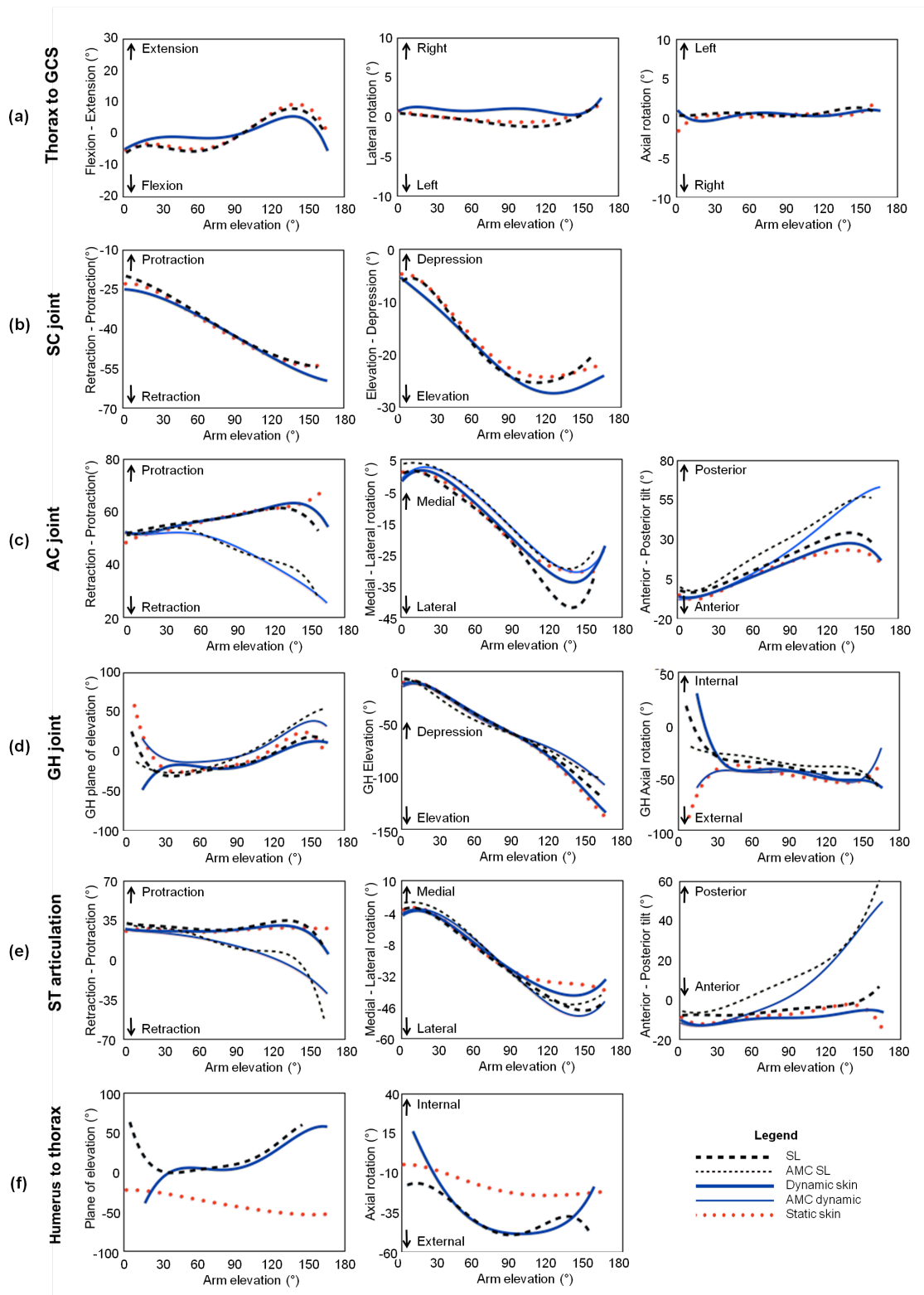


FIGURE 4.6: Complete shoulder complex kinematics during **abduction** (a) thorax in GCS, (b) sternoclavicular joint, (c) acromioclavicular joint, (d) glenohumeral joint (e) scapulathoracic articulation and (f) humerothoracic rotations

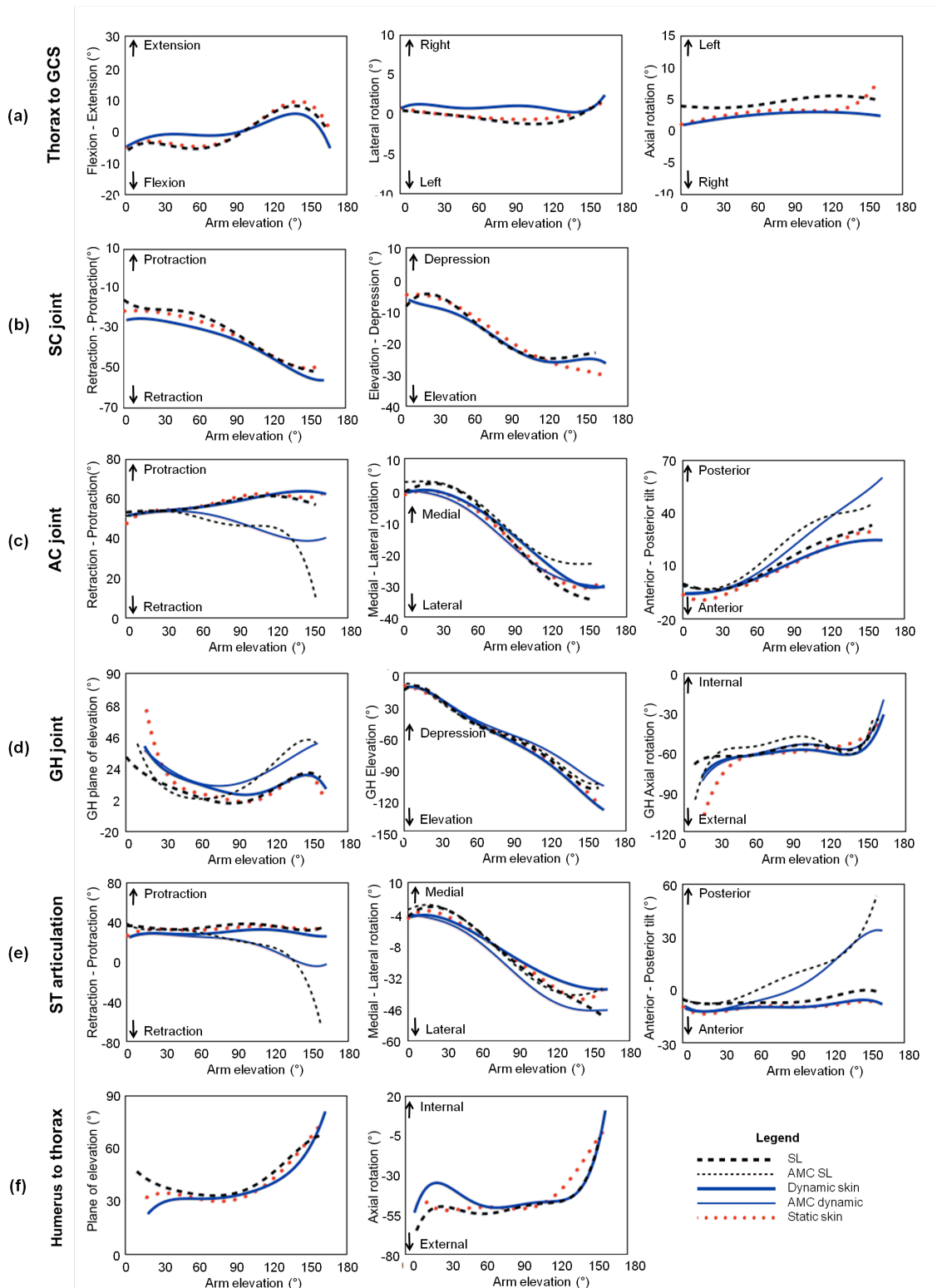


FIGURE 4.7: Complete shoulder complex kinematics during **scaption** (a) thorax in GCS, (b) sternoclavicular joint, (c) acromioclavicular joint, (d) glenohumeral joint (e) scapulathoracic articulation and (f) humerothoracic rotations

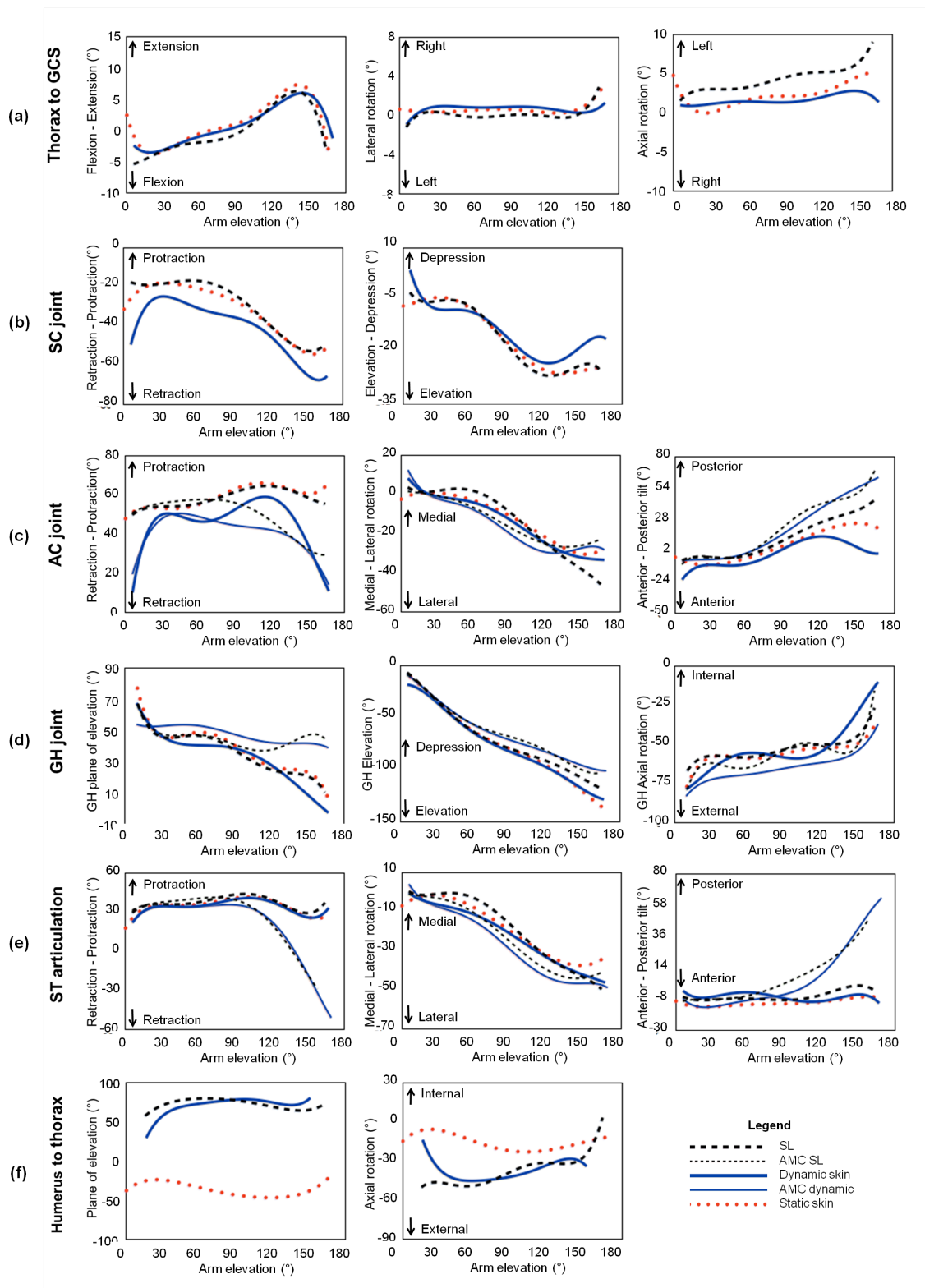


FIGURE 4.8: Complete shoulder complex kinematics during **flexion** (a) thorax in GCS, (b) sternoclavicular joint, (c) acromioclavicular joint, (d) glenohumeral joint (e) scapulathoracic articulation and (f) humerothoracic rotations

TABLE 4.5: Investigating significant differences (denoted with *) between recording protocols during physiological ROMs. sSk refers to static skin measurements, sSL refers to static SL trials and dAMC refers to dynamic AMC measurements

Joint Kinematics	Abduction			Scaption			Flexion		
	sSk&sSL	sSk&dSk	sSL&dAMC	sSk&sSL	sSk&dSk	sSL&dAMC	sSk&sSL	sSk&dSk	sSL&dAMC
Thorax									
Flexion-Extension	.707	*.000	*.005	.117	*.001	.163	1.000	.133	.369
Lateral rotation	.096	.082	*.000	*.002	*.000	.283	1.000	*.007	*.011
Axial rotation	1.000	*.021	*.002	*.026	*.010	*.000	1.000	.059	*.006
SC joint									
Retraction-Protraction	1.000	1.000	.409	.081	.107	1.000	.709	1.000	1.000
Elevation-Depression	1.000	1.000	.738	.846	*.039	.382	.971	.173	*.009
AC joint									
Retraction-Protraction	.147	.935	*.000	1.000	1.000	.111	.847	1.000	*.001
Medial-Lateral rotation	*.023	1.000	*.034	*.000	.050	.791	.401	1.000	.131
Anterior-Posterior tilt	1.000	1.000	*.000	1.000	1.000	*.000	.322	1.000	*.000
GH joint									
Plane of Elevation	1.000	1.000	.076	1.000	1.000	*.014	.349	1.000	.137
Elevation	.082	1.000	.132	.117	*.003	*.004	.503	1.000	*.020
Axial rotation	1.000	1.000	.215	*.028	*.009	.637	1.000	1.000	.144
ST artic.									
Retraction-Protraction	*.006	*.002	*.001	.092	*.003	*.005	.067	1.000	*.000
Medial-Lateral rotation	*.000	1.000	.180	*.000	*.019	.094	*.029	1.000	.166
Anterior-Posterior tilt	.154	1.000	*.000	*.007	*.000	*.000	*.001	.357	*.000
Humerus									
Plane of elevation	.523	.971	1.000	*.037	*.003	1.000	.567	.199	1.000
Elevation	1.000	1.000	.217	.154	1.000	.178	.797	.756	.059
Axial rotation	1.000	1.000	1.000	.233	*.019	.854	.754	1.000	1.000

TABLE 4.6: Average shoulder complex ROM and SD during ADL. Greatest joint rotations are denoted with *

Joint Rotation	Reach to opposite axilla		Reach opposite side of neck		Brush side and back of head		Clean lower back		Eat with hand to mouth		Drink from mug		Answer phone		Reach as far forward as possible		Lift block to shoulder height		Lift block to head height		Internal rotation	
	Thorax	SC Joint	AC Joint	GH Joint	ST artic.	HT	3±2	2±1	4±3	6±3	11±4*	4±2	5±3	5±3	6±3	6±3	9±4	6±3	9±4	7±4	10±5*	Cross body abduction
Flexion-Extension (°)	3±2	2±1	4±3	6±3	11±4*	4±2	5±3	5±3	6±3	6±3	22±10	21±9	17±11	27±14	23±9	13±5	6±3	9±4	7±4	10±5*	Internal rotation	
Lateral rotation (°)	3±3	2±1	3±1	4±1	5±2	2±1	2±1	2±1	2±1	4±2	4±2	2±1	5±3	8±3*	4±3	6±3	5±3	8±3*	5±2	4±3	Cross body abduction	
Axial rotation (°)	5±3	3±2	4±2	8±3	7±3	6±4	7±4	7±4	9±5	2±1	9±5	2±1	8±3	11±5	5±4	8±3	8±3	11±5	19±7*	5±4	Internal rotation	
Retraction-Protraction (°)	9±6	9±4	26±6*	18±7	13±4	13±7	18±8	18±8	22±10	21±9	17±11	27±14	23±9	13±5	13±5	17±11	17±11	27±14	23±9	13±5	Cross body abduction	
Elevation-Depression (°)	13±6	12±5	16±4	18±6	11±2	6±3	9±4	9±4	9±2	14±8	17±5	23±11*	22±13	11±5	11±5	17±5	17±5	23±11*	22±13	11±5	Internal rotation	
Retraction-Protraction (°)	9±3	11±6	22±14	20±11	12±4	8±3	10±3	12±6	12±6	17±8	14±7	21±13	25±13*	8±5	8±5	14±7	14±7	21±13	25±13*	8±5	Cross body abduction	
Medial-Lateral rotation (°)	17±9	21±8	29±4	25±6	19±6	11±4	15±5	17±5	17±5	20±7	18±6	25±8	30±14*	15±5	15±5	18±6	18±6	25±8	30±14*	15±5	Internal rotation	
Anterior-Posterior tilt (°)	18±10	23±10	44±13	32±11	17±5	11±3	17±7	15±6	15±6	28±11	30±10	44±11	46±10*	14±4	14±4	30±10	30±10	44±11	46±10*	14±4	Cross body abduction	
Plane of elevation (°)	37±11	28±13	40±16*	24±10	42±10	21±11	30±12	30±12	30±12	20±8	26±13	29±11	21±7	21±8	21±8	26±13	26±13	29±11	21±7	21±8	Internal rotation	
Elevation (°)	40±13	45±11	53±13	59±17	30±9	41±13	45±9	46±13	46±13	69±16	54±12	67±15*	66±16	29±11	29±11	54±12	54±12	67±15*	66±16	29±11	Cross body abduction	
Axial rotation (°)	24±9	20±11	31±10	32±11	53±17*	19±6	29±10	29±10	34±10*	25±11	26±12	32±12	21±7	34±15	34±15	26±12	26±12	32±12	21±7	34±15	Internal rotation	
Retraction-Protraction (°)	17±7	16±7	34±17*	24±5	12±4	15±7	17±7	20±8	20±8	24±7	18±4	25±9	33±8	13±7	13±7	18±4	18±4	25±9	33±8	13±7	Cross body abduction	
Medial-Lateral rotation (°)	20±9	24±6	38±8*	31±7	17±5	13±3	19±7	19±5	19±5	26±9	25±9	36±9	36±8	15±6	15±6	25±9	25±9	36±9	36±8	15±6	Internal rotation	
Anterior-Posterior tilt (°)	9±6	11±6	35±15*	16±8	16±6	7±3	11±5	10±5	10±5	16±5	15±7	23±10	17±6	11±4	11±4	15±7	15±7	23±10	17±6	11±4	Cross body abduction	
Plane of elevation (°)	61±17	57±13	44±16	37±9	37±10	25±11	34±9	33±12	33±12	34±10	30±14	35±16	78±14*	24±14	24±14	30±14	30±14	35±16	78±14*	24±14	Internal rotation	
Elevation (°)	37±12	50±13	91±13*	78±14	42±10	43±13	53±13	49±13	49±13	79±12	76±15	98±13*	73±15	33±12	33±12	76±15	76±15	98±13*	73±15	33±12	Cross body abduction	
Axial rotation (°)	18±11	17±13	41±27	27±10	53±13*	18±12	24±11	32±13	32±13	20±9	22±8	30±12	25±11	42±20	42±20	22±8	22±8	30±12	25±11	42±20	Internal rotation	

4.5.3 Discussion and Conclusions

Healthy shoulder complex kinematics was calculated in the present study during physiological ROM in abduction, scaption and flexion as well as for 12 ADLs using the ISB convention.

4.5.3.1 Physiological ROM

Physiological ROM recordings are useful measurements to determine the extent to which the individual joints in the shoulder contribute to overall arm elevation. It is widely accepted that the motion of the ST articulation facilitates arm elevation by placing the glenoid cavity in the correct position to maintain congruency between the humerus and the scapula [167]. Therefore the humerus and the scapula couple their movements, in what researchers describe as the scapulohumerual rhythm (SHR) [12, 63]. This complex relationship, between GH elevation and scapula lateral rotation, has been investigated by numerous research groups with various ratios being reported ranging from 1.25: to 2.5:1 [12, 15, 16, 99].

Arm elevation trials were measured statically and dynamically with skin markers to assess differences that may arise from muscle stabilisation as well as control of the joint during dynamic and static trials. Smaller thorax rotations were consistently measured when volunteers performed dynamic movement trials as compared to static and SL (Figure 4.6a, Figure 4.7a and Figure 4.8a for abduction, scaption and flexion respectively). Statistically different thorax lateral and axial rotations were measured between static skin and SL measurements during scaption (Table 4.5), suggesting that the SL positioning might have an effect on the volunteer adopting a different posture compared to without the SL. Furthermore, the muscular contraction required to hold the static positions may alter the positions of the scapula [26] therefore they may not be truly representative of dynamic scapula kinematics during motor tasks.

Although the majority of motion occurs at the GH joint and the ST articulation, motion at the SC and AC joints are required for full arm elevation. The strong clavicle fixation to the scapula through the coracoclavicular ligament means that clavicle rotation occurs with scapula movement [167, 168]. Similar to that reported by Fu et al [167], 30° of SC retraction and elevation were recorded in the current study. In general, no significantly different SC joint rotations were measured between static and dynamic trials, the exception being greater clavicle elevation during dynamic recordings compared to static during flexion (Figure 4.8b, Table 4.5).

Only two bony landmarks can be discerned on the clavicle: SC and AC. Hence, axial rotation cannot be determined through non-invasive palpation measurements [73]. Optimisation techniques can be applied in order to estimate clavicle function [144, 169] although they are not currently employed at Cardiff University.

AC joint rotations appear affected by skin artifact, with up to 8° (significant) difference in ROMs recorded between skin fixed and SL measurements during scaption (Figure 4.7c). Significant differences between SL and AMC recordings for AC retraction and posterior tilting during arm elevation (Table 4.5) can be explained by errors in the AMC recordings due to deltoid muscle contraction at high arm elevations.

GH joint and HT plane of elevation and axial rotation recorded were constant through mid-range arm elevation (Figure 4.6d&f, Figure 4.7d&f, and Figure 4.8d&f). However, near the beginning of the motion and at the final stage of motion, these rotations are affected by “gimbal lock”. This appears to affect the 5th order polynomial curves fitted to the data, since the GH joint externally rotates during arm elevation [19, 27] yet it appears as though it internally rotates during scaption (Figure 4.7) and flexion (Figure 4.8).

During the initial stage of arm elevation, scapula lateral rotation is limited, with 4° of rotation between 0 and 40° of arm elevation relative to the thorax. Beyond 40°, scapula motion rapidly increases with a total ROM of around 40° at full arm

elevation (Figure 4.6e, Figure 4.7e, and Figure 4.8e for abduction, scaption and flexion respectively).

From Table 4.5, ST lateral rotation was consistently underestimated using skin fixed methods. The largest difference was recorded during scaption when skin markers measured 20° less than the SL (Figure 4.7e). On the other hand, the AMC measured similar lateral rotation ROM to the SL. With this consideration, skin markers attached to scapula bony landmarks should be completely avoided since the results do not represent true scapula motion.

The SL is generally used with an electromagnetic sensor to record scapula movement [18, 94]. To the author's knowledge, just one other research group uses optical motion capture system with the SL [150].

4.5.3.2 Activities of Daily Living

Objective measurements of the shoulder complex during ADLs aid in the better understanding of the biomechanical demands on the shoulder during everyday tasks. However, measurements are challenging due to the coordinated movements from multiple joints and the between trial and between individual variability to execute the task [72]. The movement requirements of the joints that make up the shoulder complex during the ADLs are summarised in Table 4.6.

Although small thorax rotations were recorded during the physiological ROM trials, during the ADLs the thorax facilitated certain arm positions, with up to $11 \pm 4^\circ$ of flexion for activities that involved internal arm rotation behind the body (cleaning the lower back and internal rotation).

Reaching the side and back of the head as well as *lifting a block to head height* were the activities with greatest HT elevation ($91 \pm 13^\circ$ and $98 \pm 13^\circ$ respectively). They also seem to be the most challenging activities, with the greatest ROM measured in other joints, such as GH elevation and scapula lateral rotation, accompanying the arm elevation.

Cross-body abduction is also considered a highly challenging task. Although trunk axial rotation facilitated the movement, large AC joint and SC joint rotations were measured with a maximum of 46° of anterior tilting at the AC joint. Furthermore, a large plane of elevation is necessary for the completion of this task.

During *brushing opposite side of the head* task, less GH joint and HT elevation angles were measured in the current study compared to Veeger et al [170]. However, similar SC joint ROM and GH axial rotation were recorded. Differences in the elevation angle might be due to the trajectories that the volunteers chose to comb their hair.

Humerus axial rotation in the current study is affected by soft tissue artefact. van Andel et al [121] used the forearm orientation for the construction of the humerus ACS, thus reducing the effect of skin artefacts on their measurements. Discrepancies between the results may be explained by skin artefact errors underestimating humerus axial rotation in the current study. Furthermore, axial rotation and plane of elevation of the humerus relative to the scapula and the humerus relative to the thorax are affected by “gimbal lock”. At these positions, apparent extreme results were measured, which lead to SD values of up to 27° .

As highlighted by van Andel [121], the variety of functional tasks complicates standardisation as well as large variations of motor task execution in the normal population. However, day to day variability and trial to trial variability were not considered in the current study.

4.6 Repeatability of bony landmark identification and scapula locator placement

To define ACSs on segments, accurate and repeatable identification of anatomical landmarks is essential when using surface skin markers [80]. The positions of these landmarks are used to create an orthogonal coordinate system for

each segment to track their movement during arm elevation trials. The quality of the kinematics measurements is dependent on the accuracy with which these landmarks are identified.

Della Croce et al determined several factors that can difficult bony landmark identification. Anatomical differences between subject participants poses a challenge in the identification of the landmarks. Furthermore, soft tissue surrounding the segment poses a further challenge to the correct identification of the landmark since its thickness and composition vary between participants [103, 105]. Other factors to consider are that landmarks are surfaces, not points and identification is dependent on the specific palpation technique used. During movement, these issues further hinder ability to accurately locate the bony landmarks; for example, muscle contraction alters the thickness and stiffness of the soft tissue over the segment.

The kinematics data presented throughout this thesis was collected by three different observers: Mr Ferran for his MSc studies, Dr. Lovern for his PhD studies, and by the author. The aim of this study was to assess the inter-trial and intra-observer reliability of bony landmark identification and SL placement for the three observers.

4.6.1 Methods

A right handed, healthy male participant, age 26 years, weight 70 Kg, height 161.5 cm and a BMI of 21.1 Kg/m², was included in the study. The reliability of the bony landmark identification was assessed over two visits to the MA Laboratory by the three observers. During each visit, the observers performed three trials where they identified the bony landmarks, recorded a NP measurement, passive circumduction and performed bilateral scapular plane elevation from the arm hanging by the side of the body to 120° on a reference frame in 30° intervals. The humerus CoR was estimated with the IHA method and the scapula was tracked with a SL.

The ICC with 95% confidence interval was calculated for the ST joint angles measured with the SL in IBM Statistics SPSS 19.

4.6.2 Results

The mean ROM and SD measurements recorded by each observer as well as the overall values are summarised in Table 4.7.

The ICC for the three observers over the two MA sessions was calculated at 0.958.

TABLE 4.7: Intra-class and inter-class variation of measured shoulder complex kinematics (mean± SD) recorded by three observers

Joint Kinematics	Observer 1				Observer 2				Observer 3				Average		
	Session 1		Session 2		Session 1		Session 2		Session 1		Session 2		ROM	SD	
	ROM (°)	SD (°)	ROM (°)	SD (°)	ROM (°)	SD (°)	ROM (°)	SD (°)	ROM (°)	SD (°)	ROM (°)	SD (°)	ROM (°)	SD (°)	
Thorax	Flexion-Extension	6.2	1.2	6.6	2.2	7.0	1.0	7.0	0.9	8.1	2.8	5.3	3.2	7.3	2.1
	Lateral rotation	2.0	0.5	1.2	0.3	2.4	0.7	2.6	0.6	2.8	0.3	1.0	0.3	2.3	0.9
	Axial rotation	1.3	1.0	1.0	0.2	2.2	2.3	1.8	0.9	2.3	0.8	0.7	0.4	1.6	1.2
SC joint	Retraction-Protraction	25.4	3.7	18.3	2.7	21.9	2.3	17.7	4.5	22.1	1.8	17.2	4.4	20.0	4.5
	Elevation-Depression	19.7	1.5	14.0	5.3	15.5	1.4	14.4	3.9	20.2	0.6	15.2	4.1	17.3	4.2
	Retraction-Protraction	5.7	3.3	3.1	1.9	11.9	3.0	7.5	4.8	5.1	0.9	4.1	2.0	6.7	3.6
AC joint	Medial-Lateral rotation	14.6	3.2	16.9	11.2	31.0	6.9	15.9	6.8	20.7	2.1	19.7	7.0	19.2	8.0
	Anterior-Posterior tilt	25.4	3.2	18.6	8.0	22.0	3.1	17.8	6.2	25.8	3.4	21.6	2.9	22.2	5.1
	Plane of Elevation	19.1	6.6	15.4	11.3	8.6	4.3	22.2	0.1	30.4	5.2	26.7	3.1	20.7	9.1
GH joint	Elevation	63.2	4.5	60.2	1.5	52.8	9.2	45.2	4.2	52.8	3.9	42.1	1.4	51.6	11.2
	Axial rotation	17.9	3.6	14.2	7.2	3.9	4.4	13.5	6.9	28.5	9.5	20.3	8.1	18.3	8.6
	Retraction-Protraction	15.5	2.9	11.4	3.8	8.4	2.8	4.2	2.6	12.3	2.4	8.9	1.4	10.1	4.3
ST artic.	Medial-Lateral rotation	23.3	1.3	26.3	2.7	23.0	4.7	20.4	5.5	26.6	1.2	21.9	3.3	23.8	7.7
	Anterior-Posterior tilt	5.7	1.8	5.5	3.5	3.7	2.4	3.7	0.6	5.1	1.3	6.6	1.1	5.0	2.0
	Plane of elevation	14.0	2.9	10.9	3.2	15.0	0.5	15.6	2.5	13.4	1.0	14.4	4.6	13.8	2.7
Humerus	Elevation	79.6	2.6	80.7	1.2	89.8	8.1	80.9	3.9	85.6	9.1	82.2	3.3	81.3	10.0
	Axial rotation	16.3	0.6	13.2	0.3	8.2	0.4	10.8	3.0	11.8	5.3	6.9	1.6	11.6	3.9

4.6.3 Discussion and Conclusions

Discrepancies between the kinematics measured by the three observers produced standard deviations of 11° for GH joint elevation and 7.7° for scapula lateral rotation, shown in Table 4.7. Sources of inconsistencies between the observers could include bony landmark identification palpation technique as well as SL placement technique. Participant may also have experience fatigue, which would influence arm elevation [80]. By the time the last observer was performing the last trial of the day, the volunteer would have elevated his arm over 50 times. Furthermore, de Groot estimated that 48% of intra observer variability could be attributed to motor noise [104], the fact that a subject's movements are never exactly the same.

Since scapula function cannot be recorded accurately with skin fixed markers, the SL must be used. The greatest difference in scapula lateral rotation between two observers was 6° . De Groot measured similar differences in an inter-trial study at 8.8° [104] although Johnson found the intra-individual SD less than 2° [18]. Variation of the initial SL setting (due to bony landmark identification errors) would explain differences in the measured motion since the subsequent measurements would be affected. Also, detecting scapula landmarks at high elevations is difficult since the deltoid is at a close proximity to the landmarks and the subject was of athletic build. During muscle contraction, the landmark is easily wrongly identified. Greater variation in the retraction and posterior tilt since factors such as the contact force used by the observers, fat thickness and muscle bulk have an influence on the measurements [18].

Humerus rotations seems to be the most affected by the inter-class reproducibility (humerus relative to scapula and humerus relative to thorax). It is believed that the variability in the data is due to the "gimbal lock" phenomenon that occurs with the YXY rotation sequence, described in Chapter 1; with SD of up to 11° recorded in the GH plane of elevation. Even though the affected frames of

data were discarded, large variability was still measured since it may be challenging to decide in certain frames if the measured angle is due to joint motion or to the “gimbal lock”.

The high ICC value obtained (0.958) suggests that similar overall scapula function was measured by the observers. It is important to be aware of the differences in ROM and patterns measured by the three observers since data throughout the thesis was collected by the three observers.

4.7 Overall conclusions

MA is a useful non-invasive tool to quantify the movement of the shoulder complex. Even though errors in the measurement and technique exist, understanding where the errors originate have made it possible to explore different techniques that lead to improved accuracy in the measurements.

There are a very wide variety of testing protocols to measure shoulder complex function, which makes comparison with other researchers groups' measurements difficult. Conceptual and practical differences between testing protocols lead to discrepancies between shoulder kinematics data found in the literature. Even though ISB recommendations define ACSs of the shoulder bones and how to calculate shoulder kinematics seem appreciated and widely adopted by many research groups, standardisation of the MA protocols beyond the definition of ACS are still limited yet highly desirable [55, 171].

The protocol developed at Cardiff University measures shoulder kinematics data comparable to published studies that follow ISB recommendations. As well as the contribution towards the Cardiff protocol, by improving upon the original protocol, this Chapter provides the reader with an insight into shoulder kinematics and the individual contributions at the joints that make up the shoulder complex to overall arm elevation.

It would be desirable to measure GH translations, however motion capture techniques do not produce clinically significant levels of accuracy to measure translations at the GH joint [74]. More accurate imaging techniques should be used to achieve sub-millimetres levels of accuracy.

The next chapter, Chapter 5, applies the Cardiff protocol to measure and analyse patient shoulder complex kinematics.

Chapter 5

Assessing shoulder complex kinematics in injured or pathological patients

The shoulder is one of the most complex joints in the human body. A lack of bony stability provided by the anatomical structures, results in the largest range of motion (ROM) compared to any other joint complex in the body. However, this large ROM comes at a high price: the shoulder is one of the most commonly injured joints in the human body. It is vulnerable to injuries from sport or trauma as well as to injuries from repetitive loading during overhead activities. Soft tissue changes with increasing age also predispose the shoulder to injury [172].

Shoulder disorders of the joint complex are commonly associated with pain, restricted ROM, disability and atypical scapula function [95, 173–175]. To reduce pain on the affected shoulder, patients may adopt compensatory mechanisms [8, 95, 175] for the execution of biomechanically demanding tasks.

This Chapter contributes towards the better understanding of joint injury and pathology, together with their effect on shoulder motions. Improved knowledge on the subject matter may lead to enhanced patient care and rehabilitation techniques.

5.1 Background

Accurate evaluation and diagnostics of shoulder disorders is challenging due to the joint's complexity. Shoulder movement involves the simultaneous interactions of many individual bones whose direct observation is obscured by overlying muscle. Furthermore, practitioners' are less experienced on shoulder conditions compared with other joints [176].

Currently, clinical diagnosis of shoulder disorders relies on patient history taking together with physical and imaging examination [173, 176, 177]. ROM measurements play a vital role in disability assessment and the evaluation of treatment outcomes [178]; where motion is qualitatively assessed by making a subjective comparison of the injured or pathological (IoP) shoulder to the patient's contralateral (CL) shoulder.

Often, differentiation of shoulder disorders is challenging since shoulder pain can be caused by many different intrinsic and extrinsic conditions [64, 173]. Moreover, pathologies often coexist, further hindering diagnosis [172]. Additionally, pathologies and their manifestations vary from one person to another.

The previous Chapter describes the motion analysis (MA) techniques developed at Cardiff University where shoulder complex kinematics in healthy participants has been successfully measured; yielding results comparable to published studies. This Chapter focuses on measuring the kinematics of shoulder patients that presented disability due to injury or pathology (IoP); thus exploring the effect of trauma and pathology on shoulder kinematics. Comparisons between patients' affected shoulder to their CL shoulder and to healthy participants provides an indication of the effects of pathology or injury on the joint complex.

A wealth of biomechanical data is collected during MA Laboratory sessions, which can be difficult to interpret. Tools to aid in MA data interpretation have been previously developed, although they are commonly used for lower limb analysis [107–109]. At Cardiff, a classification method was developed to aid

in the interpretation of MA data by characterising knee function based on osteoarthritic (OA) and non-pathological kinematics [107]. The tool provides a visual classification of a patient's OA joint as well as his or her progress after total knee replacement (TKR) surgery. Clinicians and shoulder patients could benefit from an objective and accurate quantitative tool that would aid in a patient's diagnosis based on their shoulder complex function.

The aim of this further study was to measure shoulder function in patients that have experienced a prior injury or have pathology in the joint. A preliminary study using the classification tool available at Cardiff to characterise shoulder complex function was also performed.

5.2 Analysis of shoulder patients' kinematics using motion capture techniques

Using the protocol outlined in Chapter 3, shoulder complex function was assessed in four groups of patients that presented either pathology or injury to the shoulder complex. International Society of Biomechanics (ISB) recommendations for data collection and the reporting of motion were followed [73]. The groups of patients were as follows:

- Clavicle fracture
- Glenohumeral joint instability
 - Multidirectional instability
 - Irreparable rotator cuff tear
 - Glenohumeral joint dislocation

The NHS R&D Department and the Local Research Ethics Committee gave ethical approval to assess patients in the MA Laboratory. Written informed consent

from the study participants was sought prior to testing. The injured shoulder kinematics was recorded first followed by the CL shoulder.

Patients were instructed to perform physiological bilateral arm elevation in abduction, scaption and flexion from 0 to 120° of arm elevation (or within the limits of discomfort if they could not reach 120°) in 20° intervals marked on a reference frame. Scapula bony landmarks were identified and recorded with the scapula locator (SL). To avoid overcrowding the Chapter with numerous graphs, only the joint kinematics that are commonly reported for patients with the same or similar conditions are shown in this Chapter. For the full description of each patient cohort shoulder complex kinematics, the reader is directed to Appendix D.

The 15 activities of daily living (ADL) tasks summarised in Chapter 3, Table 3.3 were recorded for both the IoP shoulder and for the CL shoulder with an acromium marker cluster (AMC) to track the movement of the scapula.

The kinematics data from the 23 healthy participants (8♀, 15♂, age 23.7 ± 2.2 years, height 1.73 ± 0.09 m, weight 69.9 ± 14.6 Kg, and BMI 22.9 ± 2.8 Kg/m²) in Chapter 4 was used for comparison with the patients' injured and CL shoulders. Similar to the patient data, only the data collected with the SL trials and to 120° of arm elevation was reported for the physiological ROM recordings and with the use of the AMC for the ADLs.

5.2.1 Clavicle fracture patients

The clavicle serves as the only bony link between the shoulder girdle and the trunk. The segment stabilises the glenohumeral (GH) joint which in turn increases the force and ROM in the joint.

Clavicle fractures commonly occur as a result of high impact forces on the shoulder girdle or falling on the outstretched hand [179, 180]. These fractures account for 44% of all injuries to the shoulder girdle [181, 182] and between 5% and 10% of all bone fractures [181–183]. They are routinely identified in an AP

view X-ray and can be categorised into three groups: proximal, mid-shaft and distal fractures.

Conservative management is the preferred treatment of choice for the majority of mid-shaft clavicle fractures [184]. The method consists of immobilising the arm in a sling for several weeks [183–185] until clinical signs of union are observed.

Surgical intervention may be necessary if the overlying skin is severely compromised by the bony fractures; when the fracture ends are displaced by more than 2cm; for symptomatic non-union; and when neurovascular damage is suspected [184]. Several techniques are available, including plate fixation, Kirschner wires and threaded pins. [186–188].

The goal of clavicle fracture treatment is to restore shoulder strength and motion as pre-injury condition. However, there is a wide range of clinical outcomes following treatment. A loss of strength and motion of the injured shoulder following treatment may result from nonunion, malunion and shortening of the clavicle [189]. Controversial clinical outcomes have been reported following midshaft clavicle fractures with some authors suggesting poor outcomes if shortening is of more than 18mm in male patients and 14mm in female patients [190–193], whereas others have reported no association between shortening and clinical outcome [194?]. Furthermore, a specific rehabilitation program is extremely important and should be designed according to the patient.

It was thus hypothesised that the treated clavicle fracture patients will present similar shoulder girdle function in comparison to their CL shoulders and to healthy participants.

5.2.1.1 Methods

Eight patients (1♀, 7♂, mean age 23.9 ± 8.5 years, height 1.79 ± 0.07 m, weight 86.1 ± 18.2 Kg, and BMI 26.9 ± 4.8 Kg/m²) had sustained unilateral clavicle fracture between 6 months and 4 years prior to testing in the MA Laboratory. Three

patients were treated with a clavicle plate (of which one patient had it removed and the other two patients were awaiting removal); two patients were treated with a threaded pin (removed 3 and 6 months post fracture) and the remaining three patients were treated conservatively. Kinematics data was collected by Dr. Lovern and the author.

Clavicle movement is intrinsic to the kinematics of two joints: sternoclavicular (SC) and acromioclavicular (AC) joints. Statistical analysis of the SC and AC kinematics of healthy participants as well as for both the patients' injured and CL shoulders was performed using One-Way analysis of variance (ANOVA) statistics test in SPSS ($p < 0.05$). No distinction between treatment methods was made since the number of participants recruited was too few.

5.2.1.2 Results

SC and AC joint kinematics were investigated during physiological arm elevation. The average ROM and standard deviation (SD) for healthy volunteers and for both the patients' injured and CL shoulders are shown in Figure 5.1 through to Figure 5.3 for abduction, scaption and flexion respectively. Joint rotations were plotted against arm elevation relative to the thorax.

Results from the One-Way ANOVA test are summarised in Table 5.1.

5.2.1.3 Discussion and Conclusions

Physiological ROM measurements were recorded to characterise the *in vivo* SC and AC joint motions in patients with clavicle fracture treated either conservatively or with surgical intervention. Only one patient had significant pain on the shoulder which limited his ROM. The remaining participants showed no visual impairment attributable to their injury during the arm elevation trials. Figure 5.1 to Figure 5.3 show healthy shoulder kinematics and clavicle patients' injured

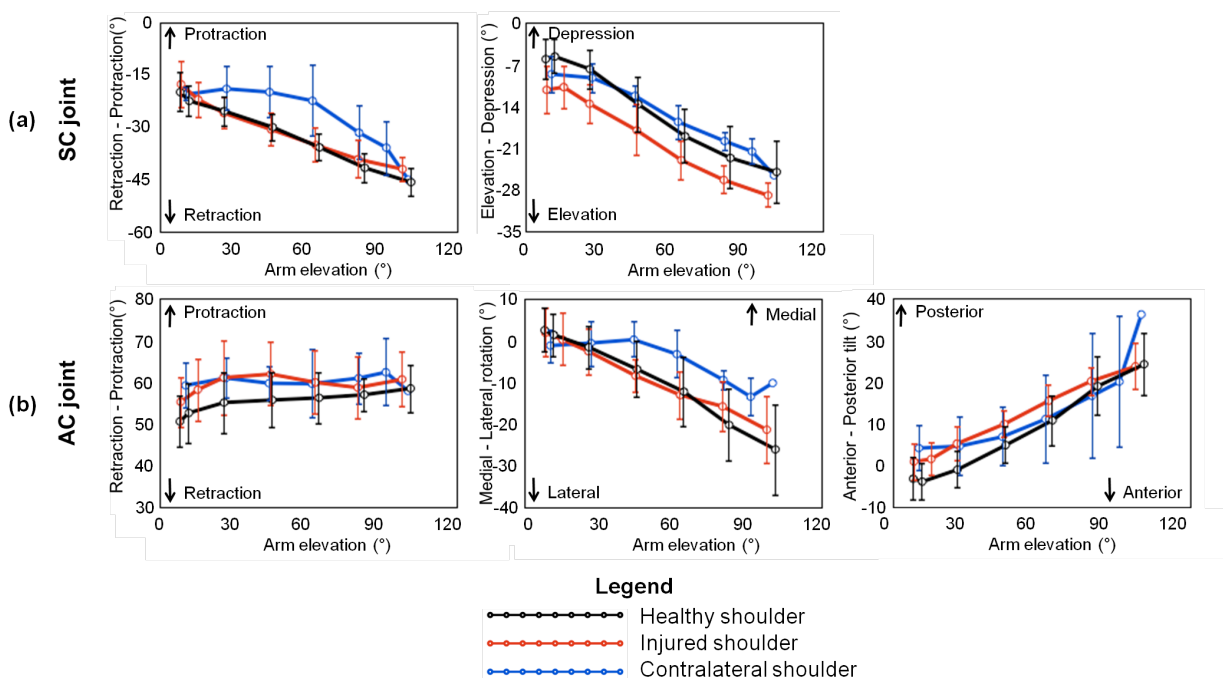


FIGURE 5.1: Average healthy participants and clavicle fracture patients' injured and contralateral (a) sternoclavicular and (b) acromioclavicular joint kinematics during **abduction**. Error bars represent SD

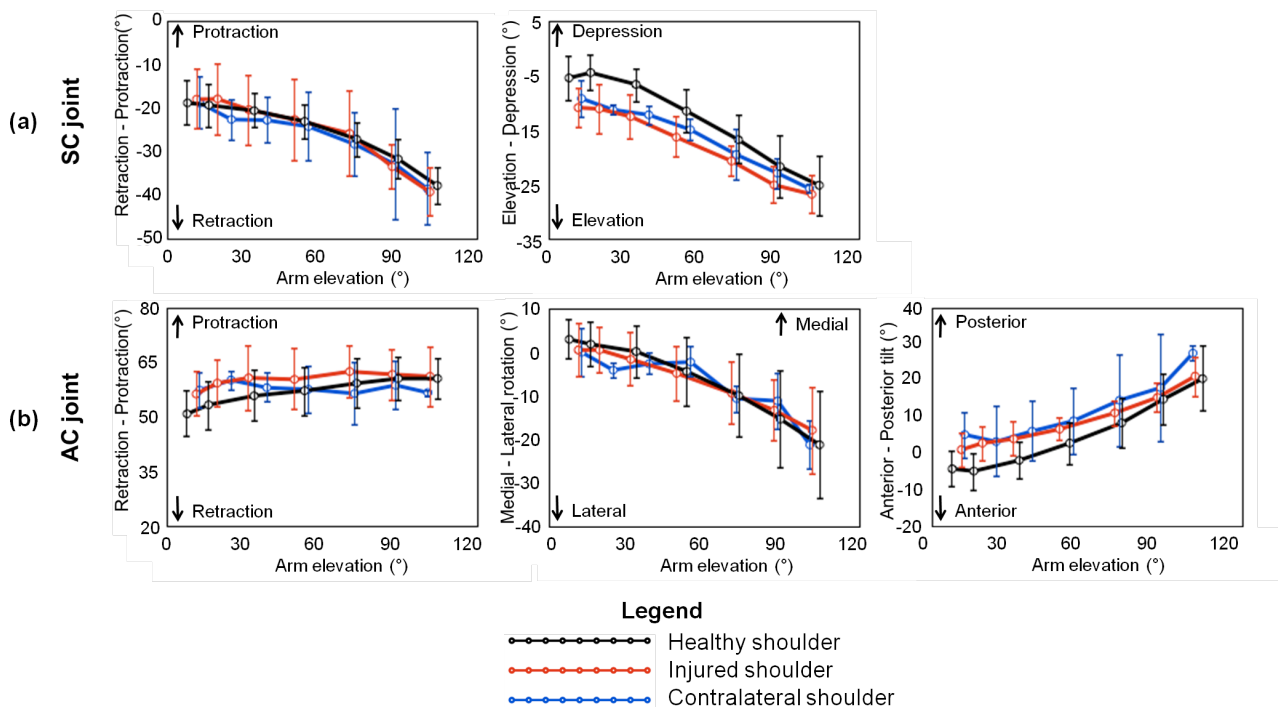


FIGURE 5.2: Average healthy participants and clavicle fracture patients' injured and contralateral (a) sternoclavicular and (b) acromioclavicular joint kinematics during **scaption**. Error bars represent SD

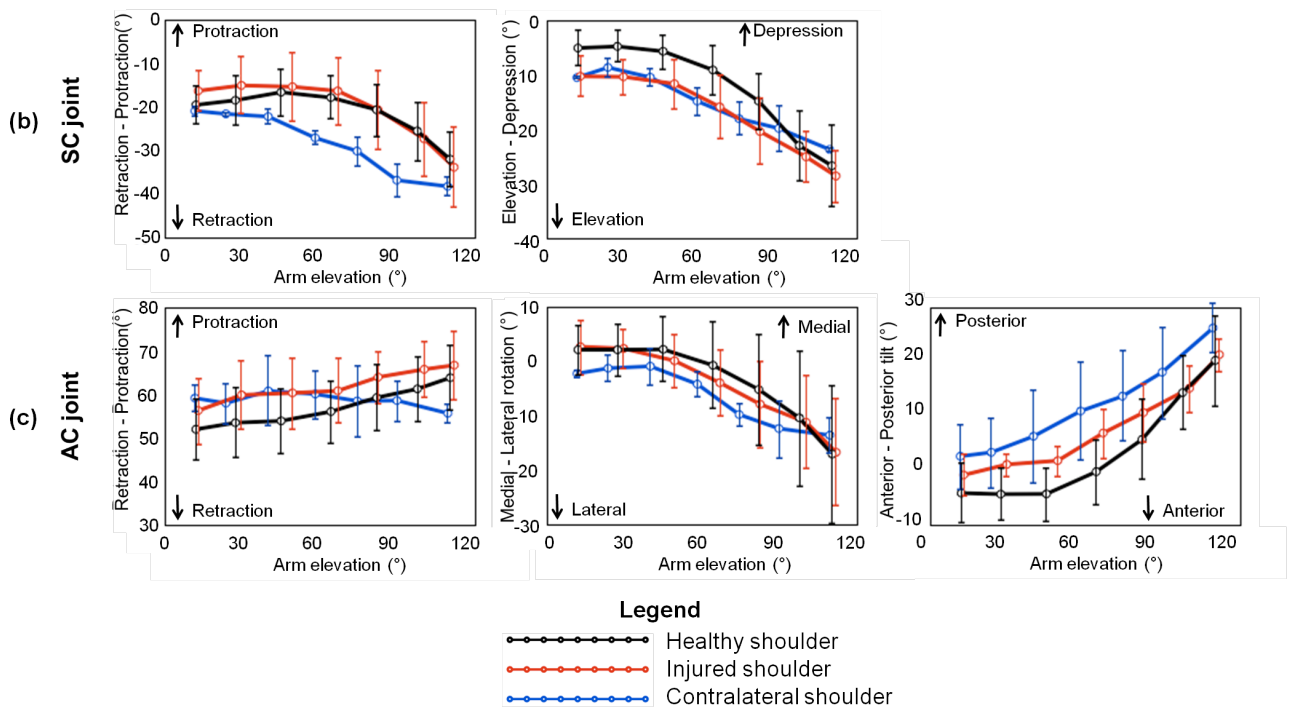


FIGURE 5.3: Average healthy participants and clavicle fracture patients' injured and contralateral (a) sternoclavicular and (b) acromioclavicular joint kinematics during **flexion**. Error bars represent SD

TABLE 5.1: ANOVA *p* values associated with SC and AC joint kinematics of healthy (HL) and clavicle fracture patients' injured (IoP) and CL (CL) shoulders during physiological ROM. Significant differences are denoted with *

Measurement		SC joint		AC joint		
		Retraction-protraction	Elevation-depression	Retraction-protraction	Medial-lateral	Anterior-posterior
Abduction	HL&IoP	1.000	.775	*.005	1.000	1.000
	HL&CL	1.000	1.000	*.001	1.000	.702
	IoP&CL	1.000	1.000	1.000	1.000	1.000
Scaption	HL&IoP	1.000	.748	.429	1.000	1.000
	HL&CL	1.000	1.000	1.000	1.000	.447
	IoP&CL	1.000	1.000	1.000	1.000	1.000
Flexion	HL&IoP	.241	.759	.052	1.000	1.000
	HL&CL	1.000	1.000	1.000	1.000	.372
	IoP&CL	.155	1.000	.278	1.000	1.000

as well as their CL shoulder kinematics during abduction, scaption and flexion respectively.

During arm elevation, the SC joint retracted and elevated. Patients' CL shoulders showed a different pattern of motion as compared to their injured and healthy shoulders during abduction (Figure 5.1a) and flexion (Figure 5.3a). However, no significant differences were recorded between the three shoulder groups (Table 5.1). This could be explained due to the data variability, with up to 18° of SD during abduction (Figure 5.1a). Similar ROMs were recorded for clavicle elevation. SC axial rotation was not measured since it cannot be calculated using the current methods employed at Cardiff University.

The AC joint protracted, laterally rotated as well as tilted posteriorly during arm elevation. Statistically greater AC protraction during abduction was measured in healthy participants compared to patients' injured and their CL shoulders (Figure 5.1b, Table 5.1). AC lateral rotations were greater in injured shoulders although differences were not statistically significant. SD values up to 10° were measured for AC rotations during flexion (Figure 5.3b).

Large SC joint rotations, in the order of 55 to 65° for axial rotation, 29° of protraction and 32° elevation, were recorded in the current study. Pronk et al [57] measured SC and AC joint rotations in healthy participants during abduction elevation. They used optimisation algorithms to minimise clavicle axial rotation and thus measured AC joint rotations at 8° protraction, 4° lateral rotation and less than 2° forward tipping. Larger clavicle elevation and posterior tilt angles were recorded in the current study as compared with studies by Fung et al [177] and Pronk et al [57]. Discrepancies may be attributed to the *in vitro* nature of their studies, as well as to differences in anatomical coordinate system (ACS) position and orientation used in the study by Fung et al in addition to their optimisation techniques used to minimise clavicle rotations [57]. Nevertheless, similar patterns of motion were recorded.

Clavicle fracture incidence predominates in the male population rather than in the female [179, 184], therefore it is not surprising that only one female patient enrolled in the current study compared to seven males.

In conclusion, shoulder function was restored for the study cohort following treatment of the clavicle fracture. The study hypothesis is accepted since the measured patients' injured shoulder ROM was similar to that of the CL and to HL participants.

5.2.2 Glenohumeral joint instability patients

Shoulder instability is the inability to maintain the humeral head within the glenoid centre during active motion. This inability can be attributed to excessive GH mobility, laxity, soft-tissue failures at the labrum, as well as to abnormal scapular kinematics [195, 196].

During arm elevation, the synchronised humerus rotation around the glenoid in the GH joint and the scapula rotation around the thorax in the scapulothoracic (ST) articulation result in the scapulohumeral rhythm (SHR) [11, 15]. Alterations to the SHR can produce movement dysfunction at the GH joint, such as instability or impingement [195].

The GH joint acts as a ball-and-socket joint, with minimal to no translations occurring in healthy shoulders [63]. However, in an unstable GH joint, translation of the humeral head relative to the glenoid is commonly measured [63, 197–199], mainly through radiographic evaluation. GH joint translations may lead to dislocations and subluxations that in turn may result in the onset of OA of the joint due to cartilage degeneration [64].

Instability at the GH joint may present itself in at least three different forms: as multidirectional instability (instability in more than one direction); rotator cuff tear (where equilibrium of the forces in the GH joint are disrupted); and dislocation or

subluxation (where, in a dislocation, the humerus and glenoid completely disarticulate whereas, in subluxation, instability is only partial). The following section investigates the kinematics of the three patient groups mentioned above.

Although it is desirable to measure GH joint translations, MA does not provide clinically meaningful levels of accuracy to measure translations and so cannot be used. Since this is the case, researchers do not report translations of the humerus relative to the scapula when measurements are taken with MA or electromagnetic systems. Instead, imaging techniques are used to measure translations.

5.2.2.1 Multidirectional instability patients

Multidirectional instability (MDI) was first described by Neer and Foster in the 1980s [200], as a symptomatic GH subluxation or dislocation occurring in more than one direction [201]. The disability can occur in both sexes, at any age, in varying activity levels within the population [202] and can be a result of a traumatic or atraumatic event [203].

Joint laxity, as a result of a loose capsule, characterises this condition [197, 204, 205] with patients often subluxating or dislocating the GH joint during daily activities [205, 206]. Over time, repetitive subluxation of the humeral head can lead to labral tears and so the patient develops shoulder pain. Patients with MDI have greatest difficulty lifting overhead and throwing [203, 207] since the arm often feels unstable.

Diagnosis and treatment of MDI is often difficult due to the complex nature of the pathology [202]. Clinical examination often includes ROM, strength, scapulothoracic rhythm and translation testing in all directions [204]. Shoulder girdle strengthening exercises and modification of the patient's routine activities are successful conservative treatments; although 20% do not respond well and thus require surgical intervention [201, 208]. Arthroscopic treatment of MDI has

been previously described with reported “satisfactory to excellent” outcomes in 75% of the cases [197].

Additional to increased GH joint translations, altered ST and GH joint kinematics have been reported in patients with MDI. Studies have reported decreased scapula lateral rotation [207, 209, 210] as well as an increase in scapula internal rotation [209, 210] and excessive GH translation with shoulder elevation while Baeyens et al reported greater GH joint external rotation during static positions using MRI [61]. It was thus hypothesised that MDI patients recruited in this study will present altered scapula and GH joint kinematics compared to a control group.

Methods

The kinematics of seven clinically diagnosed MDI shoulders in six patients (3♀, 3♂, mean age 25.7 ± 7.1 years, height 1.69 ± 0.12 m, weight 79.5 ± 17.5 Kg, and BMI 27.9 ± 6.1 Kg/m²) were measured in the MA Laboratory. The patient with bilateral MDI had arthroscopic capsular shrinkage over a year prior to testing although he still experienced shoulder subluxation. No other patient had received surgical intervention; instead they had all completed a physiotherapy regime to strengthen the rotator cuff and scapula stabilizers. The measurements were recorded by Mr Ferran with either Dr Lovern or the author working on the computer.

GH joint and ST articulation kinematics were investigated. Statistical analysis of the GH joint and ST articulation of healthy participants as well as for both the patients' injured and CL shoulders was performed using One-Way ANOVA in SPSS ($p < 0.05$). No distinction between the capsular shrinkage and non-surgical treatment patients was made due to a lack of significant cohort number.

Results

Average healthy and both the patients' injured and CL shoulders GH joint and ST articulation kinematics is shown in Figure 5.4 through to Figure 5.6 for abduction, scaption and flexion respectively. Joint kinematics are plotted against arm elevation relative to the thorax.

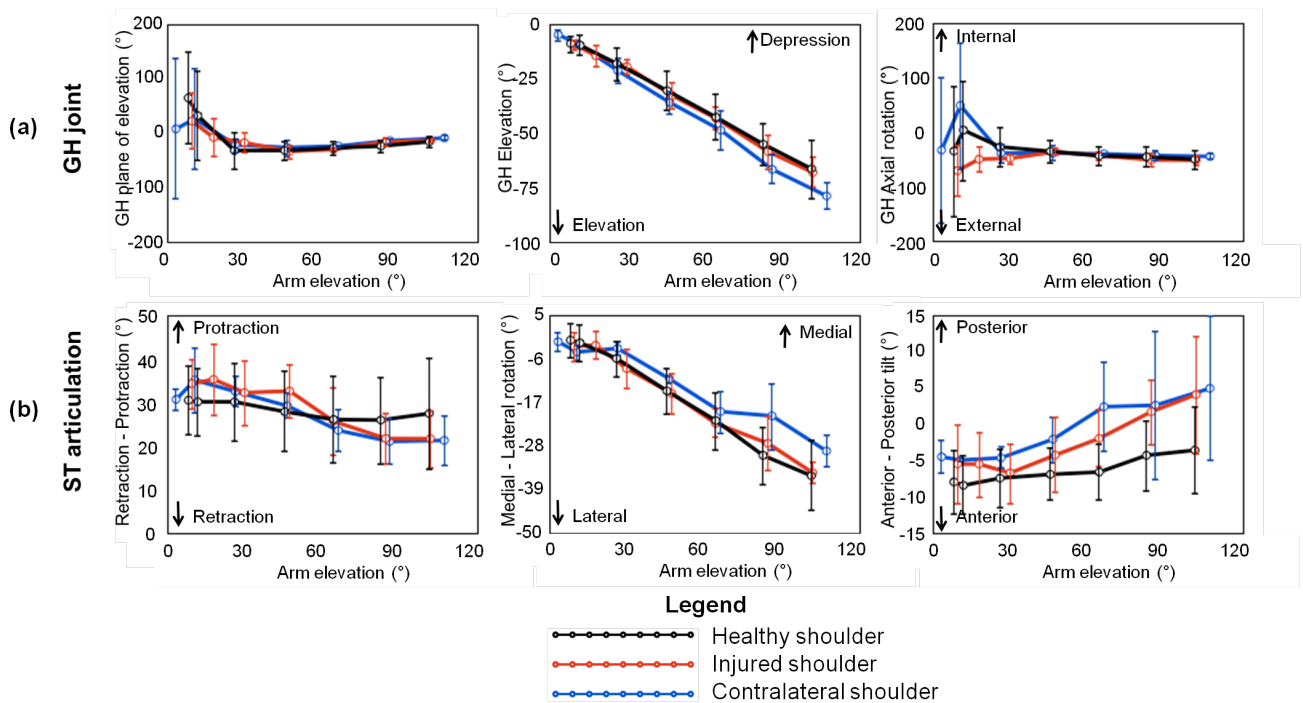


FIGURE 5.4: Average healthy and MDI patients' injured and contralateral (a) glenohumeral and (b) scapulothoracic kinematics during **abduction**. Error bars represent SD

Results from the One-Way ANOVA test are summarised in Table 5.2.

Discussion and Conclusions

Patients with MDI have an unstable GH joint and experience humerus translations in more than one direction. Mid-range arm positions, as well as overhead elevations, are problematic for these patients. One of the study participants was experiencing too much discomfort and pain during the trial, therefore decided to withdraw without completing all the elevation and ADLs trials.

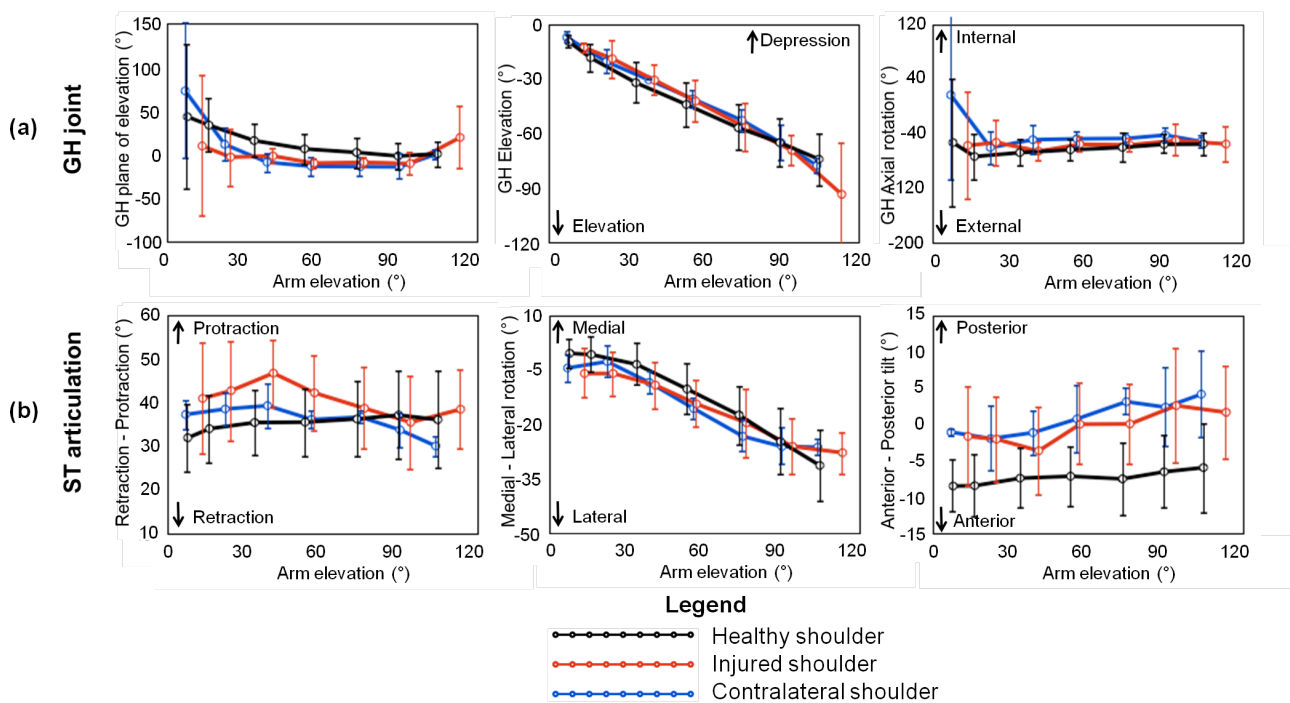


FIGURE 5.5: Average healthy and MDI patients' injured and contralateral (a) glenohumeral and (b) scapulothoracic kinematics during **scaption**. Error bars represent SD

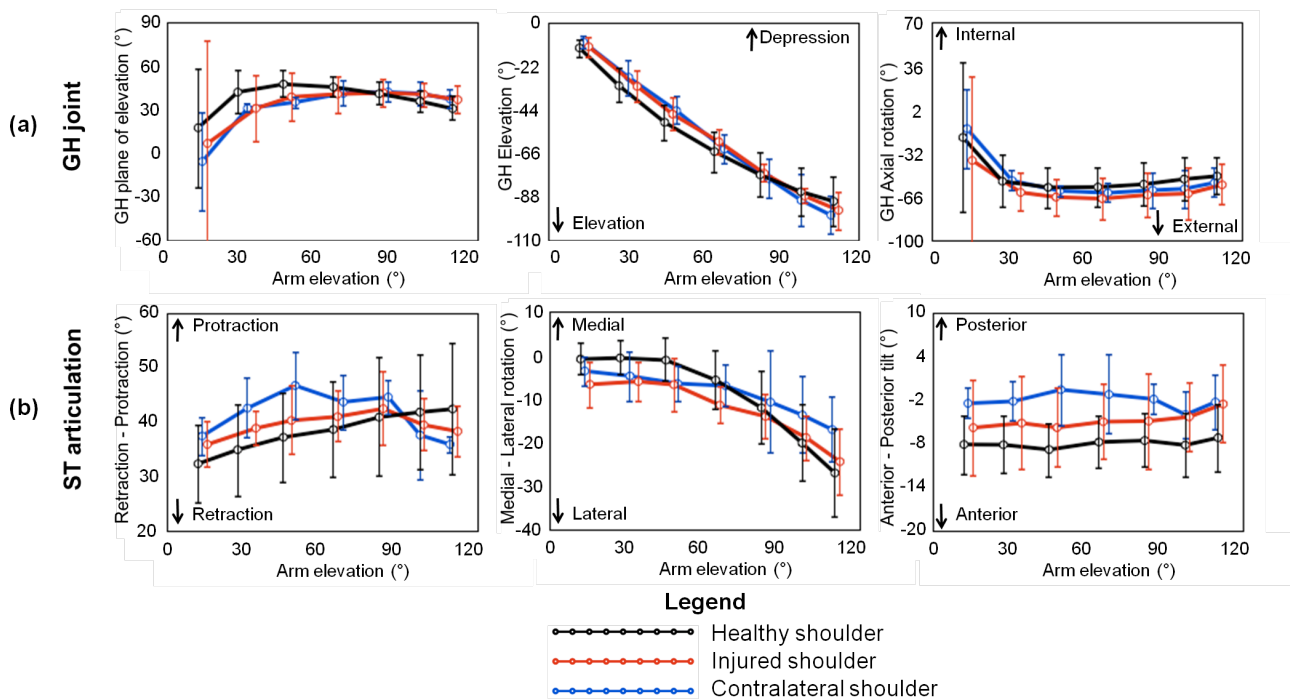


FIGURE 5.6: Average healthy and MDI patients' injured and contralateral (a) glenohumeral and (b) scapulothoracic kinematics during **flexion**. Error bars represent SD

TABLE 5.2: ANOVA *p* values associated with GH joint and ST articulation kinematics of healthy (HL) and MDI patients' loP and CL shoulders during physiological ROM. Significant differences are denoted with *

Measurement		GH joint			ST articulation		
		Plane of elevation	Elevation	Axial rotation	Retraction-protraction	Medial-lateral	Anterior-posterior
Abduction	HL&loP	.603	1.000	.318	1.000	1.000	.163
	HL&CL	1.000	1.000	1.000	1.000	1.000	*.025
	loP&CL	1.000	1.000	.382	1.000	1.000	1.000
Scaption	HL&loP	.722	1.000	.702	*.007	1.000	*.000
	HL&CL	.071	1.000	*.004	1.000	1.000	*.000
	loP&CL	.603	1.000	*.037	*.021	1.000	.652
Flexion	HL&loP	1.000	1.000	*.010	1.000	1.000	*.000
	HL&CL	1.000	1.000	.184	.405	1.000	*.000
	loP&CL	1.000	1.000	.430	1.000	1.000	*.000

Similar to shoulder kinematics data published for healthy participants [19, 27], the GH joint in the current study was responsible for the first 30 to 40° of arm elevation during abduction and scaption (Figure 5.4 and Figure 5.5 respectively). Beyond this angle, arm elevation was a combination of GH and ST rotations.

Participants did not appear to maintain the plane of elevation during arm abduction with the pathological shoulder (Figure 5.4a). In agreement with Kim et al, larger GH elevation angles were measured with the CL shoulder (up to 10° difference) during abduction and flexion elevations [202] compared with the loP shoulder; however, differences were not statistically significant (Table 5.2). Greater GH external rotation in the MDI shoulder compared to the CL was recorded.

During flexion, the scapula appeared to begin its lateral rotation at a much later stage of arm elevation (around 50° for healthy participants and nearing 60° for patients' loP and CL shoulders). However, differences in lateral rotation were not found to be statistically significant (Table 5.2) which could be due to the high SD. While protraction was recorded in healthy volunteers during arm elevations, patients showed scapula protraction and retraction during similar recordings

(Figure 5.4 to Figure 5.6 for abduction, scaption and flexion respectively). However, differences only appear significant during scaption measurements (Table 5.2). Greater posterior tilting of the scapula was also recorded in patients compared to the healthy population, yet differences were not statistically significant (Figure 5.4 to Figure 5.6 for abduction, scaption and flexion respectively). Nyiri et al also reported atypical scapula function in MDI patients [205].

Altered SHR has been reported in MDI patients treated with muscle strengthening only [202]. In their study, Kiss et al found that although the patients reached arm elevations similar to control groups, the contribution of the GH joint had decreased while ST lateral rotation contribution increased [202].

Management of MDI can result in different biomechanical shoulder outcomes depending on whether the patients were treated conservatively or surgically [202, 203, 205]. Surgical management followed by a physiotherapy regime has been shown to restore shoulder function similar to a control group [203]. In the current study, there was a lack of control regarding treatment option and thus no differentiation between the treatment methods was made.

In conclusion and in accordance with the hypothesis, significantly different shoulder girdle ROM were measured in MDI shoulders (significantly less humerus external rotation and less scapula protraction and posterior tilting) compared to the patients' CL shoulder and HL during physiological ROM.

5.2.2.2 Irreparable Rotator Cuff tear patients

The rotator cuff (RC) tendon provides dynamic stability to the GH joint by centering the humerus head in the glenoid during shoulder motion. Variations in acromium morphology can sometimes lead to mechanical abrasion of the RC, which in turn leads to tendon degeneration and tear [95, 211]. When the rotator cuff tears (RCT), the force and torque balance at the GH joint is disrupted [175]. The superior shear force of the deltoid muscle overcomes the weakened RC force [8], which results in humerus migration [8, 95, 175].

RC injuries affect 20 to 40% of the population over 60 years of age [212, 213] and 50 to 70% in population of patients over 70 years [213]. Patients usually have the greatest difficulty lifting overhead and throwing [203].

Various theories on the cause and aetiology of RCT include mechanical or anatomical factors, traumatic injury, age-related degeneration and hypovascularity of the RC [95, 213]. Other comorbidities usually follow after RCT, such as the development of OA, or superior GH subluxation [95].

RCTs are commonly treated through arthroscopic repair. However, in some instances, the RCT is irreparable (IRCT). In such cases, arthroscopic debridement is performed to reduce shoulder pain [214].

Patients with IRCT suffer from long term shoulder disability. Loss of motion is a well recognised complication [215–218] as well as residual weakness and inferior outcomes [214]. Painless loss of motion may be well tolerated, however more substantial limitations and pain or even substantial loss of motion without associated pain can be functionally disabling [217].

IRCT are often associated with proximal humeral head migration [214] often evaluated using radiographic assessment. Furthermore, “unstable kinematics” [218] have also been reported in RCT patients. Most patients will have decreased active shoulder motion and patients with a chronic weakness may have sufficient scar tissue within the joint to result in “mild limitations” [214] in passive motion. Additionally, according to Neri et al, patients may also demonstrate increased passive humerus external rotation [214].

It was hypothesised that a reduced ROM would be measured on the patient’s injured shoulder compared to their CL and HL participants shoulders as a result of altered GH joint kinematics.

Methods

Five shoulders in four subjects (1♀, 4♂, mean age 72.5 ± 13.2 years, height 1.68 ± 0.12 m, weight 75.1 ± 16.1 Kg, and BMI 26.3 ± 2.6 Kg/m²) with IRCT had

arthroscopic RC debridement since a full repair was not possible. They were all at least 1 year post operatory. The kinematics data was collected by the author with either Mr Watling or Miss Birrfelder handling the computer.

GH joint and ST articulation kinematics were recorded during the physiological arm elevation trials. Statistical analysis of the GH joint and ST articulation kinematics of healthy participants and for both the patients' IoP and CL shoulder was performed using One-Way ANOVA ($p < 0.05$) in SPSS.

Results

Average GH joint and ST articulation kinematics are shown in Figure 5.7 through to Figure 5.9 for abduction, scaption and flexion respectively. Joint rotations are plotted against arm elevation relative to the thorax.

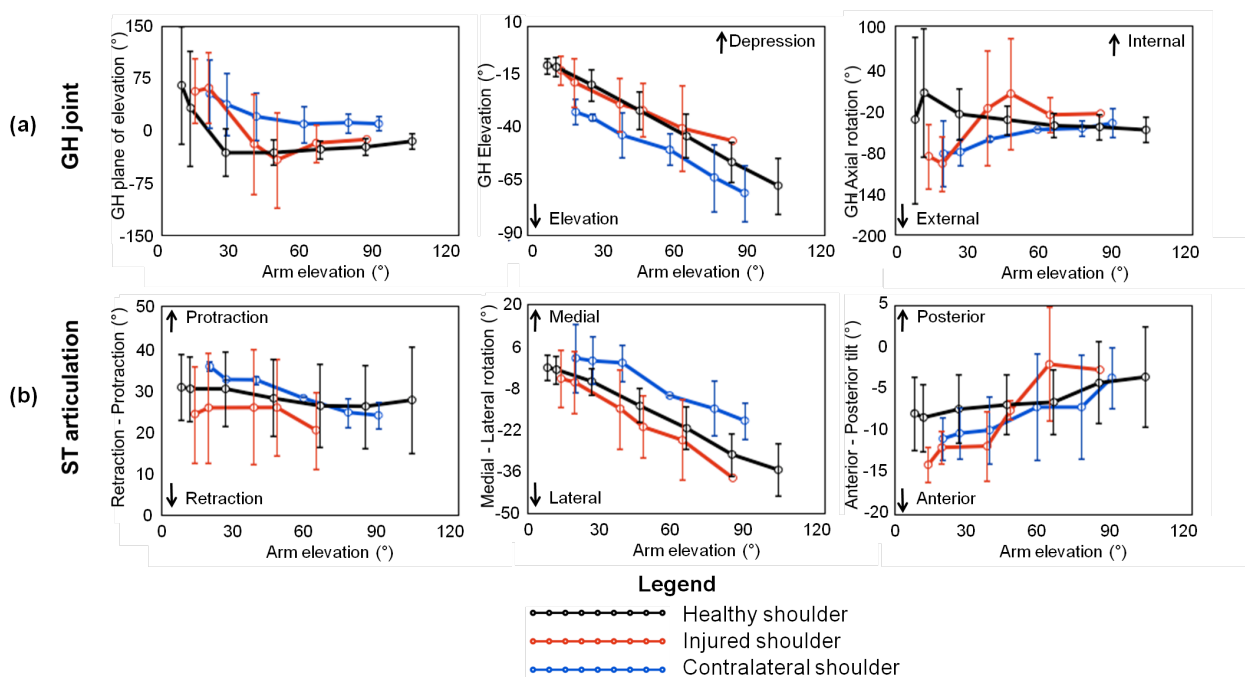


FIGURE 5.7: Average healthy and IRCT patients' injured and contralateral (a) glenohumeral and (b) scapulothoracic kinematics during **abduction**. Error bars represent SD

Results from the One-Way ANOVA test are summarised in Table 5.3.

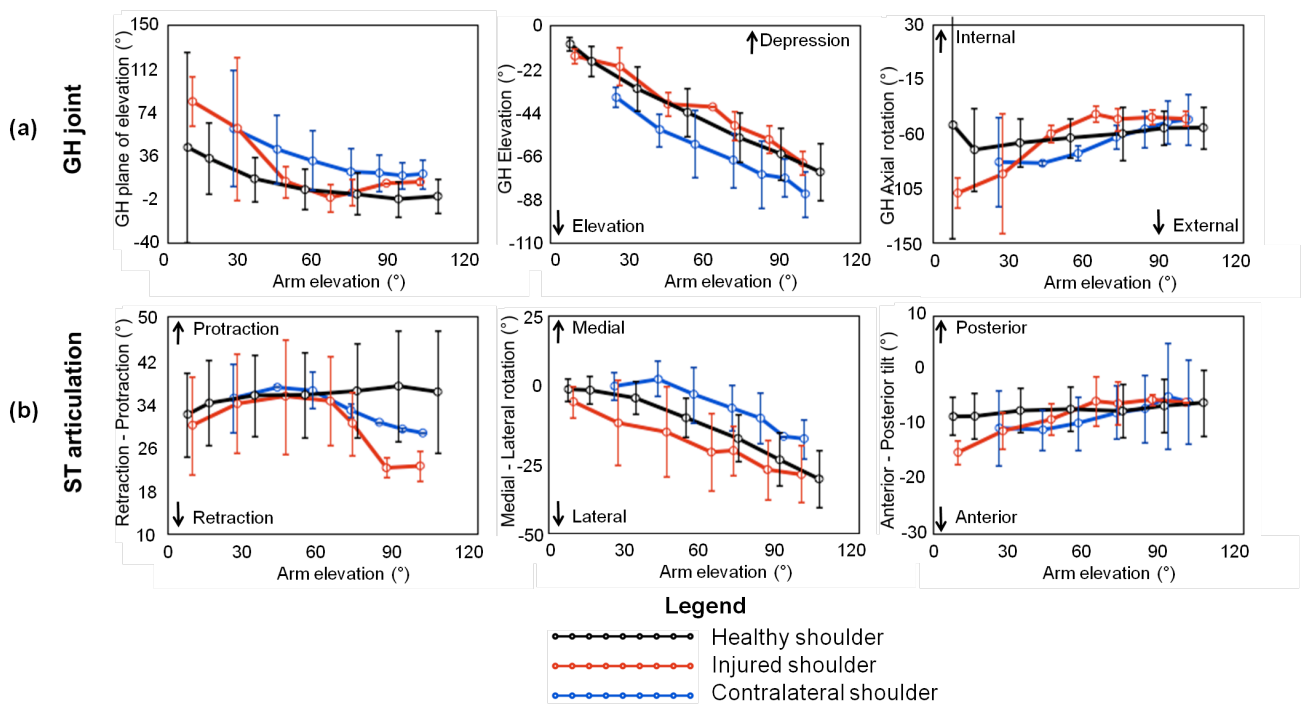


FIGURE 5.8: Average healthy and IRCT patients' injured and contralateral (a) glenohumeral and (b) scapulothoracic kinematics during **scaption**. Error bars represent SD

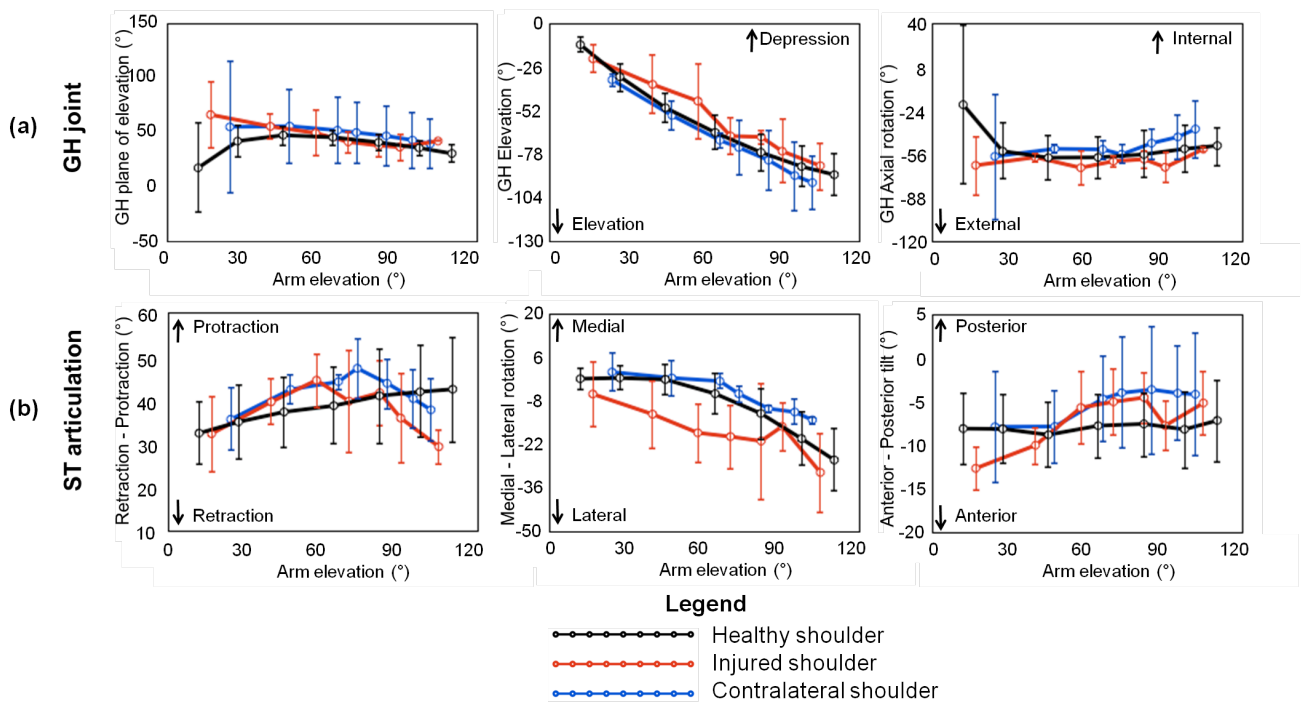


FIGURE 5.9: Average healthy and IRCT patients' injured and contralateral (a) glenohumeral and (b) scapulothoracic kinematics during **flexion**. Error bars represent SD

TABLE 5.3: ANOVA p values associated with GH joint and ST articulation kinematics of healthy (HL) and IRCT patients' loP and CL shoulders during physiological ROM. Significant differences are denoted with *

Measurement		GH joint			ST articulation		
		Plane of elevation	Elevation	Axial rotation	Retraction-protraction	Medial-lateral	Anterior-posterior
Abduction	HL&loP	.672	1.000	.309	.190	.190	1.000
	HL&CL	*.001	.253	1.000	1.000	1.000	1.000
	loP&CL	*.007	.281	.058	.162	.162	1.000
Scaption	HL&loP	1.000	1.000	*.029	.052	.722	1.000
	HL&CL	*.046	.171	1.000	.742	.945	1.000
	loP&CL	*.013	.105	*.043	.513	.112	1.000
Flexion	HL&loP	1.000	1.000	.389	1.000	.260	1.000
	HL&CL	.350	1.000	.190	.567	1.000	.069
	loP&CL	.654	.880	*.010	.315	.054	.236

Discussion and Conclusions

Conflicting scapula kinematics evidence has been reported in RCT patients [25, 162, 207, 219]. Studies supporting both an increase [25, 220] and a decrease [196, 221] of scapula lateral rotation and posterior tilting in RCT patients have been published; while others have suggested only a subset of patients with RCT present abnormal scapula kinematics [219].

As the arm elevates, the GH joint elevates and externally rotates (Figure 5.7a to Figure 5.9a for abduction, scaption and flexion respectively). During the first 40 to 50° of arm elevation, the GH plane of elevation and axial rotation were affected by “gimbal lock” therefore these elevation angles do not provide an accurate indication of GH motion and should not be considered for the analysis. Reduction in humerus external rotation has been previously reported with RCT patients [95, 222]. However, measuring accurate GH external rotation in the current study is difficult since the data is subject to “gimbal lock” during the initial movement stage. SD over 70° was recorded in GH joint rotations. The large variability in the data can be explained by presence of “gimbal lock” in the data of two participants resulting in an unrealistically large GH plane of elevation and axial rotations.

Figures 5.7b to Figure 5.9b show ST articulation rotations in abduction, scaption and flexion respectively. The current study supports the evidence that greater ST lateral rotation and posterior tilting are characteristic of RCT. However differences do not appear to be statistically significant (Table 5.3).

Kedgley et al [95] recognised different joint kinematics in RCT shoulders depending on whether the lesion to the RC is in a single tendon, extends into a portion of a second tendon; or if the lesion exceeds two tendons. They found a reduced plane of elevation angle with RCT and varying external rotation angles depending on the tear size and lesion in a cadaveric study. Furthermore, Paletta et al [8] found that normal SHR is restored following RCT repair.

Some RCT patients compensate with different muscle groups and can thus achieve similar arm elevation angles to control groups [223]. Kedgley et al [95] support the previous statement since they reported that “it is not unusual for some patients with cuff tears to exhibit near normal motion with the injured shoulder, while other patients with the same magnitude of injury are unable to achieve full elevation in the injured side”. A study participant, with bilateral RCT, showed near normal motion for both shoulders during physiological ROM. However, the patient is aware his GH joint is unstable during overhead activities.

Patients treated with debridement have reported substantial pain relief and a high rate of satisfaction although minimal strength or motion is achieved [214]. Two patients in the current study showed poor motion in their injured shoulder. Significant pain during arm elevation made it impossible for them to reach elevations beyond 50°.

In accordance to the hypothesis, altered GH joint kinematics were recorded on patient’s pathological shoulder. Greater GH joint external rotation was measured in IoP shoulders compared to the CL and HL shoulders. No significant differences were observed in scapula kinematics. A better understanding of the effects that RCT have on GH motion may lead to improved rehabilitation strategies as well as provide an appreciation as to why some patients cope better with RCT compared to others [95].

5.2.2.3 GH joint dislocation patients

The GH joint is the most commonly dislocated diarthrodial joint in the human body [7]. This inherent instability is a consequence of its extensive range of movement. Due to the lack of bony stability, the joint relies on the surrounding soft tissue for stability. Once the stabilisers have been compromised, instability at the joint occurs.

Traumatic injuries account for the majority of shoulder dislocation. The mechanism of injury may be the result of the application of a direct force, causing

translation of the humeral head, or the application of an indirect force; for example, an abduction, extension and external rotation force [224].

GH joint dislocation occurs approximately in 2% of the population with 80% of dislocations occurring in younger patients [225, 226]. Recurrence dislocation can range from 60% to 94% when the first episode occurs in patients under the age of 21 years and from 10% to 14% in patients over the age of 40 years [227].

Traditionally, patients have been managed non-operatively, with a period of immobilisation followed by rehabilitation. However, high rates of recurrence have been associated with this conservative method [228]. Early intervention following a first time dislocation has been suggested to decrease the rate of recurrent instability [198, 199]. However, not all patients develop instability following a first time dislocation; therefore these patients would be subjected to an unnecessary operation if every first time dislocator is surgically treated.

Abnormal scapula kinematics has been associated with GH joint instability [229]. Significant scapula internal rotation [162] as well as significant differences in scapulohumeral rhythm [8] have been reported. The increase in scapula internal rotation is believed to be detrimental to maintaining inferior stability at the GH joint [230]. It was hypothesised that GH joint dislocation patients will present altered GH joint and ST articulation kinematics compared to their CL shoulders and to HL participants.

Methods

Eight shoulders in seven GH joint dislocation patients (2♀, 5♂, mean age 21.8 ± 3.8 years, height 1.86 ± 0.06 m, weight 80.4 ± 9.2 Kg, and BMI 23.3 ± 2.5 Kg/m²) were tested in the MA Laboratory. Two patients were first time dislocators, while the rest were recurrent dislocators. Of the recurrent dislocators, two had undergone arthroscopic capsular tightening prior to testing.

Statistical analysis of the SC and AC joints kinematics of healthy and patients' injured and CL shoulders was performed using One-Way ANOVA ($p < 0.05$) in

SPSS. No distinction between first time dislocators and recurrent dislocators was made due to the limited number of patients recruited.

Results

Average GH joint and ST articulation kinematics and SD for healthy participants and patients' injured and CL shoulders are shown in Figure 5.10 through to Figure 5.12 for abduction, scaption and flexion respectively. Joint rotations are plotted against arm elevation relative to the thorax.

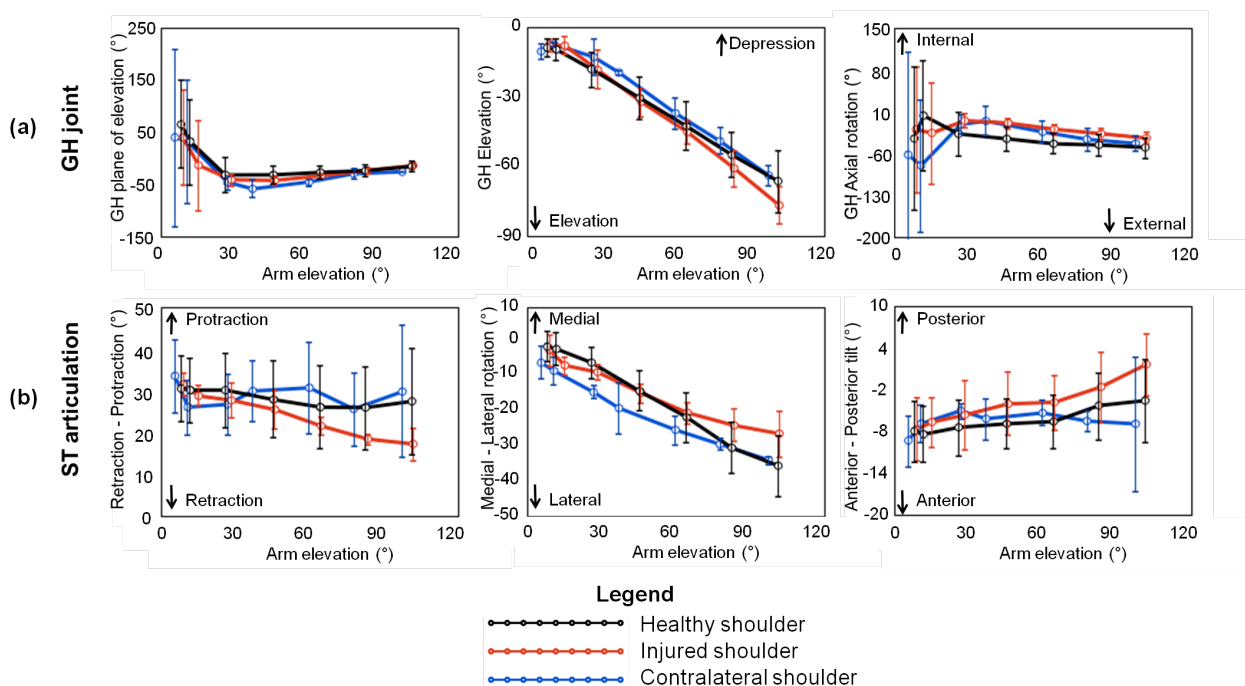


FIGURE 5.10: Average healthy and GH dislocation patients' injured and contralateral (a) glenohumeral and (b) scapulothoracic kinematics during **abduction**. Error bars represent SD

Results from the One-Way ANOVA test are summarised in Table 5.4.

Discussion and Conclusions

Accurate, detailed and specific information about patient prognosis after a first time dislocation is critical [199]. However, management of a primary traumatic GH dislocation is controversial, although increasing evidence suggests arthroscopic stabilisation is the optimal treatment option [228, 231, 232].

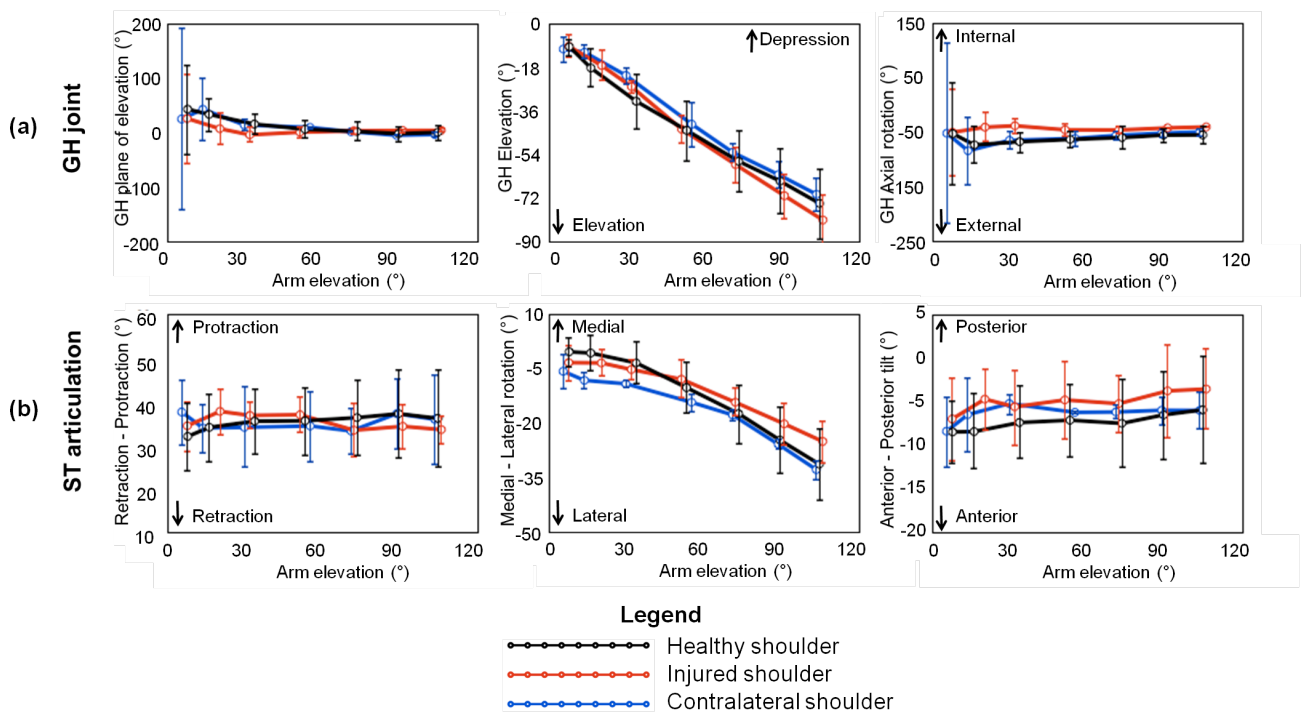


FIGURE 5.11: Average healthy and GH dislocation patients' injured and contralateral (a) glenohumeral and (b) scapulothoracic kinematics during **scaption**. Error bars represent SD

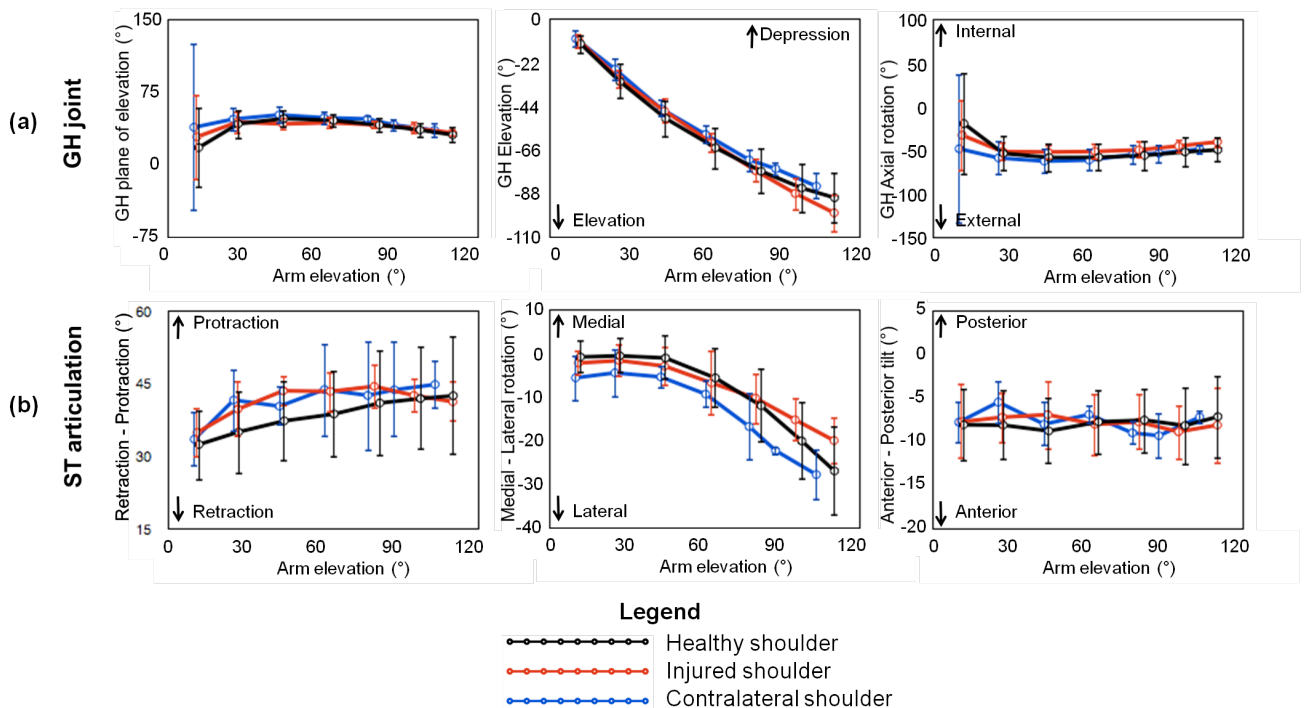


FIGURE 5.12: Average healthy and GH dislocation patients' injured and contralateral (a) glenohumeral and (b) scapulothoracic kinematics during **flexion**. Error bars represent SD

TABLE 5.4: ANOVA *p* values associated with GH joint and ST articulation kinematics of healthy (HL) and GH dislocation patients' IoP and CL shoulders during physiological ROM.

Significant differences are denoted with *

Measurement		GH joint			ST articulation		
		Plane of elevation	Elevation	Axial rotation	Retraction-protraction	Medial-lateral	Anterior-posterior
Abduction	HL&IoP	1.000	1.000	.060	.192	1.000	.173
	HL&CL	.158	1.000	.194	1.000	1.000	1.000
	IoP&CL	.518	1.000	1.000	.105	1.000	.136
Scaption	HL&IoP	1.000	1.000	*.000	1.000	1.000	*.001
	HL&CL	1.000	1.000	.916	1.000	1.000	.277
	IoP&CL	1.000	1.000	*.003	1.000	1.000	.059
Flexion	HL&IoP	1.000	1.000	.125	.418	1.000	1.000
	HL&CL	.746	1.000	1.000	.390	1.000	1.000
	IoP&CL	.558	1.000	.052	1.000	1.000	1.000

Patients' ability to reach the higher elevation on the frame was not affected by their condition, with GH joint elevation angles achieved similar to their CL shoulder and to the healthy cohort (Figure 5.10a to Figure 5.12a for abduction, scaption and flexion respectively). In fact, greater GH elevation angles were recorded on patients' injured shoulder as compared to their CL and healthy participant's shoulders, supporting Paletta's et al suggestion that SHR kinematics are altered in the unstable shoulder [8]. However, differences were not statistically significant (Table 5.4).

From Figure 5.10a, Figure 5.11a and Figure 5.12a, GH plane of elevation was maintained throughout arm movements during abduction, scaption and flexion respectively. Humerus external rotation relative to the scapula was recorded for all participants. However, significant differences between healthy and injured shoulders and between injured and CL shoulders were recorded during scaption (Table 5.4).

Small ST protraction angles were recorded and the pattern of motions were similar between the three shoulder groups for scaption and flexion (Figure 5.11b

and Figure 5.12b respectively). However, the scapula appeared to retract for patients' injured shoulder during abduction (Figure 5.10b). For patients with GH joint instability, Matias et al [195] found significant differences in retraction and posterior tilt angles between their injured and estimated healthy shoulder function.

Similar to other research groups [100, 196], patients' injured shoulders experienced less scapula lateral rotation during abduction (Figure 5.10b), scaption (Figure 5.11b) and flexion (Figure 5.12b) compared to their CL and with healthy shoulders.

In accordance to the hypothesis, altered GH and ST articulation kinematics were measured in the GH dislocation patients. However, differences only appeared significant during scaption.

5.2.3 Activities of Daily Living

Reduced ROM and pain are limiting factors of shoulder disability. Compensatory mechanisms described above were explored and described during physiological ROM. However, it is important to evaluate shoulder complex performance during everyday life, where both movement and loading are common occurrences.

Limited studies have investigated shoulder function during ADLs on patients. Most ADL investigations have been on young healthy population with no shoulder impairment [35, 121]. So there is still a need to investigate the IoP population. The aim of this study was to measure shoulder complex function during ADLs in both injured and pathological patients for comparison with healthy shoulder function.

5.2.3.1 Methods

Shoulder complex patients who enrolled onto the ROM studies described above, were instructed to perform 15 ADLs (summarised in Chapter 3, Table 3.3). The combined anthropometric data between the four patients group is (4♀, 20♂, mean age 32.4 ± 19.9 years, height 1.76 ± 0.11 m, weight 80.7 ± 16.2 Kg, and BMI 25.9 ± 4.8 Kg/m²). First their loP shoulder was tested, followed by CL shoulder measurements.

During weight bearing activities, the patients were allowed to choose the most comfortable weight of the load during lifting a block to shoulder and head height tasks.

Significant differences between healthy and loP shoulder ROMs during the ADLs were investigated using One-Way ANOVA ($p < 0.05$) in SPSS. When the data did not conform to the ANOVA requirements, the Wilcoxin sign rank non-parametric test ($p < 0.05$) was used.

5.2.3.2 Results

The four patient cohorts were recorded and analysed without making a distinction between the different shoulder conditions. The ADLs were performed with both the loP (Table 5.5) and the CL (Table 5.6) shoulder. The reader is directed to Table 4.6 in Chapter 4 for the healthy participants' ADL measurements. Significant differences between healthy and loP shoulders are shown in Table 5.5.

TABLE 5.5: Average patients' loP shoulder complex ROM and SD during ADLs. Significant differences between healthy and loP shoulders are denoted with §

Joint Rotation	Thorax											Internal rotation	
	Reach opposite axilla	Reach opposite side of neck	Brush side and back of head	Clean lower back	Eat with hand to mouth	Drink from mug	Answer phone	Reach as far forward as possible	Lift block to shoulder height	Lift block to head height	Cross body abduction		
Flexion-Extension (°)	3±2	2±3	3±2	5±3	10±4	3±3	5±3	5±3	6±4	6±3	8±4	6±4	12±5
Lateral rotation (°)	3±2	2±1	2±1	3±1	5±2	2±1	3±1	3±2	2±1	5±2	7±3	5±4	5±3
Axial rotation (°)	4±3	3±2	3±2	6±4§	7±4	4±3	4±3§	6±5§	3±2	9±4	10±4	11±7§	6±4
Retraction-Protraction (°)	7±6	8±5	25±8	14±11	11±5	10±7	12±6§	14±7§	17±8	14±7§	19±8	17±10	12±6
Elevation-Depression (°)	9±6	12±6	13±6	18±7	11±3	5±3	8±4	7±4	14±6	16±8	24±9	18±8	10±4
Retraction-Protraction (°)	7±3	11±6	22±15	14±6	10±7	8±4	9±4	10±4	11±6§	12±8	17±10	20±14	9±5
Medial-Lateral rotation (°)	5±5	18±7	25±6	24±8	16±8	9±5	14±5	13±5§	14±7	16±7	23±8	31±11	13±6
Anterior-Posterior tilt (°)	9±6	17±9	41±18	30±13	22±11	10±6	15±9	12±6	21±10	24±10	39±15§	32±16	18±9
Plane of elevation (°)	35±21	27±14	41±17	28±14	46±38	24±14	30±14	32±17	20±10	33±12	35±15	25±14	65±47§
Elevation (°)	39±16	51±13	51±16	61±15	27±11	35±12	37±11§	38±15	59±19	56±11	64±10	73±9	31±15
Axial rotation (°)	27±17	22±15	33±18§	25±10	53±43	19±11	26±13	28±16	24±11	36±17	39±19	19±18	50±40§
Retraction-Protraction (°)	15±7	16±7	28±20§	19±7§	12±5	13±7	15±8	16±9	21±8	18±7	24±12	26±10	16±13
Medial-Lateral rotation (°)	17±10	21±7	22±7§	30±9	15±8	10±5	17±5	15±6§	19±9§	21±7	33±10	35±8	12±5§
Anterior-Posterior tilt (°)	11±7	10±6	35±20	15±8	21±9	8±5	11±6	10±5	14±8	14±7	23±14	18±15	18±13§
Plane of elevation (°)	62±24	60±30	42±21	40±16	31±27§	29±20	28±11	30±12	40±18	38±15	36±17§	45±19§	40±27
Elevation (°)	31±12	48±14§	84±24	70±15	39±14	38±13	44±12	40±13	67±17§	68±17	92±10	67±21	35±13
Axial rotation (°)	22±19	23±19	32±22	24±10	41±29	20±14	22±11	24±13§	21±11	32±19	36±23§	23±19	63±34§

TABLE 5.6: Average patients' contralateral shoulder complex ROM and SD during ADLs

Joint Rotation	Reach opposite axilla										Reach opposite side of head			Brush side and back of head			Clean lower back			Eat with hand to mouth			Drink from mug			Answer phone			Reach as far forward as possible			Lift block to shoulder height			Lift block to head height			Cross body abduction			Internal rotation																																																																																																																																																				
	Thorax	2±2	2±1	4±3	5±3	9±4	4±3	5±2	5±2	8±6	8±3	9±4	5±5	11±5	SC Joint	6±3	8±3	22±9	14±8	9±3	9±4	13±5	14±7	20±12	14±6	23±10	15±7	11±6	SC Joint	11±5	12±6	11±5	14±7	9±10	7±3	14±7	15±6	21±11	17±9	10±5	AC Joint	12±8	11±4	24±17	19±10	10±3	10±3	15±10	16±13	25±15	19±11	11±6	AC Joint	15±8	20±6	27±9	27±9	12±4	10±4	14±6	16±9	18±8	24±10	28±13	13±5	GH Joint	17±11	14±8	40±14	31±14	19±7	9±5	14±12	23±10	24±11	39±12	28±12	18±10	GH Joint	37±16	30±24	36±17	27±14	31±19	27±17	33±22	33±18	23±15	33±16	38±16	24±18	41±21	Elevation	37±11	50±14	55±18	54±17	27±6	38±9	37±8	41±12	60±16	51±11	61±15	66±11	26±11	ST artic.	16±7	16±5	34±18	20±9	9±4	13±6	13±5	16±6	22±11	20±5	23±10	25±12	12±8	ST artic.	15±6	23±6	36±11	30±10	11±4	12±4	16±5	15±4	20±10	21±7	32±10	37±11	13±5	ST artic.	9±8	8±4	33±16	15±12	19±7	7±4	8±4	9±4	14±7	13±7	18±9	13±5	17±7	Plane of elevation	62±20	58±18	38±21	41±18	28±16	28±14	31±15	23±12	44±18	32±9	36±17	53±24	34±20	Elevation	37±4	46±11	97±18	65±13	36±9	41±8	46±13	46±13	74±15	70±12	91±14	63±9	36±13	Axial rotation	23±14	19±12	34±20	18±5	41±27	16±7	24±12	18±8	25±12	30±13	33±13	22±10
Thorax	2±2	2±1	4±3	5±3	9±4	4±3	5±2	5±2	8±6	8±3	9±4	5±5	11±5	SC Joint	6±3	8±3	22±9	14±8	9±3	9±4	13±5	14±7	20±12	14±6	23±10	15±7	11±6	SC Joint	11±5	12±6	11±5	14±7	9±10	7±3	14±7	15±6	21±11	17±9	10±5	AC Joint	12±8	11±4	24±17	19±10	10±3	10±3	15±10	16±13	25±15	19±11	11±6	AC Joint	15±8	20±6	27±9	27±9	12±4	10±4	14±6	16±9	18±8	24±10	28±13	13±5	GH Joint	17±11	14±8	40±14	31±14	19±7	9±5	14±12	23±10	24±11	39±12	28±12	18±10	GH Joint	37±16	30±24	36±17	27±14	31±19	27±17	33±22	33±18	23±15	33±16	38±16	24±18	41±21	Elevation	37±11	50±14	55±18	54±17	27±6	38±9	37±8	41±12	60±16	51±11	61±15	66±11	26±11	ST artic.	16±7	16±5	34±18	20±9	9±4	13±6	13±5	16±6	22±11	20±5	23±10	25±12	12±8	ST artic.	15±6	23±6	36±11	30±10	11±4	12±4	16±5	15±4	20±10	21±7	32±10	37±11	13±5	ST artic.	9±8	8±4	33±16	15±12	19±7	7±4	8±4	9±4	14±7	13±7	18±9	13±5	17±7	Plane of elevation	62±20	58±18	38±21	41±18	28±16	28±14	31±15	23±12	44±18	32±9	36±17	53±24	34±20	Elevation	37±4	46±11	97±18	65±13	36±9	41±8	46±13	46±13	74±15	70±12	91±14	63±9	36±13	Axial rotation	23±14	19±12	34±20	18±5	41±27	16±7	24±12	18±8	25±12	30±13	33±13	22±10	49±30

5.2.3.3 Discussion and conclusions

Although physiological ROM measurements provide an estimate of the disability caused by IoP, seldom do we use the shoulder complex to its maximum capabilities. A better measure of how the disability impacts the patient's life can be assessed through ADLs measurements. In the current study, four patient groups (clavicle fracture, MDI, IRCT and GH joint dislocation patients) were recorded during ADLs in the MA Laboratory. No distinctions were made between the different subgroup of patients nor between the different treatment modalities or clinical care given to them.

Three of the four IRCT patients had problems raising the injured arm to an overhead position. A MDI patient withdrew mid trial due to pain without having performed any of the ADLs. A clavicle fracture patient treated with a fixation plate experienced pain and discomfort during certain tasks therefore he did not complete all of them. No GH dislocator patient experienced difficulty during the measurements.

Significant differences were measured in various ADLs and through all shoulder complex joints and segment rotations. This highlights the importance of measuring various ADLs since they subject the shoulder to different biomechanical demands based on motion, loading and the precision with which the task is performed. Table 5.5 and Table 5.6 present a summary of the mean ROM values \pm SD of IoP shoulder complex kinematics (and significant differences with healthy shoulder complex kinematics) and of CL shoulder complex kinematics respectively.

All patients completed the *reaching to opposite axilla* task and similar ROM were obtained compared with the healthy cohort. This task does not require patients to elevate their arms beyond $31 \pm 12^\circ$ therefore did not present a challenge to patients.

Significantly lower scapula protraction and lateral rotation were measured in the patient cohort ($28 \pm 20^\circ$ and $22 \pm 7^\circ$ respectively) compared to the healthy

cohort ($34\pm 17^\circ$ and $38\pm 8^\circ$ respectively) during *reach side and back of head* task. However, similar GH elevations were measured between the two groups, with a difference of 2° . Similarly, significantly less scapula protraction ($19\pm 7^\circ$ and $24\pm 5^\circ$ respectively) was measured during *brush opposite side of head* task while similar lateral rotations ($30\pm 9^\circ$ and $31\pm 7^\circ$ respectively) as well as GH elevation ($61\pm 15^\circ$ and $59\pm 17^\circ$ respectively) were measured between patients' IoP shoulders and healthy shoulders respectively. During these two highly demanding ADLs [233, 234], great HT elevation angles are necessary to complete the tasks.

Similar GH joint (difference of 3°) and HT elevations (difference of 6°) were achieved during *lift block to head height* between the patients' IoP shoulder and healthy shoulders. This could be explained by the fact that IRCT patients with the exception of the bilateral RCT patient and another patient did not perform the task because their shoulders were painful.

Some shoulder patients resorted to individual compensation mechanisms in the shoulder girdle to perform the task, such as tilting their neck to accomplish the motion. Veeger et al found larger SC retraction in patients that were able to perform demanding tasks at high arm elevation and requiring arm external rotation compared to non-able patients. They explained this observation by the increased rotation allowing additional HT external rotation which compensates for the lower than normal external rotation ROM and GH elevation ROM [170].

All ADLs were affected by singularity, particularly in the plane of elevation and axial rotations of the GH joint and the HT relationship (this is apparent in the large SD values (up to 34°) in GH and HT measurements). The singularity in the measurements is attributable to the combination of the arm starting and ending by the side of the body and the decomposition sequence used to analyse the measurements. For some particular movements, distinguishing between the actual joint motion and singularity was challenging. However, whenever singularity was obvious, the affected range of data was eliminated.

Even excluding “gimbal lock” affected rotations, large variations were recorded between participants (up to 18° SD). The participants’ conditions affect how they move the shoulder and therefore produce varying ROM values. For example, Lin et al reported RCT patients have a decreased ability to perform ADLs [70]. Moreover, adopted compensatory mechanisms on the IoP and on the CL shoulder may affect their movement. In addition, there is no one single way of performing an ADL task. Large SD in MA measurements have also been attributed to the “parametrisation of joint rotations by Euler angles” [57]: the angles are described as rotation around axes that are previously rotated, therefore they are mutually dependent and can be highly sensitive to small position changes.

Similar to healthy participants, physiological external rotation was recorded, although the results are not reported since the movement was performed with the arm by the side of the body and “gimbal locks” gave unrealistic joint rotations.

There are different reasons why ROM may be limited in patients post-operatively or post-treatment. Soft tissue damage due to their shoulder condition may hinder their recovery [234]. It is also likely that some patients with GH instability developed OA in the GH joint. According to Kasten et al, muscle contractures and atrophies present on OA shoulders would further affect its function [234]. Pain at certain arm elevations also limits patients’ ability and willingness to perform certain tasks.

5.3 Functional classification of shoulder complex data

To decide on a shoulder patient’s best treatment option, his or her condition must be clearly defined and classified. However controversy and confusion on clear definitions for certain shoulder conditions, particularly with GH joint

instability, has led to the development of numerous classification systems with wide variations between them [235].

Questionnaires and scoring systems are commonly used to assess and classify patient shoulder function [21, 173, 236, 237]. However, an overlap between pathogenesis sometimes results in incorrect diagnosis of disorders [64]. Furthermore, these are highly subjective tools.

MA measurements can objectively quantify the movement in the shoulder. However, a wealth of biomechanical data is collected, which can be a challenge to interpret. A classification method that aids in the interpretation of shoulder kinematics data, would be most useful to characterise joint function depending on the severity of the IoP.

5.3.1 The Dempster-Shafer classification method

A Dempster-Shafer (DS) classification tool, developed and employed at Cardiff University [107], is used to aid in the interpretation of joint function measured in the MA Laboratory. It is based on the Dempster-Shafer theory of evidence and it uses mathematical probability to quantify subjective judgement. It achieves this by assigning levels of support to each variable measurement and combines them to classify joint function as either non-injured-or-pathological (NloP) or injured-or-pathological (IoP). A level of uncertainty is always accounted for. The classifier builds on the work of Safranek et al [238] and Gerig et al [239].

The Cardiff DS objective classifier is a generic method to analyse MA data. The extent of pathology or trauma to a joint can be investigated by analysing clinically relevant measurements taken in the MA Laboratory. To date, it has been used to characterise OA knee joint function using both level gait [107, 109, 240, 241] stair ascend and descend [47] as well as assessing the merits of total hip arthroplasty [47]. A novel application for the DS Cardiff functional classifier, classification of shoulder complex data, is explored in the current study.

The non-optimisation DS classifier is used to interpret shoulder complex data. There are five stages in the classification method which are summarised in Figure 5.13.

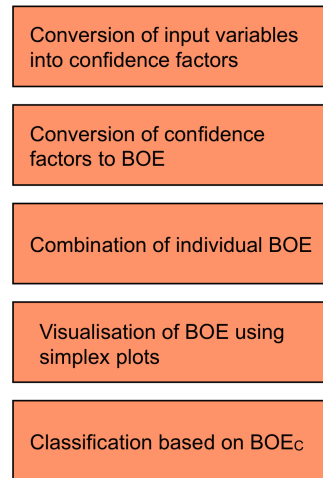


FIGURE 5.13: DS classification stages. Where BOE is body of evidence and BOE_C is the combined body of evidence

The different stages of classification are explained below, with emphasis placed on the classifier's selected menu option used to analyse shoulder complex data. The reader is directed towards [47, 107] for a more comprehensive description of the DS classifier options.

5.3.1.1 Conversion of input variables into confidence factors

The classification procedure begins by standardising each input variable, v , to a value on a scale of 0-1. The transformed variable is defined as a confidence factor $cf(v)$ which represents the level of confidence in (or not in) the variable's support that a subject's shoulder function is IoP.

The following criteria applies:

- $cf(v)$ is a monotonic function
- $cf(v) = 1$ if the measurement implies certainty in IoP
- $cf(v) = 0$ if the measurement implies certainty in NIoP

- $cf(v) = 0.5$ if the measurement favours neither IoP nor NIoP

A sigmoid function is used to transform the input variable into a $cf(v)$. The steepness of the sigmoid function is controlled with a k parameter (calculated as the Pearson's correlation coefficient) to reflect the nature of the spread of the data. The value of k indicates the degree to which v can differentiate between IoP and NIoP.

5.3.1.2 Conversion of confidence factors to BOE

A characteristic body of evidence (BOE) is calculated from the $cf(v)$ representing each input variables. The BOE is represented by a set of three belief values:

- $m_c(\{IoP\})$ is the degree of belief in the subject's joint function being IoP
- $m_c(\{NIoP\})$ is the degree of belief in the subject's joint function being NIoP
- $m_c(\Theta)$ is the degree of belief in either the subject's joint function being IoP or NIoP (i.e. level of uncertainty)

The belief values in a BOE must satisfy the condition shown in Equation (5.1)

$$m(\{IoP\}) + m(\{NIoP\}) + m(\Theta) = 1 \quad (5.1)$$

5.3.1.3 Combination of individual BOE

The individual BOE constructed for each input variable (supporting either IoP or NIoP) are combined using the Dempster's rule of combination for a final combined BOE (BOE_C).

The BOE_C comprises the three focal elements as in the individual BOE (i.e. $\{IoP\}$, $\{NIoP\}$ and $\{\Theta\}$). The combination of all characteristic BOEs is achieved

by the iterative combination of the BOE_C with another BOE. Since the classification tool is commutative [239], the order that the BOEs are combined in does not matter.

5.3.1.4 Visualisation of BOE using simplex plots

Simplex plots are used to visualise the final classification of the subject as either loP or NloP. The BOE_C is represented as a single point on a simplex plot to give a visual representation of joint function (Figure 5.14a). Simplex plots are also used to visualise the contribution that each variable has towards the final classification. Four classification regions are highlighted in the simplex plots: dominant NloP, non-dominant NloP, dominant loP, non-dominant loP (shown in Figure 5.14b).

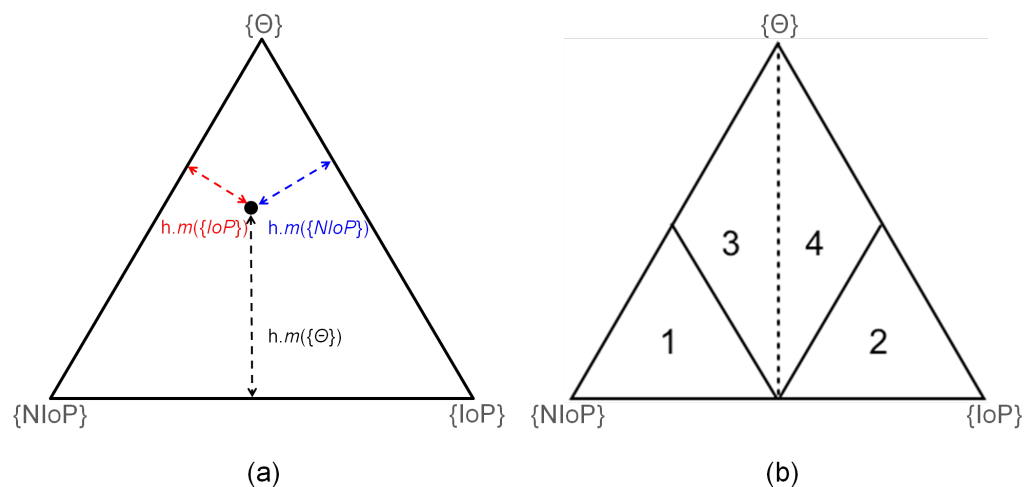


FIGURE 5.14: Visualising DS objective classification using simplex plots (a) Relationship between the belief values and position of the point in the simplex plot where h is the height of the triangle and (b) Simplex plot regions: 1) dominant NloP classification; 2) dominant loP classification; 3) non-dominant NloP and classification 4) non-dominant loP classification. The dotted vertical line is the decision boundary

5.3.1.5 Classification based on BOE_C

The following decision rule is used for the final classification:

1. If $m_c(\{IoP\}) > m_c(\{NIoP\})$ then the subject is considered to have IoP shoulder complex function
2. If $m_c(\{NIoP\}) > m_c(\{IoP\})$ then the subject is considered to have NIoP shoulder complex function

5.3.1.6 Classification accuracy and ranking of input variables

The leave-one-out (LOO) cross validation method was used to evaluate the classification accuracy. The method trains the classifier using $(n-1)$ cases to calculate the control variables. These control variables are then used to classify the remaining subject's shoulder function. The process is repeated n times.

Each variable's classification performance, and the uncertainty that it offers to the classification, is represented by an objective function (OB). The variables are ranked according to the average accuracy with which each variable classifies new subjects (LOO approach classification error rate) and the average OB measure, which is the Euclidian distance measure of the level of uncertainty in the classification. Variables with a high classification accuracy are ranked higher than those with a low accuracy. Should variables present the same accuracy, they are ranked based on their OB, where a variable with high classification accuracy will have a lower associated OB.

5.3.2 Novel application for the Cardiff DS classifier

A novel application for the Cardiff DS classification tool was developed. Measurements taken in the MA Laboratory were used to characterise shoulder complex function as either NIoP and IoP. No distinction between the different patients shoulder conditions was made.

5.3.2.1 Selecting input variables

A series of different variable combinations were explored to determine the most suitable ones for classification. Statistically significant ($p < 0.05$) variables between the two cohorts determined in Section 5.2.3 (Table 5.7) were used. Movements of the thorax relative to the GCS as well as GH joint and HT first and third rotations were excluded from the analysis because of the desire to classify motion using purely shoulder complex data and for fear of misguidance due to “gimbal lock”. Additionally, BMI and scapula orientation during the neutral position (NP) measurement were also included. Thus the variables considered for the functional classification are summarised in Table 5.7.

To characterise joint function using the DS classifier, healthy participants and shoulder patients must have a value for each of the input variables used. If there is a missing value for any of the input variables for a participant, then his or her data cannot be used for the classification. This presented a problem with the current data set since during ADL measurements, a marker may easily become occluded due to body interposition. So, once all the participants who had at least one measurement from Table 5.7 missing were discarded, eight healthy participants and 16 shoulder patients remained for classification.

The output to the classification using all the discrete values listed in Table 5.7 is given in Figure 5.15.

The in-sample classification accuracy is 81.5% and the out-of-sample classification accuracy is 70.8%. Six patients were misclassified in the dominant or non-dominant NloP regions of the simplex plot while one healthy participant laid in the decision boundary of the simplex plot.

The sample sizes were significantly reduced because a large proportion of participants could not be included in the classification process due to missing data. Furthermore, 21 variables were used to classify 24 participants. Therefore, the

TABLE 5.7: Summary of the input variables used to explore for classification

ADL	Measurement		Abbreviation
	Joint or Segment	Rotation	
N/A	N/A	N/A	IBM
NP measurement	GH joint	Elevation	NPGH2
	ST articulation	Retraction-protraction	NPST1
		Medial-lateral Anterior - posterior tilt	NPST2 NPST3
Reach opposite side of neck	HT	Elevation	ADL2HT2
Reach side and back of head	ST articulation	Retraction-protraction	ADL3ST1
		Medial-lateral rotation	ADL3ST2
Brush opposite side of head	ST articulation	Retraction-protraction	ADL4ST1
Drink from mug	SC joint	Retraction-protraction	ADL7SC1
	GH joint	Elevation	ADL7GH2
Answer phone	SC joint	Retraction-protraction	ADL8SC1
	AC joint	Medial-lateral rotation	ADL8AC2
	ST articulation	Medial-lateral rotation	ADL8ST2
Reach as far forward as possible	HT	Elevation	ADL9HT2
	AC joint	Retraction-protraction	ADL9AC1
	ST articulation	Medial-lateral rotation	ADL9ST2
Lift block to shoulder height	SC joint	Retraction-protraction	ADL10SC1
Lift block to head height	AC joint	Anterior-posterior tilt	ADL11AC3
Cross body abduction	ST articulation	Medial-lateral rotation	ADL12ST2
		Anterior-posterior tilt	ADL12ST3

top 10 ranked variables (Table 5.8) from the classification were selected to perform an additional classification. With these variables, ten NloP shoulders and 19 loP shoulders were classified.

The new calculated in-sample accuracy is 72.2% and out-of-sample accuracy is 72.4%. One healthy participant was misclassified to dominant loP and six patients were misclassified in dominant NloP. The corresponding simplex plot for the classification is shown in Figure 5.16.

A significant number of participants were also discarded for classification since data was missing from at least one of the variables. Therefore, a combination of

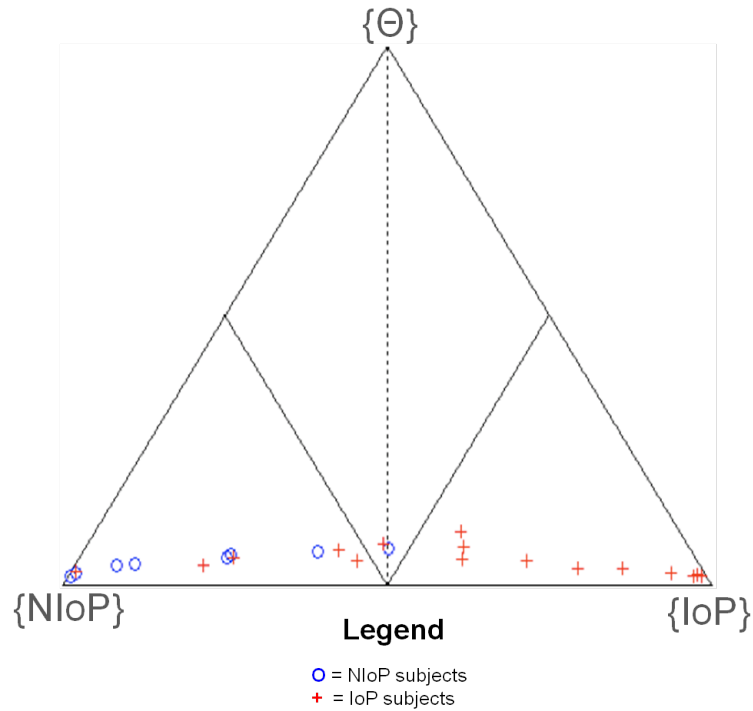


FIGURE 5.15: Simplex plot participants' shoulder classification using 21 input variables

TABLE 5.8: Ranking of input variables used in the classification

Ranking	Variable	OB	Variable accuracy
1	ADL8SC1	0.9227	54.2
2	ADL7SC1	0.8176	62.5
3	NPST2	0.8154	70.8
4	ADL3ST2	0.7864	66.7
5	ADL9ST2	0.8666	50.0
6	ADL9HT2	0.8215	54.2
7	IBM	0.8238	79.2
8	ADL10SC1	0.9496	45.8
9	ADL7GH2	0.8096	62.5
10	ADL8ST2	0.8238	54.2

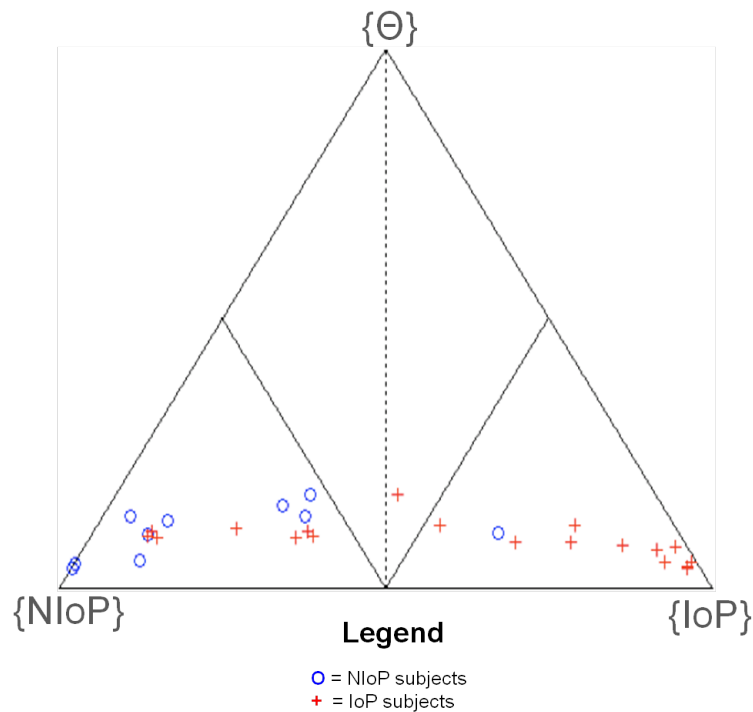


FIGURE 5.16: Simplex plot participants' shoulder classification using 10 input variables

high ranked variables that did not have too many data sets missing in combination with statistically significant variables were used for the final classification.

5.3.2.2 Shoulder function classification

Seventeen healthy shoulders and 23 patients' shoulder were classified. The BOE for all participants are recorded in Table 5.9. The corresponding simplex coordinates of DS classification are depicted in Figure 5.17.

TABLE 5.9: BOE_C values for the study participants. The most influential BOE_C in the classification are highlighted.

Participant	$m_c(\{IoP\})$	$m_c(\{NIOp\})$	$m_c(\Theta)$	
Healthy	1	0.3903	0.3443	0.2654
	2	0.3221	0.4178	0.2601
	3	0.3822	0.3421	0.2758
	4	0.0736	0.7569	0.1695
	5	0.0008	0.9280	0.0712
	6	0.2462	0.6080	0.1458
	7	0.1091	0.6690	0.2219
	8	0.0901	0.6478	0.2621
	9	0.1581	0.6224	0.2195
	10	0.1269	0.6840	0.1891
	11	0.0052	0.8266	0.1682
	12	0.0220	0.8703	0.1077
	13	0.0008	0.9090	0.0902
	14	0.1389	0.6250	0.2362
	15	0.1136	0.5987	0.2877
	16	0.0307	0.7769	0.1924
	17	0.2065	0.6346	0.1589
Clavicle fracture	18	0.3728	0.4353	0.1918
	19	0.6170	0.1782	0.2048
	20	0.9176	0.0005	0.0820
	21	0.8475	0.0459	0.1066
	22	0.3725	0.3616	0.2660
MDI	23	0.2717	0.5447	0.1836
	24	0.8035	0.0372	0.1593
	25	0.3794	0.4044	0.2162
	26	0.8703	0.0017	0.1281
	27	0.0740	0.8130	0.1130

Continued on next page

Table 5.9 – continued from previous page

Participant	$m_c(\{IoP\})$	$m_c(\{NIoP\})$	$m_c(\Theta)$	
28	0.2506	0.4779	0.2715	
IRCT	29	0.7114	0.0998	0.1888
	30	0.5032	0.2498	0.2470
	31	0.2075	0.4703	0.3223
	32	0.8469	0.0418	0.1113
	33	0.7475	0.1023	0.1502
	GH dislocation	34	0.3796	0.3799
35		0.7005	0.1228	0.1767
36		0.2259	0.5610	0.2131
37		0.8000	0.0028	0.1972
38		0.8962	0.0000	0.1038
39		0.8295	0.0483	0.1222
40		0.0009	0.8321	0.1671

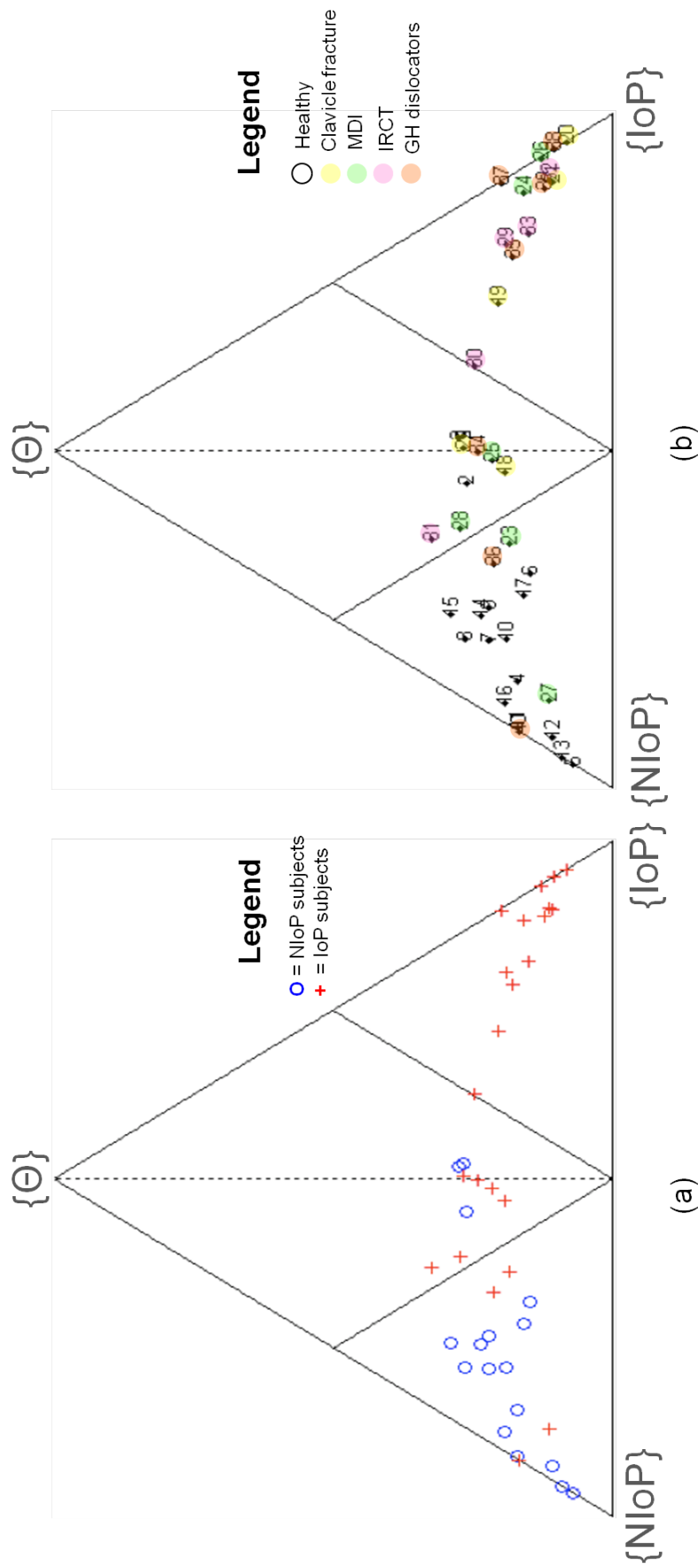


FIGURE 5.17: Simplex plot showing (a) the simplex coordinate representation of the BOE_C for all study participants and (b) each participant's classification, where the number in the Simplex plot corresponds to Table 5.9.

The in-sample classification accuracy is 81.1% and the out-of-sample classification accuracy is 72.5%. Four patients were misclassified in the dominant NIoP region of the simplex plot and a further four patients in the non-dominant NIoP. Similarly, two healthy participants were misclassified in the dominant IoP region of the Simplex plot.

The variables used to classify shoulder function and their rankings are shown in Table 5.10.

TABLE 5.10: Ranking of input variables used in the classification

Ranking	Variable	OB	Variable accuracy
1	NPST3	0.8529	65
2	ADL8AC2	0.9803	37.5
3	ADL3ST2	0.7742	62.5
4	ADL4ST1	0.7538	62.5
5	BMI	0.7495	82.5
6	ADL8SC1	0.7392	57.5
7	NPST2	0.7338	72.5

Classification using other input variables from different ADLs was investigated. The simplex plots are shown in Appendix E.

5.3.2.3 Comparing objective classification with subjective score measures

The Oxford Shoulder Score (OSS) and the Oxford Instability Score (OSIS) provide a subjective measure of how the subject perceives pain and disability due to their shoulder condition. They are each based on a set of 12 questions, ranked between 0 and 4 points. The higher the score, the less effect the IoP has impacted the patient's life.

The OSS and OSIS scores were combined (OS) due to small sample sizes. The linear association of patients' OS score and their $m_c(\{IoP\})$ and $m_c(\{NIoP\})$

of the BOE_C from the DS classification was investigated using the Pearson's correlation tests. The results from this analysis are shown in Table 5.11. The correlation coefficient sign indicates the direct relationship between the two variables. The absolute value indicates the strength of the correlation, with larger absolute values indicating stronger relationships.

TABLE 5.11: Correlation between objective classification and subjective score measures

Variables	Pearson's correlation
OS & $m_c(\{IoP\})$	-0.16298
OS & $m_c(\{NIoP\})$	0.180187

5.3.2.4 Discussion and Conclusions

Jones et al [107–109, 241] and Whatling et al [47] successfully characterised OA knee function pre-operatively and post TKR (3, 6 and 12 months) using the Cardiff DS classification tool. Their results gave a good indication of knee function following TKR. Thus, in the current study, shoulder complex classification was explored with the Cardiff DS objective classification technique.

The significantly different variables used for classification (Table 5.7) covered a range of hygiene, feeding and reaching tasks, highlighting the importance of recording various ADLs due to the biomechanical demands that they place on the shoulder. Differences were found between all 4 joint kinematics which also accentuates the interaction between the joints and the compensatory mechanisms.

Table 5.9 summarises the $m_c(\{IoP\})$, $m_c(\{NIoP\})$ and $m_c(\Theta)$ indices of classification for each subject and the relevant simplex plot is shown in Figure 5.17. A high out-of-sample classification accuracy (72.5%) was determined for the final classification. This means that, for the selected variables, the classifier was able to classify new subjects with an accuracy of 72.5%.

Seven patients were misclassified as NloP: one was a clavicle fracture patient (although very close to the decision boundary); three MDI shoulders; one shoulder in the IRCT group; the patient with bilateral asymptomatic IRCT that had good ROM despite his condition; and two were GH dislocated patients (they were both young and healthy otherwise, and their dislocation did not seem to impair their function during the MA session). Four patients were on the decision boundary line, therefore no clear indication as to whether their function is classified as NloP or loP was obtained. The remaining patients' shoulder functions were classified as dominant loP.

Retrospectively, patients that during the MA session were clearly in pain or discomfort or had trouble performing the tasks were all classified in the dominant loP region of the simplex plot; the exception being the bilateral IRCT patient who was asymptomatic and presented good ROM and function in both shoulders, however his right shoulder was classified in the boundary between dominant and non-dominant loP regions of the simplex plot (Figure 5.17). Five healthy participants were not classified in the dominant NloP region although none were classified in the dominant loP region of the simplex plot.

Of the misclassified patients as NloP, almost all had high OSS or OSIS scores (between 31 and 45 points out of a total 48 points), indicating that the patients believe they have a good shoulder function and their condition has not impaired them greatly with the exception of a GH dislocation patient that although classified as NloP, had an OSIS score of 11 points. This particular patient was dissatisfied in general, his shoulder was painful, which prevented him from playing contact sports.

The ranking of the input variables are shown in Table 5.10. BMI was considered as an input variable since an association between BMI with shoulder disorders and symptoms has been previously reported [242–244]. Scapula differences in the NP measurement might be indicative of atypical scapula kinematics during motion. The ADLs used to classify shoulder data were *reaching side and back of head, brushing opposite side of the head and drink from a mug*. The hygiene

tasks have been identified by other researchers as biomechanically demanding since high arm elevations and external rotation is required for the completion of these tasks [233, 234].

Determining the optimal functional parameters is of extreme importance to compare IoP and healthy shoulder function. Because different patient groups were used, perhaps different functional parameters are necessary in future studies. It is suggested that further work should be undertaken to investigate in more detail the DS classifier on shoulder patients. Different input variables might be more suitable between different patient subgroups. For example, RCT patients have difficulty reaching high arm elevations whereas MDI patients have altered shoulder motion at mid-arm elevation, so input variables should perhaps be different.

The OSS and OSIS scores' correlation with the classification indices were investigated using a Pearson's correlation test for 18 patients. A weak correlation, shown in Table 5.11, was found between the OSS and OSIS scores and {NloP} and {IoP} indices. This might be explained by the subjective nature of the scores. Younger patients have higher expectations of their recovery since they look forwards to regaining equivalent pre-injury physical activity. On the other hand, the elder population might be more easily satisfied with the results since they generally perform less biomechanically demanding tasks.

The visual feedback that is generated from the DS classifier makes interpretation of the results easy, with a patient lying on the regions of a triangle that indicate the severity of his or her condition. Therefore, the DS classifier might provide an answer to a much sought clinical tool that could aid surgeons in decision making process.

To conclude, a DS classification tool developed and employed at Cardiff University was used for the first time to characterise shoulder complex function. From this preliminary study, differences between shoulder patients with different levels of severity and healthy participants were detected. This line of research has

identified future directions for use of shoulder function classification and thus merits further investigation.

5.4 Limitations

Patients with different IoP were tested, and even within each group, several different treatments were given to the patients. For example the clavicle fracture subgroup have 3 treatment patients (pin, conservative and plate). There are biomechanical differences between these treatments and so, if more patients are recruited within each pathology or injury cohort, statistics may be applied to investigate variations between them.

Testing patients is more time consuming than testing healthy participants. Patients required rests since their arms were aching. Also both shoulders are tested for physiological ROM and ADLs. Some patients had not anticipated the time and asked to finish the trial early, so not all the data for the CL shoulder was always recorded. This meant that statistical analysis to compare differences between the two arms was difficult.

The effect of different input classification variables was explored. However, it was limited due to the small cohort sizes that could be classified once the participants with missing data were discarded. All variables from the top 10 ranked might have been more suitable for classification although would not have been able to classify many study participants.

Accurate GH measurements are highly desirable, since they can provide an insight into aetiologies of instability conditions (such as RCT, MDI and dislocation of the joint). However, conventional methods or approaches for measuring GH kinematics using reflective markers are highly susceptible to skin movement artifact, and their reliability for the accurate assessment of GH joint kinematics has not been established [48]. Without a sufficiently accurate measuring technique

and the necessary sample size, detecting statistically significant differences between the healthy, IoP and CL shoulders is difficult.

Furthermore, the instantaneous helical axis (IHA) method was used to calculate the GH joint centre of rotation (CoR). However, in GH joint instability patients, the IHA is not recommended since translations at the joint may occur; however, the method calculates the CoR as a fixed point relative to the scapula [77, 81]. Some authors have recommended the use of the finite helical axis (FHA) method to measure kinematics of instability patients, although the ISB proposes imaging modalities such as MRI or CT to estimate GH joint CoR for these patients [73].

Chapter 6

Conclusions and Further Work

6.1 Conclusions

Surgeons use a range of observations and physical examination techniques to determine the type and extent of an injury or pathology. It is believed that surgeons could benefit from a more accurate measurement tool contributing to improving patient care.

In accordance with the thesis hypothesis, motion analysis (MA) was found to be a useful non-invasive tool to objectively quantify the movement of the shoulder complex. Even though errors in the measurement and technique exist, understanding where the errors originate have made it possible to explore different approaches that lead to improved accuracy in the measurements.

The studies described in this thesis have contributed towards the advancement of shoulder complex kinematics studies at Cardiff University as well as with the international shoulder researchers' community. An appreciation was gained of the challenges faced when using MA to measure shoulder motion as well as a better understanding of joint function in healthy (HL), injured or pathological (IoP) and contralateral (CL) shoulders. With the combined efforts of Dr. Lovern,

Mr Ferran and the author, shoulder complex kinematics were recorded and analysed for 23 healthy participants and for 25 shoulder patients; between them, the 25 shoulder patients suffered from four different IoP. As a result, a Cardiff University shoulder kinematics database was created, with the possibility of being expanded when more participants are assessed.

A novel application for the Cardiff Dempster-Shafer (DS) objective classifier was explored to aid in the interpretation of MA data. The classifier identified differences between healthy and patient cohorts following which it was possible to classify their shoulder function with a high degree of accuracy.

Image registration techniques (IRT), involving dynamic fluoroscopy and three-dimensional (3D) bone models generated from magnetic resonance imaging (MRI) scans using Simpleware Software (Simpleware Ltd.), were developed to accurately measure glenohumeral (GH) joint rotations. The technique uses JointTrack software (Banks, S.A.) to obtain the poses of registered 3D bone models to the fluoroscopic images.

Conclusions will now be discussed according to the specific objectives outlined in Chapter 1.

Objective 1. Develop and collect data with an image based method to accurately measure glenohumeral joint function

Image registration techniques were developed in the current study to measure GH joint kinematics using dynamic single-plane fluoroscopy. 3D computer bone models of the humerus and scapula were generated from MRI scans using Simpleware Software (Simpleware Ltd.). The technique requires the accurate registration of the 3D models to the 2D fluoroscopic images of the GH joint during dynamic measurements. JointTrack software (Banks, S.A.) was used to perform the registration as well as to obtain segments' poses.

Although 3D models rendered from CT scans are highly accurate, MRI was the chosen imaging modality for this study since it is less invasive than CT.

MRI segmentation was challenging due to a lack of a specialised shoulder coil and due to the difficulty of identifying cortical bone on MRI scans. However, a registration repeatability trial was performed. No significant differences were detected between the three-times-registered poses suggesting 3D bone models of the scapula and humerus generated from MRI scans may be of sufficient accuracy to perform image registration.

Full kinematic description of the GH joint and of the scapula were obtained. The GH joint was recorded elevating $92.1 \pm 2.3^\circ$ and $85.7 \pm 1.6^\circ$ during abduction and scaption respectively. The scapula retracted ($18.8 \pm 2.8^\circ$ and $7.5 \pm 1.8^\circ$ during abduction and scaption respectively), tilted posteriorly ($29.4 \pm 2.4^\circ$ and $15.8 \pm 1.3^\circ$ during abduction and scaption respectively) and rotated laterally ($58 \pm 1^\circ$ and $54 \pm 2^\circ$ during abduction and scaption respectively). The pattern of elevation agrees with what other researchers have previously measured.

Humeral head translation was measured towards the glenoid centre ($3 \pm 0.9\text{mm}$ medially, $2.7 \pm 0.9\text{mm}$ inferiorly and then superiorly and $6.7 \pm 2\text{mm}$ posteriorly) during abduction and ($2.8 \pm 0.9\text{mm}$ medially, $3.6 \pm 0.9\text{mm}$ superiorly and then inferiorly and $5.3 \pm 2.1\text{mm}$ anteriorly) during scaption. The centering of the humeral head is believed to provide joint congruency for optimal shoulder function.

Objective 2. Develop and use the data collection and analysis method to assess shoulder complex function on healthy volunteers using Motion Analysis techniques

Additions and improvements to the Cardiff MA protocol for measuring and analysing shoulder complex biomechanics were made. Subsequently, studies were performed investigating shoulder complex asymmetry during arm elevation as well as measurements of shoulder function during physiological ranges of motion (ROM) and activities of daily living (ADLs).

Firstly, modifications to the custom developed Matlab (The MathWorks, Inc) program to estimate GH joint centre of rotation (CoR) with the instantaneous helical axes (IHA) method improved GH joint kinematics calculations. Prior to this thesis, only regression equations based on scapula geometry were used to estimate GH joint CoR. However the equations assume normal scapula and humerus geometry and do not take into account osseous deformations. Significant differences between GH joint CoR were measured in positions along the x_S and z_S scapula anatomical coordinate system (ACS) axes. The most significant difference was measured in the anterior position (x_S axis), where regression equations overestimated GH position by an average of 4cm compared to the IHA method. The regression equations also estimated the GH joint CoR laterally to the scapula ACS although imaging studies identified GH joint CoR medially to the scapula ACS.

Secondly, a light-weight acromium marker cluster (AMC) was designed, developed and used to record scapula function during dynamic activities. To evaluate the AMC's measurement accuracy, simultaneous scapula locator (SL) and AMC measurements were recorded. The AMC measured similar scapula angles to the SL up to 70° of arm elevation for retraction and posterior tilting and to 130° of arm elevation for scapula lateral rotation measurements. Due to deltoid contraction at high arm elevations, changes in the shape of the soft tissue surrounding the acromium introduce significant errors to the measurements therefore caution should be taken when reporting scapula angles measured with the AMC at high arm elevations. A 0.925 intra-class correlation coefficient (ICC) was recorded in an intra-observer repeatability trial for scapula rotations using the AMC.

Differences between unilateral (UE) and bilateral (BE) arm elevations were explored to determine the effect of thorax rotations on shoulder kinematics. BE was found to significantly decrease trunk lateral rotation (by 3.4° and 3.6° during abduction and flexion respectively) and axial rotation (by 2.4° during flexion) with respect to UE; however, trunk flexion was significantly greater during

BE ($16.3 \pm 4.0^\circ$ and $15.9 \pm 3.5^\circ$ during abduction and flexion respectively) compared to UE ($12.9 \pm 2.5^\circ$ and $11.8 \pm 3.6^\circ$ during abduction and flexion respectively). Scapula rotations are also significantly different between UE and BE. Greater scapula retraction was recorded during BE ($48.8 \pm 7.0^\circ$) compared to UE ($45.8 \pm 8.1^\circ$) in abduction.

Shoulder function asymmetry was investigated between dominant and non-dominant shoulders. Significantly greater GH elevation was measured in dominant arms compared to non-dominant arms, with a difference of up to 7.6° during scaption. Statistically different scapula rotations were also measured between dominant and non-dominant arms. Dominant arms showed 7.0° greater scapula lateral rotation compared to the non-dominant. Asymmetry between the two shoulders could be attributed to soft tissue imbalance from more frequent use of the dominant shoulder compared to the non-dominant.

Physiological ROM during static and dynamic trials and 15 activities of daily living (ADLs) were recorded with skin markers attached to bony landmarks as well as with the AMC (and the SL for physiological ROMs). Static and dynamic trials measured differences in thorax and scapula rotations which may have arisen from muscle stabilisation. Acromioclavicular (AC) and scapula lateral rotations were underestimated (by up to 8° and 20° respectively) using the skin fixed markers. The ADLs investigate the biomechanical demands placed on the shoulder complex during everyday tasks. From the ADLs measurements, *Reaching side and back of head* and *lifting a block to head height* were considered the most biomechanically demanding activities since they required the greatest humerothoracic angle ($91 \pm 13^\circ$ and $98 \pm 13^\circ$ respectively). Joint and segment rotations are comparable to published studies that follow International Society of Biomechanics (ISB) recommendations.

An intra-observer and inter-observer repeatability trial was performed to investigate differences in shoulder complex kinematics measured by three observers over two visits to the MA Laboratory. Discrepancies between the kinematics

measured by the three observers produced standard deviations (SD) of 11° for GH joint elevation and 7.7° for scapula lateral rotation. Sources of inconsistencies between the observers could include bony landmark identification palpation technique as well as SL placement technique. However, a high ICC (0.958) was calculated, suggesting that similar overall scapula function was measured by the observers.

Objective 3. Investigate skin artefact and marker placement errors in Motion Analysis measurements and compare simultaneous image registration and Motion Analysis recordings

Radio-opaque markers, created with a Zinc coat, allowed for the visual qualitative assessment of marker placement for MA measurements. It was thus possible to observe that the AI scapula marker was not accurately placed on the bony landmark, but instead was placed inferiorly. MA measurements are also sensitive to skin movement artefact. Scapula movement under the skin was observed with the radio-opaque markers, therefore skin artifact errors are to be expected in the MA results.

To investigate the errors commonly associated with MA, a comparison between the kinematics outputs from the MA measuring system and IRT was performed. However, GH joint kinematics could not be measured with MA at arm elevations ranging beyond 70° to 90° since the retro-reflective markers became occluded with the fluoroscope examination table during arm elevations.

Greater GH joint elevation was recorded with IRT (54.8° and 82.6° for abduction and scaption respectively) compared to MA (51.1° and 75.2° for abduction and scaption respectively). Furthermore, differences between IRT and MA recordings in GH joint plane of elevation (6.7° and 1.9° abduction and scaption respectively) and axial rotation (24.1° and 23.0° abduction and scaption respectively) were measured.

During axial rotation measurements, similar GH joint elevation angles were measured with the two measurement systems. Plane of elevation and axial rotation were not reported since MA measurements are affected by “gimbal lock” errors.

Discrepancies in measured rotations between MA and IRT can be attributed to factors related to differences in the analytical approach as well as the errors associated with the techniques:

Different anatomical landmarks were chosen to create the embedded axis system on the humerus and scapula. As a result, the ACSs were positioned and orientated differently.

Different rotation sequences used to analyse the kinematics data may also be responsible for discrepancies between MA and IRT measurements. MA uses the ISB recommended YXY Euler angle sequence of rotation while IRT uses the ZXY Cardan angle convention.

The scapula moves significantly under the skin therefore skin markers are not fully representative of scapula movement.

The IRT is also subject to measurement and computational errors. The 3D models were created from MRI scans although CT generated bone models are generally more accurate. Furthermore, registration errors may also affect the IRT results.

Single-plane fluoroscopy is sensitive to translations perpendicular to the image plane. Biplane would give more accurate results. However, in addition to a greater radiation dose associated with the measurement system, it also constrains the movements further.

Objective 4. Investigate differences between patients’ injured or pathological shoulder function with that of the contralateral shoulder as well as healthy shoulder function using Motion Analysis techniques

Patients with four different shoulder conditions from either a sustained IoP to the shoulder complex were invited to the MA Laboratory. The effect and the extent of the IoP was investigated during physiological ROMs elevation and ADLs recordings.

Clavicle fracture patients

Although different sternoclavicular (SC) retraction patterns of motion during abduction and flexion were observed between the patients' CL shoulder compared to their IoP shoulder and to the HL cohort, differences were not statistically significant.

During abduction, statistically greater AC retraction was measured in HL participants ($8 \pm 3^\circ$) compared to patients' IoP ($7 \pm 3^\circ$) and their CL ($4 \pm 4^\circ$) shoulders. AC lateral rotations were greater in IoP shoulders (by up to 10° compared to the patients' CL shoulder) although differences were not statistically significant.

Multidirectional instability (MDI) patients

GH joint motions were similar between patients' IoP shoulder and their CL shoulder, with the exception of axial rotation, where greater GH external rotation was measured in the MDI patients' CL shoulder during scaption (18° compared to 15° for both healthy and IoP shoulders).

Significant differences in scapulothoracic (ST) articulation retraction-protraction and posterior tilting were observed between HL and both patients' IoP and CL shoulders while similar lateral rotation ROMs were measured between all shoulders.

Irreparable rotator cuff tear (IRCT) patients

In comparison to RCT patients' IoP and CL shoulders, HL shoulders showed greater ST lateral rotation and posterior tilting, with a maximum difference of 5°

between HL and loP during scaption and 11° between HL and CL shoulders during flexion (in scapula lateral rotation). However, differences do not appear to be statistically significant. GH joint elevation was greater in HL shoulders compared to loP and CL patient shoulders during the three elevation trials. The extent to which RCT affect shoulder kinematics depends on whether the lesion to the RC is in a single tendon, extends into a portion of a second tendon; or if the lesion exceeds two tendons.

Glenohumeral joint dislocation patients

Greater GH elevation angles were recorded on patients' loP shoulder as compared to their CL and HL participant's shoulders. Significant differences in ST posterior tilting between healthy ($6 \pm 3^\circ$) and loP ($4 \pm 2^\circ$) shoulders were recorded during scaption only. Small ST protraction angles were recorded and the pattern of motions were similar between the three shoulder groups. Compared to their CL and with HL shoulders, patients' loP shoulders experienced less scapula lateral rotation during abduction, scaption and flexion; however differences are not statistically significant.

Activities of daily living measurements

It is important to consider the compensatory mechanisms on the loP as well as on the CL shoulders that patients adopt following iloP and how they affect shoulder movement during everyday tasks.

Significant differences were measured in various ADLs and through all shoulder complex joints and segment rotations in HL and loP shoulder complex kinematics. This highlights the importance of measuring various ADLs since they subject the shoulder to different biomechanical demands based on motion, loading and the precision with which the task is performed.

Objective 5. Investigate the suitability of using functional variables obtained in the Motion Analysis Laboratory to objectively characterise healthy and injured or pathological shoulder function applying the Cardiff DS objective classifier method

The DS classifier is a generic method to analyse and interpret MA data. The Cardiff DS objective classifier was used to characterise shoulder function on HL participants and patients. An initial study using 24 discrete joint complex rotation values from the ADLs as input variables was able to characterise non-injured-or-pathological (NloP) and loP subjects with 70.8% accuracy. However not all participants could be classified since they had input data values missing. Therefore, seven variables were chosen for classification. Applying the new classification variables, NloP and loP shoulder function was characterised with 72.5% accuracy. Forty participants were classified in total. Four patients were misclassified in the dominant NloP region of the simplex plot and a further four patients in the non-dominant NloP. Similarly, two healthy participants were misclassified in the dominant loP region of the simplex plot; possibly explained by the variability of ways in which a task can be executed.

A weak correlation between the Oxford Shoulder Score (OSS) and the Oxford Instability Score (OSI) with the NloP and loP classification indices was found (-0.16298 and 0.180187 respectively). This might be explained by the subjective nature of the scores.

6.2 Further work

Several areas for improvement and further investigation of shoulder complex kinematics research at Cardiff University are highlighted below:

1. The accuracy with which the magnetic resonance imaging bone models were created should be assessed, possibly segmenting a phantom model.

Furthermore, a magnetic resonance imaging segmentation inter and intra repeatability trial would give an appreciation of the segmentation errors.

2. Recruit more healthy participants and patients for the image registration study. Shoulder replacement patients would be a particularly interesting patient subgroup to analyse since the implant contour appears clear in the fluoroscopic images.
3. Explore the use of bi-planar fluoroscopy measurements to increase the in-plane registration accuracy in the image registration procedure. It would not only improve the glenohumeral joint rotation calculations, but also allow measurements of humerus translations relative to the scapula.
4. It would be beneficial to develop a mechanism that assists participants to maintain the plane of elevation when measuring physiological arm elevation. This way the movements would be better standardised.
5. The development of Matlab routines to calculate the finite helical axis method, would result in improved glenohumeral joint kinematics estimation accuracy in patients with instability.
6. Consider using the DS classifier for the four patient subgroups (i.e. clavicle fracture, multiple directional instability, irreparable rotator cuff tear, and glenohumeral dislocation patients) separately. Larger patient cohorts need to be tested in the Motion Analysis Laboratory.
7. Provided more patients from each subgroup are tested, additional studies should consider the kinematics differences between the subgroup and the healthy participants to determine the most suitable input variables for classification. It is probable that significant differences may be found in other joint angles.
8. It would be good research practise to age and gender match the recruited healthy participants to the patient cohort.

9. Continue and further develop the ongoing collaboration with Zimmer (Zimmer, Inc. Switzerland). Joint kinematics data collected in the Cardiff University Motion Analysis Laboratory was shared with colleagues in Zimmer (Zimmer, Inc. Switzerland). They developed a 3D musculoskeletal model using AnyBody software (AnyBody Technology A/S), driven with a healthy participant's Motion Analysis data collected at Cardiff University by the author (Figure 6.1). Glenohumeral joint reaction forces, as well as muscle forces were calculated for a series of physiological range of motion measurements and activities of daily living.

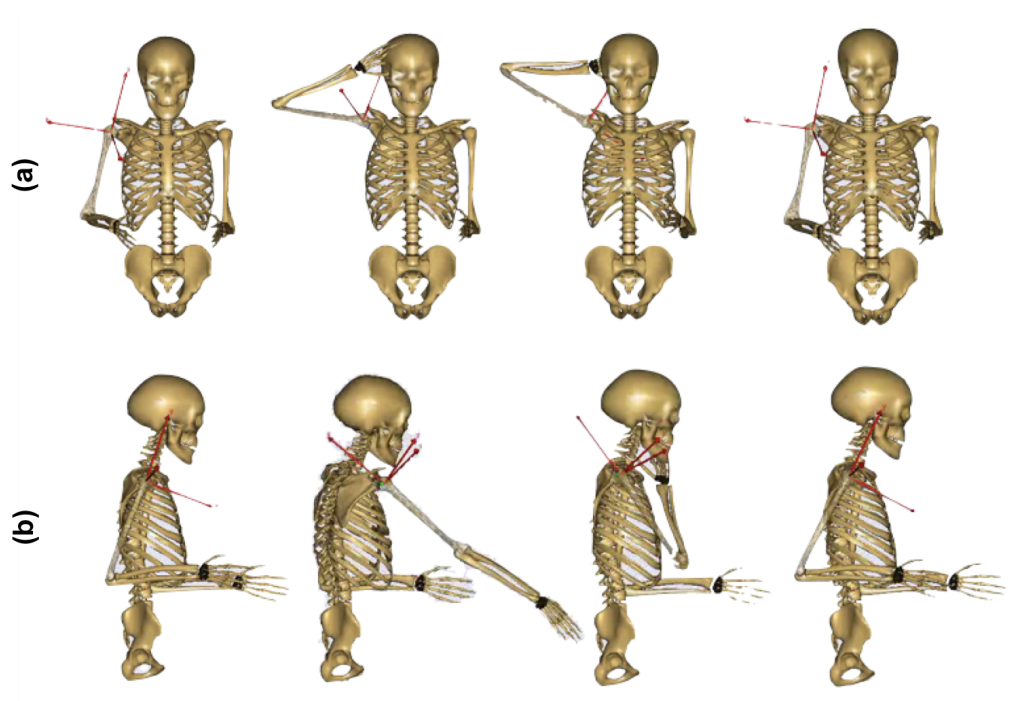


FIGURE 6.1: AnyBody (AnyBody Technology A/S) upper limb musculoskeletal model developed by Zimmer, Switzerland. The model is driven with data from the Cardiff MA Laboratory (a) Reach side and back of head and (b) eat with hand to mouth [113]

Based on the findings from the pilot study, Zimmer (Zimmer, Inc. Switzerland) expressed an interest in obtaining joint kinematics data for a further 10 healthy subjects.

Appendix A

Image registration information sheet and consent form

Part 1

VOLUNTEER INFORMATION SHEET

Assessment of shoulder function using imaging techniques

You are being invited to take part in a research study with Cardiff University. Before you decide it is important for you to understand why the research is being done and what it will involve. Please take time to read the following information carefully and discuss it with others if you wish. One of our team will go through the information sheet with you. Ask us if there is anything that is not clear or if you would like more information. Take time to decide whether or not you wish to participate. Part 1 tells you about the purpose of this study and what will happen to you if you take part. Part 2 gives you more detailed information about the conduct of the study.

What is the purpose of the study?

The shoulder has a larger range of motion than any other joint complex in the human body which aids us in the positioning of the arm and hand for everyday activities. However, this wide range of motion leaves it susceptible to a variety of injuries and pathologies.

Measurement of shoulder movement is essential for the understanding and evaluation of the function of the joint complex. Marker based motion analysis techniques are commonly used to quantify shoulder motion but errors are introduced due to relative motion of the skin and the underlying bone. Imaging techniques can be used to match 3 dimensional computer models of implants or bones to 2 dimensional low dose X-ray (fluoroscopic) images. Computer models can be constructed using MRI scans or are available for implants from the manufacturer. Recently, this technique was successfully applied abroad to measure movement in the shoulder joint and it produced very small errors. The aim of our study is to explore the feasibility of using imaging techniques to measure the 3 dimensional movement of the shoulder more accurately using low dose X-rays (fluoroscopy). This data will ultimately be compared with signals generated using marker based motion analysis to understand and help reduce the errors associated with skin movement that are produced when markers are attached to the skin.

The study is designed to compare the effects of shoulder pathology, injury, surgery or rehabilitation with what is measured to be healthy shoulder movement. It involves 20 patients from different sub groups (shoulder replacement patients, first time dislocators, and recurrent dislocators) who agree to take part at a time between 12 and 18 months after their shoulder surgery and 20 healthy volunteers with no shoulder problems.

Close work between orthopaedic surgeons, scientists and engineers is improving the tools available for shoulder patient assessment and diagnosis. Patients can clearly benefit from better diagnosis, thus promoting increased confidence in their medical care. The study that you have

been asked to take part in embraces this belief, with engineers and orthopaedic surgeons working together to help with the diagnosis of a patient's injury/pathology, and the consideration of different options available for surgery.

Why have I been chosen?

You have been chosen to take part in this study as a healthy volunteer with no previously identified shoulder injuries, disability or pain and as part of the standard recruitment procedure for this study on the request of the lead researcher.

Do I have to take part?

It is up to you to decide whether or not to take part. If you do decide to take part you will be given this information sheet to keep and be asked to sign a consent form. If you decide to take part you are still free to withdraw at any time and without giving a reason. Should you decide not to take part or withdraw at any time, you do not have to provide a reason for this decision and this will not adversely affect your current or future relationship with the NHS.

What will happen to me if I take part?

You will be asked to attend one session at the X-ray Department, University Hospital, Heath Park, Cardiff, lasting approximately 1 hour and another session at the Cardiff University Brain Research Imaging Centre lasting approximately 2 hours.

We will keep a record of your personal data for up to 5 years after the study has ended. This is intended for the possibility to invite you to take part in a reassessment should we decide to update the proposed study in the future. All data obtained during the study would remain confidential. Access to data would be available to the investigators attached to the project only.

You will be sent a map and directions and reimbursement for reasonable expenses will be provided.

What will I have to do?

Session at Cardiff University Brain Repair Imaging Centre

At the beginning of your first visit, we will explain the full study to you and ask for your consent, bearing in mind that you are free to withdraw at any time. In preparation for the MRI scan, you will first be asked a set of safety questions to make sure that you don't have anything in your body that might be affected by the scans, such as a pacemakers and other implanted devices, or metal in your body (e.g. shrapnel from war injuries). Based upon the results, you would either be included or excluded from the study.

If you are included in the study, you will be asked to remove all metal objects from your person including keys, coins, jewellery and watches and will need to remove credit cards and travel-cards, belts and under-wired bras. Your valuables will then be locked away for security reasons. If you are wearing make-up you may be asked to remove this as well.

You will be asked to lie down in a Magnetic Resonance Imaging (MRI) scanner for up to one and a half hours whilst we obtain images of your shoulder. You would lie on the bed of the MRI scanner and we would move you into the tube of the scanner so that your shoulder is in the correct position to be scanned. You would wear earplugs to protect your hearing but will still be able to hear the researcher when spoken to over the intercom. You would also be given a call button to hold throughout the scan to get the attention of the researcher who will be on the other side of a window just outside the scanner room. You can speak to the researcher via a microphone from inside the scanner.

It is very important that you keep still during the scans and try not to move your upper body at all. We would make sure that you are comfortable by providing cushions around the head and under the legs and a blanket if necessary.

Session at the X-ray department at the University Hospital of Wales

At the beginning of your visit, we will explain the full study to you and ask for your consent, bearing in mind that you are free to withdraw at any time

As part of the assessment your upper garments will need to be removed with the exception of bras. Females are advised to wear a sports bra or other suitable undergarment. Firstly you will have very light radio opaque markers placed onto the surface of your upper arm and trunk, held in place with double sided tape.

During the assessment a radiologist will ask you to perform simple arm elevation movements in a set pattern. This will be recorded for a maximum period of 60 seconds using low-dosage fluoroscopic X-ray equipment.

Throughout the sessions your shoulder movement will be recorded using standard audiovisual equipment. The recordings will be used for data verification post processing. Your face will be digitally masked from these files so that nobody can identify you from the videos. All data files, including audiovisual files will be stored in encrypted folders on Cardiff University password protected computers. Cardiff University and NHS members of staff who are directly involved with the study will have access to the files. The audiovisual files will be electronically destroyed up to 10 years from the commencement of the study.

Regular rest and toilet breaks will be provided as often as you need them to assure maximal comfort.

What happens if you find something unusual on my scan?

The researchers involved do not have expertise in MRI diagnosis. The person conducting your scans will not be able to comment on the results of your scans. You should not regard these research scans as a medical screening procedure. Occasionally when we image participants, the researchers may be concerned that a potential abnormality may exist on the scan. In this case, a report can be forwarded to the Consultant Orthopaedic Surgeon involved in the study so that he may arrange to further investigate any potential abnormality. Early detection may have the benefit of starting treatment early but, in a small number of cases, may have implications for future employment and insurance.

It is important that you realise that these scans are not intended to provide any information that may help in the diagnosis of any medical condition. If you do have any health concerns, you should contact a qualified medical practitioner in the normal way.

Are there any risks in participating in this study?

Before participating you should consider if this will affect any insurance you have and seek advice if necessary.

The X-ray effective dose per exposure is estimated to be trivially low (up to 5 microSieverts) and represents a lifetime risk of induction of malignancy (cancer) to you of less than 1 in a million. The level of risk from one exposure is approximately equivalent to one day of exposure to natural background radiation.

It is possible that if the investigation is performed on a pregnant woman it will harm the unborn child. Pregnant women must not therefore take part in this study, neither should women who plan to become pregnant during the study. Women who are at risk of pregnancy may be asked to have a pregnancy test before taking part to exclude the possibility of pregnancy. Women who could become pregnant must use an effective contraceptive during the course of this study. Any woman who finds that she has become pregnant while taking part in the study should immediately tell her doctor and the research investigator.

No serious side effects of being in an MRI scanner have been reported despite millions of scans worldwide. Although the possibility of long-term effects cannot be completely ruled out, the weight of experience and opinion is against this.

Some people find being inside an MRI scanner claustrophobic although this is less so with the more compact systems like those used in CUBRIC. The scanner also makes quite loud noises for which we provide ear plugs. The radiofrequency waves we use to create the MR scans can cause your head and body to warm up slightly. This is not a problem, and you usually won't notice it, as your blood flow will increase slightly to take the heat away; we also keep the scanner room quite cool so that you always remain comfortable.

A few people have reported minor side effects including dizziness, mild nausea, a metallic taste in the mouth, and the sensation of seeing flashing lights. These side effects, if experienced, go away soon after you leave the magnet. If you experience any of these or others please let us know as soon as possible.

If you find the experience in the scanner unpleasant, just let us know straightaway and we will stop and take you out of the scanner.

What are the possible benefits of taking part?

We hope to be able to better understand how shoulder injuries affect the motion of the shoulder. There is no intended clinical benefit to the patient from taking part in the study. The information we get from this study may help us to provide future patients who have shoulder pathology or injury with improved treatment options.

If the information in Part 1 have interested you and you are considering participation, please read the additional information in Part 2 before making any decisions.

Part 2

Assessment of shoulder function using imaging techniques

What if new information becomes available?

Sometimes during the course of a research project, new information becomes available about the investigation. If this happens, your research doctor will tell you about it and discuss with you whether you want to continue in the study. If you decide to withdraw your research doctor will make arrangements for your care to continue. If you decide to continue in the study you will be asked to sign an updated consent form.

Also, on receiving new information your research doctor might consider it to be in your best interests to withdraw you from the study. He/she will explain the reasons and arrange for your care to continue.

What will happen if I do not want to carry on with the study?

If you withdraw from the study, we will destroy all your identifiable samples, but we will need to use the data collected up to your withdrawal.

What if something goes wrong?

If you are harmed by taking part in this research project, there are no special compensation arrangements. If you are harmed due to someone's negligence, then you may have grounds for a legal action but you may have to pay for it. Regardless of this, if you wish to complain, or have any concerns about any aspect of the way you have been approached or treated during the course of this study, the normal National Health Service complaints mechanisms should be available to you.

Will my taking part in this study be kept confidential?

All information which is collected about you during the course of the research will be kept strictly confidential. Any information about you which leaves the hospital/University will have your name and address removed so that you cannot be recognized.

Will my GP be informed of my involvement in the study?

With your permission, we will send a letter to your General Practitioner informing him or her of your involvement in the study.

What will happen to the results of the research study?

The measurements taken will provide information about the movement of your shoulder. This information will then be compared with the same obtained during the corresponding clinical trial that you are kindly talking part in and used to assess the effectiveness of the measurements.

The results of the study will be presented at meetings of orthopaedic surgeons, clinical scientists, and engineers, and if accepted, published in medical and engineering journals. If interested, a copy of the published article can be made available to you.
You will not be identified in any report/publication.

Who is organizing and funding the research?

The research is being organized by Dr. Catherine Holt (Senior Lecturer in Biomechanics), Mr Richard Evans (Consultant Orthopaedic Surgeon), and Ms. Lindsay Stroud (PhD. Student). None of the doctors or engineering staff are being paid for this study.

Who has reviewed the study?

The project has been reviewed the Cardiff University Research Governance Team.
The project has the approval of the Cardiff and Vale NHS Trust and ethical approval has been granted by the NHS National Research Ethics Service.

Where can I get independent advice about taking part in the trial?

If you wish to get independent advice regarding your rights as a participant in the trial, you can contact Mr. Stuart Roy at 01443 443574. Mr. Roy is an orthopaedic knee consultant in the Royal Glamorgan Infirmary and has been a collaborator with Cardiff University on similar, but unassociated trials involving patients with total knee replacements.

What if I wish to lodge a complaint?

If you wish to make a minor complaint regarding the way you were approached or treated during the trial, please contact Ms. Lindsay Stroud (02920874000 ext 77900). If you wish to make a more formal complaint, please contact Dr. Catherine Holt, the Chief Investigator of the trial (029 2087 4533). If contacting the above mentioned researchers compromises the nature of your complaint, you can contact the Cardiff University Research Governance Team on 029 208 79277.

Contact details

For further information you can contact:

Dr. Cathy Holt
Lecturer in Biomechanics
Cardiff School of Engineering
Cardiff University
Queen's Buildings
The Parade
Cardiff CF24 0YF
Wales, UK
Tel: 029 20874533
Fax: 029 20874939

Ms. Lindsay Stroud
Research Student
Cardiff School of Engineering
Cardiff University
Queen's Buildings
The Parade
Cardiff CF24 3AA
Wales, UK
Tel: 029 20874000 ext 77900
Fax: 029 20874939

This completes Part 2

Study number:

Volunteer identification number for this trial:

VOLUNTEERS CONSENT FORM

Assessment of shoulder function using imaging techniques

Please initial box

1. I confirm that I have read and understand the information sheet dated 11th of December 2009 (Version 3) for the above study. I have had the opportunity to ask questions and have had these answered satisfactorily.

2. I understand that my participation is voluntary and that I am free to withdraw at any time, without giving any reason, without my medical care or legal rights being affected.

3. I agree to take part in the above study.

4. I agree to allow notification of my GP

Name of volunteer

Date

Signature

Name of person
taking consent

Date

Signature

When completed, 1 for volunteer; 1 for researcher site file; 1 (original) to be kept in medical notes

Appendix B

Image registration protocol



**Image Registration manual for
Shoulder complex studies**

Data Handling

Lindsay Stroud

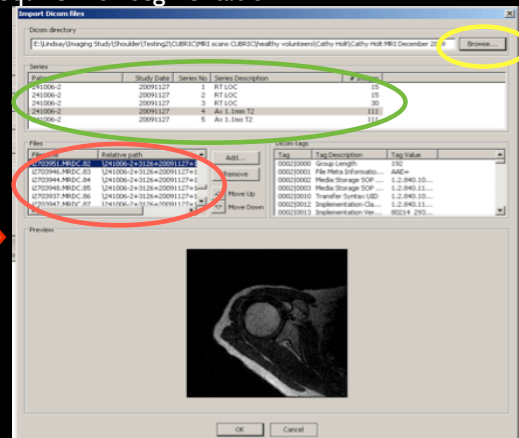
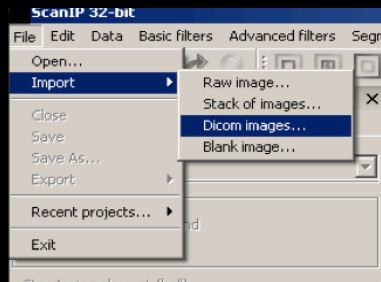


Simpleware instructions

Getting started and importing MRI images

Browse for the main image folder directory that contains the MRI scans. This way, all images subfolders can be accessed to view which one is required for segmentation

Open ScanIP and import Dicom images.

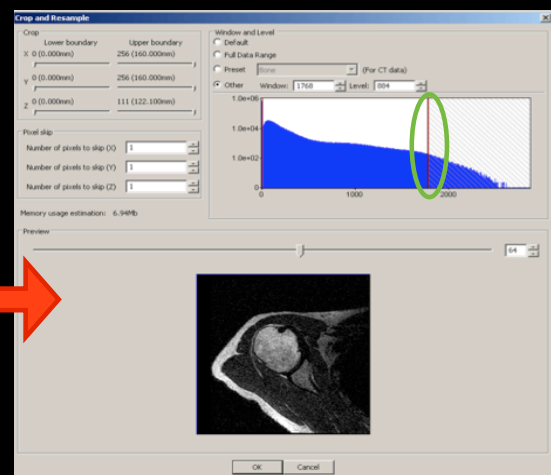
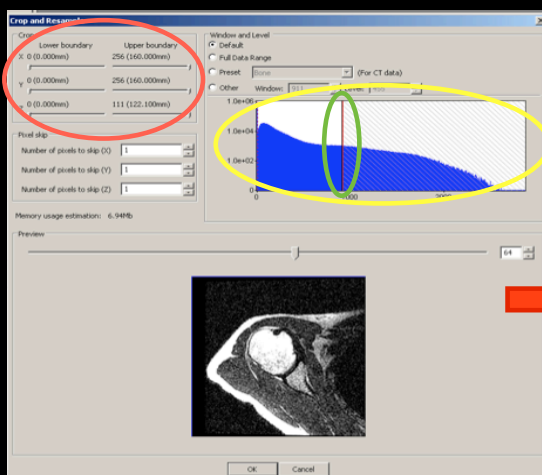


Scrawl down to view images within the selected folder

3

Getting started and importing MRI images

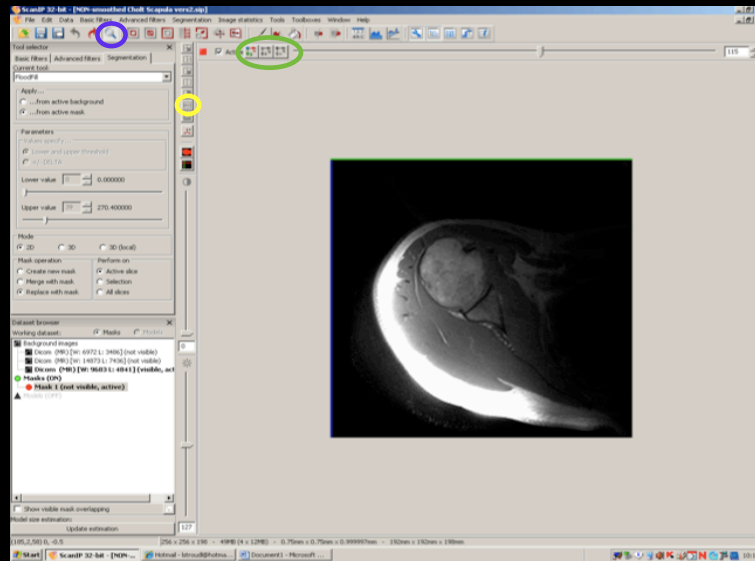
Once the folder containing the MRI images has been selected, the image light intensity can be altered in the histogram to better suit segmentation. This is performed by dragging the histogram lines in the horizontal plane. It may also be convenient to Crop the images.



4

Getting started and importing MRI images

In the **2D** view, select from the different **slice views** which view is more appropriate for segmentation. Use the **zoom** in and out tool when convenient.



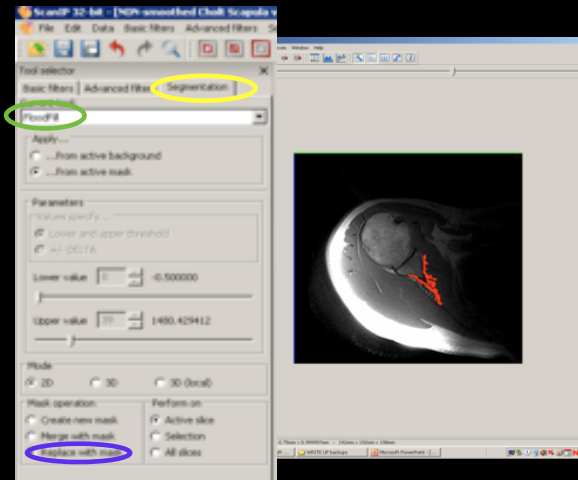
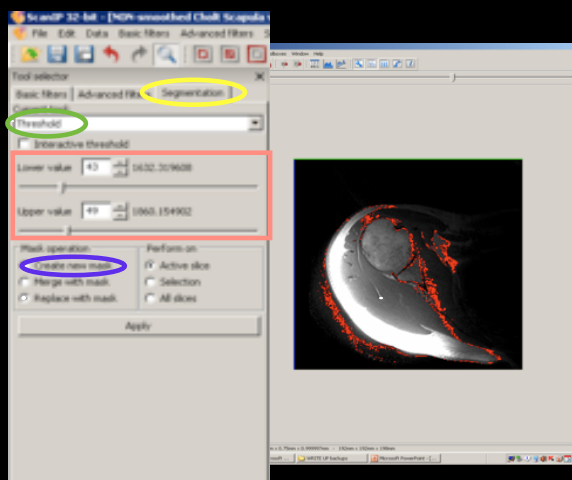
5

Segmentation

Segmenting cortical bone

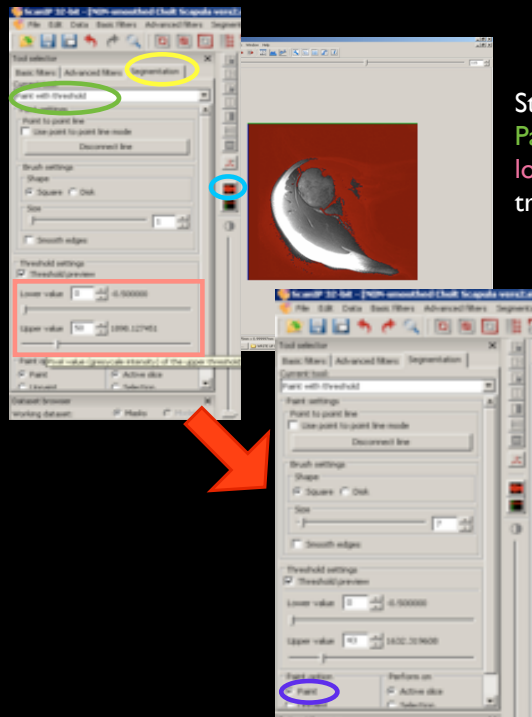
Select the **Threshold** tool and **Create new mask** to begin segmenting the scans. The **Lower and Upper values** are used to determine the pixel range

Next, use the **FloodFill** tool and **Replace with mask** option and click on a section of the mask that represents the cortical bone.



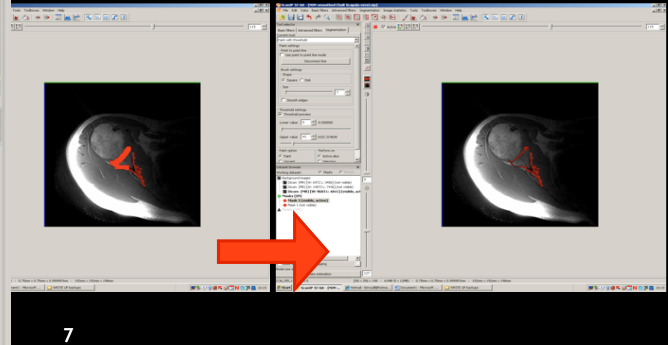
6

Segmentation



Still under the Segmentation menu, select Paint with threshold. The threshold upper and lower values. Use the tool to make the mask translucent.

When Painting with threshold, only the pixels that are shown in the mask when setting the lower and upper threshold values can be painted.

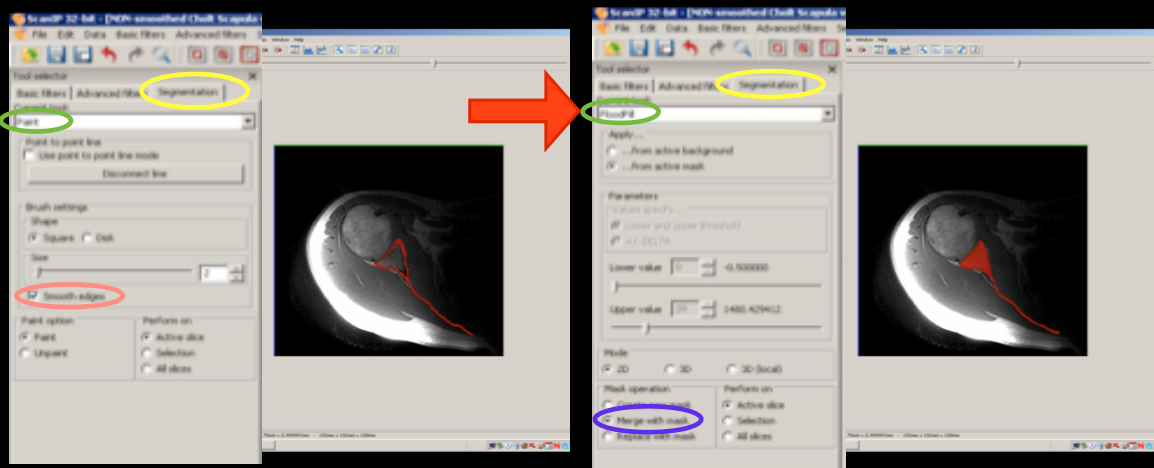


7

Segmentation

Complete the segment's outline (i.e. cortical bone) manually with the standard paint tool. Select Smooth edges option

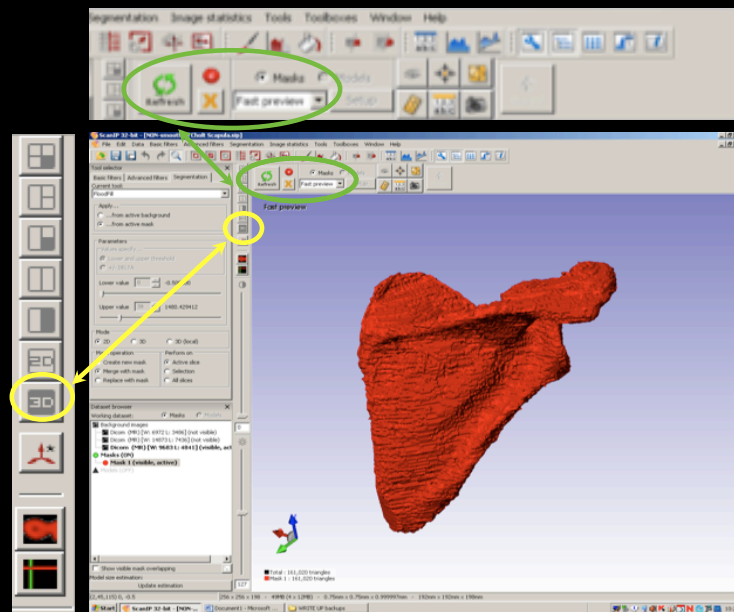
Floodfill the segment outline using Merge with mask to obtain a solid model



8

3D view

To view the segment in 3D, Refresh the view in fast preview mode



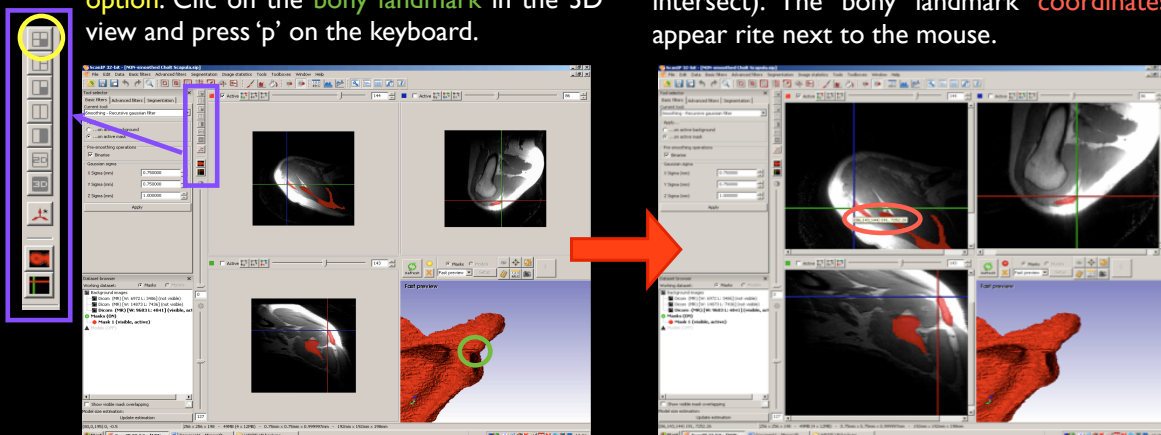
9

Changing the embedded axis system

It is necessary to change the axis system on the models so that they are in accordance with either ISB or with University of Florida axes system. Bony landmarks must be identified to create new ACSs

Select the three 2D views and the 3D view option. Click on the bony landmark in the 3D view and press 'p' on the keyboard.

Hover the mouse on top of the bony landmark on a 2D view (where the two lines intersect). The bony landmark coordinates appear next to the mouse.



Identify all bony landmarks using the technique outlined above.

10

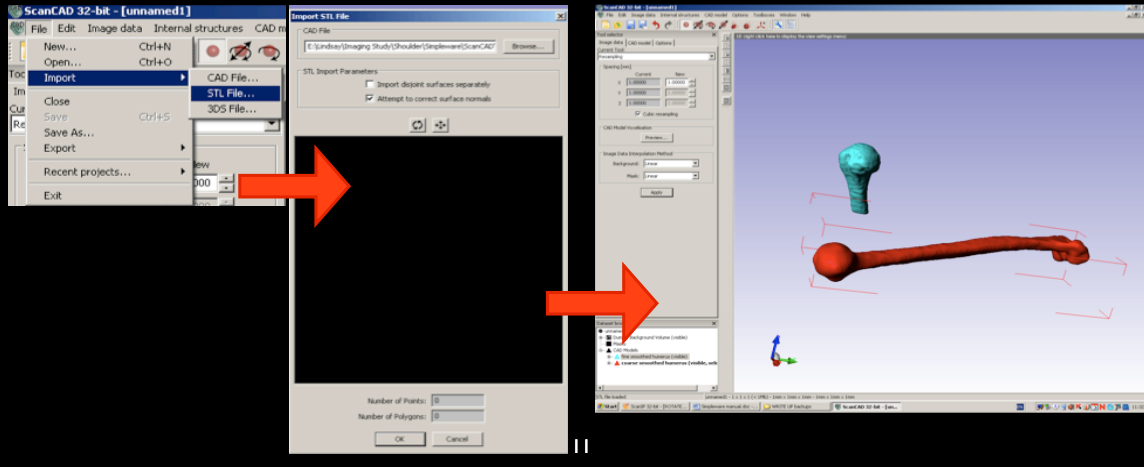
Coarse to fine model registration

NOTE - Humerus segment requires a further step for ISB recommendations before bony landmark id

To use ISB recommendations, the humerus coarse scan model needs to be registered to the fine scan model using ScanCAD. This is because the epicondyles are not segmented in the fine scan model.

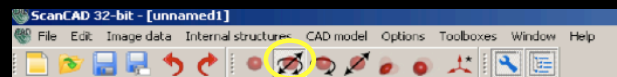
Export the models as described on slide 18.

Open ScanCAD and import the STL models of the coarse and fine humerus

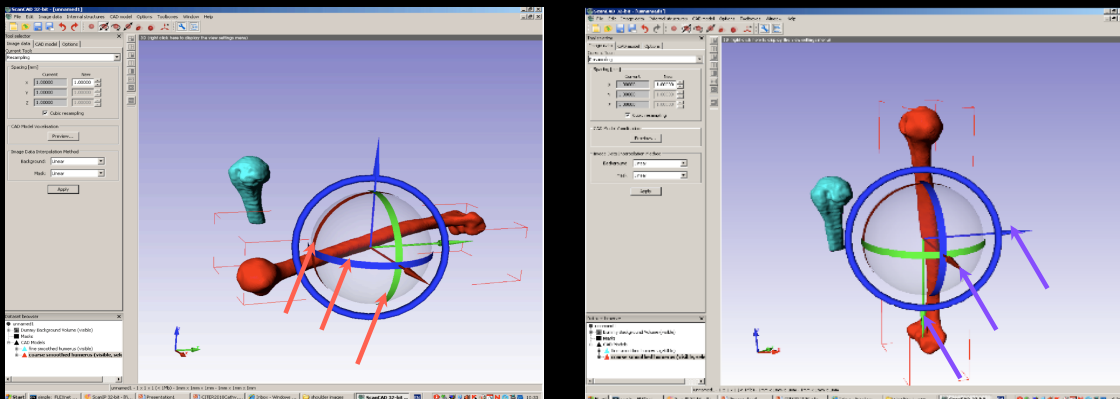


Coarse to fine model registration

To register the coarse scan model to the fine scan model, select the coarse model and use the **rotate and translate tool**.



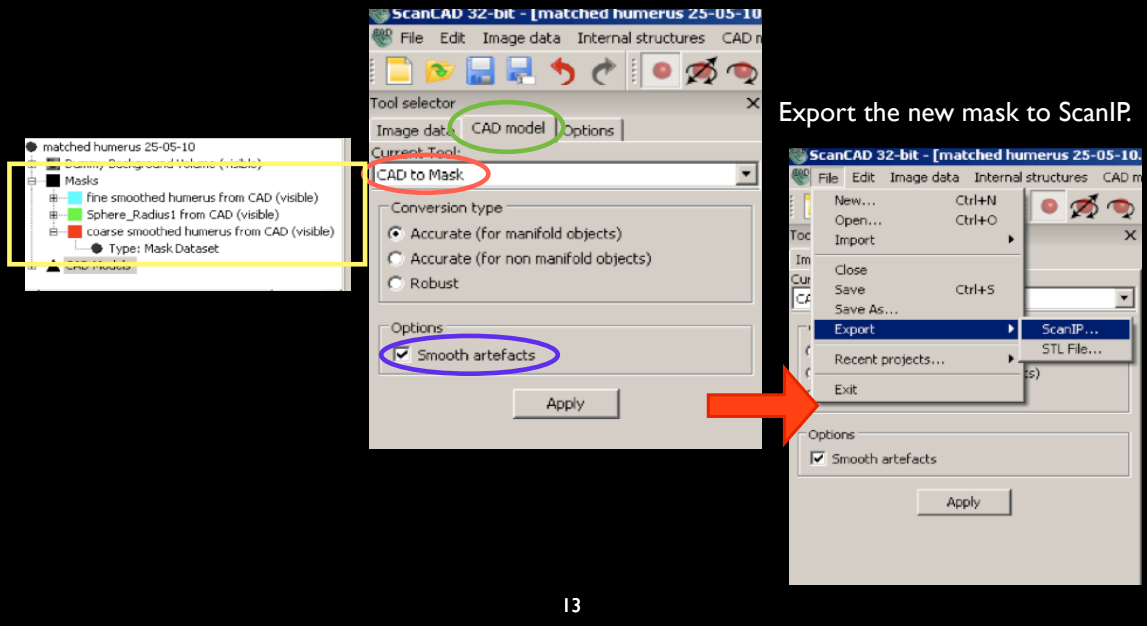
Use the blue, red and green curved lines to **rotate** the model and the blue, red and green straight lines to **translate** the model.



Import sphere.stl and register it to the fine model using the steps outlined above. Scale the sphere manually using the blue ring around the model. 12

Coarse to fine model registration

Select all masks and from the tool selector, select **CAD model** and **CAD to Mask** option from the current tool. Also select the **Smooth Artefact** option and apply.



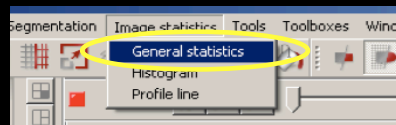
13

Registered humerus model ACS

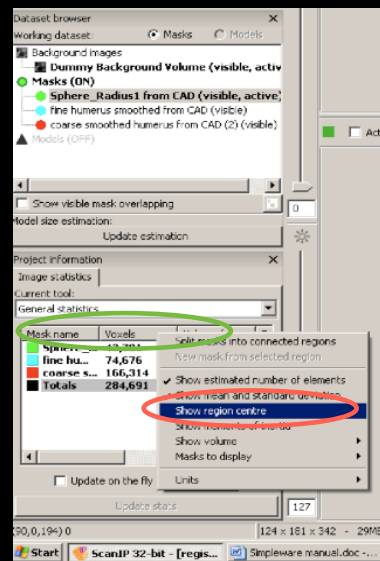
Use the registered humerus to identify the necessary bony landmarks in ScanIP as outlined on slide 10.

The GH joint centre of rotation is assumed the centre of the registered sphere.

To identify the centre of the sphere, select **General statistics** from Image statistics in the main menu.



From the project information, Image statistics, right click on the menu and select **Show region centre**. Scrawl to the far right of the image statistics to region centre. Right click on it again to select the units as pixels!!



14

Changing the embedded axis system

Open Excel spreadsheet labeled scapula and humerus to calculate the new ACSs

	X coordinates	Y coordinates	Z coordinates	
2 POSTERIOR	87	106	124.875	coordinates in mm
3 ANTERIOR	100.75	80.25	105.894	
4 INFERIOR	96.25	104	107.226	
5 SUPERIOR	100.75	83.75	131.868	
6				
7 S1	14.5	-20.25	24.642	vector length
8 a1	0.413856765	-0.577972378	0.703328165	
9 S2	13.75	-17.75	-18.981	
10 s2	0.467675344	-0.603726364	-0.645596052	
11 s3	-0.797754434	-0.596113535	-0.020447195	0.996083115
12				0.996083115
13 s4	-0.431081353	0.552620952	0.707785647	
14				
15 Xa	-0.797754434	-0.596113535	-0.020447195	Y x Z = X
16 Ya	0.413856765	-0.577972378	0.703328165	
17 Za	-0.431081353	0.552620952	0.707785647	
18				
19 Spacing X, Y and Z	0.75	0.75	0.999	USE THESE VALUES TO CHANGE THE COORDINATE SYSTEM BUT CHANGE THE SIGN
20 Scaling factor	100			
21				
22 Y axis in pixels	-106	-79	-3	bony landmark ID (in pixels)
23 Y axis in pixels	55	-77	70	
24 Z axis in pixels	-57	74	71	
25				
26 average bony landmark id in pixels				
27				
28 POSTERIOR	116	141	125	112 140 108
29 ANTERIOR	134	113	106	116 139 105
30 INFERIOR	115.00	138.67	107.33	117 137 109
31 SUPERIOR	134.3333333	111.6666667	132	INFERIOR 115.00 138.67 107.33
32				133 113 132
33				135 111 132

Input the slice spacing

Input bony landmarks coordinates in pixels

The X, Y and Z are the new axis system. When applying them in Simpleware, use the opposite sign to what is shown in the excel sheet.

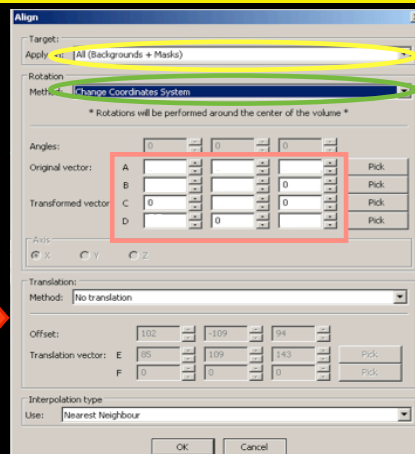
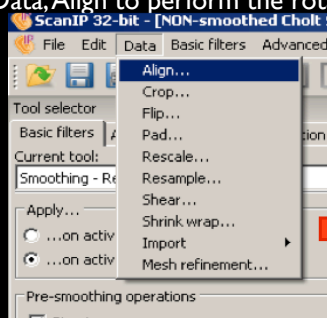
Only need to input the coordinates in pixels and the slice spacing. The rest is calculated automatically

15

Changing the embedded axis system

In ScanID:

Select Data, Align to perform the rotation



Select The rotation to be applied on All backgrounds and masks and the rotation method as Change the coordinate system.

Write the new X axis in A (positive values) and B (negative values) boxes. The new Y axis goes in C (positive value) and D (negative values). REMEMBER: the values to input should have the opposite sign to the excel sheet.

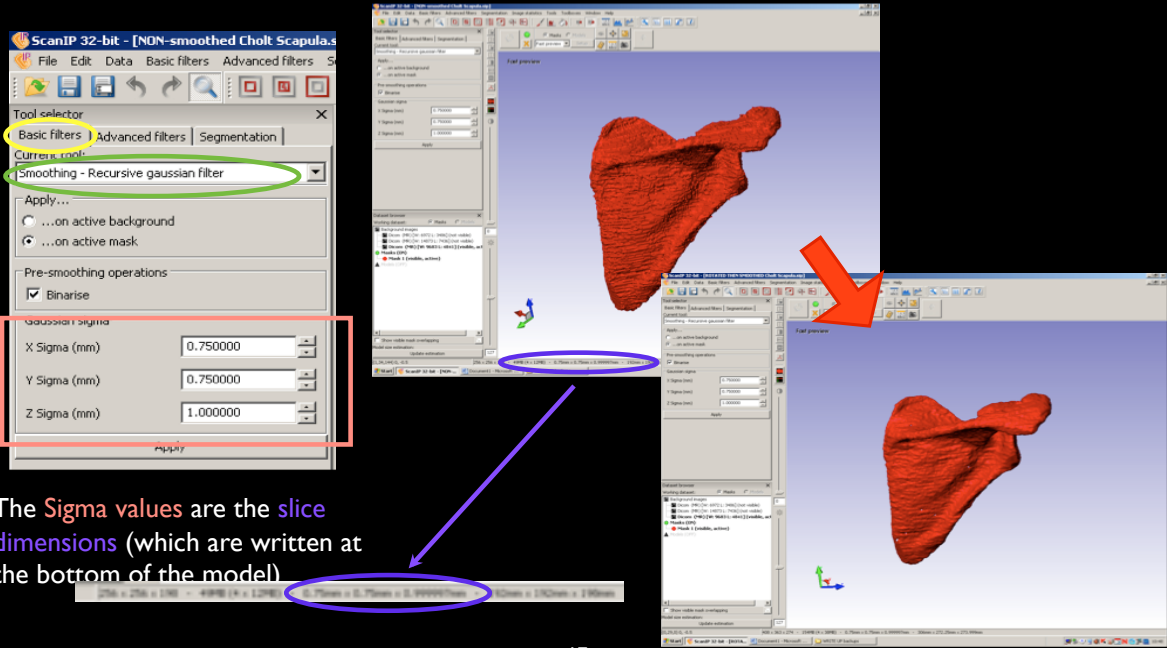
Press ok and refresh in the 3D view.

Once the segment has a new axis system, need to select the origin again since the coordinates would have changed.

16

Smoothing

To smooth the 3D model, use **Basic filters** tool and select the **Recursive gaussian filter**.



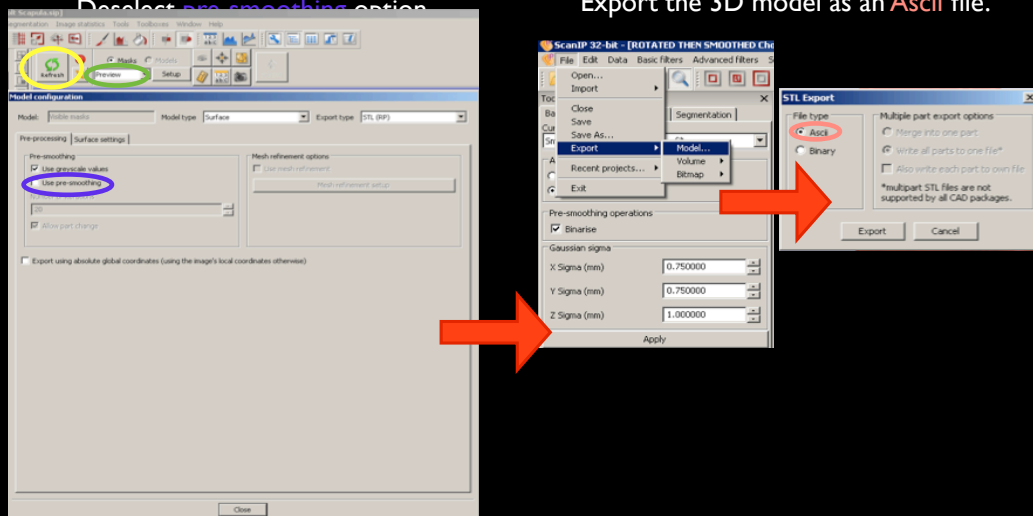
17

Exporting the 3D model

To export model as an **.stl** file, need to **refresh** the model in **preview** mode.

Redselect **use smoothing** option

Export the 3D model as an **Ascii** file.



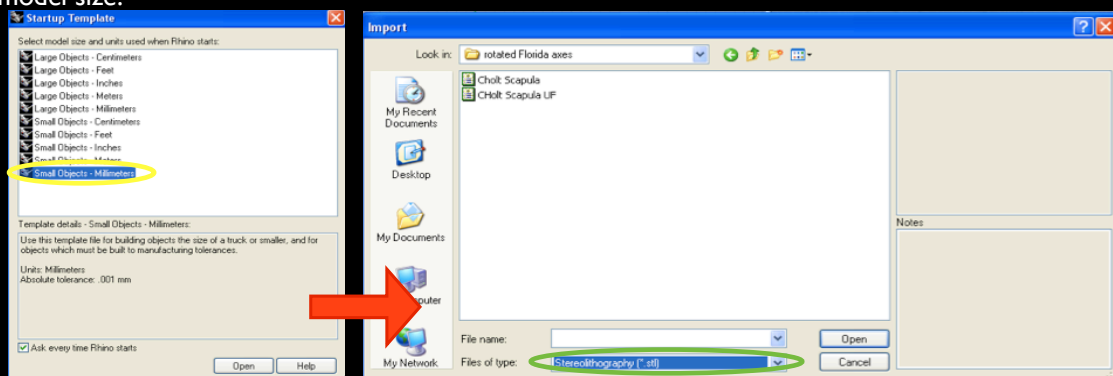
18

Rhinoceros 4.0 instructions

Performing origin translation

Start Rhinoceros 4.0
Select **Small Objects - Millimeters**
model size.

Select **.stl** file type



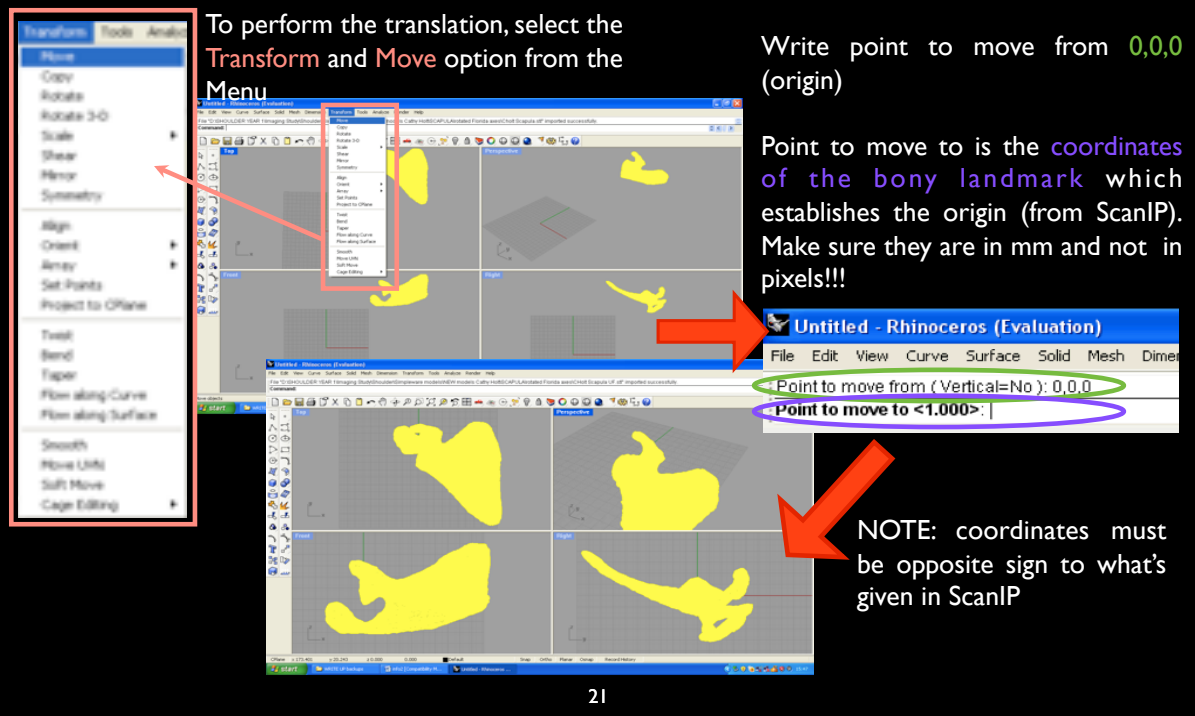
Performing origin translation

To perform the translation, select the **Transform** and **Move** option from the **Menu**

Write point to move from **0,0,0** (origin)

Point to move to is the **coordinates of the bony landmark** which establishes the origin (from ScanIP). Make sure they are in mm and not in pixels!!!

NOTE: coordinates must be opposite sign to what's given in ScanIP

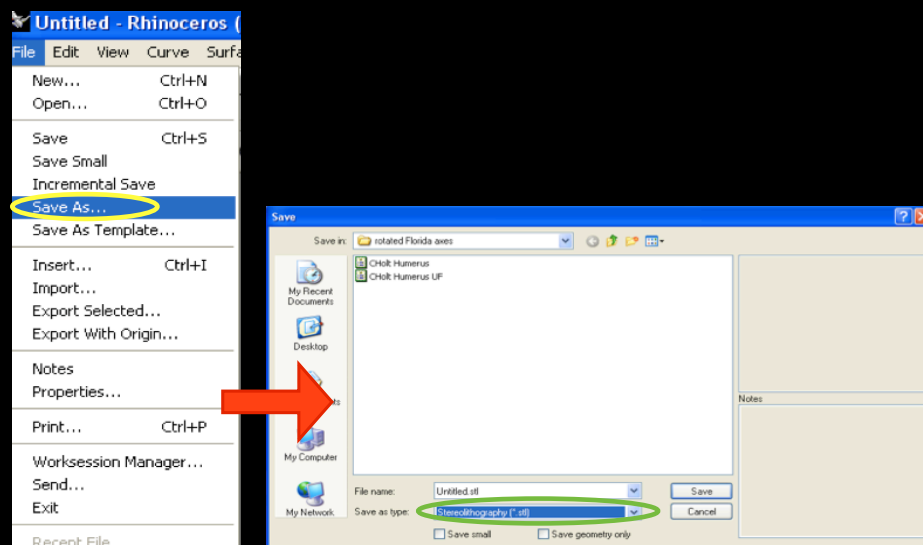


The image shows a multi-view 3D model of a bone in yellow. A red box highlights the 'Transform' > 'Move' menu path. A red arrow points from the text 'Write point to move from 0,0,0 (origin)' to the 'Point to move from' field in the command line, which contains '(Vertical=No): 0,0,0'. Another red arrow points from the text 'Point to move to is the coordinates of the bony landmark...' to the 'Point to move to' field, which contains '<1.000>:'. A third red arrow points from the text 'NOTE: coordinates must be opposite sign to what's given in ScanIP' to the same field. The command line also shows 'Point to move to <1.000>:'.

21

Exporting the 3D model

Save the model as an **stl** file to be used for the image registration



The image shows the 'File' menu with 'Save As...' highlighted. A red arrow points from 'Save As...' to the 'Save' dialog box. In the dialog box, the 'File name' field contains 'Untitled.stl' and the 'Save as type' dropdown is set to 'Stereolithography (*.stl)'. A red arrow points from the text 'Save the model as an stl file to be used for the image registration' to the 'Save as type' dropdown.

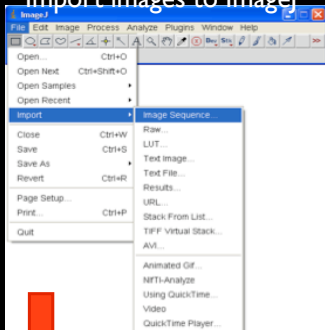
22

Fluoroscopy images handling instructions

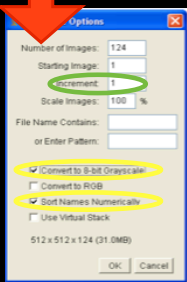
ImageJ

Save as an **Image sequence** with **TIFF** extension

Import images to ImageJ

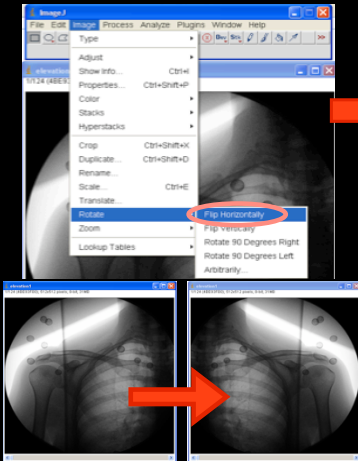


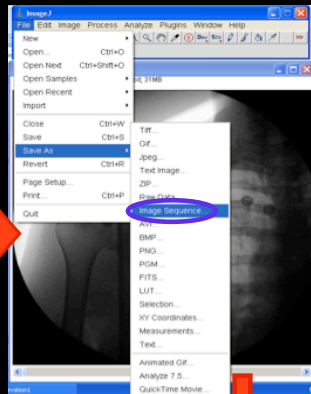
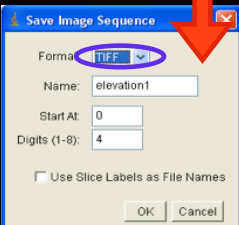
Convert images to 8-bit Greyscale and Sort Numbers Numerically



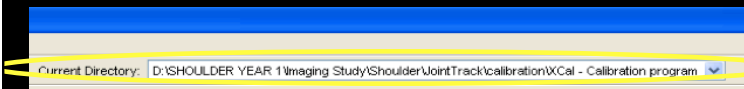
Change the total number of images in increment value if necessary

The images must be **Flipped horizontally** if they were reversed during image acquisition



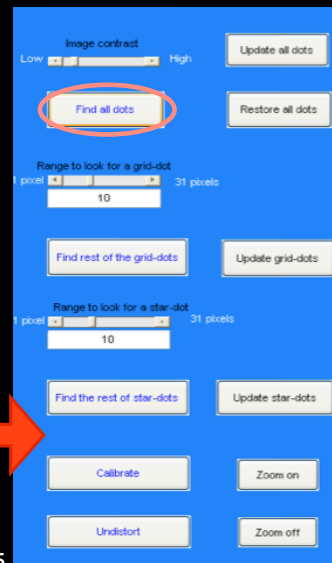
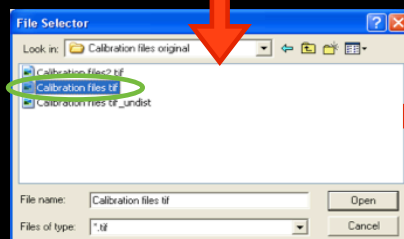
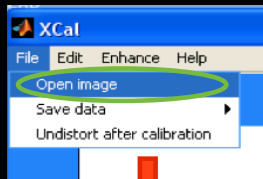
Undistorting images



Browse for the **directory** where the Matlab program is saved and run Xcal.m

Follow Help menu instructions

A Matlab Figure appears. Select **Open image** from the File Menu and find the converted **Calibration frame image 8-bit greyscale tiff file**.



Press the button: **Find all dots** and wait

25

Undistorting images

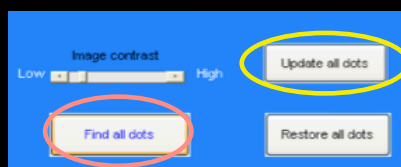
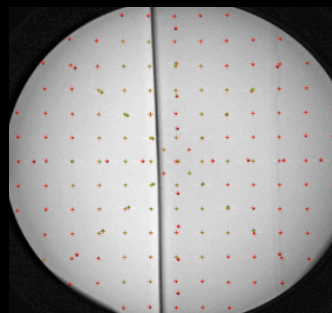
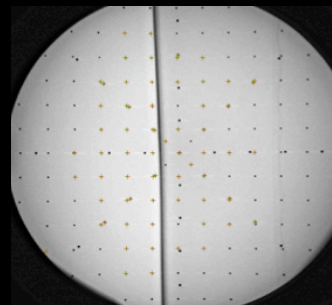
If not all are found:

- Change minimum circle radius
- Change radius range - slider
- Press the button: **Find all dots**
- Wait

If needed:

- Add a dot: a on keyboard
- Delete a dot: d on keyboard
- Press button: **Update all dots**

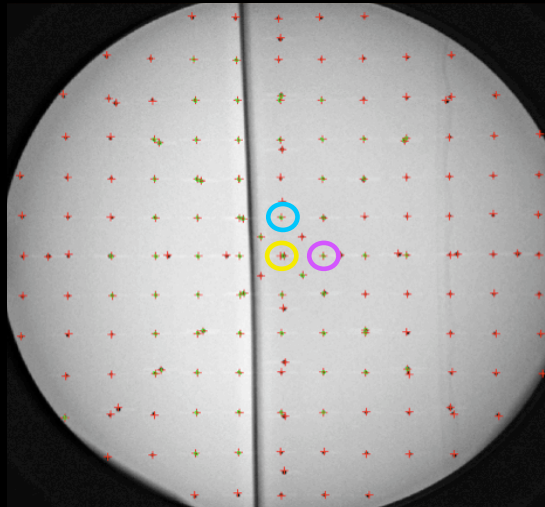
NOTE: Added dots appear as red crosses on the calibration frame



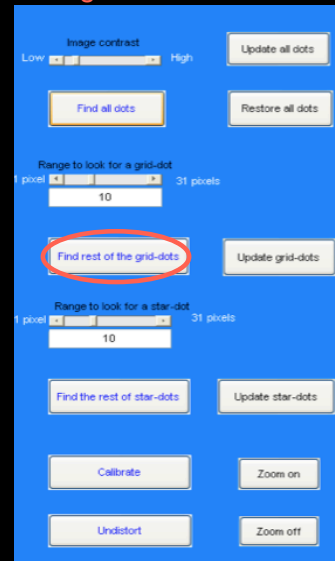
26

Undistorting images

To sort out the grid coordinates from all dots found, select (with mouse): the grid center dot, the grid dot above center, the grid dot to right of center



Press the button: Find rest of the grid-dots and wait



27

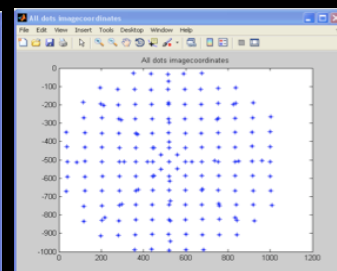
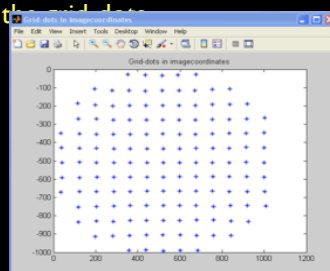
Undistorting images

If not all are found

- change range to look for a grid-dot (slider)
- Press the button: Find rest of the grid-dots
- Select (with mouse): the grid center dot, the grid dot above center, the grid dot to right of center
- Press the button: Find rest of the grid-dots
- Wait

If dot is missing in grid dots or wrong dot is found

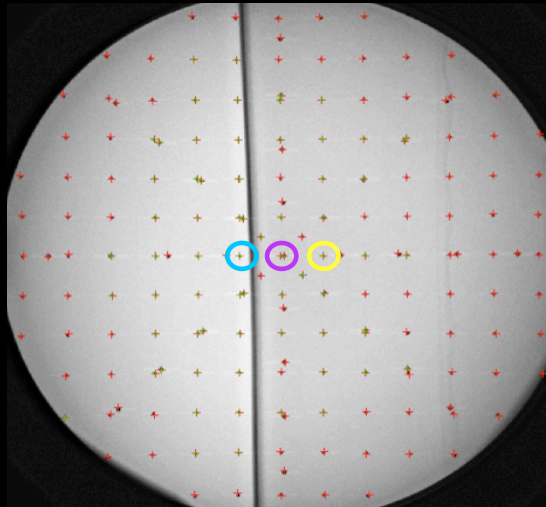
- Add a dot: a on keyboard
- Delete a dot: d on keyboard
- Press button: Update grid-dots
- Select (with mouse): the grid center dot, the grid dot above center, the grid dot to right of center
- Press the button: Find rest of the grid-dots
- Wait



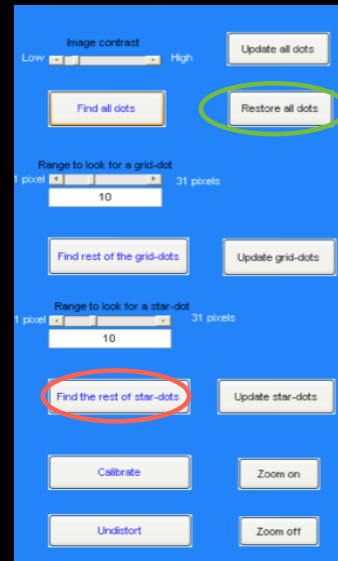
28

Undistorting images

To sort out the star coordinates from all dots found, press button **Restore all dots**. Then select (with mouse): the star to right of center, the star to left of center, the center star dot



Press the button: **Find rest of the star-dots** and wait



29

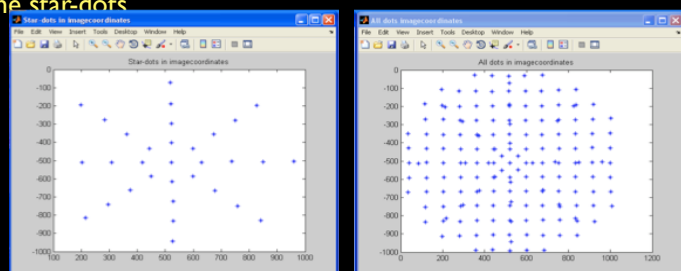
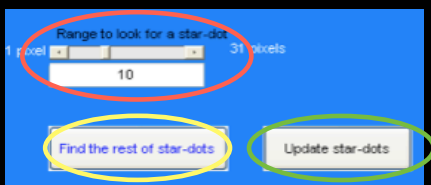
Undistorting images

If not all are found

- change range to look for a star-dot (slider)
- Press the button: **Find rest of the star-dots**
- Select (with mouse): the star to right of center, the star to left of center
- Press the button: **Find rest of the star-dots**
- Wait

If dot is missing in star-dots or wrong dot is found

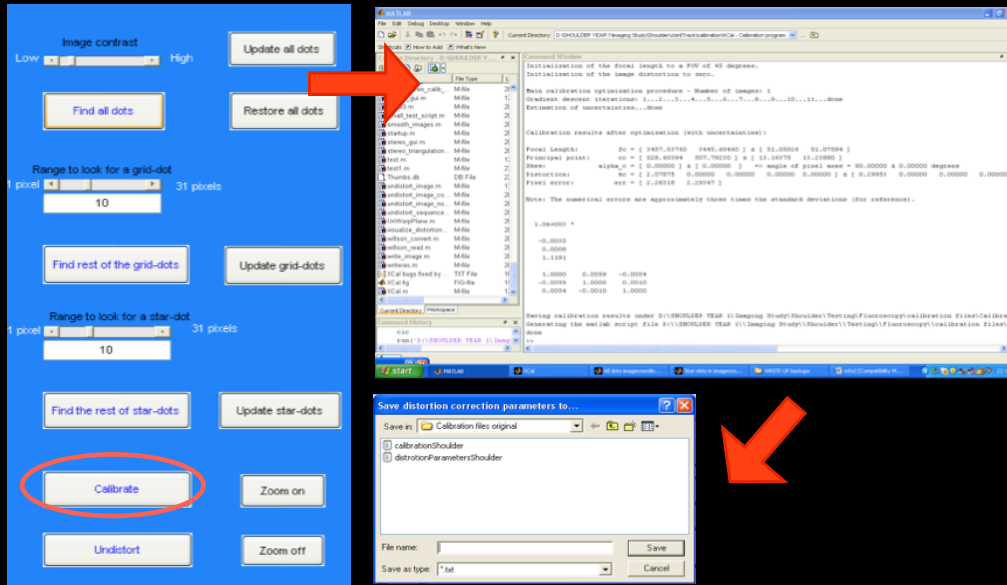
- Add a dot: a on keyboard
- Delete a dot: d on keyboard
- Press button: **update star-dots**
- Select (with mouse): the star to right of center, the star to left of center
- Press the button: **Find rest of the star-dots**
- Wait



30

Undistorting images

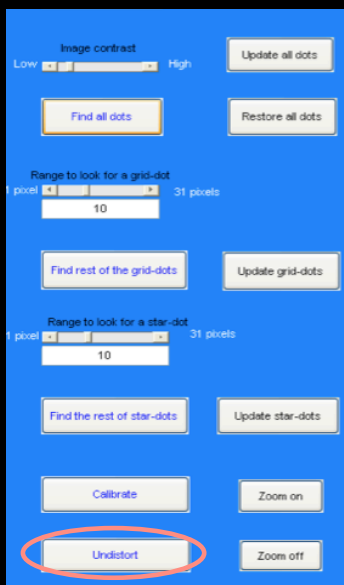
Press the button **Calibrate** and wait. You can see the results in the Matlab prompt. They are saved in an m-file called image name.m



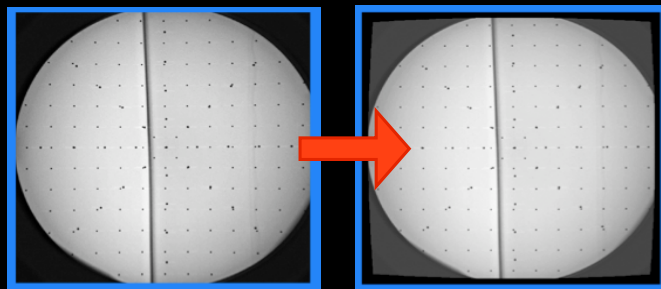
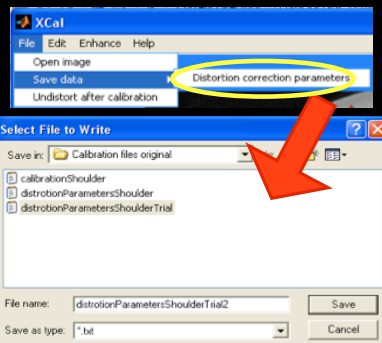
31

Undistorting images

To save the distortion parameters and thus be able to undistort other images using the calibration results, Select File, Save data, **Distortion correction parameters**.



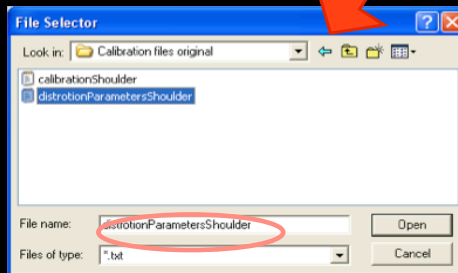
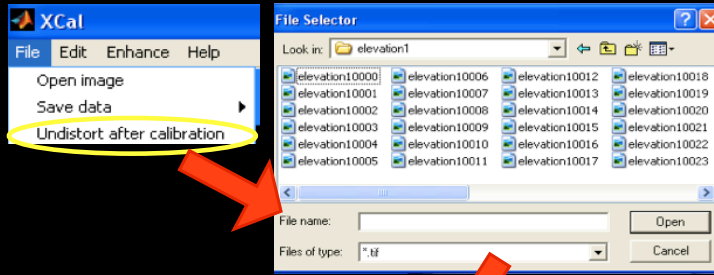
Press the button: **Undistort** and wait. Undistorted image is saved as the name of the original image _undist.tif



32

Undistorting images

Select File, **Undistort after calibration** and select the motion images (for more than one keep the ctrl key down).

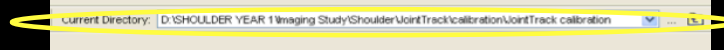


Next select the corresponding file with saved **distortion parameters**

The undistorted images are saved with **_undist** in the file name and can be found in the same path as the distorted images.

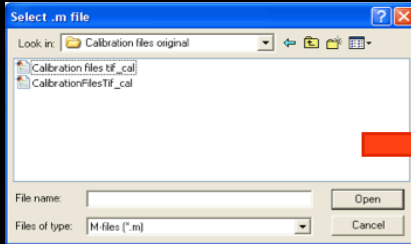
JT Calibration

Open Matlab and browse for JointTrack calibration folder in the **Current Directory**



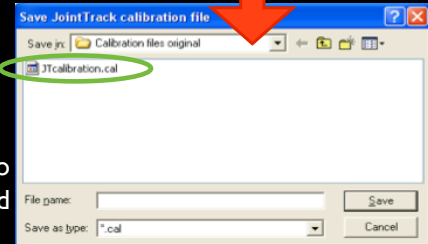
Run m2cal.m program.

Select the .m file that was created in Xcal



The units used were mm and the images were not cropped after distortion correction

What unit are you using?
 1/Enter = mm, 2 = cm, 3 = inch.
 For other units, please input its scale relative to mm (e.g. 25.4 = inch):
 1
 Did you crop the images after distortion correction?
 1 = yes, 0/Enter = no : 0



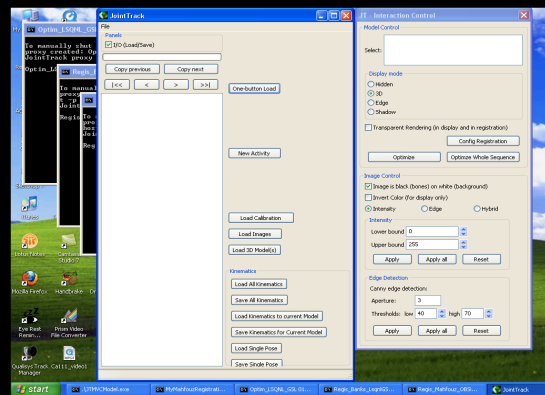
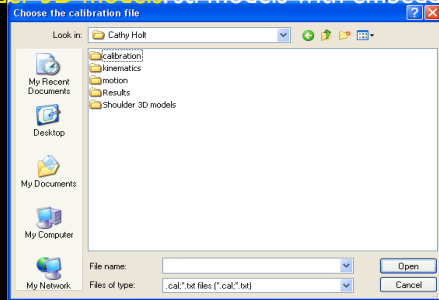
This JTcalibration.cal file is the one imported into JointTrack during the One Button load

3D to 2D registration

Make a folder with the following sub folders:

- calibration:** calibration file from m2cal.m
- kinematics:** the saved JT kinematics
- motion:** undistorted flourescopic images
- results:** the final saved results
- shoulder 3D models:** stl models with embedded ACSs

Open JointTrack for 3D to 2D image registration



If you get a message error, shut all the windows and try again.

NOTE: Close the first window and the rest should close automatically.

3D to 2D registration

1. JT calibration file

2. Fluoroscopic images

3. Select both models (humerus and scapula)

Imported files ready for registration

Perform a one button load to import all the relevant files to JT. Otherwise, can select each one manually from the menu.

37

3D to 2D registration

Change the **Upper and Lower intensity bound** and the **Low and High Threshold** values to aid with the image registration as appropriate.

JT - Interaction Control

Model Control

Select: CHob Scapula UF.stl
CHob Humerus UF.stl

Display mode

Hidden
 3D
 Edge
 Shadow

Transparent Rendering (in display and in registration)

Config Registration

Optimize

Optimize Whole Sequence

Image Control

Image is black (bones) on white (background)
 Invert Color (for display only)

Intensity

Lower bound: 0
Upper bound: 255

Apply

Apply all

Reset

Edge Detection

Canny edge detection:

Aperture: 3

Thresholds: low 40 high 70

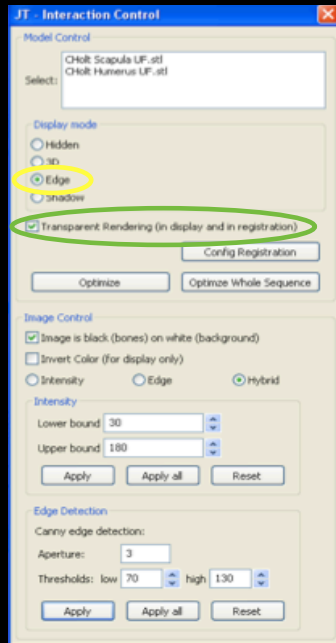
Apply

Apply all

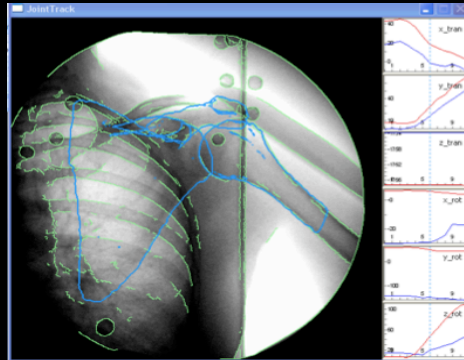
Reset

38

3D to 2D registration



When performing the image registration, it is convenient to use the **Edge Display mode with Transparent Rendering (in display and in registration)**. This is because you can use **edges from the posterior and anterior view of the segment to register to the x-rays**.



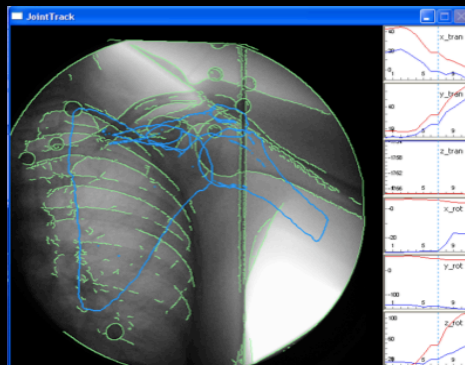
Use Shift or Control keys on the key board in conjunction with the up, down, left and right arrow keys to perform rotations and translations. To Translate model up and down and left and right use the arrow keys only.

Use the + and - keys to make the movement increments and decrements bigger or smaller, as necessary.

39

3D to 2D registration

Use the **Copy previous** option to copy the kinematics from the previous frame. This way, small adjustments are necessary to register the model to the new x-ray image rather than starting the registration from the beginning.



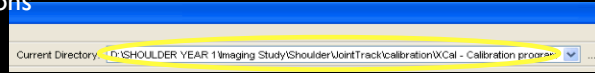
Save the absolute kinematics poses for the segments with **Save All Kinematics**.



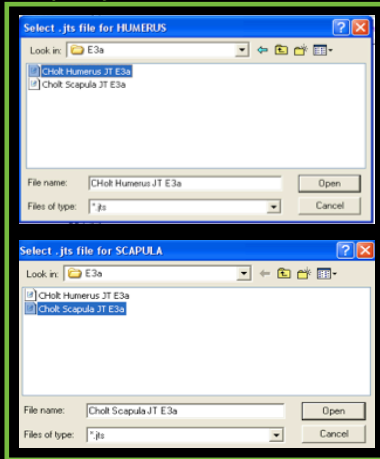
40

GH joint kinematics

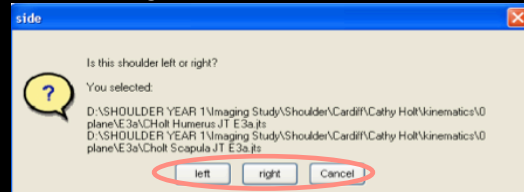
Open Matlab and Browse for the **directory** where the program (Matsuki files) is saved and run:
kin_humerus_212_GUI for ISB recommendations
kin_humerus_213_GUI for UF axes system



Search for the **Humerus** and **Scapula JT absolute kinematics**



Which shoulder was tested?
The right or the left shoulder?



The GH joint kinematics are saved in the same path as the kinematics files from JT.

JT kinematics are resampled over 100 points to compare to the kinematics measured with the mocap system

Image Registration manual for Shoulder complex studies

Data Handling

Lindsay Stroud

Appendix C

Motion analysis information pack and consent form

PATIENT INFORMATION SHEET

SHOULDER MOTION STUDY

You are being invited to take part in a research study with Cardiff University. Before you decide it is important for you to understand why the research is being done and what it will involve. Please take time to read the following information carefully and discuss it with others if you wish. Ask us if there is anything that is not clear or if you would like more information. Take time to decide whether or not you wish to take part.

What is the purpose of the study?

The shoulder has a larger range of motion than any other joint in the human body. It is able to perform a wide range of tasks e.g. reaching for objects above head level, brushing the hair, tying shoelaces etc. However, this wide range of motion leaves it susceptible to a wide range of injuries. Surgeons use a range of observations and physical examinations to decide on the type and extent of a patient's upper limb pathology. Their decision to proceed with a diagnosis and plan of surgery or therapeutic treatment is based on experience of patients with similar symptoms and their expertise and training. In some instances, this decision making process can be far from straightforward. In these cases it is believed surgeons could benefit from a detailed knowledge of the movement of the upper limb to further their understanding of the causes of upper limb disorders for clinical evaluation and rehabilitation purposes.

Why have I been chosen?

You have sustained an injury to your shoulder. The shoulder is made up of a number of joints and muscles that act together to provide a wide range of motion. We would like to assess the movement in your injured shoulder and compare it to the non-injured side and compare to other non-injured patients.

Do I have to take part?

It is up to you to decide whether or not to take part. If you do decide to take part you will be given this information sheet to keep and be asked to sign a consent form. If you decide to take part you are still free to withdraw at any time and without giving a reason. A decision to withdraw at any time, or a decision not to take part, will not affect the standard of care you receive.

What will happen to me if I take part?

If you agree to take part you will be invited to attend the Human Motion Analysis Laboratory, Cardiff School of Engineering, Cardiff University. You will ideally be assessed on four occasions at approximately 6 weeks, 3 months, 6 months and 1 year post injury.

Expenses and payment

A parking space will be provided on the grounds of Cardiff School of Engineering and local travel expenses reimbursed if requested.

What do I have to do?

You will be asked to attend the motion analysis laboratory. Maps and Directions will be provided. At the laboratory PhD Students will interview you and ask you to fill in a questionnaire about your shoulder symptoms. Your shoulder will then be assessed in the laboratory. As part of the assessment your upper garments will need to be removed with the exception of bras. Females are advised to wear a sports bra or other suitable undergarment.

During the assessment, laboratory staff will be placing very light polystyrene or cork round markers onto the skin in various places on the shoulder, arm, chest and back. The markers are placed with double sided tape and self-adhesive tape and a series of recordings will be made using cameras that record the positions of the markers placed on the patient.

The markers will then be removed and an electromagnetic tracking system will be used. As before, the electromagnetic receivers will be attached with double sided tape and self-adhesive tape. Participants will also be asked to use a supporting brace which minimises rotation of the forearm by holding the elbow flexed at 90°. The method is completely non-invasive. The duration of each assessment will be a maximum of 3 hours. Regular rest and toilet breaks will be provided as often as the patient needs them to assure maximal comfort.

Throughout the sessions your motions will be recorded using standard audiovisual equipment. The recordings will be used for data verification post processing.

All data files, including audiovisual files will be stored in encrypted folders on Cardiff University password protected computers. Cardiff University and NHS members of staff who are directly involved with the study will have access to the files. Any data relating to you that is presented publicly will be anonymised and visual information blocked facially.

Are there any risks in participating in this study?

The markers are placed onto the skin using double sided and self-adhesive tape. It is possible that there may be a slight discomfort upon the removal of the tape.

What are the possible benefits of taking part?

We hope to be able to better understand how shoulder injuries affect the motion of the shoulder. We also hope to determine whether this technology can detect subtle changes in shoulder motion that can help doctors in the diagnosis and treatment of patients with shoulder injuries. We hope that your participation will benefit future patients.

What if new information becomes available?

Sometimes during the course of a research project, new information becomes available about the treatment that is being studied. If this happens, your research doctor will tell you about it and discuss with you whether you want to continue in the study. If you decide to withdraw your research doctor will make arrangements for your care to continue. If you decide to continue in the study you will be asked to sign an updated consent form.

Also, on receiving new information your research doctor might consider it to be in your best interests to withdraw you from the study. He/she will explain the reasons and arrange for your care to continue.

What if something goes wrong?

If you are harmed by taking part in this research project, there are no special compensation arrangements. If you are harmed due to someone's negligence, then you may have grounds for a legal action but you may have to pay for it. Regardless of this, if you wish to complain, or have any concerns about any aspect of the way you have been approached or treated during the course of this study, the normal National Health Service complaints mechanisms should be available to you.

Will my taking part in this study be kept confidential?

All information which is collected about you during the course of the research will be kept strictly confidential. Any information about you which leaves the hospital/University will have your name and address removed so that you cannot be recognized from it.

What will happen to the results of the research study?

The results of the study will be presented at meetings of orthopaedic surgeons, clinical scientists, and engineers, and if accepted, published in medical and engineering journals. If interested, a copy of the published article can be made available to you. You will not be identified in any report/publication.

Who is organizing and funding the research?

The research is being organized by Dr. Catherine Holt (Senior Lecturer in Biomechanics), Mr Richard Evans (Consultant Orthopaedic Surgeon), Mr. Barry Lovern

(PhD. Student), Ms. Lindsay Stroud (PhD. Student), and Mr. Nicholas Ferran (Trauma Research Fellow)

None of the doctors or engineering staff are being paid for this study.

Who has reviewed the study?

The project has been reviewed the Cardiff University Research Governance Team. The project has the approval of the Cardiff and Vale NHS Trust and ethical approval has been granted by the National Research Ethics Service.

Where can I get independent advice about taking part in the trial?

If you wish to get independent advice regarding your rights as a participant in the trial, you can contact Mr. Stuart Roy at 01443 443574. Mr. Roy is an orthopaedic knee consultant in the Royal Glamorgan Infirmary and has been a collaborator with Cardiff University on similar, but unassociated trials involving patients with total knee replacements.

What if I wish to lodge a complaint?

If you wish to make a minor complaint regarding the way you were approached or treated during the trial, please contact Mr. Barry Lovern or Ms. Lindsay Stroud (02920874000 ext 77900). If you wish to make a more formal complaint, please contact Dr. Catherine Holt, the Chief Investigator of the trial (029 2087 4533). If contacting the above mentioned researchers compromises the nature of your complaint, you can contact the Cardiff University Research Governance Team on 029 208 79277.

Contact for Further Information

For further information you can contact:

Dr. Cathy Holt
Lecturer in Biomechanics
Cardiff School of Engineering
Cardiff University
Queen's Buildings
The Parade
Cardiff CF24 0YF
Wales, UK
Tel: 029 20874533
Fax: 029 20874939

Mr. Barry Lovern or Ms. Lindsay Stroud
Research Student
Cardiff School of Engineering
Cardiff University
Queen's Buildings
The Parade
Cardiff CF24 3AA
Wales, UK
Tel: 029 20874000 ext 77900
Fax: 029 20874939

For independent advice you can contact:

Mr. Stuart Roy
Dept of Orthopaedics
Royal Glamorgan Hospital
Ynysmaerdy
Llantrisant
Tel. 01443 443574

Thank you for taking part in this study.

You will be given a copy of this information sheet and a copy of the signed consent form.

Oxford Shoulder Instability Score

Subject: «First_Name» «Surname» («Visit_ID»)

Visit: «Visit_Type»

Date: «Date_of_Visit»

Time: «Time_of_Visit»

Affected Shoulder: «Shoulder»

The Oxford Shoulder Instability Score

During the past four weeks:

1. **During the last six months, how many times has your shoulder slipped out of joint (or dislocated)?**

L R

- Not at all
 1 or 2 times in 6 months
 1 or 2 times per month
 1 or 2 times per month
 More often than 1 or 2 times per week

2. **During the last three months, have you had any trouble (or worry) dressing because of your shoulder?**

L R

- No trouble at all
 Slight trouble or worry
 Moderate trouble or worry
 Extreme difficulty
 Impossible to do

3. **During the last three months, how would you describe the worst pain you have had from your shoulder?**

L R

- None
 Mild ache
 Moderate
 Severe
 Unbearable

4. **During the last three months, how much has the problem with your shoulder interfered with your usual work (including school, college or housework)?**

L R

- Not at all
 A little bit
 Moderately
 Greatly
 Totally

5. **During the last three months, have you avoided any activities due to worry about your shoulder– feared that it might slip out of joint?**

L R

- Not at all
 Very occasionally
 Some days
 Most days or more than one activity
 Every day or many activities

6. **During the last three months, has the problem with your shoulder prevented you from doing things that are important to you?**

L R

- No, not at all
 Very occasionally
 Some days
 Most days or more than one activity
 Every day or many activities

7. **During the last three months, how much has the problem with your shoulder interfered with your social life (including sexual activity – if applicable)?**

L R

- Not at all
 Occasionally
 Some days
 Most days
 Every day

8. During the last four weeks, how much has the problem with your shoulder interfered with your sporting activities or hobbies?

L R

- Not at all
 A little/occasionally
 Some of the time
 Most of the time
 All of the time

9. During the last four weeks, how often has your shoulder been 'on your mind' – how often have you thought about it?

L R

- Never, or only if someone asks
 Occasionally
 Some days
 Most days
 Every day

10. During the last four weeks, how much has the problem with your shoulder interfered with your ability or willingness to lift heavy objects?

L R

- Not at all
 Occasionally
 Some days
 Most days
 Every day

11. During the last four weeks, how would you describe the pain which you usually had from your shoulder?

L R

- None
 Very mild
 Mild
 Moderate
 Severe

12. During the last four weeks, have you avoided lying in certain positions, in bed at night, because of your shoulder?

L R

- | | | |
|--------------------------|--------------------------|--------------------|
| <input type="checkbox"/> | <input type="checkbox"/> | No nights |
| <input type="checkbox"/> | <input type="checkbox"/> | Only 1 or 2 nights |
| <input type="checkbox"/> | <input type="checkbox"/> | Some nights |
| <input type="checkbox"/> | <input type="checkbox"/> | Most nights |
| <input type="checkbox"/> | <input type="checkbox"/> | Every night |

Oxford Shoulder Score

Subject: «First_Name» «Surname» («Visit_ID»)

Visit: «Visit_Type»

Date: «Date_of_Visit»

Time: «Time_of_Visit»

Affected Shoulder: «Shoulder»

The Oxford Shoulder Score

During the past four weeks:

1. How would you describe the worst pain you had from your shoulder

- | L | R | |
|--------------------------|--------------------------|------------|
| <input type="checkbox"/> | <input type="checkbox"/> | None |
| <input type="checkbox"/> | <input type="checkbox"/> | Mild |
| <input type="checkbox"/> | <input type="checkbox"/> | Moderate |
| <input type="checkbox"/> | <input type="checkbox"/> | Severe |
| <input type="checkbox"/> | <input type="checkbox"/> | Unbearable |

2. Have you had any trouble dressing yourself because of your shoulder?

- | L | R | |
|--------------------------|--------------------------|---------------------|
| <input type="checkbox"/> | <input type="checkbox"/> | No trouble at all |
| <input type="checkbox"/> | <input type="checkbox"/> | Very little trouble |
| <input type="checkbox"/> | <input type="checkbox"/> | Moderate trouble |
| <input type="checkbox"/> | <input type="checkbox"/> | Extreme difficulty |
| <input type="checkbox"/> | <input type="checkbox"/> | Impossible to do |

3. Have you had any trouble getting in and out of a car or using public transport because of your shoulder?

- | L | R | |
|--------------------------|--------------------------|---------------------|
| <input type="checkbox"/> | <input type="checkbox"/> | No trouble at all |
| <input type="checkbox"/> | <input type="checkbox"/> | Very little trouble |
| <input type="checkbox"/> | <input type="checkbox"/> | Moderate trouble |
| <input type="checkbox"/> | <input type="checkbox"/> | Extreme difficulty |
| <input type="checkbox"/> | <input type="checkbox"/> | Impossible to do |

4. Have you been able to use a knife and fork – at the same time?

- | L | R | |
|--------------------------|--------------------------|--------------------------|
| <input type="checkbox"/> | <input type="checkbox"/> | Yes, easily |
| <input type="checkbox"/> | <input type="checkbox"/> | With little difficulty |
| <input type="checkbox"/> | <input type="checkbox"/> | With moderate difficulty |
| <input type="checkbox"/> | <input type="checkbox"/> | With extreme difficulty |
| <input type="checkbox"/> | <input type="checkbox"/> | No, impossible |

5. Could you carry household shopping on your own?**L R**

- Yes, easily
 With little difficulty
 With moderate difficulty
 With extreme difficulty
 No, impossible

6. Could you carry a tray containing a plate of food across a room?**L R**

- Yes, easily
 With little difficulty
 With moderate difficulty
 With extreme difficulty
 No, impossible

7. Could you brush/comb your hair with the affected arm?**L R**

- Yes, easily
 With a little difficulty
 With moderate difficulty
 With extreme difficulty
 No, impossible

8. How would you describe the pain you usually had from your shoulder?**L R**

- None
 Very mild
 Mild
 Moderate
 Severe

9. Could you hang your clothes up in a wardrobe, using the affected arm? (whichever you tend to use)

L R

- Yes, easily
 With little difficulty
 With moderate difficulty
 With extreme difficulty
 No, impossible

10. Have you been able to wash and dry yourself under both arms?

L R

- Yes, easily
 With little difficulty
 With moderate difficulty
 With extreme difficulty
 No, impossible

11. How much has pain from your shoulder interfered with your usual work (including housework)?

L R

- Not at all
 A little bit
 Moderate
 Greatly
 Totally

12. Have you been troubled by pain from your shoulder in bed at night?

L R

- No nights
 Only 1 or 2 nights
 Some nights
 Most nights
 Every night

Centre Number:
Study Number:
Patient Identification Number for this trial:

CONSENT FORM

Title of Project: Shoulder Motion Study
Name of Researchers: Dr Cathy Holt and Mr Richard Evans

Please
initial
box

1. I confirm that I have read and understand the information sheet dated..... (version.....) for the above study. I have had the opportunity to consider the information, ask questions and have had these answered satisfactorily.
2. I understand that my participation is voluntary and that I am free to withdraw at any time without giving any reason, without my medical care or legal rights being affected.
3. I understand that relevant sections of my medical notes and data collected during the study may be looked at by individuals from regulatory authorities or from the NHS Trust, where it is relevant to my taking part in this research. I give permission for these individuals to have access to my records.
4. I agree to take part in the above study.

Name of Patient Date Signature

Name of Person Date Signature
taking consent

When completed, 1 for patient; 1 for researcher site file; 1 (original) to be kept in medical notes

Appendix D

Complete healthy and patient shoulder complex kinematics description during physiological ROM

Complete kinematics description of healthy (HL), injured or pathological (IoP) and contralateral (CL) patient shoulder function are shown in Figure D.1 through to Figure D.3 for clavicle fracture patients during abduction, scaption and flexion respectively; Figure D.4 through to Figure D.6 for MDI patients during abduction, scaption and flexion respectively; Figure D.7 through to Figure D.9 for IRCT patients during abduction, scaption and flexion respectively; and Figure D.10 through to Figure D.12 for GH dislocation patients during abduction, scaption and flexion respectively.

Significant differences in shoulder function were investigated using One-Way ANOVA ($p > .05$) in SPSS. Post Hoc was performed using Bonferroni test. The results from this analysis is summarised in Table D.1 through to Table D.4 for clavicle fracture, MDI, IRCT and GH dislocation patients respectively.

D.1 Clavicle fracture patients

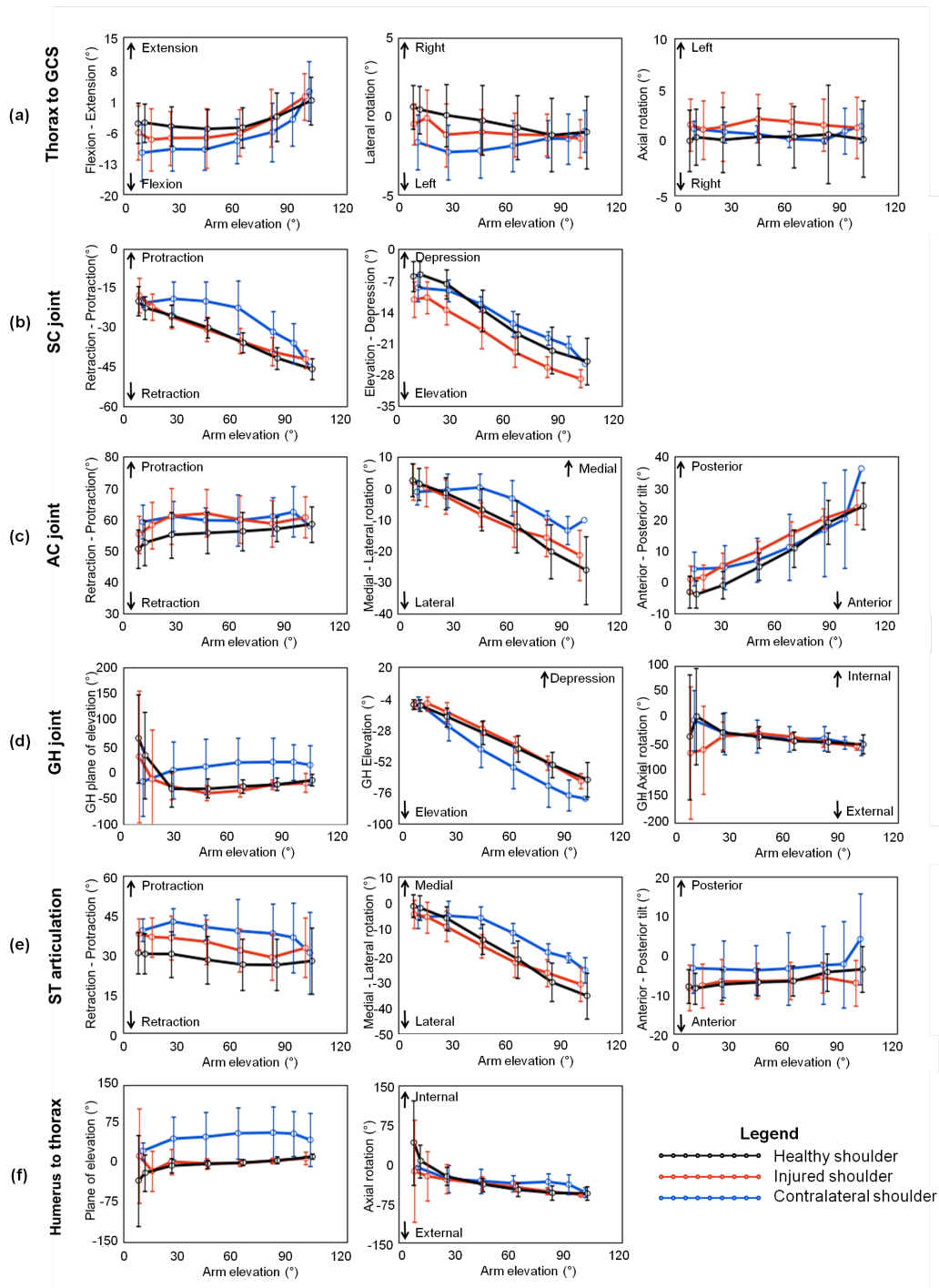


FIGURE D.1: Complete healthy and clavicle fracture patient shoulder complex kinematics during **abduction** (a) thorax in GCS, (b) sternoclavicular joint, (c) acromioclavicular joint, (d) glenohumeral joint (e) scapulathoracic articulation and (f) humerothoracic rotations. Error bars represent SD

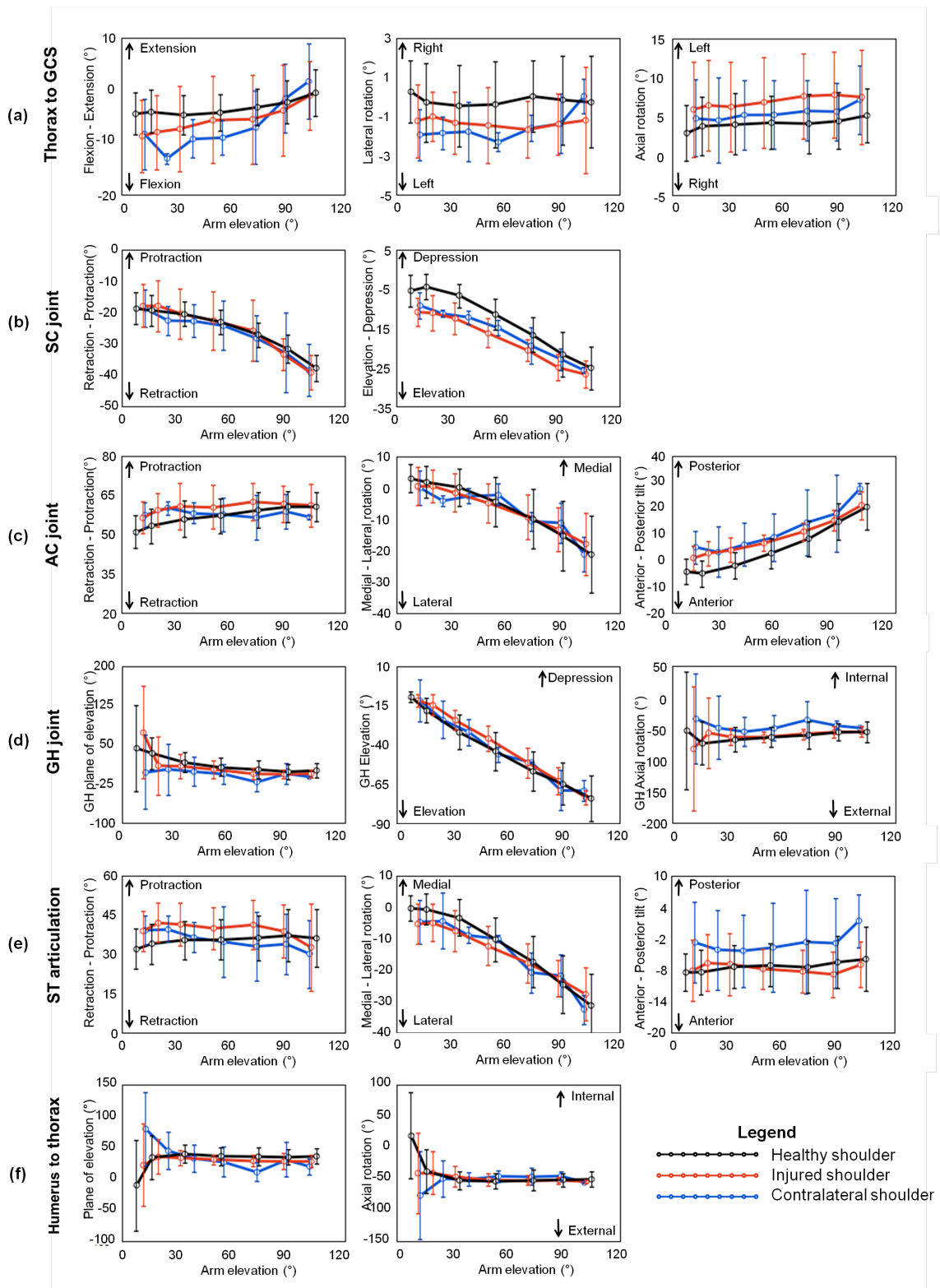


FIGURE D.2: Complete healthy and clavicle fracture patient shoulder complex kinematics during **scaption** (a) thorax in GCS, (b) sternoclavicular joint, (c) acromioclavicular joint, (d) glenohumeral joint (e) scapulathoracic articulation and (f) humerothoracic rotations. Error bars represent SD

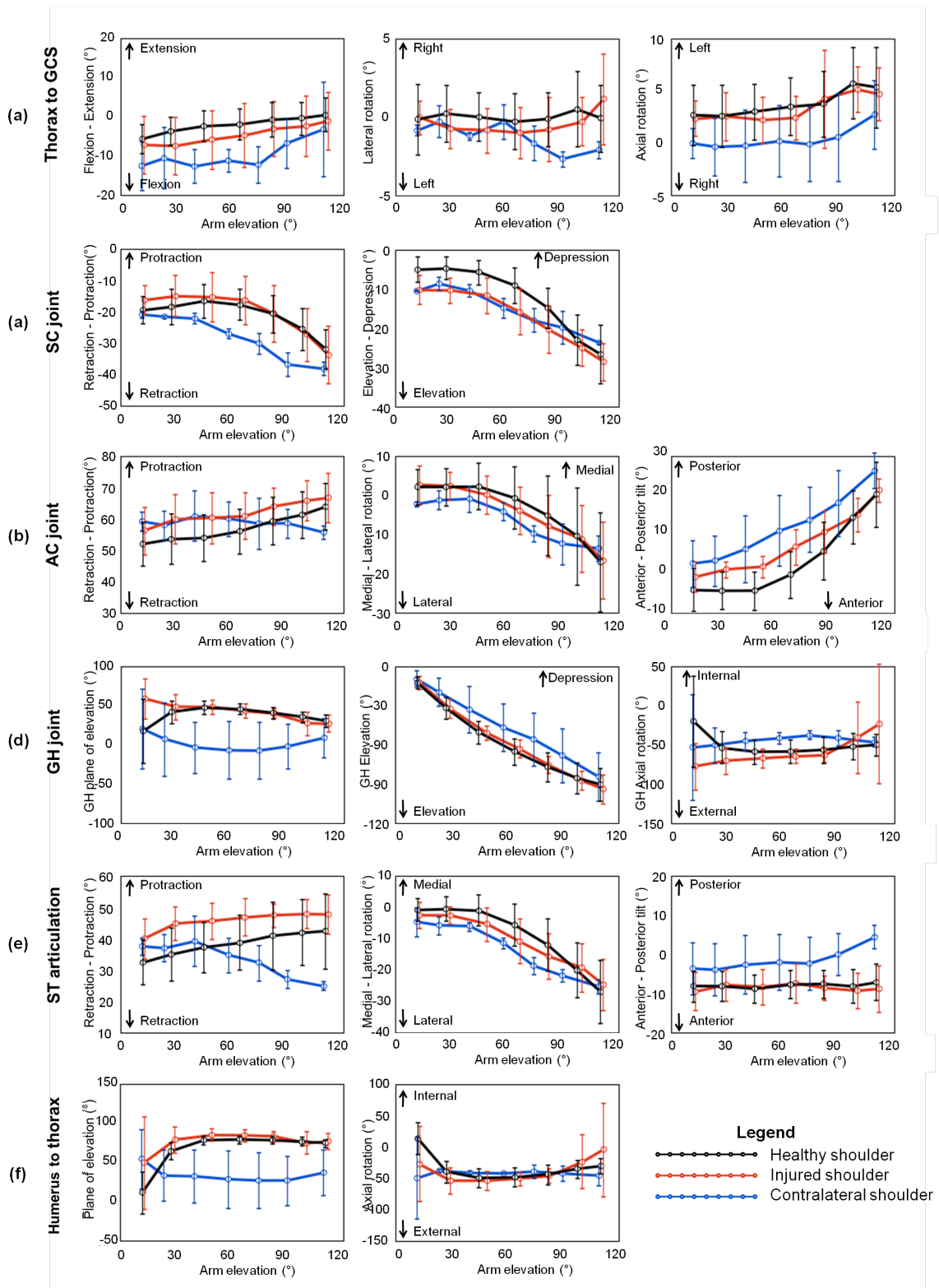


FIGURE D.3: Complete healthy and clavicle fracture patient shoulder complex kinematics during **flexion** (a) thorax in GCS, (b) sternoclavicular joint, (c) acromioclavicular joint, (d) glenohumeral joint (e) scapulathoracic articulation and (f) humerothoracic rotations. Error bars represent SD

TABLE D.1: Differences between healthy and clavicle fracture patient shoulder complex kinematics during physiological ROM. Significant differences are denoted with *

Joint Rotation	Abduction			Scaption			Flexion			
	HL&IoP	HL&CL	IoP&CL	HL&IoP	HL&CL	IoP&CL	HL&IoP	HL&CL	IoP&CL	
Thorax	Flexion-Extension	1.000	.502	1.000	.656	.266	1.000	.339	*.000	*.006
	Lateral rotation	.143	*.001	.063	*.001	*.000	1.000	.966	*.007	.066
	Axial rotation	*.000	.098	*.003	*.000	*.010	*.007	1.000	*.000	*.001
SC Joint	Retraction-Protraction	1.000	1.000	1.000	1.000	1.000	1.000	1.000	.241	.155
	Elevation-Depression	.775	1.000	1.000	.748	1.000	1.000	.759	1.000	1.000
AC Joint	Retraction-Protraction	*.005	*.001	1.000	.429	1.000	1.000	.052	1.000	.278
	Medial-Lateral rotation	1.000	1.000	1.000	1.000	1.000	1.000	1.000	1.000	1.000
	Anterior-Posterior tilt	1.000	.702	1.000	1.000	.447	1.000	1.000	.372	1.000
GH Joint	Plane of elevation	1.000	*.000	*.000	.672	*.027	.280	1.000	*.000	*.000
	Elevation	1.000	.508	.409	1.000	1.000	1.000	1.000	1.000	1.000
	Axial rotation	1.000	1.000	1.000	1.000	*.014	.052	1.000	.478	.948
ST artic.	Retraction-Protraction	*.008	*.000	.084	*.049	1.000	.052	*.011	.101	*.000
	Medial-Lateral rotation	1.000	1.000	1.000	1.000	1.000	1.000	1.000	1.000	1.000
	Anterior-Posterior tilt	1.000	*.002	*.001	1.000	*.000	*.000	1.000	*.000	*.000
HT	Plane of elevation	1.000	*.000	*.000	.178	*.014	.560	.557	*.000	*.000
	Elevation	1.000	1.000	1.000	1.000	1.000	1.000	1.000	1.000	1.000
	Axial rotation	1.000	1.000	1.000	.867	.372	1.000	1.000	1.000	.700

D.2 Multiple directional instability patients

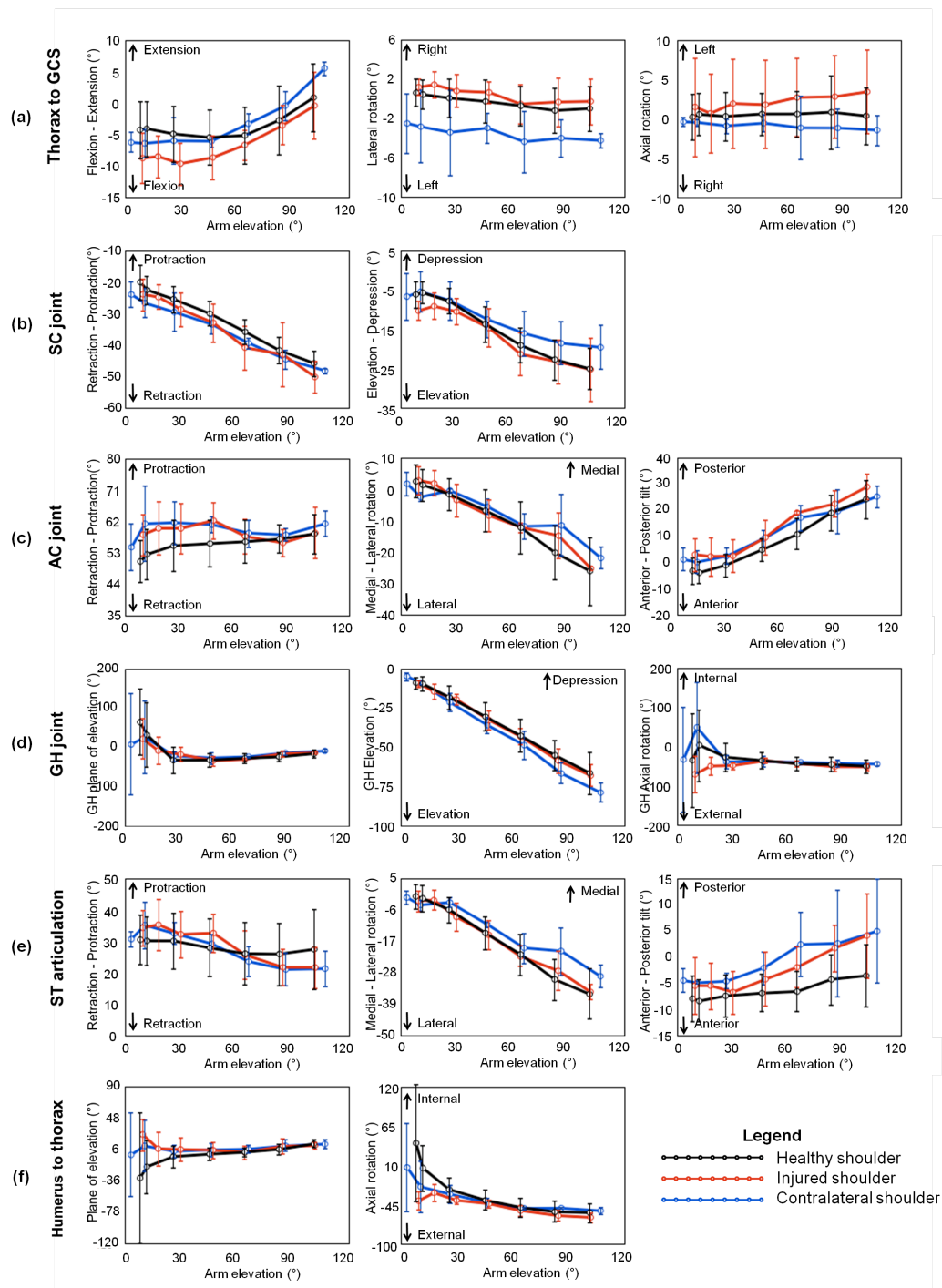


FIGURE D.4: Complete healthy and MDI patient shoulder complex kinematics during **abduction** (a) thorax in GCS, (b) sternoclavicular joint, (c) acromioclavicular joint, (d) glenohumeral joint (e) scapulathoracic articulation and (f) humerothoracic rotations. Error bars represent SD

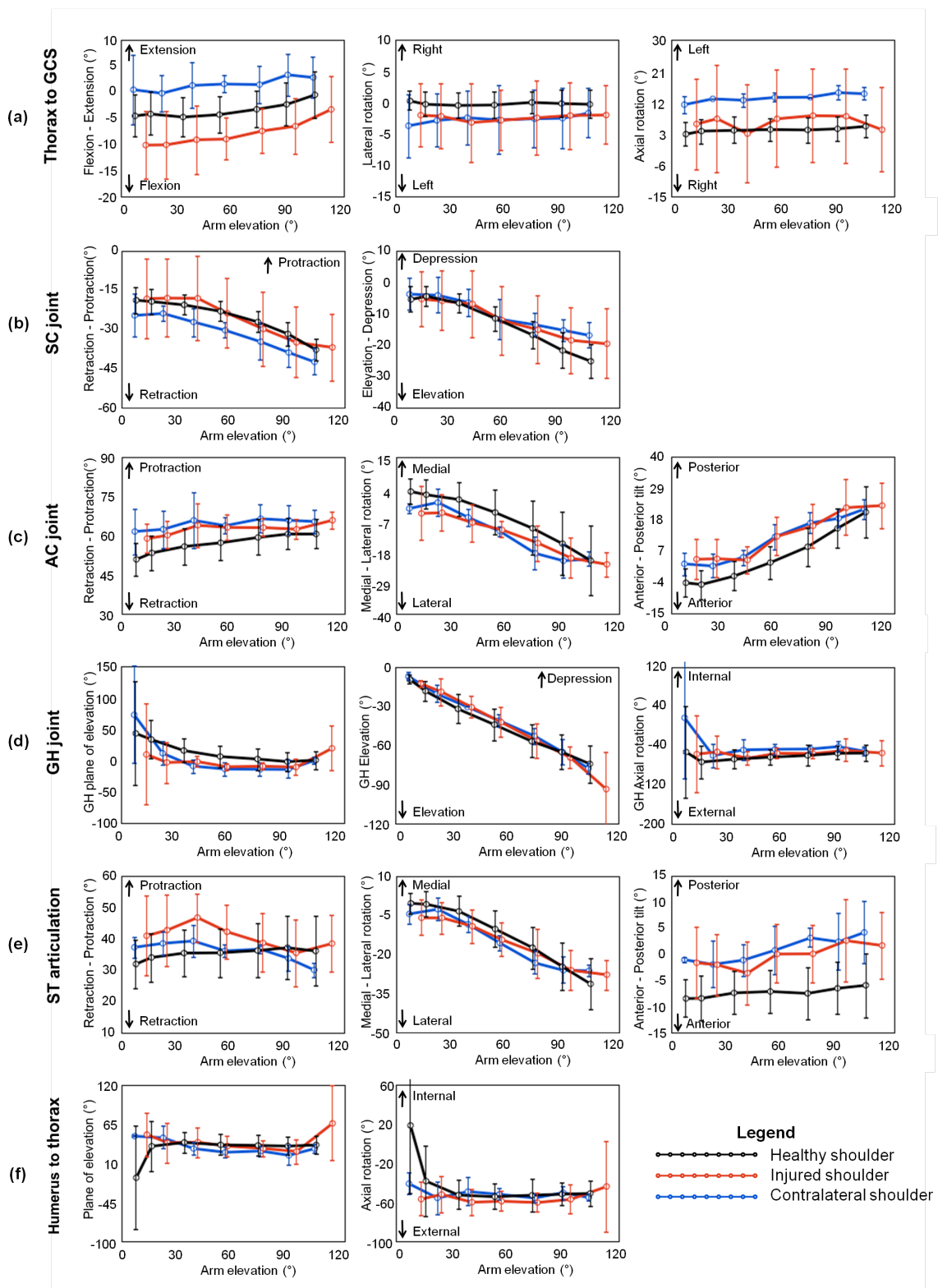


FIGURE D.5: Complete healthy and MDI patient shoulder complex kinematics during **scaption** (a) thorax in GCS, (b) sternoclavicular joint, (c) acromioclavicular joint, (d) glenohumeral joint (e) scapulathoracic articulation and (f) humerothoracic rotations. Error bars represent SD

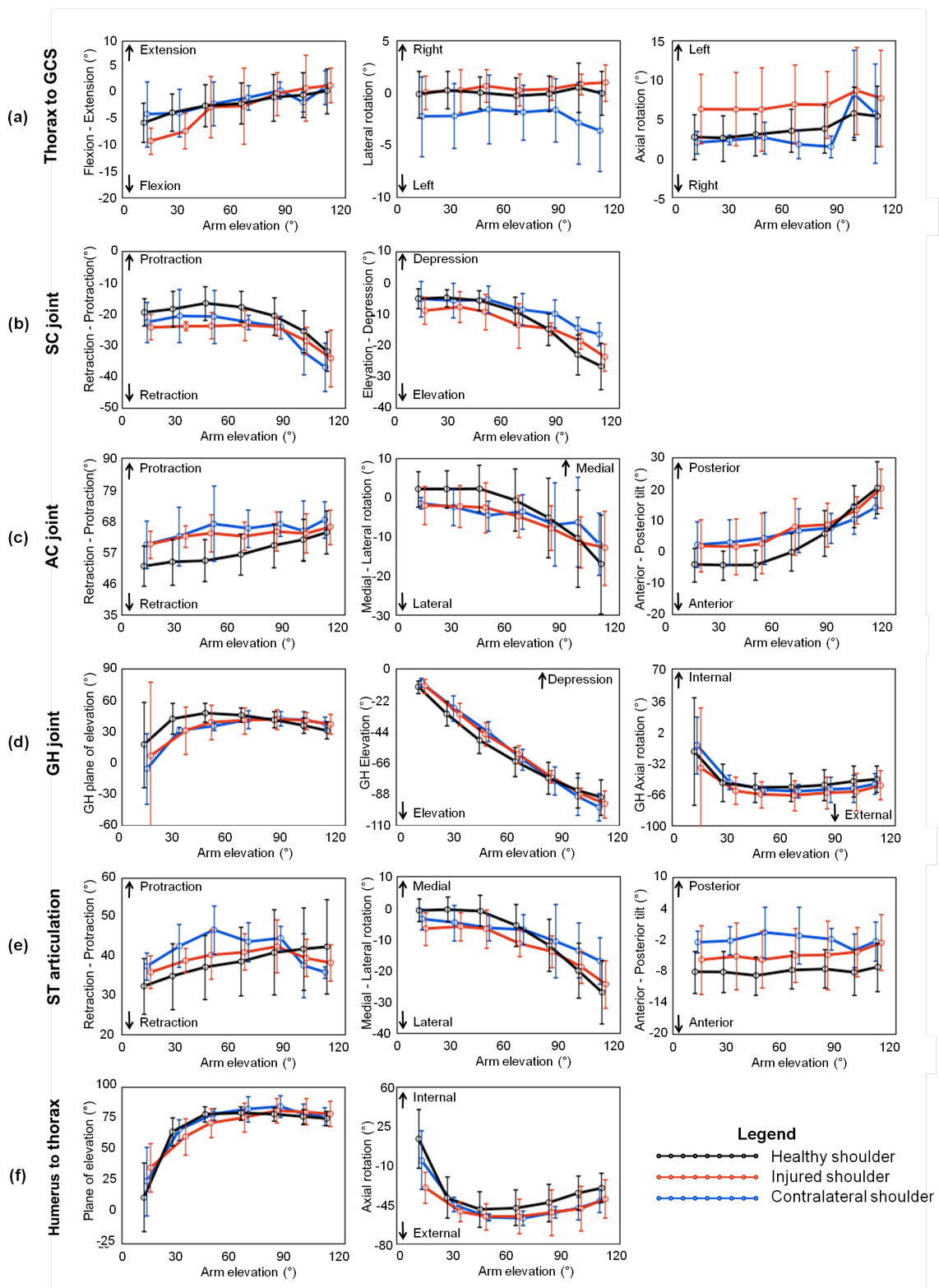


FIGURE D.6: Complete healthy and MDI patient shoulder complex kinematics during **flexion** (a) thorax in GCS, (b) sternoclavicular joint, (c) acromioclavicular joint, (d) glenohumeral joint (e) scapulathoracic articulation and (f) humerothoracic rotations. Error bars represent SD

TABLE D.2: Differences between healthy and MDI patient shoulder complex kinematics during physiological ROM. Significant differences are denoted with *

Joint Rotation	Abduction			Scaption			Flexion		
	HL&IoP	HL&CL	IoP&CL	HL&IoP	HL&CL	IoP&CL	HL&IoP	HL&CL	IoP&CL
Thorax	Flexion-Extension	.400	1.000	.272	*.001	*.000	1.000	1.000	1.000
	Lateral rotation	.265	*.000	*.000	*.000	.905	.294	*.000	*.000
	Axial rotation	.085	*.022	*.000	*.026	*.000	*.009	1.000	*.004
SC Joint	Retraction-Protraction	1.000	1.000	1.000	1.000	.419	.374	.470	1.000
	Elevation-Depression	1.000	1.000	.894	1.000	1.000	1.000	1.000	.717
AC Joint	Retraction-Protraction	*.024	*.009	1.000	*.004	*.000	*.009	*.001	1.000
	Medial-Lateral rotation	1.000	1.000	1.000	.673	.819	1.000	1.000	1.000
	Anterior-Posterior tilt	1.000	1.000	1.000	.471	.677	1.000	1.000	1.000
GH Joint	Plane of elevation	.603	1.000	1.000	.722	.071	1.000	1.000	1.000
	Elevation	1.000	1.000	1.000	1.000	1.000	1.000	1.000	1.000
	Axial rotation	.318	1.000	.382	.702	*.004	*.037	*.010	.430
ST artic.	Retraction-Protraction	1.000	1.000	1.000	*.007	1.000	1.000	.405	1.000
	Medial-Lateral rotation	1.000	1.000	1.000	1.000	1.000	1.000	1.000	1.000
	Anterior-Posterior tilt	.163	*.025	1.000	*.000	*.000	.652	*.000	*.000
HT	Plane of elevation	.902	.583	1.000	1.000	.465	1.000	.635	.584
	Elevation	1.000	1.000	1.000	1.000	1.000	1.000	1.000	1.000
	Axial rotation	.982	1.000	1.000	.688	1.000	.645	.185	1.000

D.3 Irreparable rotator cuff tear patients

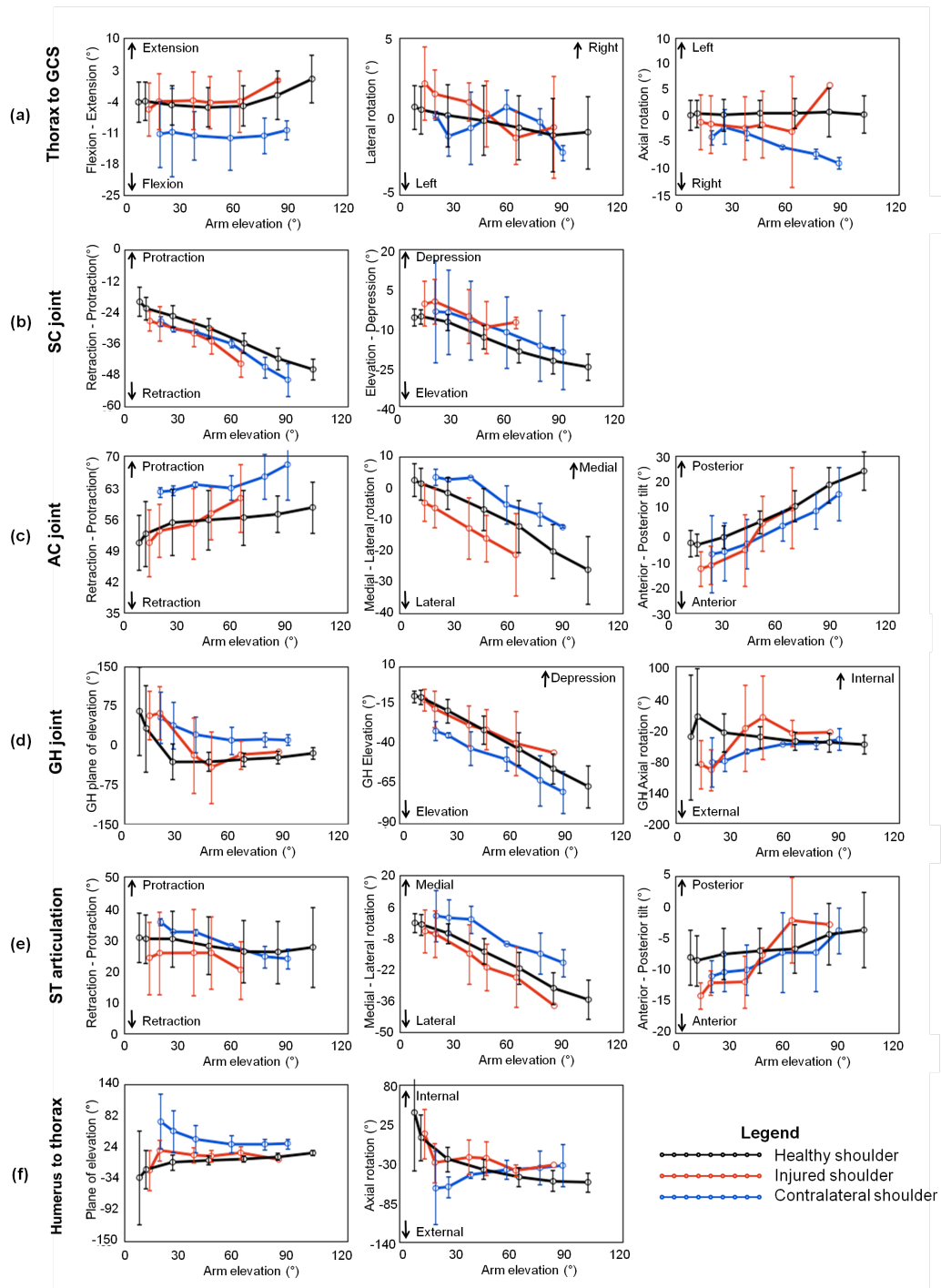


FIGURE D.7: Complete healthy and IRCT patient shoulder complex kinematics during **abduction** (a) thorax in GCS, (b) sternoclavicular joint, (c) acromioclavicular joint, (d) glenohumeral joint (e) scapulathoracic articulation and (f) humerothoracic rotations. Error bars represent SD

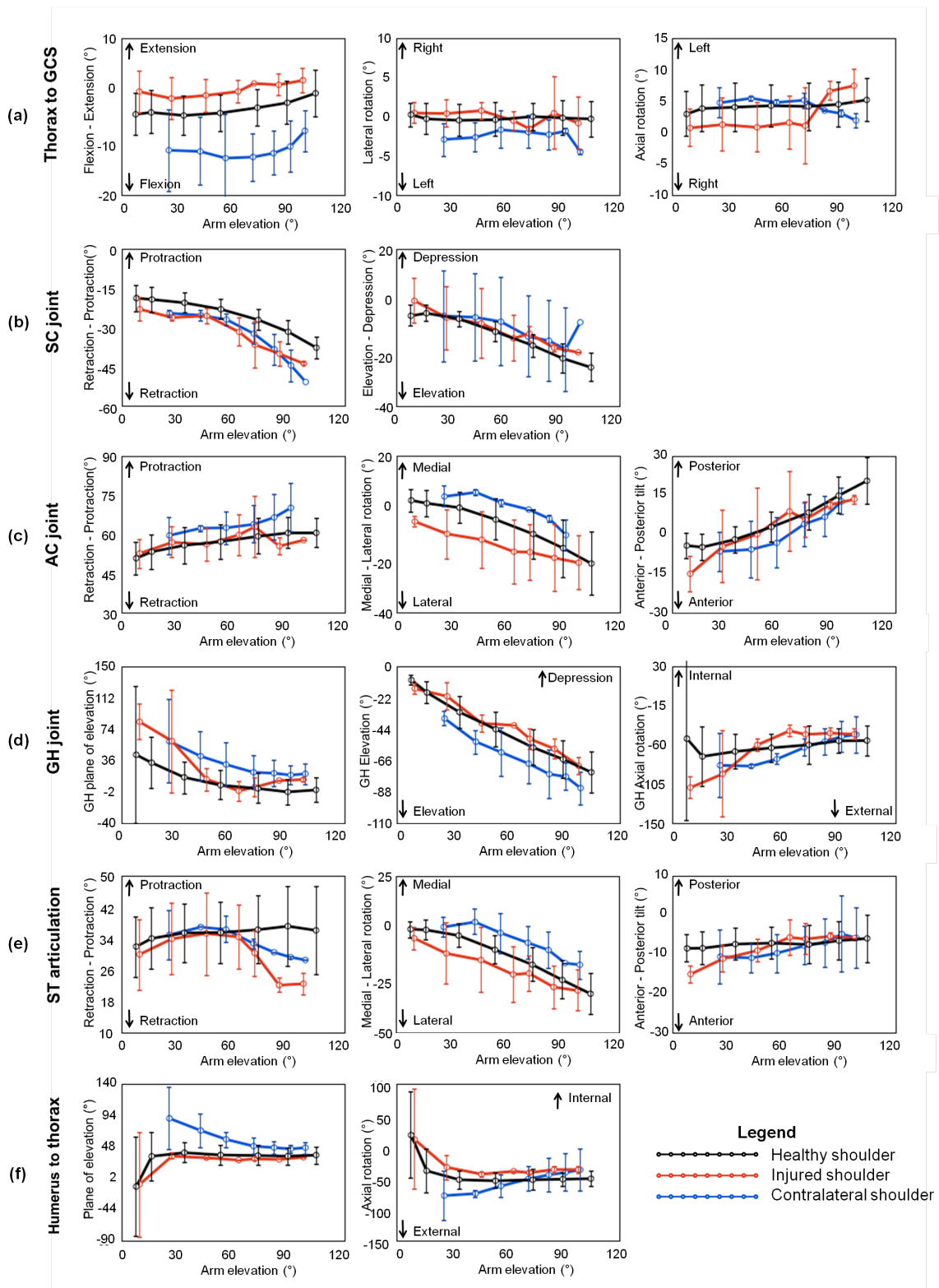


FIGURE D.8: Complete healthy and IRCT patient shoulder complex kinematics during **scaption** (a) thorax in GCS, (b) sternoclavicular joint, (c) acromioclavicular joint, (d) glenohumeral joint (e) scapulathoracic articulation and (f) humerothoracic rotations. Error bars represent SD

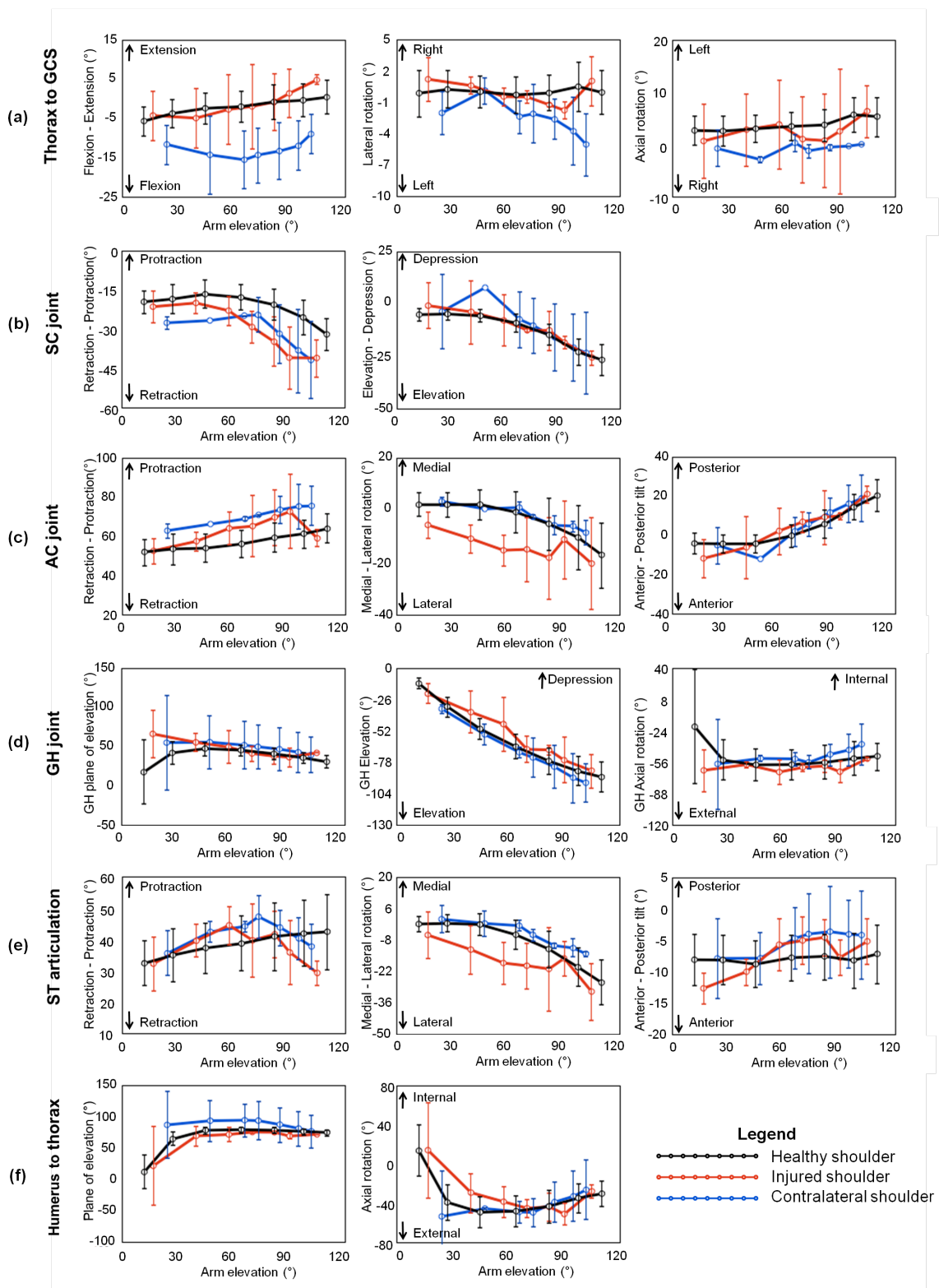


FIGURE D.9: Complete healthy and IRCT patient shoulder complex kinematics during **flexion** (a) thorax in GCS, (b) sternoclavicular joint, (c) acromioclavicular joint, (d) glenohumeral joint (e) scapulathoracic articulation and (f) humerothoracic rotations. Error bars represent SD

TABLE D.3: Differences between healthy and IRCT patient shoulder complex kinematics during physiological ROM. Significant differences are denoted with *

Joint Rotation	Abduction			Scaption			Flexion		
	HL&IoP	HL&CL	IoP&CL	HL&IoP	HL&CL	IoP&CL	HL&IoP	HL&CL	IoP&CL
Thorax	Flexion-Extension	1.000	*.000	*.000	*.000	*.000	1.000	*.000	*.000
	Lateral rotation	.643	1.000	.138	*.000	*.000	1.000	*.002	*.003
	Axial rotation	1.000	*.001	*.004	.597	1.000	.644	.456	*.002
SC Joint	Retraction-Protraction	1.000	1.000	1.000	.433	.173	1.000	.124	1.000
	Elevation-Depression	.148	.439	1.000	1.000	1.000	1.000	1.000	1.000
AC Joint	Retraction-Protraction	1.000	.323	.455	1.000	*.005	*.010	.198	*.001
	Medial-Lateral rotation	1.000	.669	.284	.176	.428	*.009	*.015	1.000
	Anterior-Posterior tilt	.267	.883	1.000	1.000	1.000	1.000	1.000	1.000
GH Joint	Plane of elevation	.672	*.001	*.007	1.000	*.046	*.013	1.000	.350
	Elevation	1.000	.253	.281	1.000	.171	.105	1.000	.880
	Axial rotation	.309	1.000	.058	*.029	1.000	*.043	.389	*.010
ST artic.	Retraction-Protraction	.190	1.000	.162	.052	.742	.513	1.000	.567
	Medial-Lateral rotation	.190	1.000	.162	.722	.945	.112	.260	1.000
	Anterior-Posterior tilt	1.000	1.000	1.000	1.000	1.000	1.000	1.000	.069
HT	Plane of elevation	.264	*.000	*.001	1.000	*.023	*.011	.432	*.032
	Elevation	1.000	1.000	1.000	1.000	1.000	1.000	1.000	1.000
	Axial rotation	.259	.905	1.000	.215	1.000	.934	1.000	1.000

D.4 GH dislocation patients

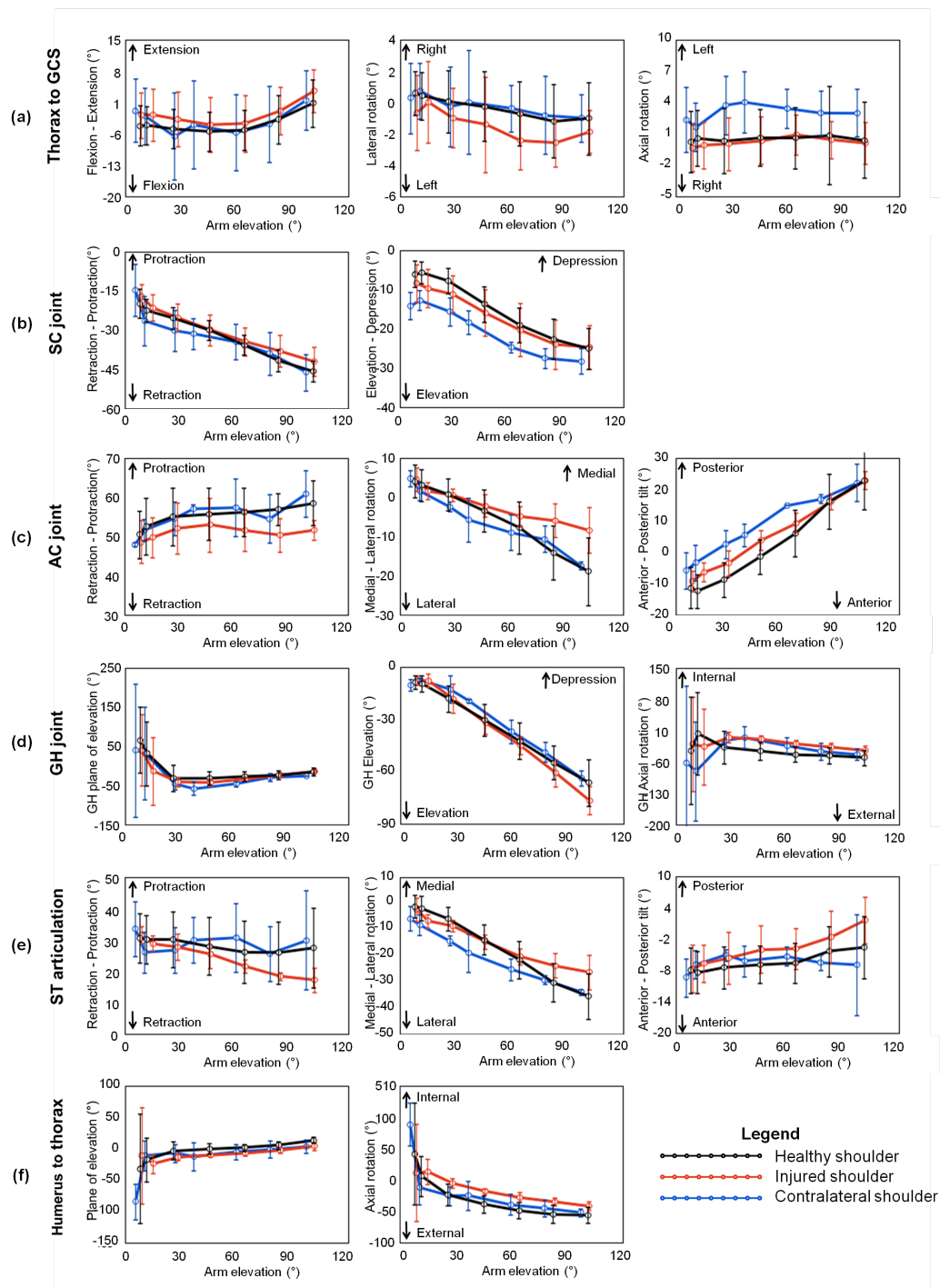


FIGURE D.10: Complete healthy and GH dislocation patient shoulder complex kinematics during **abduction** (a) thorax in GCS, (b) sternoclavicular joint, (c) acromioclavicular joint, (d) glenohumeral joint (e) scapulathoracic articulation and (f) humerothoracic rotations. Error bars represent SD

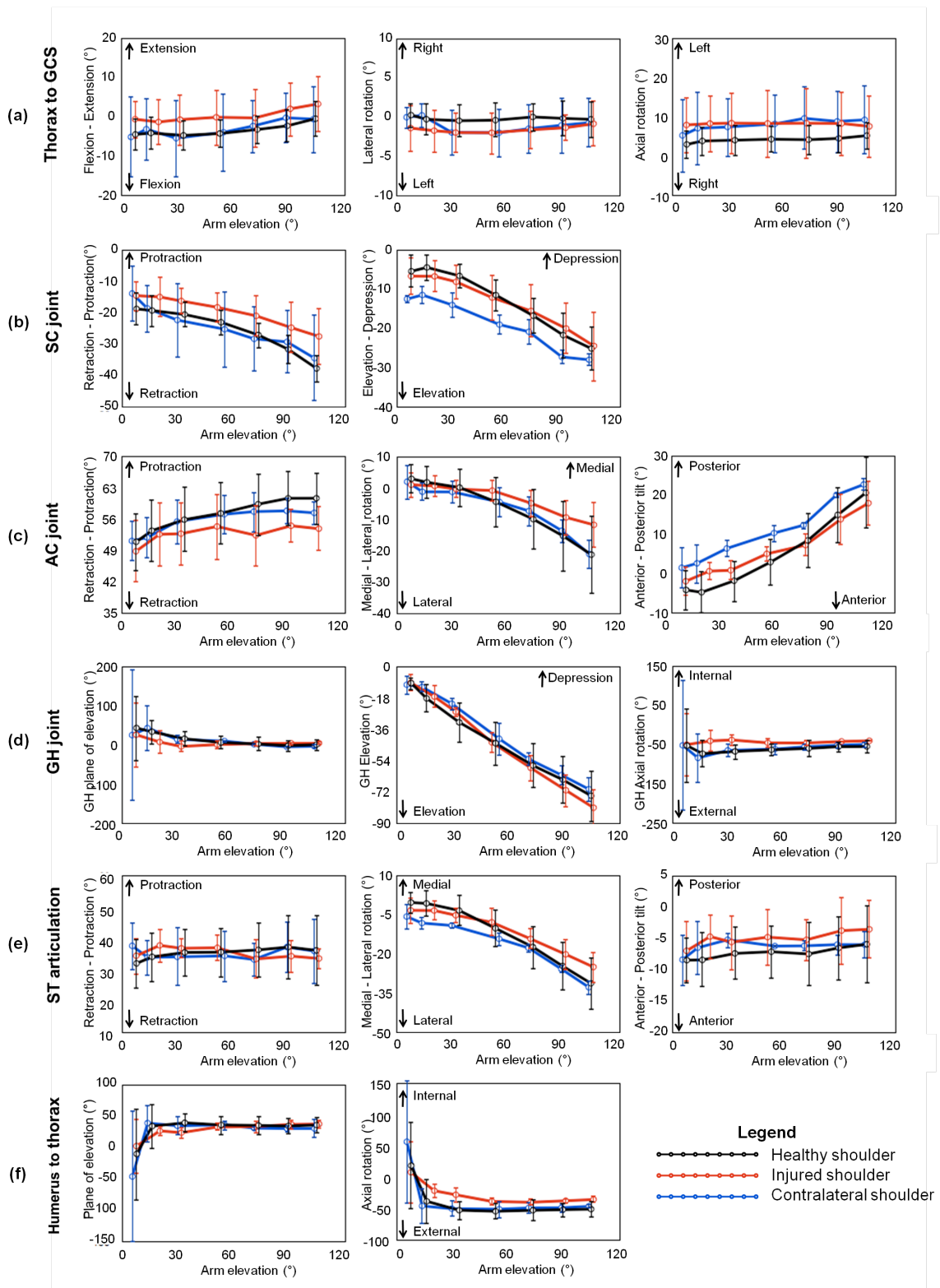


FIGURE D.11: Complete healthy and GH dislocation patient shoulder complex kinematics during **scaption** (a) thorax in GCS, (b) sternoclavicular joint, (c) acromioclavicular joint, (d) glenohumeral joint (e) scapulathoracic articulation and (f) humerothoracic rotations. Error bars represent SD

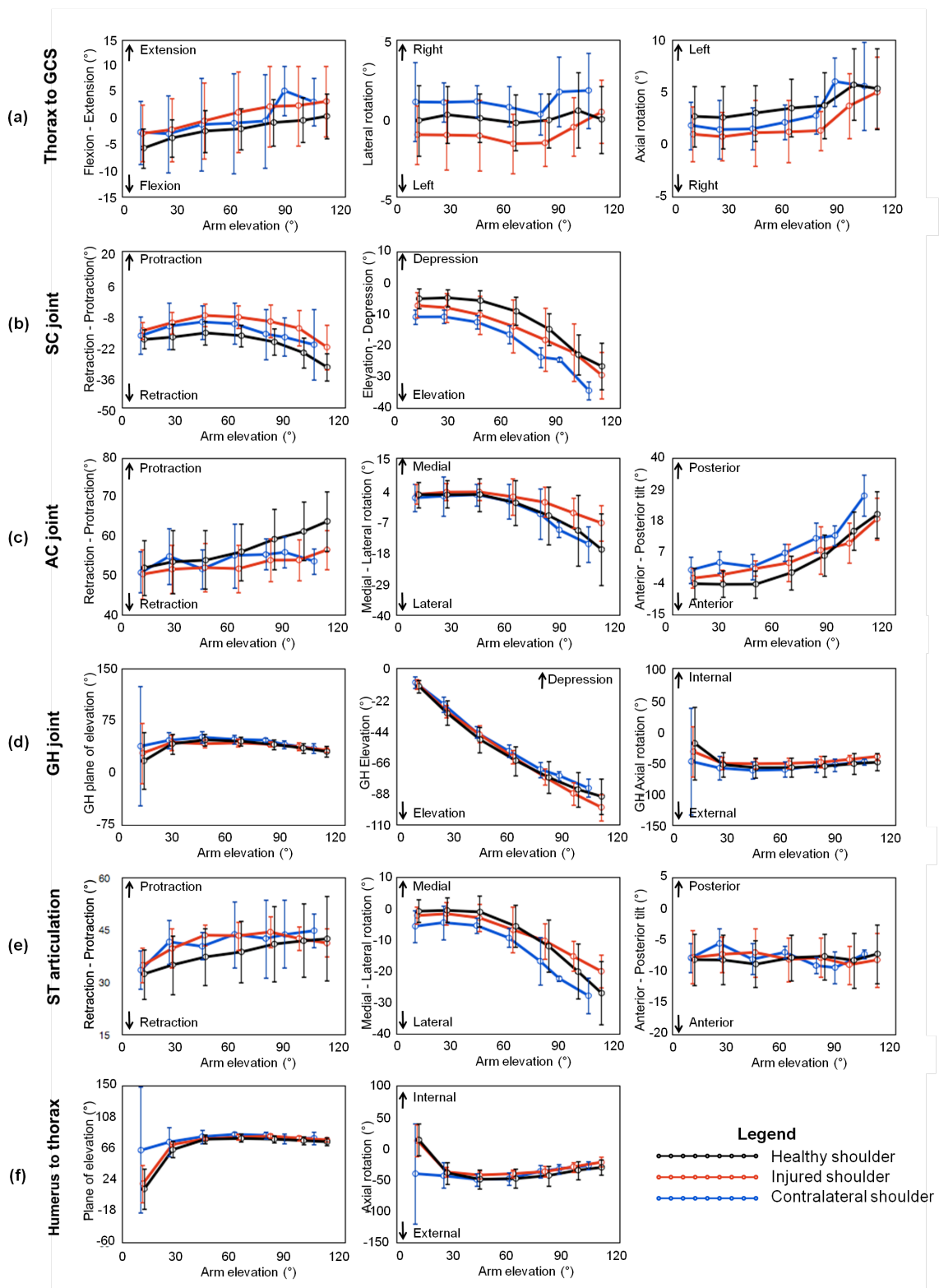


FIGURE D.12: Complete healthy and GH dislocation patient shoulder complex kinematics during **flexion** (a) thorax in GCS, (b) sternoclavicular joint, (c) acromioclavicular joint, (d) glenohumeral joint (e) scapulathoracic articulation and (f) humerothoracic rotations. Error bars represent SD

TABLE D.4: Differences between healthy and GH dislocation patient shoulder complex kinematics during physiological ROM. Significant differences are denoted with *

Joint Rotation	Abduction			Scaption			Flexion			
	HL&IoP	HL&CL	IoP&CL	HL&IoP	HL&CL	IoP&CL	HL&IoP	HL&CL	IoP&CL	
Thorax	Flexion-Extension	.426	1.000	.865	*.003	1.000	*.008	.216	.408	1.000
	Lateral rotation	*.042	1.000	*.025	*.001	*.050	.257	*.010	*.004	*.000
	Axial rotation	.931	*.000	*.000	*.000	*.000	1.000	.174	1.000	.776
SC Joint	Retraction-Protraction	1.000	1.000	1.000	.322	1.000	.496	*.016	.142	.940
	Elevation-Depression	1.000	.419	.973	1.000	.448	.510	1.000	.570	1.000
AC Joint	Retraction-Protraction	.063	1.000	.085	*.050	1.000	.289	.054	.194	1.000
	Medial-Lateral rotation	1.000	1.000	1.000	1.000	1.000	1.000	.958	1.000	1.000
	Anterior-Posterior tilt	1.000	1.000	1.000	1.000	.688	.973	1.000	.854	1.000
GH Joint	Plane of elevation	1.000	.158	.518	1.000	1.000	1.000	1.000	.746	.558
	Elevation	1.000	1.000	1.000	1.000	1.000	1.000	1.000	1.000	1.000
	Axial rotation	.060	.194	1.000	*.000	.916	*.003	.125	1.000	.052
ST artic.	Retraction-Protraction	.192	1.000	.105	1.000	1.000	1.000	.418	.390	1.000
	Medial-Lateral rotation	1.000	1.000	1.000	1.000	1.000	1.000	1.000	1.000	1.000
	Anterior-Posterior tilt	.173	1.000	.136	*.001	.277	.059	1.000	1.000	1.000
HT	Plane of elevation	.127	.235	1.000	.558	.430	1.000	.263	*.016	.457
	Elevation	1.000	1.000	1.000	1.000	1.000	1.000	1.000	1.000	1.000
	Axial rotation	.134	1.000	.574	*.000	.279	*.000	.732	1.000	1.000

Appendix E

Functional classification using different input variables

Objective classification was investigating using input variables from anthropometric data, the neutral position (NP) and two activities of daily living (ADL), *Reach side and back of head* and *Lift block to shoulder height*. These two activities were determined as biomechanically demanding in Chapter 4. The input variables for each classification attempt, as well as their ranking and the classification accuracy are summarised in Table E.1. The corresponding Simplex Plots are shown in Figure E.1.

TABLE E.1: Classification trials

Classification attempt	Accuracy		Ranking	Input variable	OB	Variable accuracy
	in-sample	out-of-sample				
a	61.1	55	1	NPGH2	0.83335	72.5
			2	NPST3	0.9427	60.0
			3	NPST1	0.8195	67.5
			4	ADL11ST3	0.9552	52.5
			5	BMI	0.8335	72.5
			6	ADL11GH2	0.8734	60.0
			7	ADL3ST1	0.9741	47.5
			8	ADL11ST1	0.8348	57.5
			9	ADL11ST2	0.9733	52.5
			10	ADL3ST3	0.9805	22.5
			11	ALD3ST2	0.9328	47.5
			12	NPST2	0.8425	62.5
			13	ADL3GH2	0.8405	50.0
b	72.9	72.5	1	NPGH2	0.8279	67.5
			2	NPST3	0.9052	60.0
			3	NPST1	0.7024	67.5
			4	BMI	0.7242	72.5
			5	ADL11ST3	0.7922	60.0
c	74.9	67.5	1	NPST1	0.7940	67.5
			2	NPST3	0.6452	67.5
			3	BMI	0.6704	72.5
			4	ADL3ST2	0.9626	22.5
			5	ADL3GH2	0.6899	62.5
d	80.3	75	1	NPST1	0.8279	67.5
			2	NPST3	0.7024	67.5
			3	NPGH2	0.7242	72.5
			4	ADL3ST2	0.9684	22.5
			5	ADL11GH2	0.7400	62.5
			6	ADL11ST2	0.7922	60.0
			7	ADL3GH2	0.7293	57.5

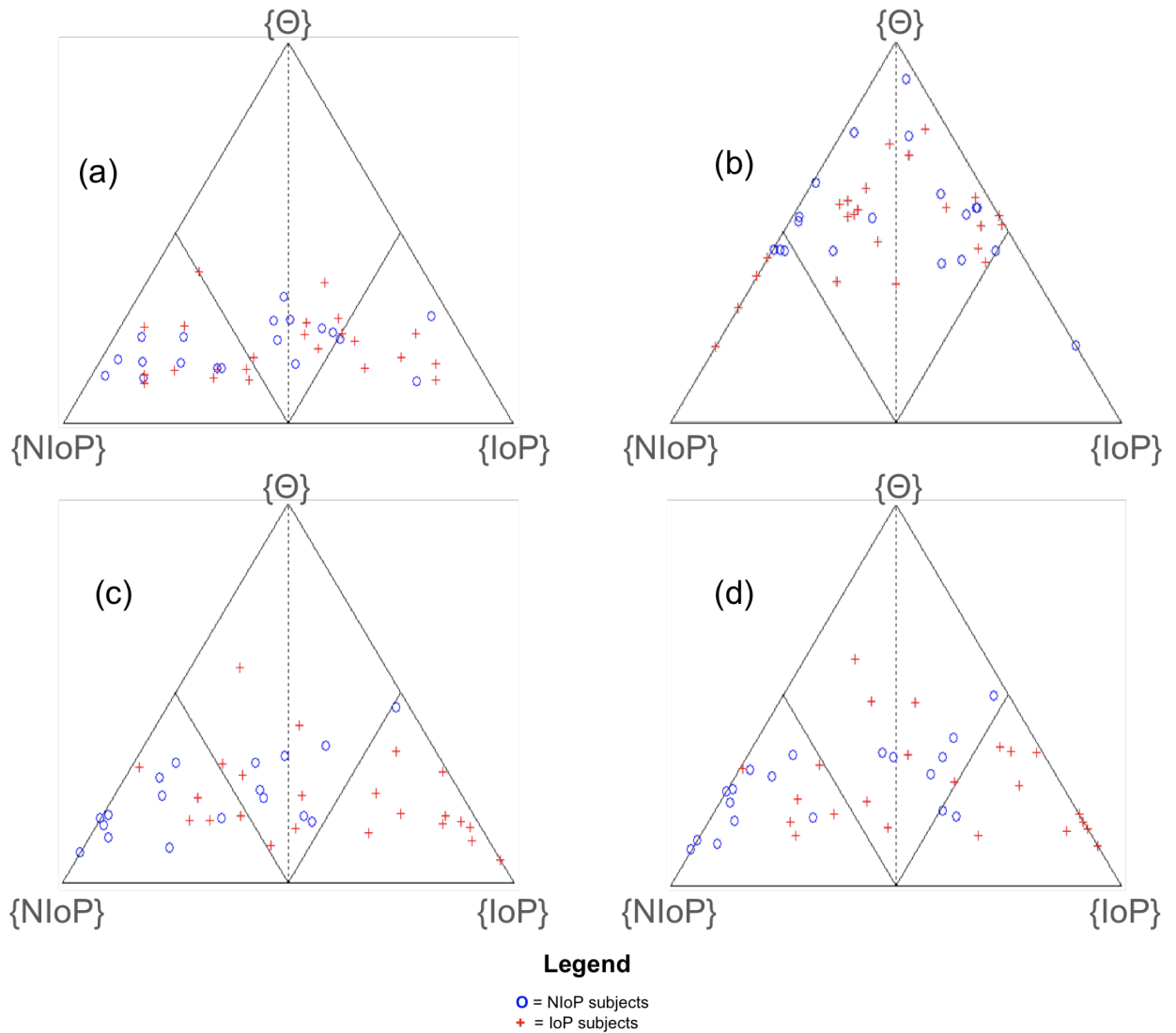


FIGURE E.1: Simplex plot showing the simplex coordinate representation of the BOE_C for all study participants using different input variables (a), (b), (c) and (d) correspond to the classification attempts summarised in Table E.1

Bibliography

- [1] Zatsiorsky. *Kinematics of human Motion*. Human Kinetics, 1998.
- [2] Visible body. <http://www.visiblebody.com/>, March 2011.
- [3] R. Drake, W. Vogl, and A.V.M. Mitchell. *Gray's Anatomy for Students: with student consult access*. 2004.
- [4] M. Nordin and V. Frankel. *Basic Biomechanics of the Musculoskeletal System*. 2001.
- [5] F.H. Netter, J. Craig, and C. Machado. Netter images. <http://www.netterimages.com/>, March 2011.
- [6] W.B. Kibler. Closed kinematic chain rehabilitation for sports injuries. *Phys Med Rehab Clin N Am*, 58A:195–201, 2000.
- [7] R.J. Hawkins and S.R. Saddemi. Shoulder instability. *Current Orthopaedics*, 4(4):242–252, 1990.
- [8] G.A. Paletta, J.J. Warner, R.F. Warren, A. Deutsch, and D.W. Altchek. Shoulder kinematics with two-plane x-ray evaluation in patients with anterior instability or rotator cuff tearing. *J Shoulder Elbow Surg*, 6(6):516–527, 1997.
- [9] W.B. Kibler. Rehabilitation of rotator cuff tendinopathy. *Clinics in Sports Medicine*, 22(4):837–847, 2003.

- [10] A.M. Hill, A.M.J. Bull, J. Richardson, A.H. McGregor, C.D. Smith, C.J. Barrett, P. Reilly, and A.L. Wallace. The clinical assessment and classification of shoulder instability. *Current Orthopaedics*, 22(3):208–225, 2008.
- [11] V.T. Inman, J.B.deC. M. Saunders, and L.C. Abbott. Observations on the function of the shoulder joint. *J Bone Joint Surg.*, 26:1–30, 1944.
- [12] J.P. Braman, S.C. Engel, R.F. LaPrade, and P.M. Ludewig. In vivo assessment of scapulohumeral rhythm during unconstrained overhead reaching in asymptomatic subjects. *J Shoulder Elbow Surg.*, 18(6):960–967, 2009.
- [13] F. Fayad, A. Roby-Brami, C. Yazbeck, S. Hanneton, M.M. Lefevre-Colau, V. Gautheron, S. Poiraudreau, and M. Revel. Three-dimensional scapular kinematics and scapulohumeral rhythm in patients with glenohumeral osteoarthritis or frozen shoulder. *J Biomech.*, 41:326–332, 2008.
- [14] J. Yoshizaki, K. and Hamada, K. Tamai, R. Sahara, T. Fujiwara, and T. Fujim. Analysis of the scapulohumeral rhythm and electromyography of the shoulder muscles during elevation and lowering: Comparison of dominant and nondominant shoulders. *J Shoulder Elbow Surg.*, 18(5):156–763, 2009.
- [15] Y. Kon, N. Nishinaka, K. Gamada, H. Tsutsui, and S.A. Banks. The influence of handheld weight on the scapulohumeral rhythm. *J Shoulder Elbow Surg.*, 17(6):943–946, 2008.
- [16] J. Crosbie, S.L. Kilbreath, and L. Hollmann. Scapulohumeral rhythm and associated spinal motion. *Clin Biomech.*, 23:184–192, 2008.
- [17] N. D. Barnett, R. D. D. Duncan, and G. R. Johnson. The measurement of three dimensional scapulohumeral kinematics: a study of reliability. *Clin Biomech.*, 14:287–290, 1999.
- [18] G. R. Johnson, P.R. Stuart, and S. Mitchell. A method for the measurements of three-dimensional scapular movement. *Clin Biomech.*, 8:269–273, 1993.

- [19] F.C.T. Van der Helm and G.M. Pronk. Three dimensional recording and description of motions of the shoulder mechanism. *J Biomech Eng.*, 177: 27–40, 1995.
- [20] C.W. Carter, W.N. Levine, C.P. Kleweno, L.U. Bigliani, and C.S. Ahmad. Assessment of shoulder range of motion: Introduction of a novel patient self-assessment tool. *Arthroscopy: The Journal of Arthroscopic & Related Surgery*, 24(6.):712–717, 2008.
- [21] J. Dawson, G. Hill, R. Fitzpatrick, and A. Carr. The benefits of using patient-based methods of assessment. medium-term results of an observational study of shoulder surgery. *J Bone Joint Surg.*, 83(6):877–882, 2001.
- [22] A. Khan, T.D. Bunker, and J.B. Kitson. Clinical and radiological follow-up of the aequalis third-generation cemented total shoulder replacement. *The Journal of Bone and Joint Surgery Br.*, 91B(7):1594–1600, 2009.
- [23] B. Coley, B.M. Jolles, A. Farron, A. Bourgeois, F. Nussbaumer, C. Pichonnaz, and K. Aminian. Outcome evaluation in shoulder surgery using 3d kinematics sensors. *Gait & Posture*, 25(4):523–532, 2007.
- [24] A. Deutsch, D.W. Altchek, E. Schwartz, J.C. Otis, and R.F. Warren. Radiologic measurement of superior displacement of the humeral head in the impingement syndrome. *J Shoulder Elbow Surg.*, 5:186–193, 1996.
- [25] P.W. McClure, L.A. Michener, and A.R. Karduna. Shoulder function and 3-dimensional scapular kinematics in people with and without shoulder impingement syndrome. *Phys Ther.*, 86:1075–1090, 2006.
- [26] F. Fayad, G. Hoffmann, S. Hanneton, C. Yazbeck, M.M. Lefevre-colau, S. Poiraudeau, M. Revel, and A. Roby-Brami. 3d scapular kinematics during arm elevation: Effect of motion velocity. *Clin Biomech.*, 21:932–941, 2006.

- [27] C.G.M. Meskers, H.M. Vermeulen, J.H. de Groot, F.C.T. van der Helm, and Rozing P.M. 3d shoulder position measurements using six-degree-of-freedom electromagnetic tracking device. *Clin Biomech.*, 12:280–292, 1998.
- [28] L. Roux, S. Hanneton, and A. Roby-Brami. Shoulder movements during the initial phase of learning manual wheelchair propulsion in able-bodied subjects. *Clin Biomech.*, 21(1):S45S51, 2006.
- [29] L. Ng, A. Burnett, A. Campbell, and P. OSullivan. Caution: the use of an electromagnetic device to measure trunk kinematics on rowing ergometers. *Sports Biomech*, 8(3):255–259, 2009.
- [30] C. van Andel, K. van Hutten, M. Eversdijk, D. Veeger, and J. Harlaar. Recording scapular motion using an acromion marker cluster. *Gait & Posture*, 29:123–128, 2009.
- [31] P. Salvia, S. Bouilland, R. Moletta, V. Sholukha, S. Van Sint Jan, and M. Rooze. Three-dimensional shoulder kinematics by optoelectronic stereophotogrammetry. *J Biomech.*, 39(1):S78–, 2006.
- [32] A. Bonnefoy-Mazure, J. Slawinski, A. Riquet, J.M. Lvque, C. Miller, and L. Chze. Rotation sequence is an important factor in shoulder kinematics. application to the elite players flat serves. *J Biomech.*, 43(10):2022–2025, 2010.
- [33] N. Klopkar and J. Lenarc. Bilateral and unilateral shoulder girdle kinematics during humeral elevation. *Clin Biomech.*, 21:S20–S26, 2006.
- [34] P. Salvia, S. Van Sint Jan, A. Crouan, L. Vanderkerken, F. Moiseev, V. Sholukha, C. Mahieu, and O. Snoeck. Precision of shoulder anatomical landmark calibration by two approaches: A cast-like protocol and a new anatomical palpator method. *Gait & Posture*, 29(4):587–591, 2009.

- [35] B. Lovern, L.A. Stroud, N.A. Ferran, R.O. Evans, S.L. Evans, and C.A. Holt. Motion analysis of the glenohumeral joint during activities of daily living. *Gait & Posture*, 13(6):803–809, 2010.
- [36] M.M.B. Morrow, K.R. Kaufman, and K.N. An. Scapula kinematics and associated impingement risk in manual wheelchair users during propulsion and a weight relief lift. *Clin Biomech.*, 26(4):352–357, 2011.
- [37] A.G. Cutti, G. Paolini, M. Troncossi, A. Cappello, and A. Davalli. Soft tissue artefact assessment in humeral axial rotation. *Gait & Posture*, 21(3):341–349, 2008.
- [38] E.A. Hassan, T.R. Jenkyn, and C.E Dunning. Direct comparison of kinematic data collected using an electromagnetic tracking system versus a digital optical system. *J Biomech.*, 40(4):930–935, 2007.
- [39] H. Graichen, T. Stammberger, H. Bonel, M. Haubner, K.H Englemeier, M. Reiser, and F Eckstein. Magnetic resonance-based motion analysis of the shoulder during elevation. *Clin Orthop.*, 370:154–163, 2000.
- [40] H. Graichen, T. Stammberger, H. Bonel, K.H Englemeier, M. Reiser, and F Eckstein. Glenohumeral translation during active and passive elevation of the shoulder - a 3d open-mri study. *J Biomech.*, 33:609–613, 2000.
- [41] H. Graichen, T. Stammberger, H. Bonel, M. Haubner, K.H Englemeier, M. Reiser, and F Eckstein. 3d mr-based motion analysis of the supraspinatus and shoulder bones during elevation. *Clin Orthop.*, pages – , 2000.
- [42] J.M. Polster, N. Subhas, J.J. Scalise, J.A. Bryan, M.L. Lieber, and M.S. Schickendantz. Three-dimensional volume-rendering computed tomography for measuring humeral version. *J Shoulder Elbow Surg.*, 19(6): 899–907, 2010.

- [43] S.A. Banks. *Model based 3D kinematic estimation from 2D perspective silhouettes: application with total knee prostheses*. PhD thesis, University of Florida, 1992.
- [44] S.A. Banks and W.A. Hodge. Accurate measurement of three - dimensional knee replacement kinematics using single-plane fluoroscopy. *IEEE Trans. Biomed. Eng.*, 43:638–649, 1996.
- [45] Y. Kim, K.I. Kim, J.H Choi, and K. Lee. Novel methods for 3d postoperative analysis of total knee arthroplasty using 2d/3d image registration. *Clin Biomech.*, 26(4):384–391, 2010.
- [46] A. Kitagawa, N. Tsumura, T. Chin, K. Gamada, S.A. Banks, and M. Kurosaka. In vivo comparison of knee kinematics before and after high-flexion posterior cruciate-retaining total knee arthroplasty. *The Journal of Arthroplasty*, 25:964–969, 2010.
- [47] G.M. Whatling. *A contribution to the clinical validation of a generic method for the classification of osteoarthritic and non-pathological knee function*. PhD thesis, Cardiff University, 2009.
- [48] M.J. Bey, R. Zael, S.K. Brock, and S. Tashman. Validation of a new model-based tracking technique for measuring three-dimensional, in vivo glenohumeral joint kinematics. *J Biomech Eng.*, 128(4):604–609, 2006.
- [49] M.J. Bey, S.K. Kline, R. Zael, T.R. Lock, and P.A. Kolowich. Measuring dynamic in-vivo glenohumeral joint kinematics: Technique and preliminary results. *J Biomech.*, 41:711–714, 2008.
- [50] N. Nishinaka, H. Tsutsui, K. Mihara, K. Suzuki, D. Makiuchi, Y. Kon, T.W. Wright, M.W. Moser, K. Gamada, H. Sugimoto, and S.A. Banks. Determination of in vivo glenohumeral translation using fluoroscopy and shape-matching techniques. *J Shoulder Elbow Surg.*, 17(2):319–322, 2008.

- [51] J.L. Bishop, S.K. Kline, K.J. Aalderink, R. Zauel, and M.J. Bey. Glenoid inclination: In vivo measurements in rotator cuff tear patients and associations with superior glenohumeral joint translation. *J Shoulder Elbow Surg.*, 18:231–236, 2009.
- [52] K.O. Matsuki, K. Matsuki, S. Mu, T. Sasho, K. Nakagawa, N. Ochiai, K. Takahashi, and S.A. Banks. In vivo 3d kinematics of normal forearms: Analysis of dynamic forearm rotation. *Clin Biomech.*, 25:979–983, 2010.
- [53] T.B. Johnston. The movements of the shoulder joint. a plea for the use for the ‘plane of the scapula’ as the plane of reference for movements occurring at the humero-scapular joint. *J Bone Joint Surg.*, 25:252–260, 1937.
- [54] S.W. Alpert, M.M. Pink, F.W. Jobe, P.J. McMahon, and W. Mathiyakom. Multidirectional instability of the glenohumeral joint. *J Shoulder Elbow Surg.*, 9(1):47–58, 2000.
- [55] A. Kontaxis, A.G. Cutti, G.R. Johnson, and H.E.J. Veeger. A framework for the denition of standardized protocols for measuring upper-extremity kinematics. *Clin Biomech.*, 24:246–253, 2009.
- [56] S.T. Tumer and A.E. Engin. Three-dimensional modelling of the human shoulder complex - part ii: mathematical modelling and solution via optimization. *J Biomech Eng*, 111:113–121, 1989.
- [57] G.M. Pronk, F.C.T. van der Helm, and L.A. Rozendaal. Interaction between the joints in the shoulder mechanism: the function of the costoclavicular, conoid and trapezoid ligaments. *Proc Instn Mech Engrs*, 207: 219–229, 1993.
- [58] G. Pronk. *The Shoulder Girdle*. PhD thesis, University of Delft, Netherlands, 1991.

- [59] F. Camargo Forte, M. Peduzzi de Castro, J. Mahnic de Toledo, D. Cury Ribeiro, and J. Fagundes Loss. Scapular kinematics and scapulothoracic rhythm during resisted shoulder abduction – implications for clinical practice. *Physical Therapy in Sport*, 10(3):105–111, 2009.
- [60] W. Sahara, K. Sugamoto, M. Murai, T. Hiroyuki, and H. Yoshikawa. The three-dimensional motions of the glenohumeral joint under semi-loaded condition during arm abduction using vertically open mri. *Clin Biomech.*, 22:304–312, 2007.
- [61] J.P. Baeyens, P. Van Roy, A. De Schepper, G. Declercq, and J.P. Clarijs. Glenohumeral joint kinematics related to minor anterior instability of the shoulder at the end of the late preparatory phase of throwing. *Clin Biomech.*, 16(9):752–757, 2001.
- [62] K.J. McQuade and A.M. Murthi. Anterior glenohumeral force/translation behavior with and without rotator cuff contraction during clinical stability testing. *Clin Biomech*, 19(1):10–15, 2004.
- [63] N.K. Poppen and Walker P.S. Normal and abnormal motion of the shoulder. *J Bone Joint Surg.*, 58(2):195–201, 1976.
- [64] K. Maruyama, S. Sano, K. Saito, and Y. Tamaguchi. Trauma-instability-voluntarism classification for glenohumeral instability. *J Shoulder Elbow Surg*, 4(3):241–246, 1995.
- [65] P.J. Rundquist, D.D. Anderson, C.A. Guanche, and P.M. Ludewig. Shoulder kinematics in subjects with frozen shoulder. *Arch Phys Med Rehabil.*, 84(10):1473–1479, 2003.
- [66] H.M. Vermeulen, M. Stokdijk, P.H. Eilers, C.G. Meskers, P.M. Rozing, and T.P. Vliet Vlieland. Measurement of three dimensional shoulder movement patterns with an electromagnetic tracking device in patients with a frozen shoulder. *Annals of the Rheumatic Diseases*, 61:115–120, 2002.

- [67] F. Fayad, A. Roby-Brami, C. Yazbeck, S. Hanne-ton, M.M. Lefevre-Colau, V. Gautheron, S. Poiraudau, and M. Revel. Three-dimensional scapular kinematics and scapulohumeral rhythm in patients with glenohumeral osteoarthritis or frozen shoulder. *J Biomech.*, 41:326–332, 2007.
- [68] J.E. Kuhn, K.D. Plancher, and R.J. Hawkins. Scapular winging. *J Am Acad Orthop Surg*, 3:319–325, 1995.
- [69] K. Akgun, I. Aktas, and Y Terzi. Winged scapula caused by a dorsal scapular nerve lesion: A case report. *Arch Phys Med Rehabil.*, 89(10): 2017–2020, 2008.
- [70] J.C. Lin, N. Weintrub, and D.R. Aragaki. Nonsurgical treatments for rotator cuff injury in the elderly. *Journal of the American Medical Directors Association*, 9:626–632, 2008.
- [71] P.J. Royer, E.J. Kane, K.E. Parks, J.C. Morrow, R.R. Moravec, D.S. Cristie, and D.S. Teyhen. Fluoroscopic assessment of rotator cuff fatigue on glenohumeral arthrokinematics in shoulder impingement syndrom. *J Shoulder Elbow Surg.*, 18:968–975, 2009.
- [72] A. Sheikhzadeh, J. Yoon, V.J. Pinto, and Y.W. Kwon. Three-dimensional motion of the scapula and shoulder during activities of daily living. *J Shoulder Elbow Surg.*, 17(6):936–942, 2008.
- [73] G. Wu, F.C.T. van der Helm, H.E.J. Veeger, M. Makhsous, P. Van Roy, C. Anglin, J. Nagels, A.R. Karduna, K. McQuade, X. Wang, F.W. Werner, and B. Bucholz. Isb recommendation on definitions of joint coordinate systems of various joints for the reporting of human joint motion - part ii: shoulder, elbow, wrist and hand. *J Biomech.*, 38:982–992, 2005.
- [74] D.F. Massimini, G. Li, and J.J.P. Warner. Non-invasive determination of coupled motion of the scapula and humerus: An in-vitro validation. *J Biomech.*, 44(3):408–412, 2011.

- [75] T. Monnet, E. Desailly, M. Begon, C. Vallee, and P. Lacouture. Comparison of the score and ha methods for locating in vivo the glenohumeral joint centre. *J Biomech.*, 40:3487–3492, 2007.
- [76] H.E.J. Veeger, B. Yu, K.N. An, and R.H. Rozendal. Parameters for modelling the upper extremity. *J Biomech.*, 30:647–652, 1997.
- [77] M. Stokdijk, J. Nagels, and P.M. Rozing. The glenohumeral joint rotation centre in vivo. *J Biomech.*, 33:1629–1636, 2000.
- [78] C.G.M. Meskers, F.C.T. van der Helm, L.A. Rozendaal, and P.M. Rozing. In vivo estimation of the glenohumeral joint rotation center from scapular bony landmarks by linear regression. *J Biomech.*, 31(1):93–96, 1998.
- [79] C.A. Campbell, D.G. Lloyd, J.A. Alderson, and B.C. Elliott. Mri validation of a new regression model for glenohumeral centre of rotation estimation. *J Biomech.*, 41:S165–, 2008.
- [80] C.A. Campbell, D.G. Lloyd, J.A. Alderson, and B.C. Elliott. Mri development and validation of two new predictive methods of glenohumeral joint centre location identification and comparison with established techniques. *J Biomech.*, 42:1527–1532, 2009.
- [81] H.E.J. Veeger. The position of the rotation center of the glenohumeral joint. *J Biomech.*, 33:1711–1715, 2000.
- [82] M. Lempereur, F. Leboeuf, S. Brochard, J. Rousset, V. Burdin, and O. Rmy-Nris. In vivo estimation of the glenohumeral joint centre by functional methods: Accuracy and repeatability assessment. *J Biomech.*, 43(2):370–374, 2010.
- [83] H.J. Woltring, R. Huiskes, and A. de Lange. Finite centroid and helical axis estimation from noisy landmark measurements in the study of human joint kinematics. *J Biomech.*, 18(5):379–389, 1985.

- [84] H.J. Woltring, . A de Lange, J.M.G. Kauer, and A. Huiskes. *Instantaneous helical axis estimation via natural cross-validates splines*. Dordrecht/Boston/Lancaster: Martinus Nijhoff Publishers, 1987.
- [85] H.J. Woltring. *Data processing and error analysis*. Berlec Corporation, Worthington, OH, 1990.
- [86] A. Leardini, A. Cappozzo, F. Catani, S. Toksvig-Larsen, A. Petitto, V. Sforza, G. Cassanelli, and Giannini. S. Validation of a functional method for the estimation of hip joint centre location. *J Biomech.*, 32: 99–103, 1999.
- [87] K.J. Faber, K. Homa, and R.J. Hawkins. Translation of the glenohumeral joint in patients with anterior instability: Awake examination versus examination with the patient under anesthesia. *J Shoulder Elbow Surg.*, 8(4): 320–323, 1999.
- [88] E.A. Yoldas, K.J. Faber, and R.J. Hawkins. Translation of the glenohumeral joint in patients with multidirectional and posterior instability: Awake examination versus examination under anesthesia. *J Shoulder Elbow Surg.*, 10(5):416–420, 2001.
- [89] C.M. Werner, R.W. Nyffeler, H.A. Jacob, and C. Gerber. The effect of capsular tightening on humeral head translations. *J Orthop Res.*, 22(1): 194–201, 2004.
- [90] H.E.J. Veeger, F.C.T. van der Helm, E.K.J. Chadwick, and D.J. Magermans. Toward standardized procedures for recording and describing 3-d shoulder movements. *Behav. Res. Methods. Instrum. Comput.*, 35:440–446, 2003.
- [91] T. Tsung-Yuan, L. Tung-Wu, K. Mei-Ying, and L. Cheng-Chung. Effects of soft tissue artifacts on the calculated kinematics and kinetics of the knee during stair-ascent. *J Biomech.*, 44(6):1182–1188, 2011.

- [92] L. Lucchetti, A. Cappozzo, A. Cappello, and U. Della Croce. Skin movement artefact assessment and compensation in the estimation of knee-joint kinematics. *J Biomech.*, 31(11):977–984, 1998.
- [93] R. Schmidt, C. Disselhorst-Klug, J. Silny, and G. Rau. A marker-based measurement procedure for unconstrained wrist and elbow motions. *J Biomech*, 2002(35):1279–1283, 1999.
- [94] M.A.J. Meskers, C.G.M. van de Sande and J.H. de Groot. Comparison between tripod and skin-fixed recording of scapular motion. *J Biomech.*, 40(4):941–946, 2007.
- [95] A.E. Kedgley, G.A. Mackenzie, L.M. Ferreira, J.A. Johnson, and K.J. Faber. In vitro kinematics of the shoulder following rotator cuff injury. *Clin Biomech.*, 22:1068–1073, 2007.
- [96] R. Kelkar, V.M. Wang, E.L. Flatow, P.M. Newton, G.A. Ateshian, L.U. Bigliani, R.J. Pawluk, and V.C. Mow. Glenohumeral mechanics: a study of articular geometry, contact, and kinematics. *J Shoulder and Elbow Surg*, 10:73–84, 2001.
- [97] L.A. Stroud, B. Lovern, R. Evans, L. Jones, S.L. Evans, and C. Holt. Measuring scapula orientation during arm elevation. In *CMBBE 2008 proceedings*, 2008.
- [98] A.F. Shaheen, C.M. Alexander, and A.M.J. Bull. Tracking the scapula using the scapula locator with and without feedback from pressure-sensors: A comparative study. *J Biomech.*, 44(8):1633–1636, 2011.
- [99] P.W. McClure, L.A. Michener, B.J. Sennett, and A.R. Karduna. Direct 3-dimensional measurement of scapular kinematics during dynamic movements in vivo. *J Shoulder Elbow Surg*, 10(3):269–277, 2001.
- [100] A. Karduna, P. McClure, L. Michener, and Sennett B. Dynamic measurements of three-dimensional scapular kinematics: a validation study. *J Biomech Eng.*, 123(2):184–190, 2001.

- [101] S. Brochard, M. Lempereur, and O. Remy-Neris. Double calibration: An accurate, reliable and easy-to-use method for 3d scapular motion analysis. *J Biomech.*, 44:751–754, 2011.
- [102] A. Leardini, L. Chiari, U.D. Croce, and A. Cappozzo. Human movement analysis using stereophotogrammetry. part 3. soft tissue artifact assessment and compensation. *Gait Posture*, 21(2):212–225, 2005.
- [103] D. Bourne, A. Choo, W. Regan, D. MacIntyre, and T. Oxland. Accuracy of digitization of bony landmarks for measuring change in scapular attitude. *Proc. IMechE. J. Engineering in Medicine, Part H*, 223:349–361, 2009.
- [104] J. H. de Groot. The variability of shoulder motions recorded by means of palpation. *Clin Biomech.*, 12(7/8):461–472, 1997.
- [105] U. Della Croce, A. Leardini, and L. Chiari. Human movement analysis using stereophotogrammetry. part 4: assessment of anatomical landmark misplacement and its effects on joint kinematics. *Gait & Posture*, 21(2): 226–237, 2005.
- [106] N.A. Jacobs, J. Skorecki, and J. Charnley. Analysis of the vertical component of force in normal and pathological gait. *J Biomechanics*, 5:11–34, 1972.
- [107] L. Jones. *The development of a novel method for the classification of osteoarthritic and normal knee function*. PhD thesis, Cardiff University, 2004.
- [108] L. Jones, C.A Holt, and M.J. Beynon. Reduction, classification and ranking of motion analysis data: an application to osteoarthritic and normal knee function data. *Computer Methods in Biomechanics and Biomedical Engineering*, 11(1):31–40, 2007.
- [109] L. Jones, M.J. Beynon, C.A. Holt, and S. Roy. An application of the Dempster-Shafer theory of evidence to the classification of knee function

- and detection of improvement due to total knee replacement. *J Biomech.*, 39:2512–2520, 2006.
- [110] L.A. Stroud and C. Whatling, G.M. Holt. Combining image and motion capture: A route to quantifying shoulder function. In *British Elbow & Shoulder Society Meeting*, 2011.
- [111] L.A. Stroud, B. Lovern, R. Evans, L. Jones, S.L. Evans, and C. Holt. Estimating the glenohumeral joint centre of rotation: regression equations versus helical axis. In *Proceedings of the 9th Symposium of Computer Methods in Biomechanics and Biomedical Engineering, Valencia*, 2010.
- [112] L.A. Stroud, B. Lovern, N. Ferran, R. Evans, S.L. Evans, and C. Holt. Measuring glenohumeral joint translations using motion analysis techniques. In *Proceedings of the 22nd Congress of the International Society of Biomechanics, Cape Town*, 2009.
- [113] A.R. Hopkins, D. Emmenegger, L.A. Stroud, C. Scharer, B. Lovern, C. Holt, and J. Seebeck. Generation of subject specific shoulder kinematic models from motion capture data and anybody simulation. In *Proceedings of the XXIII Congress of the International Society of Biomechanics, Brussels*, 2011.
- [114] L.A. Stroud, B. Lovern, R. Evans, L. Jones, S.L. Evans, and C. Holt. Quantifying glenohumeral joint translation in multidirectional instability patients and healthy volunteers. In *Proceedings of the 17th Congress of European Society of Biomechanics, Edinburgh*, 2010.
- [115] L.A. Stroud, B. Lovern, L. Jones, R. Evans, S.L. Evans, and C. Holt. In vivo non-invasive measurements of scapula kinematics: Effect of bilateral arm elevation on scapula lateral rotation. In *Proceedings of the 10th International Symposium of the ISB Technical Group of the 3D Analysis of Human Movement, Amsterdam*, 2008.

- [116] S.K. Chen, P.T. Simonian, T.L. Wickiewicz, J.C. Otis, and R.F. Warren. Radiographic evaluation of glenohumeral kinematics: a muscle fatigue model. *J Shoulder Elbow Surg.*, 8(1):49–52, 1999.
- [117] K.G. Hermann, M. Backhaus, U. Scheneider, K. Labs, D. Loreck, S. Suhlsforf, T. Schink, T. Fischer, B. Hamm, and M. Bollow. Rheumatoid arthritis of the shoulder joint: comparison of conventional radiography, ultrasound, and dynamic contrast-enhanced magnetic resonance imaging. *Arthritis Rheumatol*, 48(12):3338–3349, 2003.
- [118] T. Kido, E. Itoi, N. Konno, A. Sano, M. Urayama, and K. Sato. The depressor function of biceps on the head of the humerus in shoulders with tears of the rotator cuff. *J Bone Joint Surg., Br.*, 82(3):416–419, 2000.
- [119] D.S. Teyhen, J.M. Miller, T.R. Middag, and E.J. Kane. Rotator cuff fatigue and glenohumeral kinematics in participants without shoulder dysfunction. *J Athl Train.*, 43(4):352–358, 2008.
- [120] D.G. Mandalidis, B.S. Mc Glone, R.F. Quigley, D. McInerney, and M. O'Brian. Digital fluoroscopic assessment of the scapulohumerual rhythm. *Surg. Radiol. Anat.*, 21(4):194–198, 1999.
- [121] C. van Andel, N. Wolterbeek, A. Doorenbosch, H.E.J. Veeger, and J. Harlaar. Complete 3d kinematics of upper extremity functional tasks. *Gait & Posture*, 27:120–127, 2008.
- [122] P.M. Ludewig and T. Cook. Translations of the humerus in persons with shoulder impingement symptoms. *J Orthop Sports Phys Ther.*, 32(6): 248–259, 2002.
- [123] L. Tung-Wu, T. Tsung-Yuan, K. Mei-Ying, H. Horng-Chaung, and C. Hao-Ling. In vivo three-dimensional kinematics next term of the normal knee during active extension under unloaded and loaded conditions using single-plane fluoroscopy. *Medical Engineering & Physics*, 30(8):1004–1012, 2008.

- [124] K.J. Fischer, T.T. Manson, H.J. Pfaeffle, M.M. Tomaino, and Woo S. L. Y. A method for measuring joint kinematics designed for accurate registration of kinematic data to models constructed from ct data. *J Biomech.*, 34(3): 377–383, 2001.
- [125] D.F.L. Southgate, A.M. Hill, S. Alexander, A.L. Wallace, U.N. Hansen, and A.M.J. Bull. The range of axial rotation of the glenohumeral joint. *J Biomech.*, 42:1307–1312, 2009.
- [126] A.E. Kedgley, G.A. Mackenzie, L.M. Ferreira, D.S. Drosdowech, J.F. Kenneth, and J.A. Johnson. The effect of muscle loading on the kinematics of in vitro glenohumeral abduction. *J Biomech.*, 40(7):2953–2960, 2007.
- [127] M.R. Mahfouz, W.A. Hoff, R.D. Komistek, and D.A. Dennis. A robust method for registration of three-dimensional knee implant models to two-dimensional fluoroscopy images. *IEEE Trans Med Imaging*, 22(12):1561–1574, 2003.
- [128] S. Yamaguchi, K. Gamada, T. Sasho, H. Kato, M. Sonoda, and S.A. Banks. In vivo kinematics of anterior cruciate ligament deficient knees during pivot and squat activities. *Clin Biomech.*, 24:71–76, 2009.
- [129] R.D. Komistek, D.A. Dennis, and M. Mahfouz. In vivo fluoroscopic analysis of the normal human knee. *Clin Orthop.*, 410:69–81, 2003.
- [130] T. Asano, M. Akagi, K. Tanaka, J. Tamura, and T. Nakamura. In vivo three dimensional knee kinematics using biplanar image matching technique. *Clin Orthop.*, 388:157–166, 2001.
- [131] L.E. DeFrate, H. Sun, T.J. Gill, H.E. Rubash, and G. Li. In vivo tibiofemoral contact analysis using 3d mri-based knee models. *J Biomech.*, 37(10): 1499–1504, 2004.
- [132] T. Moro-oka, S. Hamai, H. Miura, T. Shimoto, H. Higaki, B.J. Fregly, Y. Iwamoto, and S.A. Banks. Can magnetic resonance imaging derived bone models be used for accurate motion measurement with single-plane

- three-dimensional shape registration? *Wiley InterScience*, DOI 10.1002 (jor.20355), 2007.
- [133] S.J. Doran, L. Charles-Edwards, S.A. Reinsberg, and M.O. Leach. A complete distortion correction for mr images: I. gradient ward correction. *Phys Med Biol*, 50:1343–1361, 2005.
- [134] D.L. Hill, C.R. Jr. Maurer, J.M. Studholme, C. Fitzpatrick, and D.L. Hawkes. Correcting scaling errors in tomographic images using a nine degree of freedom registration algorithm. *J Comput Assist Tomogr*, 22: 317–323, 1998.
- [135] B.M. You, P. Siy, W. Anderst, and S. Tashman. In vivo measurement of 3-d skeletal kinematics from sequences of biplane radiographs: Application to knee kinematics. *IEEE Trans. Biomed. Eng.*, 20(6):514–525, 2001.
- [136] T. Ohnishi, M. Suzuki, A. Nawata, S. Naomoto, T. Iwasaki, and H. Haneishi. Three-dimensional motion study of femur, tibia, and patella at the knee joint from bi-plane fluoroscopy and ct images. *Radiological Physics and Technology*, 3(2):151–158, 2004.
- [137] W.A. Wallace and F. Johnson. Detection and correction of geometrical distortion in x-ray fluoroscopic images. *J Biomech.*, 14(2):123–125, 2004.
- [138] V. Phadke, J.P. Braman, and P.M. LaPrade, R.F. and Ludewig. Comparison of glenohumeral motion using different rotation sequences. *J Biomech.*, 44(4):700–705, 2011.
- [139] M. Senk and L. Cheze. Rotation sequence as an important factor in shoulder kinematics. *Clin Biomech.*, 21(Supplement 1):S3–S8, 2005.
- [140] A.B. Mazure, J. Slawinski, A. Riquet, J.M. Leveque, C. Miller, and L. Cheze. Rotation sequence is an important factor in shoulder kinematics: Application to the elite players' flat serves. *J Biomech.*, 43:2022–2035, 2010.

- [141] L. Jones, C.A. Holt, and A. Bowers. Movement of the shoulder complex: The development of a measurement technique based on proposed isb standards. In *Proc Intl. Society of Biomechanics: 8th. Intl. Symposium on 3D Motion*, 2006.
- [142] L. Jones, C.A. Holt, and A. Bowers. Movement of the shoulder complex: The development of a measurement technique based on proposed isb standards. In *Proc Intl. Society of Biomechanics: 8th. Intl. Symposium on 3D Motion Analysis*, 2006.
- [143] I.A. Murray. *Upper limb kinematics and dynamics during everyday tasks*. PhD thesis, University of Newcastle upon Tyne, 1999.
- [144] I. Charlton and G.R. Johnson. A model for the prediction of the forces at the glenohumeral joint. *J Engineering in Medicine*, 220:801–812, 2006.
- [145] I. Soderkvist and P.A. Wedin. Determining the movements of the skeleton using well-configured markers. *J Biomech.*, 26:1473–1477, 1993.
- [146] International Shoulder Group. <http://internationalshouldergroup.org>, June 2011.
- [147] R.M. Ehrig, R.T. Taylor, G.N. Duda, and M.O. Heller. A survey of formal methods for determining the centre of rotation of ball joints. *J Biomech.*, 39(15):2798–2809, 2006.
- [148] B. Lovern, L.A. Stroud, R.O. Evans, S.L. Evans, and C.A. Holt. Dynamic tracking of the scapula using skin mounted markers. *J. Engineering in Medicine, Part H*, 223(7):823–831, 2009.
- [149] B. Lovern. *Functional Analysis of the Shoulder Complex in Healthy and Pathological Subjects using Three-Dimensional Motion Analysis Techniques*. PhD thesis, Cardiff University, 2010.
- [150] A.F. Shaheen, C.M. Alexander, and A.M.J. Bull. Effects of attachment position and shoulder orientation during calibration on the accuracy of the acromial tracker. *J Biomech.*, 44(7):1410–1413, 2011.

- [151] D. Theodoridis and S. Ruston. The effect of shoulder movements on thoracic spine 3d motion. *Clin Biomech.*, 17:418–421, 2002.
- [152] M. Kebaetse, P. McClure, and N.A. Pratt. Thoracic position effect on shoulder range of motion, strength, and three-dimensional scapular kinematics. *Arch Phys Med Rehabil*, 80(8):945–950, 1999.
- [153] A. Gil, F.F.C.T. van der Helm, P. Pezarat, and I. Carita. Effects of different arm external loads on the scapulo-humeral rhythm. *Clin Biomech.*, 15: S21–S24, 2000.
- [154] M.A. Finley and R.Y. Lee. Effect of sitting posture on 3-dimensional scapular kinematics measured by skin mounted electromagnetic tracking sensors. *Arch Phys Med Rehabil*, 84:563–568, 2003.
- [155] G.N. Gantchev and Dimitrova D.M. Anticipatory postural adjustments associated with arm movements during balancing on unstable support surface. *International Journal of Psychophysiology*, 22:117–122, 1996.
- [156] M. Peat, E. Culham, and K.E. Wilk. Functional anatomy of the shoulder complex. *The Athlete's Shoulder*, 2:3–16, 1990.
- [157] F. Fayad, S. Hanne-ton, M.M. Lefevre-Colau, S. Poiraudreau, M. Revel, and A. Roby-Brami. The trunk as a part of the kinematic chain for arm elevation in healthy subjects and in patients with a frozen shoulder. *Brain Res.*, 29;1191:107–115, 2008.
- [158] S.G. Stewart, G.A. Jull, J.K.F. Ng, and J.M. Willems. An initial analysis of thoracic spine movement during unilateral arm elevation. *J Manual Manipul Therapy*, 3:15–20, 1995.
- [159] D.C. Boone and S.P. Azen. Normal range of motion of joints in male subjects. *J. Bone and Joint Surg. Am.*, 61:756–759, 1979.
- [160] I. Gunal, N. Kose, O. Erdogan, E. Gokturk, and S. Seber. Normal range of motion of the joints of the upper extremity in male subjects, with special reference to side. *J Bone Joint Surg Am.*, 78:1401–1404, 1996.

- [161] K. Matsuki, K.O. Matsuki, S. Mu, S. Yamaguchi, N. Ochiai, T. Sasho, H. Sugaya, T. Toyone, Y. Wada, K. Takahashi, and S.A. Banks. In vivo 3 dimensional analysis of scapular kinematics: Comparison between dominant and nondominant shoulders. *J Shoulder Elbow Surg.*, 20(4):659–665, 2011.
- [162] J.J.P. Warner, L.J. Micheli, L.E. Arslanian, J. Kennedy, and R. Kennedy. Scapulothoracic motion in normal shoulders and shoulders with glenohumeral instability and impingement syndrome: A study using moire topographic analysis. *Clin Orthop Relat Res*, 285:191–199, 1992.
- [163] C.J. Barnes, S.J. Van Steyn, and R.A. Fischer. The effect of age, sex, and shoulder dominance on range of motion of the shoulder. *J Shoulder Elbow Surg.*, 10(3):242–246, 2001.
- [164] L.G. Macedo and D.J. Magee. Differences in range of motion between dominant and nondominant sides of upper and lower extremities. *Journal of Manipulative and Physiological Therapeutics*, 31(8):577–582, 2008.
- [165] J.C. Otis, R.F. Warren, S.I. Backus, T.J. Santner, and J.D. Mabrey. Torque production in the shoulder of the normal young adult male. *Am J Sports Med.*, 18:119–123, 1990.
- [166] M.A. Gallagher, F. Zuckerman, J.D. Cuomo, and J. Ortiz. The effect of age, speed, and arm dominance on shoulder function in untrained men. *J Shoulder Elbow Surg.*, 5(1):25–31, 1996.
- [167] F. Fu, M. Seel, and R. Berger. Relevant shoulder biomechanics. *Operative Techniques in Orthopaedics*, 1(2):134–146, 1991.
- [168] E.A. Codman. *The Shoulder: Rupture of the Supraspinatus Tendon and Other Lesions in or about the Subacromial Bursa*. Thomas Todd Co., 1934.
- [169] F.C.T. Van der Helm. A finite musculoskeletal model of the shoulder mechanism. *J Biomech.*, 27(5):551–569, 1994.

- [170] H.E.J. Veeger, D.J. Magermans, J. Nagels, E.K.J. Chadwick, and F.C.T. van der Helm. A kinematical analysis of the shoulder after arthroplasty during a hair combing task. *Clin Biomech.*, 21:S39–S44, 2006.
- [171] A.G. Cutti and H.E.J. Veeger. Shoulder biomechanics: today’s consensus and tomorrow’s perspectives. *Med Biol Eng Comput.*, 47:463–466, 2009.
- [172] New Zealand Guidelines Group. The diagnosis and management of soft tissue shoulder injuries and related disorders. <http://www.acc.co.nz>, June 2011.
- [173] A.F. de Winter, M.P. Jans, R.J.P.M. Scholten, W. Deville, D. van Schaardenburg, and L.M. Bouter. Diagnostic classification of shoulder disorders: interobserver agreement and determinants of disagreement. *Ann Rheum Dis*, 58:272–277, 1999.
- [174] B.W. Hickey, S. Milosavljevic, M.L. Bell, and P.D. Milburn. Accuracy and reliability of observational motion analysis in identifying shoulder symptoms. *Manual Therapy*, 12:263–270, 2007.
- [175] F. Steenbrink, J.H. de Groot, H.E.J. Veeger, F.C.T. van der Helm, and P.M. Rozing. Glenohumeral stability in simulated rotator cuff tears’. *J Biomech.*, 42:1740–1745, 2009.
- [176] E.G. McFarland, J. Garzon-Muvdi, and X. Jia. Clinical and diagnostic tests for shoulder disorders: a critical review. *Br J Sports Med.*, 44:328–332, 2010.
- [177] M. Fung, S. Kato, P.J. Barrance, J.J. Elias, E.G. McFarland, K. Nobuhara, and E.Y. Chao. Scapular and clavicular kinematics during humeral elevation: A study with cadavers. *J Shoulder Elbow Surg.*, 10(3):278–285, 2001.
- [178] C.B. Terwee, A.F. de Winter, R.J. Scholten, M.P. Jans, W. Deville, D. van Schaardenburgh, and L.M. Bouter. Interobserver reproducibility of the

- visual estimation of range of motion of the shoulder. *Arch Phys Med Rehabil*, 86:1356–1361, 2005.
- [179] Y.L. Moon, K.I. Lee, A.M. Jacir, and L.U. Bigliani. Review of the literature on sports related clavicle fractures and analysis on the biomechanics of lesion. *Sports Orthopaedics and Traumatology*, 23(1):30–34, 2007.
- [180] J. Nowak, H. Mallmin, and S. Larsson. The aetiology and epidemiology of clavicular fractures: A prospective study during a two-year period in uppsala, sweden. *Injury*, 31(5):353–358, 2000.
- [181] C.R. Rowe. An atlas of anatomy and treatment of midclavicular fractures. *Clin Orthop Relat Res.*, 58:29–42, 1968.
- [182] F. Postacchini, S. Gumina, P. De Santis, and F. Albo. Epidemiology of clavicle fractures. *J Shoulder Elbow Surg*, 11(5):452–456, 2002.
- [183] Y.C. Tsuei, M.K. Au, and W. Chu. Comparison of clinical results of surgical treatment for unstable distal clavicle fractures by transacromial pins with and without tension band wire. *J Chin Med Assoc*, 73(12):638–643, 2010.
- [184] P.J. Hughes and B. Bolton-Maggs. Fractures of the clavicle in adults. *Current Orthopaedics*, 16(2):133–138, 2002.
- [185] J. Gille, A.P. Schulz, S. Wallstable, C. Voigt, and M. Faschingbauer. Hook plate for medial clavicle fracture. *Indian J Orthop*, 44(2):221–223, 2010.
- [186] N. Matsumura, H. Ikegami, N. Nakamichi, T. Nakamura, T. Nagura, N. Imanishi, S. Aiso, and Y. Toyama. Effect of shortening deformity of the clavicle on scapular kinematics: A cadaveric study. *Am J Sports Med.*, 38(5):1000–1006, 2010.
- [187] M. Zlowodzki, B.A. Zelle, P.A. Cole, K. Jeray, and M.D. McKee. Treatment of acute midshaft clavicle fractures: systematic review of 2144 fractures: on behalf of the evidence-based orthopaedic trauma working group. *J Orthop Trauma.*, 19(7):504–507, 2005.

- [188] The Canadian Orthopaedic Trauma Society. Nonoperative treatment compared with plate fixation of displaced midshaft clavicular fractures. a multicenter, randomized clinical trial. *J Bone Joint Surg. Am.*, 89:1–10, 2007.
- [189] M.Y. Bajuri, S. Maidin, A. Rauf, M. Baharuddin, and S. Harjeet. Functional outcomes of conservatively treated clavicle fractures. *Clinics (Sao Paulo)*, 66(4):635–639, 2011.
- [190] S. Lazarides and G. Zafiropoulos. Conservative treatment of fractures at the middle third of the clavicle: the relevance of shortening and clinical outcome. *J Shoulder Elbow Surg*, 15:191–194, 2006.
- [191] M. Ledger, N. Leeks, T. Ackland, and A. Wang. Short malunions of the clavicle: an anatomic and functional study. *J Shoulder Elbow Surg*, 14: 349–354, 2005.
- [192] J.M. Hill, M.H. McGuire, and L.A. Crosby. Closed treatment of displaced middle-third fractures of the clavicle gives poor results. *J Bone Joint Surg Br*, 79:537–539, 1997.
- [193] M. Wick, E.J. Muller, E. Kollig, and G. Muhr. Midshaft fractures of the clavicle with a shortening of more than 2cm predispose to nonunion. *Arch Orthop Trauma Surg*, 121:207–211, 2001.
- [194] A. Nordqvist, I. Redlung-Johnell, S.A. von, and C.J. Petersson. Shortening of clavicle after fracture. incidence and clinical significance, a 5-year follow up of 85 patients. *Acta Orthop Scan*, 68:349–351, 1997.
- [195] R. Matias and A. Gil Pascoal. The unstable shoulder in arm elevation: A three-dimensional and electromyographic study in subjects with glenohumeral instability. *Clin Biomech.*, 21:S52–S58, 2006.
- [196] P.M. Ludewig and T. Cook. Alterations in shoulder kinematics and associated muscle activity in people with symptoms of shoulder impingement. *Phys Ther.*, 80:276–291, 2000.

- [197] S.H. Treacy, F.H. Savoie, and L.D. Field. Arthroscopic treatment of multidirectional instability. *J Shoulder Elbow Surg*, 8:344–349, 1999.
- [198] T.O. Smith. Immobilisation following traumatic anterior glenohumeral joint dislocation. a literature review. *Injury, Int J Care Injured*, 37:228–237, 2006.
- [199] R.C. Mather, L.A. Orlando, R.A. Henderson, J.T.R. Lawrence, and Taylor D.C. A predictive model of shoulder instability after a first-time anterior shoulder dislocation. *J Shoulder Elbow Surg.*, 20:259–266, 2011.
- [200] C.S. Neer and C.R. Foster. Inferior capsular shift for involuntary inferior and multidirectional instability of shoulder. *J. Bone Joint Surg Am*, 62:897–908, 1980.
- [201] Y.H. An and R.J. Friedman. Multidirectional instability of the glenohumeral joint. *Orthop Clin of North Am*, 31(2):275–283, 2000.
- [202] R.M. Kiss, A. Illyes, and J. Kiss. Physiotherapy vs. capsular shift and physiotherapy in multidirectional shoulder joint instability. *J Electrom and Kines*, 20:489–501, 2010.
- [203] H. Inui, K. Sugamoto, T. Miyamoto, H. Yoshikawa, A. Machida, J. Hashimoto, and K. Nobuhara. Three-dimensional relationship of the glenohumeral joint in the elevated position in shoulders with multidirectional instability. *J Shoulder Elbow Surg.*, 2116(5):510–515, 2002.
- [204] S.H. Kim. Arthroscopic treatment of posterior and multidirectional instability. *Operative Techniques in Sports Medicine*, 12(2):111–121, 2004.
- [205] P. Nyiri, A. Illyes, R. Kiss, and J. Kiss. Intermediate biomechanical analysis of the effect of physiotherapy only compared with capsular shift and physiotherapy in multidirectional shoulder instability. *J Shoulder Elbow Surg*, 19:802–813, 2010.

- [206] L. Beasley, D.A. Faryniarz, and J.A. Hannafin. Multidirectional instability of the shoulder in the female athlete. *Clin Sports Med.*, 19:331–349, 2000.
- [207] J. Ozaki. Glenohumeral movements of the involuntary inferior and multidirectional instability. *Clin Orthop*, 238:107–111, 1990.
- [208] J.K. Bell. Arthroscopic management of multidirectional instability. *Orthop Clin of North Am.*, 41(3):357–365, 2010.
- [209] J.B. Ogston and P.M. Ludewig. Differences in 3-dimensional shoulder kinematics between persons with multidirectional instability and asymptomatic controls. *Am J Sports Med.*, 35:1361–1370, 2007.
- [210] R. von Eisenhart-Rothe, F.A. Jørgensen, F. Eckstein, T. Vogl, and H. Graichen. Pathomechanics in atraumatic shoulder instability: scapular positioning correlates with humerus head centering. *Clin. Orthop. Relat. Re.*, pages 82–89, 2005.
- [211] E. Jeffrey and M.D. Budoff. The etiology of rotator cuff disease and treatment of partial-thickness pathology. *Journal of the American Society for Surgery of the Hand*, 5(3):269–273, 2005.
- [212] C. Milgrom, M. Schaffler, S. Gilbert, and C. van Holsbeeck. Rotator cuff changes in asymptomatic adults. the effect of age, hand dominance and gender. *J Shoulder Elbow Surg. Br*, 77(2):296–298, 1995.
- [213] S.M. Kane, A. Dave, A. Haque, and K. Langston. The incidence of rotator cuff disease in smoking and non-smoking patients: a cadaveric study. *Orthopaedics*, 29(4):363, 2006.
- [214] B.R. Neri, K.W. Chan, and Y.W. Kwon. Management of massive and irreparable rotator cuff tears. *J Shoulder Elbow Surg.*, 18(5):808–818, 2009.
- [215] J.J.P. Warner and P.E. Greis. The treatment of stiffness of the shoulder after repair of the rotator cuff. *Instr Course Lect*, 47:67–75, 1998.

- [216] K.J. Brislin, L.D. Field, and F.H. Savoie. Complications after arthroscopic rotator cuff repair. *Arthroscopy*, 23:124–128, 2007.
- [217] S. Namdari and A. Green. Range of motion limitation after rotator cuff repair. *J. Shoulder Elbow Surg.*, 19:290–296, 2010.
- [218] S.S. Burkhart. Fluoroscopic comparison of kinematic patterns in massive rotator cuff tears. a suspension bridge model. *Clin Orthop Relat*, 284:144–152, 1992.
- [219] H. Graichen, T. Stammberger, H. Bonel, E. Wiedmann, K.H. Englmeier, and M. Reiser. Three-dimensional analysis of shoulder girdle and supraspinatus motion patterns in patients with impingement syndrome. *J. Orthop*, 19:1192–1198, 2001.
- [220] A.C. Lukasiewicz, P. McClure, L. Michener, N. Pratt, and B. Sennett. Comparison of 3-dimensional scapular position and orientation between subjects with and without shoulder impingement. *J. Orthop. Sports Phys. Ther.*, 29:574–583, 1999.
- [221] K. Endo, T. Ikata, S. Katoh, and Y. Takeda. Radiographic assessment of scapular rotational tilt in chronic shoulder impingement syndrome. *J. Orthop. Sci.*, 6:3–10, 2001.
- [222] J. H. de Groot, M.A.J. van de Sande, C.G.M. Meskers, and P.M. Rozing. Pathological teres major activation in patients with massive rotator cuff tears alters with pain relief and or salvage surgery transfer. *Clin Biomech.*, 21:S27–S32, 2006.
- [223] B.T. Kelly, R.J. Williams, F.A. Cordasco, S.L. Backus, J.C. Otis, D.E. Weiland, D.W. Altchek, E.V. Craig, T.L. Wickiewicz, and R.F. Warren. Differential patterns of muscle activation in patients with symptomatic and asymptomatic rotator cuff tears. *J Shoulder and Elbow Surg*, 14:165–171, 2005.

- [224] S.E. Dalton and S.J. Snyder. Glenohumeral instability. *Bailliere's Clinical Rheumatology*, 3(3):511–534, 1989.
- [225] L. Hovelius. Incidence of shoulder dislocation in sweden. *Clin Orthop Relat Res*, 166:127–131, 1982.
- [226] B.D. Owens, M.L. Duffey, B.J. Nelson, T.M. DeBerardino, D.C. Taylor, and S.B. Mountcastle. The incidence and characteristics of shoulder instability at the united states military academy. *Am J Sports Med.*, 35(7):1168–1173, 2007.
- [227] S.M. Moore, V. Musahl, P.J. McMahon, and R.E. Debski. Multidirectional kinematics of the glenohumeral joint during simulated simple translation tests: impact on clinical diagnoses. *J Orthop Res*, 22(4):889–894, 2004.
- [228] J.A. Bishop, T.S. Crall, and M.S. Kocher. Operative versus nonoperative treatment after primary traumatic anterior glenohumeral dislocation: expected-value decision analysis. *J Shoulder Elbow Surg.*, pages –, 2011.
- [229] P.M. Ludewig and J. Reynolds. The association of scapular kinematics and glenohumeral joint pathologies. *J. Orthop. Sports Phys. Ther.*, 39(2): 90–104, 2009.
- [230] E. Itoi, N.E. Motzkin, B.F. Morrey, and K.N. An. Scapular inclination and inferior stability of the shoulder. *J Shoulder Elbow Surg.*, 1:131–139, 1992.
- [231] R.A. Arciero, D.C. Taylor, R.J. Snyder, and J.M. Uhorchak. Arthroscopic bioabsorbable tack stabilization of initial anterior shoulder dislocations: a preliminary report. *Arthroscopy*, 11:410–417, 1995.
- [232] H. Boszotta and W. Helperstorfer. Arthroscopic transglenoid suture repair for initial shaft fracture: a decision analysis model. *Arthroscopy*, 16:462–470, 2000.
- [233] J. Aizawa, T. Masuda, T. Koyama, K. Nakamaru, K. Isozaki, A. Okawa, and S. Morita. Three-dimensional motion of the upper extremity joints

- during various activities of daily living. *J Biomech.*, 43(15):2915–2922, 2008.
- [234] P. Kasten, M. Maier, P. Wendy, O. Rettig, P. Raiss, S. Wolf, and M. Loew. Can shoulder arthroplasty restore the range of motion in activities of daily living? a prospective 3d video motion analysis study. *J Shoulder Elbow Surg.*, 19(2):S59–S65, 2010.
- [235] J.E. Kuhn. A new classification system for shoulder instability. *Br J Sports Med.*, 44:341–346, 2010.
- [236] J. Dawson, R. Fitzpatrick, and A. Carr. Questionnaire on the perceptions of patients about shoulder surgery. *J Bone Joint Surg.*, 78(4):593–600, 1996.
- [237] J. Dawson, R. Fitzpatrick, and A. Carr. The assessment of shoulder instability. the development and validation of a questionnaire. *J Bone Joint Surg.*, 81(3):420–426, 1999.
- [238] R.J. Safranek, S. Gottschlich, and A.C. Kak. Evidence accumulation using binary frames of discernment for verification vision. *IEEE Trans Robotics and Automation*, 6(4):405–417, 1990.
- [239] G. Gerig, D. Welti, C.R.G. Guttman, A.C.F. Colchester, and G. Szekely. Exploring the discrimination power of the time domain for segmentation and characterization of active lesions in serial mr data. *Medical Image Analysis*, 4(1):31–42, 2000.
- [240] M.J. Beynon, L. Jones, and C.A. Holt. Classification of osteoarthritic and normal knee function using three-dimensional motion analysis and the dempster-shafer theory of evidence. *IEEE Trans Syst Man Cybern A.*, 36(1):173–186, 2006.
- [241] L. Jones and C.A. Holt. An objective tool for assessing the outcome of total knee replacement surgery. *Proc Inst Mech Eng [H]*, 222(5):647–655, 2008.

- [242] E. Viikari-Juntura, H. Riihimaki, E. Takala, S. Rauas, A. Peppanen, and A. Malmivaara. Factors predicting pain in the neck, shoulders and upper limbs in forestry work. *People Work Res Rep*, 7:233–253, 1993.
- [243] E. Viikari-Juntura, R. Shiri, S. Soloviera, J. Karppinen, P. Leino-Arjas, and H. Varonen. Risk factors of artherosclerosis and shoulder pain - is there an association? a systematic review. *Eur J Pain*, 12:412–426, 2008.
- [244] A.M. Wendelboe, K.T. Hegmann, L.H. Gren, S.C. Alder, G.L. White, and J.L. Lyon. Associations between body-mass index and surgery for rotator cuff tendinitis. *J Bone Joint Surg. Am.*, 86:743–747, 2004.